# Revision and Extension of a COSMO-RS Based Model for Electrolyte Systems: From Infinite Dilution to the Fused Salt State

Vom Promotionsausschuss der
Technischen Universität Hamburg

zur Erlangung des akademischen Grades

Doktor-Ingenieur (Dr.-Ing.)

genehmigte Dissertation (Monografie)

von
Andrés González de Castilla Mena

aus
Mexiko City, Mexiko

2025

DOI: https://doi.org/10.15480/882.16280

ORCID: https://orcid.org/0000-0003-0536-7402

1. Gutachterin: Prof. Dr.-Ing. Irina Smirnova
2. Gutachter: Prof. Dr. Andreas Klamt

Vorsitzender des Prüfungsausschusses: Prof. Dr.-Ing. Mirko Skiborowski

Datum der mündlichen Prüfung: 24.10.2025

# Acknowledgements

The present work was developed during my time as a research assistant at the Institute of Thermal Separation Processes in Hamburg University of Technology. I am very thankful to Prof. Dr.-Ing. Irina Smirnova for her continuous support throughout these years and for always having an open ear and the right words for all circumstances.

I am also very thankful to Prof. Dr. Andreas Klamt for his role as second reviewer and his support and feedback, which were always very motivating. I gratefully acknowledge scientific discussions with his former team: Dr. Frank Eckert, Dr. Michael Diedenhofen and the team from BIOVIA (Dassault Systèmes Germany).

I wish to express gratitude to Prof. em. Roland Kjellander for his kindness, clarity and patience with my questions, which inspired me to take a deeper dive into electrolyte theory.

Several students provided support for the results in this manuscript with a thesis or as scientific assistants. I celebrate their success, wish them the best for their future and hope that our paths will meet again someday.

I am thankful to all my colleagues at Hamburg University of Technology for their friendship, the discussions, the sports and the relaxed environment and to my colleague and friend Dr.-Ing. Simon Müller for his constant support and enthusiasm. My good friends Zsolt Kállai and David García Luna took it upon themselves to proof-read some excerpts of this work and I gratefully acknowledge their constructive comments.

Being far away from my homeland is difficult and made me more appreciative of older friendships that never waned in Mexico and in the U.S., and of the newer friendships in Germany and Europe that quickly turned Hamburg into a second home. My family remains a constant in my life, and I am deeply grateful for having my parents, my brother and my sisters who always supported and encouraged me. Lastly, I want to thank my dearest Carla: we pursued our goals and went through challenging times together with endless humor, love and mutual understanding.

# Summary

Electrolyte thermodynamics remains an active field of study and current industrial requirements highlight the need for more standardized, predictive approaches. COSMO-RS-ES is a promising electrolyte model that can describe aqueous electrolytes, including salt and solvents partitioning in liquid-liquid systems. It is also capable of predicting the solubility of a wide range of salts in mixed aqueous solvents. The present thesis extends the COSMO-RS-ES model beyond aqueous systems by enhancing its performance especially for non-aqueous electrolyte systems. It builds a bridge between COSMO-RS-based modelling of conventional electrolytes and pure ionic liquids leading to the first consistent model of its kind, applicable from infinite dilution to the pure ionic liquid state.

To achieve this goal, a modification to the long-range electrostatics term is introduced. This modification corrects large systematic deviations at low relative permittivity values. Subsequently, the compositional derivatives of the molar mass, density and relative permittivity of the mixture are used to re-derive an extension of the modified long-range electrostatics term. The resulting expression is Gibbs-Duhem consistent and improves the performance of the COSMO-RS-ES model, particularly for the prediction of salt solubility in non-aqueous solvents. In a parallel step, the modified extended long-range electrostatics term is combined with conventional COSMO-RS theory for the description of ionic liquid systems to gain insights into the physical significance of the approach.

In a conclusive step, the tested methodologies for salts and for ionic liquids are integrated to develop a generalized model called the COSMO-RS-ES+ model. This model can deal with salts and ionic liquids using the same basis and parameters for all ions. It is trained with available salt-based electrolyte system datasets from its COSMO-RS-ES predecessor, as well as with infinite dilution activity coefficients of neutral molecules in pure ionic liquids and data from ternary liquid-liquid equilibria with an ionic liquid component. The predictive power of the model is tested with salt solubility in pure and mixed solvents, temperature dependent ionic liquid solubility in neat solvents and the temperature dependent mean ionic activity coefficients of diverse salts in water. The resulting model demonstrates consistent predictive capabilities, shows the advantage of handling ionic liquids as electrolytes and takes a step closer to meeting industrial needs.

# Symbols

**Latin symbols**

| | |
|---|---|
| $a$ | distance of closest approach |
| a | activity |
| $\boldsymbol{a_{eff}}$ | COSMO-RS effective segment interaction contact area |
| $A$ | Helmholtz free energy / adjustable parameter |
| $\mathbf{A}$ | Coulomb interaction matrix |
| $\boldsymbol{A_{IJ}}$ | COSMO-RS total segment-pair interaction energy |
| $\boldsymbol{A_{\phi}^{(c)}}$, $\boldsymbol{A_{\phi}^{(m)}}$, $\boldsymbol{A_{\phi}^{(x)}}$ | Debye-Hückel parameter (molar, molal, mole fraction) |
| $\boldsymbol{b^{(c)}}$, $\boldsymbol{b^{(m)}}$, $\boldsymbol{b^{(x)}}$ | parameter of closest approach (molar, molal, mole fraction) |
| $\boldsymbol{B}$ | adjustable parameter / McMillan-Mayer state function |
| $\boldsymbol{c}$ | molar concentration / fitting parameter |
| $\boldsymbol{c_{ij}(r)}$ | direct pair correlation function |
| $\boldsymbol{c_{hb}(T)}$ | COSMO-RS hydrogen bonding energy interaction parameter |
| $\tilde{\mathbf{C}}(\boldsymbol{k})$ | matrix notation for the Fourier transforms of $c_{ij}(r)$ |
| $\boldsymbol{C}$ | capacitance / adjustable parameter |
| $\boldsymbol{d_i}$, $\overline{\boldsymbol{d}}$ | density of compound $i$, averaged density |
| $\boldsymbol{d_{IJ}}$ | euclidean distance between surface segments $I$ and $J$ |
| $\mathbf{D}$ | Green's function (matrix) / adjustable parameter |
| $\boldsymbol{e}$ | electron charge |
| $E$ | dielectric factor / interaction energy / energy |
| E | electric field |
| $\boldsymbol{E_{IJ}^{mf}}$ | COSMO-RS electrostatic misfit energy for surface contact $IJ$ |
| $\boldsymbol{f}$ | fugacity / fraction |
| $\boldsymbol{f_{sc}}$ | scaling factor |
| $\boldsymbol{f^{\perp}}$ | parameter for COSMO-RS orthogonal misfit energy |
| $\boldsymbol{F}$ | force / adjustable parameter |
| $g$ | molar Gibbs free energy |
| $\boldsymbol{g_{ij}(r)}$ | radial distribution function |
| $\mathbf{g}_{\boldsymbol{i}}$ | Kirkwood g-factor |
| $G$ | Gibbs free energy |
| $\boldsymbol{G_{IJ}^{hb}}$ | COSMO-RS hydrogen bonding interaction energy |
| $h$ | molar enthalpy |
| $\boldsymbol{h_{ij}(r)}$ | total pair correlation function |

| | |
|---|---|
| $\widetilde{\mathbf{H}}(\boldsymbol{k})$ | matrix notation for the Fourier transforms of $h_{ij}(r)$ |
| $\widehat{\boldsymbol{H}}$ | Hamiltonian operator |
| $\boldsymbol{I^{(c)}}$, $\boldsymbol{I^{(m)}}$, $\boldsymbol{I_x}$ | ionic strength (molar, molal, mole fraction) |
| $\boldsymbol{I_x^{IL}}$ | ionic strength at the pure molten salt state (mole fraction) |
| $\mathbf{I^{(0)}}$ | identity matrix |
| $I$ | energy level $I$ |
| $\mathbf{K_{assoc}}$ | association constant |
| $\boldsymbol{k_B}$ | Boltzmann constant |
| $\boldsymbol{\ell}$ | amount of accessible quantum energy levels $I$ |
| $\boldsymbol{m}$ | molal concentration |
| $\boldsymbol{M}$, $\boldsymbol{\bar{M}}$ | molar mass, averaged molar mass |
| $\boldsymbol{n_i}$ , $\boldsymbol{n_T}$ | moles of component $i$, total number of moles |
| $\boldsymbol{n_D}$ | refractive index |
| $N$ | number of particles in an ensemble |
| $\boldsymbol{N_A}$ | Avogadro´s number |
| $P$ | pressure |
| P | polarization |
| $\boldsymbol{\mathcal{P}}$ | component/mixture property |
| $q$ | charge |
| $\mathbf{Q^X}$ | charge density (matrix representation) |
| $\boldsymbol{r}$ | radius / radial distance |
| $\boldsymbol{r_{av}}$ | averaging radius |
| $R$ | ideal gas constant |
| $\boldsymbol{R_i}$ | radius of spherical ion $i$ |
| $\boldsymbol{s}$ | COSMO surface segment |
| $S$ | entropy |
| $T$ | temperature |
| $\boldsymbol{u_{ij}}$ | pair interaction potential between entities $i$ and $j$ |
| $U$ | internal energy |
| $\mathbf{v}$ | molar volume |
| $V$ | volume |
| w | mass fraction |
| $\boldsymbol{x}$ | mole fraction |
| $\boldsymbol{z_i}$ | valence of species $i$ |
| $\boldsymbol{z}$ | coordination number |
| $\boldsymbol{Z}$ | partition function |

**Greek symbols**

| | |
|---|---|
| $\boldsymbol{\alpha}$ | energy parameter / association degree / parameter |
| $\boldsymbol{\alpha_{sc}}$ | scaling parameter |
| $\boldsymbol{\alpha_0}$ | polarizability tensor |
| $\boldsymbol{\beta}$ | inverse of the product $k_B T$ |
| $\boldsymbol{\gamma}$ | activity coefficient |
| $\boldsymbol{\Gamma}$ | surface segment activity coefficient |
| $\boldsymbol{\Gamma}$ | MSA screening parameter |
| $\boldsymbol{\delta_{ij}}$ | Kronecker delta |
| $\boldsymbol{\delta^{(3)}(r)}$ | Dirac delta |
| $\boldsymbol{\varepsilon_0}$ | vacuum permittivity |
| $\boldsymbol{\varepsilon}$ | relative permittivity |
| $\boldsymbol{\eta}$ | expansion term of a PB solution |
| $\boldsymbol{\theta}$ | coordination angle |
| $\boldsymbol{\Theta_I}$ | surface fraction of molecular surface segments of type $I$ |
| $\boldsymbol{\kappa}$ | screening length |
| $\boldsymbol{\kappa_D}$ | Debye screening length |
| $\boldsymbol{\lambda_B}$ | Bjerrum length |
| $\boldsymbol{\Lambda}$ | electrostatic coupling parameter |
| $\boldsymbol{\mu}$ | chemical potential |
| $\boldsymbol{\nu_i}$ | stoichiometric coefficient of species $i$ |
| $\boldsymbol{\nu}$ | sum of the stoichiometric coefficients |
| $\boldsymbol{\rho}$ | number density |
| $\boldsymbol{\sigma}$ | surface charge density |
| $\boldsymbol{\tau}$ | interaction energy parameter |
| $\boldsymbol{\phi}$ | volume fraction |
| $\boldsymbol{\varphi}$ | osmotic coefficient |
| $\boldsymbol{\Pi}$ | osmotic pressure |
| $\boldsymbol{\Phi^{X}}$ | surface electrostatic potential (matrix) |
| $\boldsymbol{\psi}$ | electrostatic potential |
| $\boldsymbol{\Psi}$ | sphericity |
| $\boldsymbol{\Psi(r)}$ | wave function |

# Abbreviations

| | |
|---|---|
| AIOMFAC | Aerosol Inorganic-Organic Mixtures Functional-groups Activity Coefficients |
| AAD | Average Absolute Deviation |
| AARD | Average Absolute Relative Deviation |
| ARD | Average Relative Deviation |
| BiDH | Binding Debye-Hückel |
| COSMO | Conductor-like Screening Model |
| COSMO-RS | COSMO for Realistic Solvation |
| COSMO-RS-ES | COSMO-RS for Electrolyte Systems |
| COSMO-SAC | COSMO Surface Activity Coefficients |
| CPA | Cubic Plus Association |
| DFT | Density Functional Theory |
| DH | Debye-Hückel |
| DIT | Dressed Ion Theory |
| DME | Dimethoxyethane |
| EoS | Equation of State |
| E-PDH | Extended Pitzer-Debye-Hückel |
| IDAC | Infinite Dilution Activity Coefficient |
| IL | Ionic Liquid |
| JESS | Joint Expert Speciation System |
| LLE | Liquid-Liquid Equilibrium |
| LMWA | Law of Matching Water Affinities |
| LPB | Linearized Poisson-Boltzmann |
| LR | Long-Range |
| MDE-DH | Multiple Decay Extension of the Debye-Hückel Theory |
| ME-PDH | Modified Extended Pitzer-Debye-Hückel |
| MIAC | Mean Ionic Activity Coefficient |
| M-PDH | Modified Pitzer-Debye-Hückel |
| MSA | Mean Spherical Approximation |
| NRTL | Non-Random Two Liquid |
| NRTL-SAC | NRTL – Surface Activity Coefficient |
| OF | Objective Function |
| OZ | Ornstein-Zernike |
| PB | Poisson-Boltzmann |
| PC-SAFT | Perturbed Chain SAFT |

| | |
|---|---|
| PDH | Pitzer-Debye-Hückel |
| PM | Primitive Model |
| PPC-SAFT | Polar PC-SAFT |
| PR | Peng-Robinson |
| RKS | Redlich-Kwong-Soave |
| RMSE | Root Mean Square Error |
| RPM | Restricted Primitive Model |
| RP-MSA | Restricted Primitive Mean Spherical Approximation |
| RTIL | Room-Temperature Ionic Liquid |
| SAFT | Statistical Associating Fluid Theory |
| SAFT-VR | SAFT Variable Range |
| SAFT-VRE | SAFT-RV for Electrolytes |
| SLE | Solid-Liquid Equilibrium |
| SR | Short-Range |
| UNIFAC | UNIQUAC Functional-groups Activity Coefficients |
| UNIQUAC | Universal Quasi-Chemical |
| VLE | Vapor-Liquid Equilibrium |

# Contents

# List of figures

# List of tables

# 1 Introduction

Electrolyte thermodynamics remain a challenge for practical industrial applications and, while the demand for predictive capability grows, even modern chemical engineering models for electrolytes lack true predictive, universal applicability.[1,2] This is attributed to the nature of ions in an electrolyte mixture. Ions are charged species that interact with each other over long distances due to coulombic forces and can significantly influence molecular interactions.[3] Furthermore, the available experimental data for phase equilibria in electrolytes is seldom transferable to industrial settings and its description with conventional electrolyte models requires extensive parameterization, particularly if the conditions significantly depart from room temperature, atmospheric pressure and low to moderate electrolyte concentrations.[1]

For these reasons, the most abundantly applied electrolyte models still rely on system- or chemical group specific binary interaction parameters.[1,4–6] In contrast, a robust, well established predictive method for thermodynamic properties in systems with neutral components is the COSMO-RS model, introduced by Klamt et al.[7,8] The widespread use of the COSMO-RS model inevitably lead to strive for electrolyte extensions. The first developments of COSMO-RS-based electrolyte models involved a COSMO-RS-based contribution combined with a long-range electrostatics term to describe mostly aqueous and some mixed aqueous systems with simple salts.[9–13] Gerlach et al.[14] introduced the COSMO-RS-ES model, which was the first COSMO-RS based approach to systematically reproduce a broad database of mixed aqueous biphasic electrolytes and mean ionic activity coefficients. In previous works, Müller et al.[15,16] introduced new data types into the training set and an effective ionization degree, thereby improving the capabilities of COSMO-RS-ES to predict the solubility of a wide variety of salts in water and mixed aqueous solvent systems. However, significant systematic deviations remained present in the description of highly concentrated, non-aqueous electrolytes.

The objective of the present work is to address the consistent extension of the COSMO-RS-ES model for highly concentrated, non-aqueous electrolytes in the entire concentration range spanning from infinitely diluted ions to the pure ionic liquid/molten salt state. For this purpose, a modified, Gibbs-Duhem consistent extension of the long-

range electrostatics term is developed and introduced into the model. Subsequently, the training dataset of the model is enlarged with experimental data from ionic liquid systems consisting of experimentally measured liquid-liquid equilibria and infinite dilution activity coefficients of neutral species in pure ionic liquids. These were extracted from the recent literature and a public database from the National Institute of Standards and Technology. Finally, the short-ranged COSMO-RS-based equations for ionic interactions are reformulated from scratch to handle both monoatomic and large polyatomic ions with the same basis, the same parameters and accounting for all binary contact interactions in a predictive manner. The resulting extended model, denominated COSMO-RS-ES+, has a comparable performance to that of its predecessors for aqueous salt systems, while extending its reach and predictive power towards non-aqueous salt and ionic liquid-based electrolytes including the pure ionic liquid state.

Some results of the present manuscript have been published by González de Castilla et al.[17,18] Developments derived in the present work have been applied in a different setting by Marques et al.[19] and Arrad et al.[20]

# 2 Fundamentals

## 2.1 Basic Thermodynamic Principles

The word “Thermodynamics” comes from the Greek *therme* and *dynamikos*: the force of heat; the dynamics due to heat. In its beginnings, thermodynamics dealt with steam engines and the conversion of heat into the ability to do work. In time, it was observed that the mathematical groundwork for the steam engines can be universally applied and used at the molecular level to describe macroscopic observations.[21]

### 2.1.1 Statistical Mechanics and Thermodynamic Relations

A system is any formally defined part of the universe that becomes an object of study. The system is closed if it does not exchange mass with its surroundings and isolated if it does not exchange energy with its surroundings.[21,22] A closed, isolated system with constant volume $V$ that filled with a material content will contain an energy inherent to this material content and find itself at a given temperature. If the material content consists of e.g. a given number ($N$) of discretized, inert, microscopic, hard, identical spherical particles of species $i$, then this system can be analyzed as a microcanonical ensemble.[22]

The instantaneous position and momenta of these particles determine the internal energy $U$ of the system. A snapshot of these particles at any given instant would reveal them at fixed positions with given momenta, which equate to potential and kinetic energy, respectively. These constitute the instantaneous internal energy $\breve{U}$ of the snapshot and the snapshot is called a microstate. The total number $\Omega$ of possible configurations that yield the same instantaneous internal energy $\breve{U}$ is called the degeneracy of the system.[22]

If two of these systems are in thermal contact, the total internal energy is given by the sum of their initial states $U^{tot} = U_1^0 + U_2^0$. The equilibrated values of $U_1$ and $U_2$ after the energy exchange are unknown and lie somewhere within a range of 0 and $U^{tot}$ with the condition $U^{tot} = U_1 + U_2$. Statistics provide a powerful tool to analyze this problem.[22,23]

The total degeneracy is $\Omega^{tot} = \Omega_1(U_1) \cdot \Omega_2(U_2)$: for every microstate contained in $\Omega_1(U_1)$, system 2 can find itself in any microstate contained in $\Omega_2(U_2)$. The most probable state is found at the maximum of the distribution $\frac{\partial(\Omega_{1,i}\Omega_{2,i})}{\partial U_{1,i}} = 0$. For evaluation purposes one can assume that the degeneracy is approximated based on the following statistical formula:[21]

$$\Omega(U) = \frac{N!}{(N^{(I)}!)(N^{(II)}!)\ldots(N^{(\ell)}!)} \tag{2.1}$$

where $N$ is the total number of particles, $N^{(I)}$ are the number or particles that find themselves at configurational (quantum) energy level $(I)$ and this can go up to any amount $(\ell)$ of quantum energy levels which become accessible at higher $U$ values.[22,23]

A simple exercise[22] reproduced with equation (2.1) can demonstrate that the observable (macroscopic) value of the internal energy is an average $\langle U_1 \rangle$ given by the sum of the energies system 1 has at different energy levels *i* weighted by their probability $p(U_{1,i})$:

$$\langle U_1 \rangle = \sum_i U_{1,i} \cdot p(U_{1,i}) = \sum_i U_{1,i} \cdot \frac{\Omega_{1,i}\Omega_{2,i}}{\sum_j \Omega_{1,j}\Omega_{2,j}} \tag{2.2}$$

where $U_{1,i}$ and $\Omega_{1,i}$ stand for the energy and degeneracy of system 1 at a given energy distribution *i* of the total energy. The same applies to system 2. This average leads to the condition $\frac{\partial \ln(\Omega_{1,i})}{\partial U_{1,i}} = \frac{\partial \ln(\Omega_{2,i})}{\partial U_{2,i}}$ for thermal equilibrium and a definition of entropy:[21,22]

$$S = k_B \ln(\Omega^{\mathrm{tot}}) \tag{2.3}$$

from which it is inferred that $S \geq 0$ due to $\Omega(U \to 0) = 1$ based on equation (2.1). It can also be inferred from equation (2.2) that the equilibrated macroscopic average $\langle U_1 \rangle$ distributes around the maximum of $\Omega_{1,i}\Omega_{2,i}$, i.e. the entropy is maximized at equilibrium.

Thus, by fixing ($N$, $V$), entropy $S$ is defined and the natural variables of $U$ in the microcanonical ensemble are $N_i$, $V$ and $S$. Partial derivation of $U$ leads to equation (2.4):

$$dU = \left(\frac{\partial U}{\partial S}\right)_{N_i,V} dS + \left(\frac{\partial U}{\partial V}\right)_{N_i,S} dV + \left(\frac{\partial U}{\partial N_i}\right)_{S,V} dN_i \tag{2.4}$$

where $\left(\frac{\partial U}{\partial S}\right)_{N_i,V}$ corresponds to the temperature of the system, $\left(\frac{\partial U}{\partial V}\right)_{N_i,S}$ to the pressure of the system and the definition $\left(\frac{\partial U}{\partial N_i}\right)_{S,V} = \mu_i$ is introduced. The term $\mu_i$ is called the

chemical potential[22,23] of species $i$ and equation (2.4) corresponds to the first law of thermodynamics:

$$dU = TdS - PdV + \mu_i dN_i \tag{2.5}$$

Diverse relations, including the second law of thermodynamics, can be obtained from equation (2.5) by introducing concepts like e.g. reversible and irreversible work or by its application in the analysis of a system with *N, V, T* as the natural variables of $U$ (canonical ensemble), or *N, P, T* as the natural variables of $U$ (isobaric-isothermic ensemble).[21,22]

The chemical potential corresponds to the change in energy brought upon infinitesimal addition of particles of component $i$ while keeping the number of particles of other components and the natural variables of an ensemble constant:[22,23]

$$\mu_i = \left(\frac{\partial U}{\partial n_i}\right)_{S,V,n_j} = \left(\frac{\partial A}{\partial n_i}\right)_{T,V,n_j} = \left(\frac{\partial G}{\partial n_i}\right)_{T,P,n_j} \tag{2.6}$$

The derivative of the internal energy $U$ corresponds to the microcanonical ensemble, the derivative of the Helmholz free energy $A$ corresponds to the canonical ensemble and the derivative of the Gibbs free energy $G$ corresponds to the isobaric-isothermic ensemble.[22] The basis $n_i$ for moles of component $i$ replaces the basis $N_i$ for particles as the convention in chemical engineering calculations (i.e. $R = N_A \cdot k_B$).

### 2.1.2 Classical Thermodynamics and Phase Equilibria

A system is said to be at phase equilibrium when the phases present in it have mechanical stability (same pressure $P$), thermal stability (same temperature $T$) and chemical equilibrium (composition of each phase remains constant). This is formulated for two phases in contact (e.g. phase $\alpha$ and $\beta$) with any number $i$ of components as follows:

$$P^\alpha = P^\beta \tag{2.7}$$

$$T^\alpha = T^\beta \tag{2.8}$$

$$\mu_i^\alpha = \mu_i^\beta \tag{2.9}$$

where $\mu_i^\pi$ is the chemical potential of component $i$ in phase $\pi$.

In line with the principles described in section 2.1.1, a system will naturally move towards equilibrium by maximizing the total entropy and minimizing the total free energy.[21] By applying the first law of thermodynamics (equations (2.4) and (2.5)) to a multicomponent system, the change in internal energy is expressed as follows:

$$dU = TdS - PdV + \sum_i \mu_i dn_i \tag{2.10}$$

The total derivative of $dU$ is equal to equation (2.10) plus several missing terms. If the condition expressed for equation (2.10) is to be true, then it is a mathematical requirement (Legendre transform) that the missing terms of the total derivative add up to zero:

$$0 = SdT - VdP + \sum_i n_i d\mu_i \tag{2.11}$$

Equation (2.11) is known as the Gibbs-Duhem relation.[4] At equilibrium in the isobaric-isothermic ensemble, equation (2.11) reduces to the summation $\sum_i n_i d\mu_i = 0$ over all $i$ components present in the mixture. This implies that the chemical potential of all the species present in a phase $\pi$ are not independent from each other and need to meet the condition $\sum_i n_i^\pi d\mu_i^\pi = 0$. This is a requirement for thermodynamic consistency.[4]

Moving on to more details about the chemical potential, it is classically defined in terms of the fugacity $f$. Upon integration of the Gibbs-Duhem relation in combination with the ideal gas equation, one may obtain the following expression for the isothermic case:[4]

$$\mu_i - \mu_i^+ = RTln\left(\frac{P}{P^+}\right) \tag{2.12}$$

where the subscript + stands for an arbitrary standard reference state. Equation (2.12) is derived at the ideal gas limit and the concept of fugacity represents a corrected pressure to describe the non-ideal case. Thus, equation (2.12) is generalized as follows:[4]

$$\mu_i - \mu_i^+ = RTln\left(\frac{f_i}{f_i^+}\right) \tag{2.13}$$

In a liquid phase, the ratio $\frac{f_i}{f_i^+}$ is also known as the activity of component $i$ and it is related to the concentration of component $i$ in the mixture by means of its activity coefficient $\gamma_i$ through the following definition:[4]

$$\frac{f_i}{f_i^+} = x_i \gamma_i \tag{2.14}$$

Expression (2.14) implies that the activity coefficient is a function of concentration that requires a fixed standard reference state and describes the non-ideal departure from this chosen standard reference state. Subsequent substitution of equations (2.13) and (2.14) in equation (2.9) lead to the equilibrium condition between two phases:

$$x_i^\alpha \gamma_i^\alpha = x_i^\beta \gamma_i^\beta \tag{2.15}$$

provided that $f_i^{+,\alpha} = f_i^{+,\beta} \therefore \ \mu_i^{+\alpha} = \mu_i^{+\beta}$, that is, applying the same standard reference state for component $i$ in both phases.[4]

### 2.1.3 Intermolecular Forces

As described in sections 2.1.1 and 2.1.2, phase equilibria is reached when a system with two or more phases (e.g. vapor + liquid, liquid + liquid, triple point, etc.) has achieved mechanical, thermal and chemical equilibrium. If pressure and temperature remain constant throughout a process, the equilibrium solely depends on the chemical potential and is effectively governed by intermolecular forces.[21] These in turn can be described as a function of the pair interaction potential $u_{ij}$ between two interacting particles.

In a hard sphere approach the interaction energy between two colliding particles in a gas can be thought of as a repulsive, impenetrable wall. This is a blunt approximation and many expressions have been proposed to more realistically describe interatomic repulsion. A widely known expression is the Lennard-Jones (LJ) potential.[4,21]

**Table 1. Proportionality of the pair interaction potential with respect to the distance between interacting particles for diverse interaction types.[21,24]**

| Interaction Type | Proportionality of $u_{ij}$ to separation |
|---|---|
| **Ion – Ion** | $r^{-1}$ |
| **Ion – Dipole** | $r^{-2}$ |
| **Dipole – Dipole** | $r^{-3}$ |
| **Dipole – Induced Dipole** | $r^{-6}$ |
| **Dispersion Forces** | $r^{-6}$ |
| **Interatomic Repulsion** | $r^{-12}$ |

Other intermolecular forces make their appearance as the modelled system increases in complexity. Some of the most relevant, and their proportionality to the radial distance $r$ between the interacting particles are shown in Table 1.

In the following chapter, some aspects of the traditional thermodynamic formalism for hard, charged spheres (the simplest representation of ions) will be summarized.

## 2.2 Thermodynamics of Electrolytes in Solution

"*In short, if you do not understand the spherical case, then you cannot claim to understand the basic physics of the object." – Neil DeGrasse Tyson*

In the simplest case, ions are described as charged spheres embedded in a dielectric medium. These charged entities interact with each other over short distances through direct molecular contact and interact with each other and with the medium via Coulombic forces of a considerably longer nature than that of neutral molecules.

### 2.2.1 The Primitive Model

The spherical case of ions embedded in a medium is called the primitive model (PM),[25] conceptually shown in Figure 1. The PM defines ions as hard, charged spheres of radius $R$ embedded in a dielectric continuum of relative permittivity $\varepsilon_r$ .[22,25] In the crudest approach, these are modelled as point charges with a spherical volume that is excluded from the electrostatic interactions (further details in section 2.2.2) The relative permittivity is a material property that represents how much electric flux a material is able to retain with respect to vacuum. In practical terms, if a material is deposited between two oppositely charged plates, the force of attraction between the plates is inversely proportional to the relative permittivity of the material. The molecules of the material can redistribute their internal charge in the presence of an electric field and even reorient themselves in the case of a fluid, thereby interfering with the electric field.[26] In the PM the relative permittivity and density are the only properties that describe the solvent in which ions of nature $i$ and counter-ions of nature $j$ are dissolved. This representation is crude[25] and yet the foundation for the most commonly applied electrostatic theories.

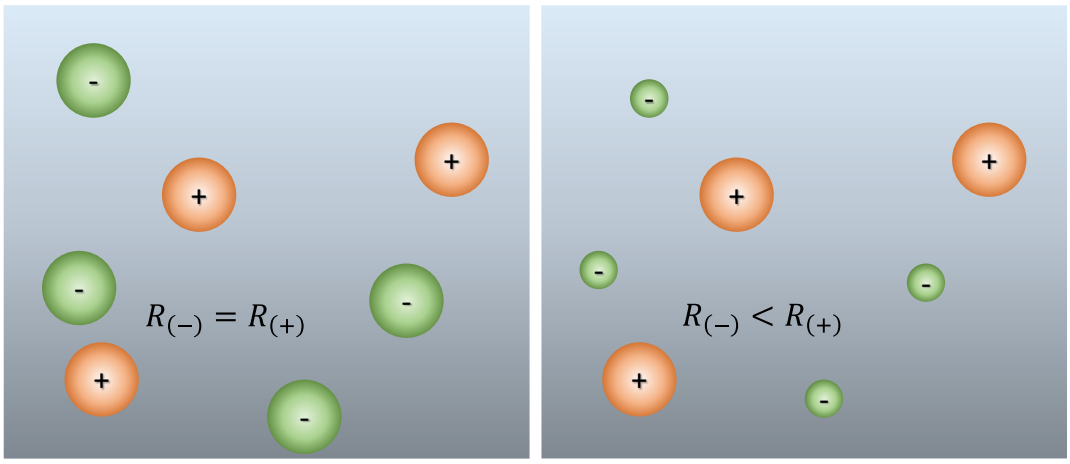


**Figure 1. The restricted PM with equally sized hard spherical ions (left) and the unrestricted PM with hard spherical ions of different sizes (right).**

Assuming equally sized hard spherical ions of radius $R$ and that all correlations between two ions $i$ and $j$ are of coulombic nature, the interaction potential $u_{ij}$ is given by:[22,27]

$$u_{ij} = \begin{cases} \infty, & r < a \quad hard\ sphere \\ \dfrac{q_i q_j}{4\pi\varepsilon_0\varepsilon_r r}, & r \geq a \quad Coulomb \end{cases} \tag{2.16}$$

where $\varepsilon_0$ is the permittivity of vaccum, $\varepsilon_r$ is the medium's relative permittivity, $q_i = z_i e$ is the charge of a sphere of species $i$ with valence $z_i$ being $e$ the electron charge. The spherical radii define the distance of closest approach between the ions: $a = (R_i + R_j)$.

The German physicist Max Born proposed one of the simplest applications of the restricted primitive model (hereafter RPM) to describe solvation of a single ion at infinite dilution. Solvation at infinite dilution is the process of transferring a single solute particle from the ideal gas state into a condensed liquid phase. Born suggested[28] that the standard molar free energy of solvation of this process was equivalent to the energetic difference (work) resulting from charging the ion in the gas phase and charging the ion in the liquid phase. Thus, by taking the coulombic potential $\psi$ in a medium, shown in equation (2.17):

$$\psi_r = \frac{q}{4\pi\varepsilon_0\varepsilon_r r} \tag{2.17}$$

the energy difference is given in the RPM by the following charging process:[28]

$$\Delta g_s^{+,\infty} = N_A \int_0^{z_i e} (\psi_s - \psi_{ig}) dq = \frac{N_A}{4\pi R_{ion}} \left(\frac{1}{\varepsilon_s \varepsilon_0} - \frac{1}{\varepsilon_0}\right) \int_0^{z_i e} q dq$$
$$= \frac{z_i^2 e^2 N_A}{8\pi \varepsilon_0 R_{ion}} \left(\frac{1}{\varepsilon_s} - 1\right) \tag{2.18}$$

where the relative permittivity of the medium $\varepsilon_r$ has been replaced by the relative permittivity of a solvent ($\varepsilon_s$) and $N_A$ is Avogadro's constant. The subscript $ig$ stands for ideal gas and the superscript ∞ stands for infinite dilution.

While equation (2.18) overestimates the value of $\Delta g_s^{+,\infty}$ when applied with experimentally measured crystal or van der Waals radii (e.g. Bondi[29] radii) and therefore requires larger than expected $R_{ion}$ values,[30] it can reasonably describe qualitative physical trends. Equation (2.18) is known as the Born term or Born equation and is applied in some electrolyte models to describe single ion solvation and transfer, particularly in the case of Equations of State (EoS) for electrolytes.[6]

Having briefly mentioned the case of a single ion, one evidently wishes to describe a mixture with multiple ions that correlate with each other. The Born equation is ill-suited for multiple ion systems as it does not capture any ion-ion pair correlations.

### 2.2.2 Debye-Hückel Theory

Peter Debye and Erich Hückel proposed a well-known theory[31] (hereafter, DH theory) to approximate the situation shown in Figure 1 (left frame) by estimating the value of the three-dimensional averaged coulombic potential $\psi_i^{av}(r)$ of the interacting charges. Firstly, the potential of an ion $i$ of radius $\frac{a}{2}$ in a medium of constant volume and relative permittivity $\varepsilon_r$ is considered by the following system of differential equations:[25,31]

$$\nabla^2 \psi_i^{av}(r) = 0 \quad \forall \quad r \leq a$$
$$\nabla^2 \psi_i^{av}(r) = -\frac{\rho_{E,i}^{tot}}{\varepsilon_0 \varepsilon_r} \quad \forall \quad r > a \tag{2.19}$$

where $\rho_{E,i}^{tot}$ stands for the total charge density surrounding the central ion. In this situation, the central ion $i$ will have a potential of interaction with all the surrounding

charges of type $j$ in its vicinity. This is essentially a mean field approximation where particle density is expressed in terms of a radial distribution function $g_{ij}(r)$ as follows:[22]

$$\rho_{E,i}^{tot} = \sum_j q_j \rho_j \, g_{ij}(r) = \sum_j q_j \rho_j \exp\left(-\beta q_j \psi_i^{av}(r)\right) \tag{2.20}$$

where $q_j$ and $\rho_j = N_j/V$ stand for the charge and number density of all ions in a fixed volume, $\beta$ stands for $(k_B T)^{-1}$ and $\psi_i^{av}(r)$ is the mean potential of the central ion.

The combination of equations (2.19) and (2.20) is known as the Poisson-Boltzmann (PB) equation and it does not have a straightforward analytical solution. As a simplified approach to approximate a solution to the inexact PB equation, Debye and Hückel linearized the exponential on the right hand side of equation (2.20) by taking the first two terms of its McLaurin expansion:[31]

$$g_{ij}^{DH}(r) = \exp\left(-\beta q_j \psi_i^{av}(r)\right)_{trunc} \approx \left[1 - \beta q_j \psi_i^{DH}(r)\right] \tag{2.21}$$

The combination of equation (2.19) and the approximation given by equation (2.21) is the (inexact) linearized Poisson-Boltzmann (LPB). For this reason, the DH theory is said to be a linearized theory, valid only at low concentrations.[25] Furthermore, the logical requirement $g_{ij}^{DH}(r) = g_{ji}^{DH}(r)$ is met only for charge symmetric ($|q_i| = |q_j|$) systems.

The LPB formulation from Debye and Hückel when the central sphere has a given volume is schematically represented in Figure 2 and mathematically expressed as follows:

$$\begin{gathered} \nabla^2 \psi_i^{DH}(r) = 0 \quad \forall \quad r \le a \\ \nabla^2 \psi_i^{DH}(r) = \frac{-1}{\varepsilon_0 \varepsilon_r} \left( \sum_j q_j \rho_j \left[1 - \beta q_j \psi_i^{DH}(r)\right] \right) = \kappa_D^2 \psi_i^{DH}(r) \;\; \forall \quad r > a \end{gathered} \tag{2.22}$$

where the term $\sum_j q_j \rho_j = 0$ is the electroneutrality condition (the sum of all charges equals zero) and where $\kappa_D$ is the Debye screening parameter given by equation (2.23):[25]

$$\kappa_D^2 = \beta \sum_j q_j q_j \rho_j \, \varepsilon_0^{-1} \varepsilon_r^{-1} \tag{2.23}$$

The proposed solution outside of the excluded dielectric volume $r > a$ is given by:[22,31]

$$\psi_i^{DH}(r) = \frac{C_1}{r}\exp(-\kappa_D r) + \frac{C_2}{r}\exp(\kappa_D r) \quad \forall \quad r > a \tag{2.24}$$

where several boundary conditions of the electric field from the central ion $i$ are valid.[25]

The first boundary condition consists of evaluating the potential at the limit $r \to \infty$. At an infinite distance the potential should vanish. However, one may note the limit:

$$\lim_{r\to\infty} \frac{C_2}{r}\exp(\kappa_D r) > 0 \tag{2.25}$$

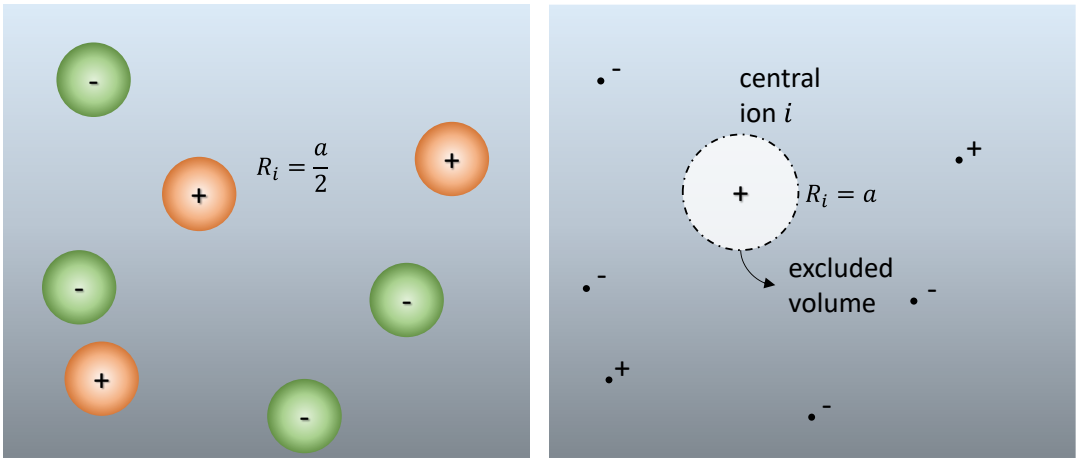


**Figure 2. The RPM (left) compared to the situation described by DH Theory (right), where the ion cloud is treated as uncorrelated point charges with no excluded dielectric volume.**

Thus, for equation (2.24) to be physically meaningful, the constant $C_2$ must be zero and the Debye-Hückel potential $\psi_i^{DH}(r)$ reduces to the following:

$$\psi_i^{DH}(r) = \frac{C_1}{r}\exp(-\kappa_D r) \quad \forall \quad r > a \tag{2.26}$$

where, if the central ion is treated as a point charge at infinite dilution ($a = 0$ and $\sum_j \rho_j = 0 \ \therefore \ \kappa_D \to 0$), the Coulomb potential $\psi_i(r)$ is obtained:

$$\lim_{\kappa_D\to 0} \psi_i^{DH}(r) = \frac{q_i}{4\pi\varepsilon_0\varepsilon_r r} \tag{2.27}$$

However, it is more realistic to evaluate $\psi_i^{DH}(r)$ at $r \geq a$ (assigns a volume to the central ion) in the presence of a surrounding ion cloud ($\kappa_D > 0$). Hence, the electro-neutrality principle is invoked in the sense that the charge $q_i$ of the central ion $i$ equals the opposing screening charge of the ion cloud $q_j^{cloud}$ at the surface of the spherical volume

encompassing the central ion.[22] This is expressed by a volume integral (spherical coordinates, hence the factor $\int_0^{2\pi} \partial\omega \int_0^{\pi} \sin(\theta)\partial\theta = 4\pi$ ) as follows:

$$4\pi \int_a^{\infty} \rho_{E,i}\, r^2 \mathrm{d}r = -4\pi \cdot \kappa_D^2 \varepsilon_0 \varepsilon_r C_1 \int_a^{\infty} \exp(-\kappa_D r)\, r \mathrm{d}r = -q_i \tag{2.28}$$

Upon integration by parts, equation (2.28) leads to the following result for $C_1$:

$$C_1 = \frac{q_i}{4\pi\varepsilon_0\varepsilon_r}\left(\frac{\exp(\kappa_D a)}{\kappa_D a + 1}\right) \tag{2.29}$$

This result can be directly applied to equation (2.26) and one may observe that this is consistent with the Coulomb potential of an infinitely diluted single charged sphere.

The chemical potential of electrostatic origin is then calculated as the work of having the isolated central ion not interacting with its surroundings and then allowing it to interact step by step with its surroundings via a coupling factor $\xi$, the interaction potential and the radial distribution function.[22,32] This is expressed by the following equation:[32]

$$\begin{aligned} \mu_i^{el} = k_B T ln\left(\gamma_i^{el}\right) &= \sum_j \int_0^1 \mathrm{d}\xi \int_a^{\infty} 4\pi r^2\, u_{ij}(r) \rho_j g_{ij}^{DH}(r;\xi) dr \\ &= -\frac{q_i^2}{8\pi\varepsilon_0\varepsilon_r}\left(\frac{\kappa_D}{\kappa_D a + 1}\right) \end{aligned} \tag{2.30}$$

An older (and the simplest) derivation route relates to the energy difference of the Güntelberg charging process (similar to the Born's equation (2.18)) of the central ion between two states defined as infinite dilution and some arbitrary concentration:[31,33]

$$\begin{aligned} \mu_i^{el} = k_B T ln\left(\gamma_i^{el}\right) &= \lim_{r\to a} \int_0^{q_i} (\psi_{i,\kappa_D>0,r>a}^{DH} - \psi_{i,\kappa_D\to 0,r>a}^{DH}) \mathrm{d}q_i \\ &= -\frac{q_i^2}{8\pi\varepsilon_0\varepsilon_r}\left(\frac{\kappa_D}{\kappa_D a + 1}\right) \end{aligned} \tag{2.31}$$

The most traditional derivation is the Debye charging process,[31] which includes a solution to $\nabla^2 \psi_i^{DH}(r) = 0$ in the vicinity of the central ion and leads to the same result for $\mu_i^{el}$. For the sake of brevity, the detailed Debye charging process is omitted here, but can be consulted in the Appendix. Setting any theoretical discussions about the different derivation routes aside, equation (2.30) is the more formal pathway.[22,32]

The excess chemical potential of electrostatic origin $\mu_i^{el}$ and its corresponding Helmholtz free energy are the central results of DH theory. For practical application the permittivity of the hypothetical medium $\varepsilon_0\varepsilon_r$ is replaced by the permittivity of a solvent $\varepsilon_0\varepsilon_s$ and $N_A$ is used to obtain molar concentration basis instead of particle number density.

### 2.2.3 The Pitzer-Debye-Hückel Term

Despite it being a very successful theory for the past 100 years, DH theory comes with several drawbacks. Some are briefly addressed in the present and upcoming subchapters.

The situation shown in Figure 1 requires a solution theory to describe particle (ion-ion) interactions in a medium. The natural variables are $N$, $V$, $T$ and the liquid solvent is an implicit species only described by its relative permittivity. Reformulated as an osmotic setup, it is captured by the McMillan-Mayer framework,[34] where the chemical potential of the implicit solvent is kept constant.[35] This allows to estimate the osmotic pressure of electrostatic origin $\Pi^{el}$ and hard-core effects that are absent in the traditional Debye and Güntelberg charging processes[36] described previously in section 2.2.2.

In statistical mechanics, the osmotic pressure can be very well approximated via the pressure equation when the radial distribution function is exact.[37] Kenneth Pitzer proposed applying the RPM interaction potential from equation (2.16) with the radial distribution function $g_{ij}^{DH}(r)$ from equation (2.21) in order to formally include kinetic hard sphere effects in DH theory.[36] This is expressed by equation (2.32):

$$\Pi^{DH} - \rho k_B T = -\frac{2\pi}{3}\sum_{ij}\rho_i\rho_j\int_0^{\infty}\frac{\partial u_{ij}}{\partial dr}\,g_{ij}^{DH}(r)r^3\mathrm{d}r \qquad (2.32)$$

To solve the integral, Pitzer divided it into two ranges: from 0 to $a$ and from $a$ to infinity, in accordance with the ansatz from equation (2.16).[27] The value at $r = a$ relates to the kinetic pressure effect of the ions in contact: repulsion forces that do not allow the ions to overlap. The integral from $a$ to infinity relates to the purely electrostatic effect of the ion cloud. Upon integration and rearrangement, the osmotic coefficient from DH theory $\varphi^{DH} = \frac{\Pi^{DH}}{\rho_j k_B T}$ is expressed as follows:[36]

$$\varphi^{DH} - 1 = \rho \frac{2\pi a^3}{3} - \frac{\kappa_D^3}{24\pi\rho(1+\kappa_D a)} \tag{2.33}$$

where $\rho$ is the total ion number density. The theoretical result for the hard sphere effect is the first term of the right-hand side of equation (2.33). For practical application, Pitzer replaced the hard-core term with a virial expansion, resulting in the well-known empirical Pitzer equations.[27,36,38] This choice was justified given that, as concentration rises, the contact correlations and hard sphere effects between particles in Figure 1 can be described as an expansion in powers of the concentration at the McMillan-Mayer level, in direct analogy to the virial corrections applied to describe a gas.[39]

The chemical potential of the ions can be obtained from the purely theoretical result from equation (2.33) through a Gibbs-Duhem transformation according to:[4,36]

$$\ln(\gamma_i) = \varphi^{DH} - 1 + 2\int_0^{\rho^{\frac{1}{2}}} \frac{\varphi^{DH} - 1}{\rho^{\frac{1}{2}}} d\rho^{\frac{1}{2}} \tag{2.34}$$

The transformation at infinite dilution isolates the electrostatic term and yields:[36]

$$\mu_i^{el} = k_B T \ln\left(\gamma_i^{el}\right) = -\frac{q_i^2}{24\pi\varepsilon_0\varepsilon_r}\left\{\left(\frac{\kappa_D}{1+\kappa_D a}\right) + \frac{2}{a}\ln(1+\kappa_D a)\right\} \tag{2.35}$$

The result that includes the hard-core term can be found in the literature.[36] Reformulation of equation (2.35) in molar basis, denoted by superscript $(c)$ where $N_A \sum_j c_j = \rho$, leads to:

$$\mu_i^{el,(c)} = RT \ln\left(\gamma_i^{el}\right) = -A_\phi^{(c)}\left(\frac{2z_i^2}{b^{(c)}}\ln\left(1 + b^{(c)}\sqrt{I^{(c)}}\right) + \frac{\sqrt{I^{(c)}}}{1 + b^{(c)}\sqrt{I^{(c)}}}\right) \tag{2.36}$$

which is a known theoretical result from Pitzer with the following definitions:[27,36]

$$A_\phi^{(c)} = \frac{1}{3}(2\pi N_A)^{0.5}(\lambda_B)^{1.5} \tag{2.37}$$

$$b^{(c)} = \frac{\kappa_D^{(C)} a}{\sqrt{I^{(c)}}} = a\sqrt{8\pi\lambda_B N_A} \tag{2.38}$$

$$I^{(c)} = \frac{1}{2}\sum_j z_j^2 c_j \tag{2.39}$$

$A_\phi^{(c)}$ is commonly referred to as the Debye-Hückel parameter, $b^{(C)}$ is called the parameter of closest approach and $I^{(c)}$ is called the ionic strength, being $c_j$ the molar concentration of ions of type $j$, and $\lambda_B = \frac{e^2}{4\pi\varepsilon_0\varepsilon_r k_B T}$ is called the Bjerrum length with $\varepsilon_r = \varepsilon_s$ for a pure solvent of relative permittivity $\varepsilon_s$. The result here is presented in the molarity convention, but in practice it is applied in the molality convention (eqs. (2.41), (2.42) and (2.43)). Equation (2.37) can sometimes be found in the literature with a factor of 1000, which is only a unit conversion factor for the volume. This and other conversion factors can cause confusion (e.g. outdated use of $cm^3$ for volume as the standard) and are deliberately ignored throughout this manuscript under the assumption of pertaining properties with consistent units (note that $\kappa_D = \kappa_D^{(c)}/N_A^{0.5}$).

Several years later, Pitzer sought to describe the activity of water diluted in eutectic molten salt mixtures.[40] For this purpose, the impact of electrostatic origin on the excess chemical potential of water can be estimated from equation (2.33) if the hard-sphere term is neglected. This corresponds to a state of infinite dilution where the electrostatic term is isolated. Equation (2.33) describes this in the molality ($m$) scale as follows:

$$\varphi_{el}^{DH(m),\infty} = -\frac{\kappa_D^3}{24\pi\sum_j c_j^{(m)}(1+\kappa_D a)} = -\frac{A_\phi^{(m)}}{\sum_j m_j}\left(\frac{2I^{(m)^{1.5}}}{1+b\sqrt{I^{(m)}}}\right) \tag{2.40}$$

Thus, assuming that the density of the medium remains constant regardless of the ion concentration, the following re-definitions ensue:[36]

$$A_\phi^{(m)} = \frac{1}{3}(2\pi N_A d_s)^{0.5}(\lambda_B)^{1.5} \tag{2.41}$$

$$b^{(m)} = \frac{\kappa_D^{(m)} a}{\sqrt{I^{(m)}}} = a\sqrt{8\pi\lambda_B N_A d_s} \tag{2.42}$$

$$I^{(m)} = \frac{1}{2}\sum_j z_j^2 m_j \tag{2.43}$$

where $d_s$ is the density of the solvent and $m_j$ stands for the molal concentration of ions. The conversion to molal scale applies to the screening length as well: $\kappa_D^{(m)} = \kappa_D^{(c)} \cdot d_s^{0.5}$.

Through thermodynamic relations for the osmotic pressure and the activity of the solvent, Pitzer[27,36] extracted the corresponding activity coefficient of electrostatic origin for the solvent from expression (2.40) in the molality convention:

$$\frac{\Pi^{el(m),\infty}}{\rho k_B T} = -\left(\frac{\partial G^{DH}}{\partial n_s}\right)_{T,P,n_j} \frac{1}{RT\sum_j m_j} = -\ln\left(\gamma_s^{(m)el}\right)\cdot\left(\sum_j m_j\right)^{-1}$$
$$\ln\left(\gamma_s^{(m)el}\right) = -A_\phi^{(m)}\left(\frac{-2I^{(m)^{1.5}}}{1+b\sqrt{I^{(m)}}}\right) \tag{2.44}$$

Under the assumption that $\Delta A^{el} \equiv \Delta G^{el}$, equation (2.44) is the slope of the excess Gibbs free energy when described as a function of concentration. Thus, integration of equation (2.44) leads to the excess Gibbs free energy of electrostatic origin in the molality basis.

However, the molality $m$ in moles of solute per kilograms of solvent tends to infinity when the solvent is being diluted in molten salt. Thus, the set of equations (2.41), (2.42), (2.43) and (2.44) required reformulation[40] in the mole fraction scale as follows (with $\kappa_D^{(x)} = \kappa_D^{(m)}/M_s^{0.5}$):

$$A_\phi^{(x)} = \frac{1}{3}\left(\frac{2\pi N_A d_s}{M_s}\right)^{0.5}(\lambda_B)^{1.5} \tag{2.45}$$

$$b^{(x)} = \frac{\kappa_D^{(x)} a}{\sqrt{I_x}} = a\sqrt{\frac{8\pi\lambda_B N_A d_s}{M_s}} \tag{2.46}$$

$$I_x = \frac{1}{2}\sum_j z_j^2 x_j \tag{2.47}$$

$$\ln\left(\gamma_s^{(x)el}\right) = -A_\phi^{(x)}\left(\frac{-2I_x^{1.5}}{1+b^{(x)}\sqrt{I_x}}\right) \tag{2.48}$$

where $M_s$ is the molar mass of the solvent. In contrast to the originally published equations,[40] the term $(1/M_s)^{0.5}$ is included as part of $A_\phi^{(x)}$ for simplicity. This choice is based on the grounds of having a consistent convention: if $N_A$ is factored in $A_\phi^{(c)}$ and the

density $d_s$ is factored in $A_\phi^{(m)}$, then the molar mass $M_s$ should be factored in $A_\phi^{(x)}$. All these changes originate from concentration conversions of the ion number density $\rho$.

Integration of equation (2.48) with respect to $n_s$ moles of solvent yields the following relation for the excess Gibbs free energy of electrostatic origin in the mole fraction scale:[40]

$$\frac{G^{DH(x)}}{RT} = -\frac{4A_\phi^{(x)} n_T I_x}{b^{(x)}} \ln\left(1 + b^{(x)}\sqrt{I_x}\right) \tag{2.49}$$

The aforementioned procedure makes use of the following definition:

$$\frac{\partial I_x}{\partial n_i} = \frac{z_i^2}{2n_T} - \frac{I_x}{n_T} \tag{2.50}$$

and thereby the generalized expression for $\gamma_i^{PDH}$ is given by the full derivative:[40]

$$\ln\left(\gamma_i^{PDH(x)}\right) = \left(\frac{\partial G^{DH(x)}}{RT\partial n_i}\right)_{T,P,n_j} = -A_\phi^{(x)}\left[\frac{2z_i^2}{b^{(x)}}\ln\left(1 + b^{(x)}\sqrt{I_x}\right) + \frac{z_i^2\sqrt{I_x} - 2I_x^{1.5}}{1 + b^{(x)}\sqrt{I_x}}\right] \tag{2.51}$$

where a neutral solvent $i = s$ with $z_s = 0$ reduces the expression to equation (2.48). The subscript PDH stands for Pitzer-Debye-Hückel and equation (2.51) is commonly referred to as the PDH term. It constitutes a purely electrostatic contribution and should not be confused with the so-called Pitzer equations which constitute equation (2.36) in the molality convention followed by a virial expansion with empirical parameters.

A full expression for $\gamma_i^{PDH}$ evaluated for molten salts presents the opportunity to evaluate the symmetrical and unsymmetrical reference states. This was also performed by Pitzer.[40] The change in reference state requires subtracting the value at the fused salt state in equation (2.49), which yields:

$$\frac{G_{symm}^{DH}}{RT} = -\frac{4A_\phi^{(x)} n_T I_x}{b^{(x)}} \ln\left(\frac{1 + b^{(x)}\sqrt{I_x}}{1 + b^{(x)}\sqrt{I_x^{IL}}}\right) \tag{2.52}$$

where the subscript *symm* stands for symmetrical reference state and the subscript *IL* stands for evaluation at the pure fused salt state and will be used interchangeably for ionic liquids (ILs). The ionic strength at the fused salt state is easily calculated as the constant $I_x^{IL} = \frac{1}{2}\sum_j \frac{z_j^2 v_j}{v}$, where $v_j$ is the stoichiometric coefficient of the ion and $v$ is the sum of all

stoichiometric coefficients. Assuming that $I_x^{IL}$ is indeed a constant and $\frac{\partial I_x^{IL}}{\partial n_i} = 0$, the derivative of the residual Gibbs-free energy of electrostatic origin with respect to the moles of any species $n_i$ (i.e. $\frac{1}{RT}\frac{\partial(G_{symm}^{DH})}{\partial n_i}$) leads to the result from Pitzer:[40]

$$\ln\left(\gamma_{i,\ symm}^{PDH}\right) = -A_\phi^{(x)}\left[\frac{2z_i^2}{b^{(x)}}\ln\left(\frac{1+b^{(x)}\sqrt{I_x}}{1+b^{(x)}\sqrt{I_x^{IL}}}\right) + \frac{z_i^2\sqrt{I_x} - 2I_x^{1.5}}{1+b^{(x)}\sqrt{I_x}}\right] \tag{2.53}$$

The correctness of equations (2.52) and (2.53) are discussed further ahead in section 6.2.1. Finally, Pitzer recommended[40] an empirical value of $b^{(m)} = 2$ equivalent to $b^{(x)} = 14.9$ for water in these eutectic molten salt mixtures to replace the physical value from equation (2.46). The use of $b_{constant}^{(x)} = 14.9$ as a fixed value is discussed in section 6.1.3.

### 2.2.4 Dressed Ion Theory

Approaches like that of Pitzer introduce a volume to the point charges in the cloud but additional phenomenology remains unaccounted for. Other systematic deviations of the PB equation were attributed to its inability to describe hydration effects or surface adsorption but not to its formulation.[41] The PB equation as formulated in section 2.2.2 actually neglects correlated ion-ion interactions as well as the closest approach of the ions in the ion cloud:[41,42] these are treated as uncorrelated point charges. To clarify this, one can break the Debye-Hückel potential $\psi_i^{DH}(r)$ into three components:

$$\psi_i^{DH}(r) = \frac{q_i}{4\pi\varepsilon_0\varepsilon_r r}\left(\frac{\exp\left(-\kappa_D(r-a)\right)}{\kappa_D a+1}\right) = \overbrace{\frac{1}{4\pi\varepsilon_0\varepsilon_r}}^{\substack{unit\ Coulomb\\ potential}}\ \overbrace{\frac{\exp(-\kappa_D r)}{r}}^{\substack{Yukawa\\ form}} \cdot \overbrace{q_i\frac{\exp(\kappa_D a)}{\kappa_D a+1}}^{\substack{effective\\ charge}} \tag{2.54}$$

and perform a thought experiment.[22] If a point charge finds itself far away from the central ion $i$, it should not "see" the electric field arising from the net sum of the charges of the central ion and its ion cloud, but the electric field that results from the ion-ion correlations near the central ion $i$. In other words, the faraway charge sees an *effective* charge $q_i^*$ of the central ion $i$ and its immediate ion cloud. The effective charge in DH theory is:

$$q_i^{*DH} = q_i\frac{\exp(\kappa_D a)}{\kappa_D a+1} \tag{2.55}$$

If the faraway charge is also treated as another central ion $k$ with its own ion cloud, the pair interaction potential between these two central ions with their corresponding ion clouds would be proportional to the following:

$$u_{ik}(r) \propto \frac{q_i^* q_k^* \exp\left(-\kappa_D |r_i - r_k|\right)}{4\pi\varepsilon_0\varepsilon_r |r_i - r_k|} \tag{2.56}$$

Ion $k$ and its immediate cloud should correlate with ion $i$ and its immediate cloud: all ions should correlate with each other. This is not accounted for in the calculation of the Debye screening parameter $\kappa_D$ from equation (2.23), which deals with bare uncorrelated point charges, and thus also not accounted for in the Debye-Hückel potential $\psi_i^{DH}(r)$. For this reason, the DH theory is said to have an asymmetric (or unequal) treatment of the ions.[22]

Consequently, one can intuitively hypothesize that the theoretical $\kappa_D$ has to be renormalized to account for the effective charges ($q_j^*$) of the ions in the ion cloud:

$$\kappa^2 = \beta \sum_j q_j q_j^* \rho_j \, \varepsilon_0^{-1} \varepsilon_r^{-1} \tag{2.57}$$

Equation (2.57) expresses that the ions of type $j$ in the ion cloud should also have effective charges, in contrast to the uncorrelated point charges expressed by $\kappa_D$. The exact formalism based on this concept, assuming that the ions of the ion cloud around a central ion are symmetrically distributed[41] and treated on the same basis,[42] is the Dressed Ion Theory (hereafter DIT) from Kjellander and Mitchell.[42]

### *The Dressed Ion Theory and its Limiting Law*

The present subchapter briefly summarizes the essential concepts of the DIT. The interested reader may refer to the original publication,[42] its background[41] and its subsequent developments[32,43–49] for further details.

Several definitions are required to proceed. Firstly, the total correlation function $h_{ij}(r)$ is introduced, which is defined in terms of the radial distribution function as follows:

$$h_{ij}(r) = g_{ij}(r) - 1 \tag{2.58}$$

and is applied to calculate the direct pair correlation function $c_{ij}(r)$ from the Ornstein-Zernike (OZ) equation:[39]

$$h_{ij}(r) = c_{ij}(r) + \sum_k \int c_{ik}(|r - r'|)\rho_k h_{kj}(r')dr' \tag{2.59}$$

A direct correlation function aids in the calculation of activity in terms of density as an independent variable by accounting for single- and multiple body interactions. For instance, it can be demonstrated that the single body (one particle) direct correlation function for an homogeneous fluid relates to the virial expansion.[39] The OZ equation expresses the correlation between two particles when under the influence of a third or more particles and this can be formulated in terms of all pair correlations. The distribution of particles of nature $j$ around the central particle $i$ is not independent from the $i - k$ and $k - j$ correlations that arise in the presence of additional $k$ particles in their vicinity. The notation $r'$ relates to the origin taken for each particle (e.g. $|r - r'| = r$ for a point charge in Coulomb's law: with the origin $r' = 0$).

Kjellander and Mitchel[41] split the direct pair correlations into two contributions: at the vicinity of the central ion (denoted by superscript 0) and at a further distance from the central ion (denoted by superscript #). The former is a region that encloses the effective charge of the central ion; the latter a region of the remaining ion cloud. Consistency requires that both regions fulfill the OZ equation when treated separately. Thus, $c_{ij}(r) = c_{ij}^0(r) + c_{ij}^\#(r)$, $h_{ij}(r) = h_{ij}^0(r) + h_{ij}^\#(r)$ and consequently the charge density around the central ion $i$ in the PB equation is also split into two contributions $\rho_{E,i}^0$ and $\rho_{E,i}^\#$ and the PB equation is reformulated in a generalized, exact fashion as follows:

$$-\varepsilon_0\varepsilon_r\nabla^2\psi_i^{av}(r) = \rho_{E,i}^0(r) + \rho_{E,i}^\#(r) = \rho_{E,i}^0(r) - \int \alpha(|r - r'|)\psi_i^{av}(r')dr' \tag{2.60}$$

where $\rho_{E,i}^0$ describes the internal charge density distribution of particle $i$ and its immediate vicinity, thereby accounting for its effective charge. The term $\rho_{E,i}^\#$ is the external charge density distribution outside of the immediate vicinity of the central ion (the Debye-Hückel-like term) and related to the entirety of the ion cloud.[41,42] The integral in equation (2.60) that replaces $\rho_{E,i}^\#$ is called the polarization response and the value $\alpha(r)$ is called the polarization response function,[41] which is in turn defined by:

$$\alpha(r) = \beta \sum_j \int \rho_j \rho_{E,j}^0(r')dr' = \beta \sum_j \rho_j\, q_j \delta^{(3)}(r) + \beta \sum_{ij} q_i q_j \rho_i \rho_j h_{ij}^0(r) \tag{2.61}$$

where $\delta^{(3)}(r)$ is the Dirac delta function. The Appendix can be consulted for further details on the origin of $\alpha(r)$ (see equation (8.14)).

This formalism contains DH theory within its framework as a simplified case.[41,42] This is made visible as follows: equation (2.60) expresses the LPB reformulation in terms of a total charge density given by the central ion with its effective charge plus a polarization response of a medium with distant charges that also correlate with each other via a linear response function.[42] If one where to neglect the renormalization, then $h_{ij}^{0}(r) = 0$ (the dress ions are not correlated with each other), $\kappa = \kappa_D$, $\rho_{E,i}^{0} = q_j\delta^{(3)}(r) = 0 \;\forall\; r > 0$, $\rho_{E,i}^{\#} = -\beta \sum_j \rho_j\, q_j^2 \psi_i^{av}(r)$ and equation (2.60) would reduce to the "inexact" LPB developed in section 2.2.2 and yield DH theory.

Following this framework for DH theory a bit further, it then follows from equation (2.58) that the total correlation function in DH theory ($h_{ij}^{DH}(r)$) is expressed in terms of the McLaurin expansion of the exponential in $g_{ij}^{DH}(r)$ applied by Debye and Hückel in equation (2.21) as follows:

$$g_{ij}^{DH}(r) = 1 + h_{ij}^{DH}(r) = 1 - \beta q_j \psi_i^{DH}(r) + \frac{1}{2!}\left(\beta q_j \psi_i^{DH}(r)\right)^2 + \cdots \qquad (2.62)$$

where the total correlation function in DH theory (only the linear term included) is therefore $h_{ij}^{DH}(r) = -\beta q_j \psi_i^{DH}(r)$ outside of the volume excluded for the central ion $i$. In combination with equations (2.54) and (2.55) one obtains:

$$h_{ij}^{DH}(r) = \frac{-\beta q_i q_j}{4\pi\varepsilon_0\varepsilon_r r}\left(\frac{\exp\big(-\kappa_D(r-a)\big)}{\kappa_D a + 1}\right) = \frac{-\beta \exp(-\kappa_D r)}{4\pi\varepsilon_0\varepsilon_r r} q_j q_i^{*DH} \quad \forall \quad r > a \qquad (2.63)$$

Once again, the aforementioned asymmetric or unequal treatment of the ions $i$ and $j$ in DH theory is evident in equation (2.63), where $h_{ij}^{DH}(r) \propto q_j q_i^{*DH}$, but $h_{kj}^{DH}(r) \propto q_j q_k$. As demonstrated by Kjellander and Mitchel,[41,42] the total correlation function with renormalized, effective charges in the linear regime is expressed as follows:

$$h_{ij}^{\#}(r) = -\frac{\beta \exp(-\kappa r)}{4\pi E r} q_j^* q_i^* \quad \forall \quad r > a \qquad (2.64)$$

where $\kappa$ is being used instead of $\kappa_D$. Thus, for the linearized regime at infinite dilution (where DH is strictly valid and $\kappa \to \kappa_D$ and $E \to \varepsilon_0\varepsilon_r$), the deviation of $h_{ij}^{DH\infty}(r)$ from its exact formulation $h_{ij}^{\#\infty}(r)$ is well approximated with the help of equation (2.55) as follows:

$$\frac{h_{ij}^{\#\infty}(r)}{h_{ij}^{DH\infty}(r)} = \frac{q_i^*}{q_i} = \frac{\exp(\kappa a)}{(1+\kappa a)} \quad \forall \quad r > a \tag{2.65}$$

from which the following relationship can be obtained:

$$\left(\frac{\kappa}{\kappa_D}\right)^2 = \frac{q_i^*}{q_i} = \frac{\exp(\kappa a)}{(1+\kappa a)} \tag{2.66}$$

In equation (2.64) the meaning of the effective charges (denoted by the superscript $*$) has been explained. However, the variable $E$ called the dielectric factor (with the property $E \to \varepsilon_0\varepsilon_r$ at infinite dilution) is introduced. Thus, DH theory in the DIT framework can now be set aside and a few words on the exact PB, the dielectric factor, the renormalized $\kappa$ and the origin of $h_{ij}^{\#}(r)$ are needed.

The long-ranged $h_{ij}^{\#}(r)$ in equation (2.64) comes from splitting the direct correlation function ($c_{ij}(r) = c_{ij}^0(r) + c_{ij}^{\#}(r)$) with the requirement that each separate part fulfills the OZ equation, from which the formal definition of $h_{ij}^{\#}(r)$ can be expressed by:[41]

$$h_{ij}^{\#}(r) = -\beta \int \rho_{E,j}^0(|r-r'|)\psi_i^{av}(r')\,dr' \tag{2.67}$$

The Fourier transforms of equations (2.60) and (2.67) at infinite dilution yield equation (2.64), among other results, and analysis of their residues leads to the following definitions for any ion:[41,42]

$$\begin{aligned} q_i^* &= \frac{4\pi}{\kappa}\int_0^\infty \rho_{E,j}^0(r) r \sinh(\kappa r)\,dr = q_i + \sum_j q_j\rho_j \hat{h}_{ij}^0(\mathrm{i}\kappa) \\ &= q_i + \frac{4\pi}{\kappa}\sum_j q_j\rho_j \int_0^\infty h_{ij}^0(r) r \sinh(\kappa r)\,dr \end{aligned} \tag{2.68}$$

$$E = \varepsilon_0\varepsilon_r + \frac{2\pi}{\kappa^3}\int_0^\infty \alpha(r) r(\sinh(\kappa r) - \kappa r \cdot \cosh(\kappa r))dr \tag{2.69}$$

where the hat symbol (^) denotes Fourier space. The choice of solving in Fourier space is based on the fact that this facilitates performing operations with the OZ equation.[39] Furthermore, the pair correlations are expected to oscillate past a certain concentration. The concentration at which the radial distribution function of electrostatic origin becomes complex valued and oscillates is known as the Kirkwood crossover.[50] The electrostatic potential is expected to have an exponential decay below this point (as described by DH theory) and an oscillatory exponential decay above this point.[48] From equations (2.68) and (2.69) derived at low concentrations, one can observe at the limit of infinite dilution that $q_j^* \to q_j$ (therefore, $\kappa \to \kappa_D$), $E \to \varepsilon_0 \varepsilon_r$ and one obtains DH theory.

The physical meaning of $E$ relates to effective screening.[48] One may picture this as the consideration that a single point charge (or a charged sphere) at infinite dilution is ideally screened by the dielectric medium in accordance to Coulomb's law. It is de facto an ideal dielectric screening state. However, as concentration rises, the screening of this charge (the polarization of the medium) is gradually affected by other charges in the near vicinity, which are also being screened. Therefore, as concentration rises the dielectric factor accounts for the deviations that arise from the dielectric response of the electrolyte with respect to ideal screening at infinite dilution.

With these definitions, and circling back to $h_{ij}^{\#}(r)$, the only possible manner in which the # component of the exponential expansion of $g_{ij}(r)$ can be consistent with $h_{ij}^{\#}(r)$ is evidently defining its Debye-Hückel-like component $g_{ij}^{\#}(r)$ as follows:

$$g_{ij}^{\#}(r) = 1 + h_{ij}^{\#}(r) = 1 - \beta q_j^* \psi_i^{av}(r) + \frac{1}{2!}\left(\beta q_j^* \psi_i^{av}(r)\right)^2 - \cdots \qquad (2.70)$$

which forcefully leads to the definition of $\kappa$ shown in equation (2.57) in the linear regime, in exactly the same fashion as the use of equation (2.62) lead to the original Debye screening parameter $\kappa_D$ in section 2.2.2. Consequently, the truncated (two term) $g_{ij}^{\#}(r)$ in the PB equation is a fundamentally exact LPB formulation, whereas the truncated $g_{ij}^{DH}(r)$ in section 2.2.2 that leads to DH theory is an inexact LPB formulation.[41]

In the linearized regime, the approximation $h_{ij}^{\#}(r) \approx -\beta q_j^* \psi_i^{av}(r)$ is therefore present (analogous to $h_{ij}^{DH}(r) \approx -\beta q_j \psi_i^{DH}(r)$ in DH theory) and it is proposed[41] that $\psi_i^{av}(r)$

should have a similar form to that of $\psi_i^{DH}(r)$ in equation (2.54): the product of a Yukawa potential and an effective charge of the central ion $i$:

$$\psi_i^{av}(r) = \frac{\exp(\kappa r)}{4\pi E r} q_i^* \tag{2.71}$$

Thus, the new challenge is calculating the effective charges $q_i^*$, $q_j^*$ and the dielectric factor $E$ in order to evaluate $h_{ij}^{\#}(r) = h_{ji}^{\#}(r) = -\frac{\beta \exp(-\kappa_D r)}{4\pi E r} q_j^* q_i^*$. Equation (2.55) is **not** a good candidate, since it is formulated in terms of $\kappa_D$ and not in terms of $\kappa$.

It then follows that one of the central questions in the DIT deals with finding approximations to evaluate the effective charges $q_i^*$, $q_j^*$ and the components of $\kappa$ and of the dielectric factor $E$, which become complex valued above the Kirkwood crossover.[42]

Unfortunately, the fact that $\kappa$ and $E$ have multiple values (multiple components), makes it difficult to estimate thermodynamic properties at higher concentrations, given that these multiple components are unknown. Hence, additional structural information of the Coulomb fluid under consideration is required. In spite of the multiple components of $\kappa$ and $E$ being unknown, the full framework for their application is found in the literature.[48]

This is the reason why a central result of the DIT is derived at infinite dilution and only applicable to very diluted systems. At infinite dilution and very low concentrations one may safely assume that $\kappa$ has a leading component near the value of $\kappa_D$ and that $E$ also has a leading component near the value of $\varepsilon_0 \varepsilon_r$. Furthermore, the leading component of $\kappa$ dominates and the use of $E = \varepsilon_0 \varepsilon_r$ is a valid assumption. Thus, by considering the dilute region, $q_j^*$ is well approximated by the leading contribution to $h_{ij}^0$, which in turn depends on the contributions of $h_{ji}^{\#}(r)$. With these considerations and assuming that all ions are of equal size, the leading contribution to the direct correlation function of the dress is in turn given by the expansion of the correlated electrostatic contributions as follows:[42]

$$\hat{h}_{ij}^0(\mathrm{i}\kappa) \approx \sum_{n=2}^{\infty} \frac{1}{n!} \left( h_{ij}^{\#}(r) \right)^x \tag{2.72}$$

With the aforementioned assumptions, the use of equations (2.64) and (2.72) inserted in (2.68) lead to the following relationship:

$$q_i^* = q_i + z_i q_i \frac{\Lambda \ln(3)}{4} \frac{\sum_j z_j^3 v_j}{\sum_j z_j^2 v_j} + q_j z_j^2 \frac{\Lambda^2 \ln(\Lambda)}{6} \frac{\sum_j z_j^4 v_j}{\sum_j z_j^2 v_j} + \mathcal{O}(\Lambda^2) \qquad (2.73)$$

where the definitions previously introduced are kept ($z_i$ is the valence of ion $i$, $v_i$ is the stoichiometric coefficient of ion $i$), $\Lambda$ is called a coupling factor given by $\Lambda = \kappa_D \lambda_B$ and $\mathcal{O}(\Lambda^2)$ would denote the next term of second order. Subsequent insertion of equation (2.73) in (2.57) normalized by $\kappa_D^2$ leads to the DIT generalized limiting law:

$$\left(\frac{\kappa}{\kappa_D}\right)^2 = 1 + \frac{\Lambda \ln(3)}{4} \left(\frac{\sum_j z_j^3 v_j}{\sum_j z_j^2 v_j}\right)^2 + \frac{\Lambda^2 \ln(\Lambda)}{6} \left(\frac{\sum_j z_j^4 v_j}{\sum_j z_j^2 v_j}\right)^2 + \mathcal{O}(\Lambda^2) \qquad (2.74)$$

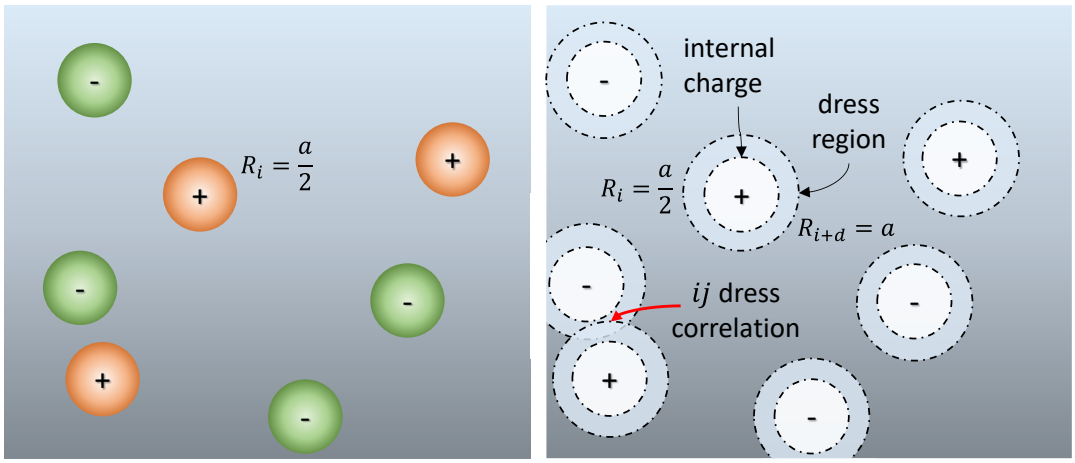


**Figure 3. The RPM (left) compared to the situation described by the DIT (right), where the central and cloud ions are treated as correlated point charges with their own excluded volume that encloses an internal charge of the central ion plus its immediate vicinity. A much more rigorous situation when compared to the DH case in Figure 2.**

In summary, the reformulation of a formally exact LPB presents the necessity for a normalized screening parameter $\kappa$. This formalism leads to an approximate expression to estimate $\kappa$ numerically in equation (2.66) valid only for the simplest charge symmetrical case (1: 1) in agreement with the valid assumptions for DH theory in section 2.2.2. The exact limiting law beyond the linear regime is given by equation (2.74) and it estimates the leading component of $\kappa$ at infinite dilution, valid for both charge symmetric and charge asymmetric ions, and for the case of high coupling ($|z_i|, |z_j| \gg 1$ and/or very low relative permittivity values). Equation (2.74) is a formally exact, central result of the DIT.

### *The Multiple-Decay Extension of the Debye-Hückel Theory*

A modification of the DH theory based on the linear regime of the DIT and the use of the approximate equation (2.66) (valid for weakly coupled 1:1 electrolytes), is the Multiple-Decay Extension of the Debye-Hückel Theory (hereafter MDE-DH) by Kjellander.[49] MDE-DH demonstrates the principles of the DIT beyond the diluted regime. It is in essence a re-derivation of DH theory including the oscillatory exponential decay of the pair correlations and therefore a prediction of the Kirkwood crossover.

Firstly, $\kappa$ hast multiple components. In the linearized approximation from equation (2.66) two roots for $\kappa$ are found and, as concentration rises, these roots merge and $\kappa$ becomes complex valued above the Kirkwood crossover.[49] This is exemplified in Figure 4.

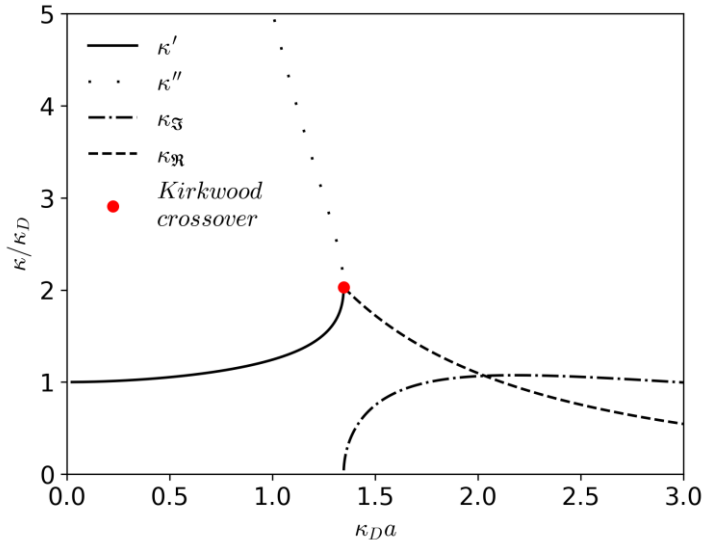


**Figure 4. The two components of $\kappa$ calculated as the roots of equation (2.66) where $\kappa'$ and $\kappa''$ merge at the Kirkwood crossover. Above the Kirkwood crossover $\kappa$ becomes complex valued and charge density oscillations are expected. Calculations for $a = 4.25$ Å, $\varepsilon_r = 78.65$ and $T = 298.15$ K. The Kirkwood crossover is found at $c \approx 0.931 \frac{mol}{L}$.**

Therefore, in accordance with the superposition principle and taking the corresponding conjugate complex pole pairs of equation (2.71), a more exact LPB is given by:

$$\nabla^2 \psi_i^{av}(r) = 0 \quad \forall \quad r < a$$

$$\nabla^2 \psi_i^{av}(r) = \frac{-\sum_j q_j \rho_j \left[1 - \beta q_j^* \psi_i^{av}(r)\right]}{\varepsilon_0 \varepsilon_r} \tag{2.75}$$

$$= \frac{\beta}{\varepsilon_0 \varepsilon_r}\left(\frac{(\kappa')^2 q_i^{*\prime}}{4\pi \mathcal{E}'} \frac{\exp(-\kappa' r)}{r} + \frac{(\kappa'')^2 q_i^{*\prime\prime}}{4\pi \mathcal{E}''} \frac{\exp(-\kappa'' r)}{r}\right) \quad \forall \quad r \geq a$$

where the dielectric factor is given by $E = \varepsilon_0 \varepsilon_r \mathcal{E}$ in order to separate the dimensionless effectiveness component from the permittivity. The term $\mathcal{E}$ is called the effective dielectric permittivity of the electrolyte.[49] The prime and double prime superscripts denote the two solutions of the complex conjugate pole pair.

In exactly the same fashion as DH theory in section 2.2.2, there is a proposed solution where the constants proportional to $\exp(\kappa r)$ must be zero. The remaining part shown in equation (2.76) is very similar to its homologue from DH theory (equation (2.26)):

$$\psi_i^{av}(r) = \frac{C_1}{r}\exp(-\kappa' r) + \frac{C_2}{r}\exp(-\kappa'' r) \tag{2.76}$$

In the DIT, equation (2.71) applies for this case[49] to rewrite equation (2.76) as follows:

$$\psi_i^{av}(r) = \frac{q_i^{*\prime}}{4\pi\varepsilon_0\varepsilon_r\mathcal{E}' r}\exp(-\kappa' r) + \frac{q_i^{*\prime\prime}}{4\pi\varepsilon_0\varepsilon_r\mathcal{E}'' r}\exp(-\kappa'' r) \tag{2.77}$$

As previously stated, one can again observe the challenge of applying principles of the DIT beyond the dilute regime: there are already 4 unknowns ($q_i^{*\prime}, q_i^{*\prime\prime}, \mathcal{E}', \mathcal{E}''$) in the simplest case (1:1 electrolyte, no strong ion coupling). As part of the approximation, equation (2.66) can be used to estimate the components of $\kappa$ and the components of $q_i^*$. Yet, 2 unknowns ($\mathcal{E}', \mathcal{E}''$) still remain and therefore, two additional equations are required.

Firstly, the electro-neutrality principle is applied in the same fashion as in equation (2.28):

$$4\pi\varepsilon_0\varepsilon_r \int_a^\infty \left( \frac{(\kappa')^2 q_i^{*\prime}\exp(-\kappa' r)}{4\pi\varepsilon_0\varepsilon_r\mathcal{E}' r} + \frac{(\kappa'')^2 q_i^{*\prime\prime}\exp(-\kappa'' r)}{4\pi\varepsilon_0\varepsilon_r\mathcal{E}'' r} \right) r\mathrm{d}r = q_i \tag{2.78}$$

After integration by parts the terms evaluated at $r \to \infty$ vanish and the terms with $r = a$ remain. Thus, by introducing the approximation from equation (2.65), the result of the integral from equation (2.78) reduces to a simple expression:

$$\left(\frac{1}{\mathcal{E}'} + \frac{1}{\mathcal{E}''}\right) = 1 \tag{2.79}$$

A second equation is still required to solve for the two components of $\mathcal{E}$. For this purpose, the second moment of the OZ equation can be applied.[49] The second moment of the OZ expresses a constraint on the pair correlations, similar to the electro-neutrality

condition.[39] Its application in the McMillan-Mayer framework is known as the Stillinger-Lovett condition,[51,52] expressed in equation (2.80) for the electrostatic component (#):

$$1 = -\frac{1}{6\varepsilon_0\varepsilon_r}\beta\sum_{ij} q_i q_j \rho_i \rho_j \int_a^\infty h_{ij}^{\#}(r) r^4 dr \tag{2.80}$$

As demonstrated by Attard,[39] application of equation (2.80) in DH theory is only self-consistent when the screening length is allowed to take a value different than $\kappa_D$. The proposed DH approximation to equation (2.80), according to Attard, should have the form:

$$1 = \frac{\kappa_D^2}{\kappa^2}\cdot\frac{\left(1+\kappa a+\frac{\kappa^2 a^2}{2}+\frac{\kappa^3 a^3}{6}\right)}{1+\kappa a} \tag{2.81}$$

Provided that one applies a modified DH theory, which is the case for MDE-DH, one can rewrite the Stillinger-Lovett condition in terms of the components of $\kappa$ as follows:

$$\begin{aligned} 1 = \frac{\kappa_D^2}{(\kappa')^2}\frac{\left(1+\kappa' a+\frac{(\kappa')^2 a^2}{2}+\frac{(\kappa')^3 a^3}{6}\right)}{\mathcal{E}'(1+\kappa' a)} \\ +\frac{\kappa_D^2}{(\kappa'')^2}\frac{\left(1+\kappa'' a+\frac{(\kappa'')^2 a^2}{2}+\frac{(\kappa'')^3 a^3}{6}\right)}{\mathcal{E}''(1+\kappa'' a)} \end{aligned} \tag{2.82}$$

where the known roots of $\left(\frac{\kappa}{\kappa_D}\right)^2$ from equation (2.66) can be readily applied (e.g. $\left(\frac{\kappa'}{\kappa_D}\right)^2 = \frac{\exp(\kappa' a)}{1+\kappa' a}$) in combination with equation (2.79) to obtain the values of $\mathcal{E}'$ and $\mathcal{E}''$.[49]

Having obtained values for $\mathcal{E}'$ and $\mathcal{E}''$, the electrostatic excess chemical potential, analogous to DH theory in section 2.2.2, is given by:

$$\begin{aligned} \mu_i^{el} = k_B T \ln(\gamma_i^{el}) = \sum_j \int_0^1 \mathrm{d}\xi \int_a^\infty 4\pi r^2 u_{ij}(r)\rho_j g_{ij}^{\#}(r;\xi) dr \\ = -\frac{q_i^2}{8\pi\varepsilon_0\varepsilon_r}\left(\frac{\kappa'}{\mathcal{E}'(1+\kappa' a)}+\frac{\kappa''}{\mathcal{E}''(1+\kappa'' a)}\right) \end{aligned} \tag{2.83}$$

At the Kirkwood crossover the pair correlations become complex valued and $\kappa$ is given by the complex pair conjugates $\kappa' = \kappa_{\Re} + \mathrm{i}\kappa_{\Im}$ and $\kappa'' = \kappa_{\Re} - \mathrm{i}\kappa_{\Im}$. The values of $\kappa_{\Re}$ and $\kappa_{\Im}$ are known from the roots of $\kappa$ as exemplified in Figure 4. The effective dielectric screening factor is reformulated[48] in terms of $\kappa_{\Re}$ and $\kappa_{\Im}$ as follows:

$$\mathcal{E}' = \mathcal{E}(\kappa_{\Re} + \mathrm{i}\kappa_{\Im}) = |\mathcal{E}|\exp(-\mathrm{i}\vartheta)$$
$$\mathcal{E}'' = \mathcal{E}(\kappa_{\Re} - \mathrm{i}\kappa_{\Im}) = |\mathcal{E}|\exp(\mathrm{i}\vartheta) \tag{2.84}$$

where $\vartheta$ is a phase shift from the summation of the exponentials in the Yukawa potentials as demonstrated by Kjellander.[48,49] Thus, introducing the complex conjugates of $\kappa$ in the electro-neutrality condition from equation (2.78) along with the definitions $\mathcal{E}' = |\mathcal{E}|\exp(-\mathrm{i}\vartheta)$, $\mathcal{E}'' = |\mathcal{E}|\exp(\mathrm{i}\vartheta)$ and by use of Euler's formula and some algebra one obtains an electro-neutrality condition above the Kirkwood crossover given by:

$$\frac{1}{|\mathcal{E}|}\cdot\left(\cos\vartheta + \mathrm{i}\cdot\sin\vartheta + \frac{\cos\vartheta - \mathrm{i}\cdot\sin\vartheta}{\cos^2\vartheta + \sin^2\vartheta}\right) = 1 \tag{2.85}$$

which evidently leads to $|\mathcal{E}| = 2\cos(\vartheta)$. The value of $\vartheta$ can be obtained from the Stillinger-Lovett condition by introducing the components of $\kappa$ and $\mathcal{E}$ as defined above the Kirkwood crossover.[49] With these components and equation (2.82) one can readily calculate the phase shift $\vartheta$ (included in the Appendix).[49]

Having values for $\kappa_{\Re}$, $\kappa_{\Im}$ and $\vartheta$, one now only needs to reformulate equation (2.83) by means of the introduction of the definitions $\kappa' = \kappa_{\Re} + \mathrm{i}\kappa_{\Im}$, $\kappa'' = \kappa_{\Re} - \mathrm{i}\kappa_{\Im}$, $|\mathcal{E}| = 2\cos(\vartheta)$ $\mathcal{E}' = |\mathcal{E}|\exp(-\mathrm{i}\vartheta)$ and $\mathcal{E}'' = |\mathcal{E}|\exp(\mathrm{i}\vartheta)$. With the help of Euler's formula and some rearrangements (included in the Appendix), this leads to:[49]

$$\begin{aligned}\mu_i^{el} = k_B T\ln(\gamma_i^{el}) &= \sum_j \int_0^1 \mathrm{d}\xi \int_a^\infty 4\pi r^2\, u_{ij}(r)\rho_j g_{ij}^{\#}(r;\xi)dr \\ &= -\frac{q_i^2}{8\pi\varepsilon_0\varepsilon_r}\left(\frac{\kappa_{\Re} + \kappa_{\Re}^2 a + a\kappa_{\Im}^2 - \kappa_{\Im}\tan\vartheta}{(1+\kappa_{\Re}a)^2 + a^2\kappa_{\Im}^2}\right)\end{aligned} \tag{2.86}$$

Figure 5 compares the three-term expansion of the radial distribution function as described by DH theory and MDE-DH at a concentration where charge inversion in the ion cloud occurs for a system with $\varepsilon_r = 78.65$ at room temperature and $a = 4.25$ Å (same as Figure 4). One may observe that at higher concentration regimes, the oscillatory exponential decay of the electrostatic correlations is predicted by MDE-DH.

Figure 5 compares the three-term expansion of the radial distribution function as described by DH theory and MDE-DH at a concentration where charge inversion in the ion cloud occurs for a system with $\varepsilon_r = 78.65$ at room temperature and $a = 4.25$ Å (same as

Figure 4). One may observe that at higher concentration regimes, the oscillatory exponential decay of the electrostatic correlations is predicted by MDE-DH.

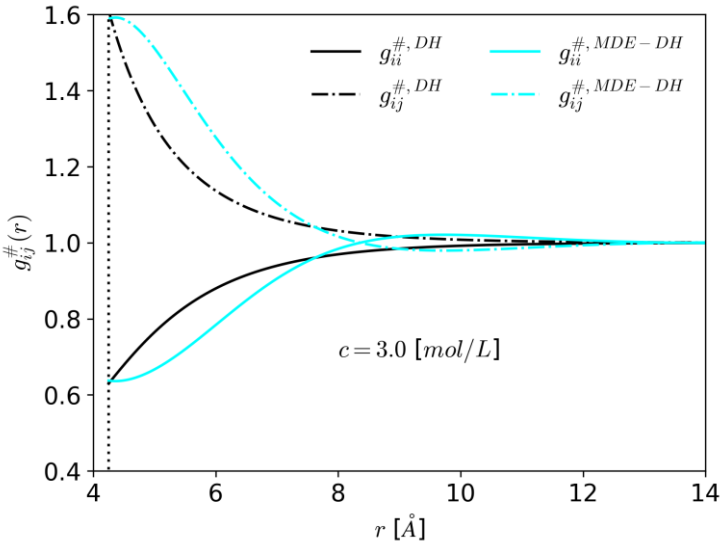


**Figure 5. Squared (three term) electrostatic component of $g_{ij}^{\#}(r)$ from DH theory and MDE-DH theory for a 1:1 electrolyte at a concentration of 3 molar. Calculated for $a = 4.25$ Å, $\varepsilon_r = 78.65$ and $T = 298.15$ K. Charge density oscillations of purely electrostatic origin, independent from the hard-core related oscillations, are predicted here by MDE-DH.**

It is noteworthy to mention that the three term expansion of $g_{ij}^{\#}$ has been used in Figure 5 for a more realistic representation that meets the requirement $g_{ii}(r) \geq 0$. Conventional equations (DH theory, the PDH term and MDE-DH) use the two-term expansion only.

### 2.2.5 Integral equations and the Mean Spherical Approximation

The OZ equation, introduced in section 2.2.4 (equation (2.59)), is an integral equation. Integral equations express the influence of multiple body correlations upon each other, as previously discussed. Diagrammatic techniques are commonly applied to describe their additive contributions and good summaries of these can be found in the literature.[22,25,39,53] These techniques represent cluster series that contribute to the total correlation function $h_{ij}(r)$. The DIT makes use of this concept within the framework of the DH theory.

An alternative approach proposed by Lesser Blum also seeks to approximate the situation in Figure 1 by assuming that the charged spheres are soft or hard. The hard sphere case corresponds to the Percus-Yevick approximation.[54] Blum applied the hard sphere concept for electrolyte systems.[55,56] The pertaining total correlation function is the lowest order

approximation of the cluster expansions for $h_{ij}(r)$ and the resulting equations are known as the Mean Spherical Approximation (hereafter, MSA).[53,55,56]

The restricted primitive MSA (RP-MSA) is only used in section 6.1.1 as a qualitative comparator for the logarithmic activity coefficients of electrostatic origin. It is neither altered nor applied in any other significant way. Therefore, its lengthy derivation will not be presented in detail. The interested reader may consult a chapter published by Blum[53], as well as the original publications[55,56] and updated literature on the topic.[22,25,57–59]

Firstly, the MSA considers the OZ equation in Fourier space. The Fourier transform of equation (2.59) is expressed as follows:[53]

$$\left[\mathrm{I}^{(0)} + \tilde{\mathrm{H}}(k)\right]\left[\mathrm{I}^{(0)} - \tilde{\mathrm{C}}(k)\right] = \mathrm{I}^{(0)} \tag{2.87}$$

where $\tilde{\mathrm{H}}(k)$ is the matrix of the transforms of $h_{ij}(r)$, $\tilde{\mathrm{C}}(k)$ is the matrix of the transforms of $c_{ij}(r)$ and $\mathrm{I}^{(0)}$ is the identity matrix. By considering the simplest case of the RPM (all spheres of the same size with radius $\frac{a}{2}$ and $|z_i| = |z_j| = 1$), Blum obtained the following conditions for the total correlations:[53]

$$h^0(r) = 0.5h_{ii}^0(r) + 0.5h_{ij}^0(r) \quad \forall \quad r \leq a \tag{2.88}$$

$$h^{\#}(r) = h_{ii}^{\#}(r) - h_{ij}^{\#}(r) = h_{jj}^{\#}(r) - h_{ji}^{\#}(r) \quad \forall \quad r > a \tag{2.89}$$

where a notation similar to that of the DIT is kept: superscript 0 denotes some shorter-ranged contribution which is, in this case, the hard-sphere from Percus and Yevick[54] (equation (2.88)). Superscript # denotes a (linearized, in the simplest case) longer-ranged contribution where all ions are correlated hard spheres, instead of uncorrelated point charges as in DH theory (a situation corrected by MDE-DH). At the limit of infinite dilution, the following boundary conditions are given:

$$h_{ij}^{\#}(r) = -1 \quad \forall \quad r < a \tag{2.90}$$

$$c_{ij}^{\#,\infty}(r) = h_{ij}^{\#,\infty}(r) = -\beta w_{ij}^{av}(r) \quad \forall \quad r \geq a \tag{2.91}$$

where equation (2.90) is only the logical requirement for $g_{ij}^{\#}(r) = 0$ inside the hard sphere (which obviously remains valid beyond infinite dilution) and equation (2.91)

comes from the OZ equation with the definition $h_{ij}^{\#}(r) = -\beta q_j \psi_i^{av}(r) = -\beta u_{ij}^{av}(r)$, which was introduced in section 2.2.4.

With the definition of $h_{ij}^{\#}(r)$ in combination with equations (2.20), (2.28) and (2.70), one can additionally express the electro-neutrality condition in terms of $h_{ij}^{\#}(r)$ as follows:

$$4\pi \int_a^\infty \rho_{E,i}\, r^2 \mathrm{d}r = 4\pi \sum_j \rho_j q_j \int_a^\infty h_{ij}^{\#}(r) r^2 dr = -q_i \tag{2.92}$$

The interaction potential $\psi_{ij}^{av}(r)$ requires a Yukawa form in the Wiener-Hopf factorization method (an algorithm for the calculation of $h_{ij}(r)$) applied by Blum.[25,53] In line with the convention, the averaged interaction potential is expressed by:[53]

$$w_{ij}^{av}(r) = \lim_{x \to 0} \frac{q_i q_j \beta}{4\pi\varepsilon_0\varepsilon_r r} \exp(-x|r|) \tag{2.93}$$

where $x$ therefore stands for a screening length. A brief summary of the Wiener-Hopf factorization algorithm related to the derivation of the MSA can be found in Chapter 4 of Barthel et al.[25] The solution method with these considerations has the objective of obtaining $h_{ij}(r)$ which in turn is applied to calculate the excess internal energy (denoted by $\Delta E$ in Blum's notation, equivalent to the Helmholtz free energy $\Delta A$). The corresponding calculation is analogous to the charge density of the system divided by the capacitance $\varepsilon_0\varepsilon_r C$ of a sum of spherical capacitors:[53]

$$\Delta E = \frac{\rho q_j^2}{8\pi}\left(\frac{1}{\varepsilon_0\varepsilon_r C}\right) = \frac{\sum_{ij} \rho_j \rho_i q_j q_i}{4\pi\varepsilon_0\varepsilon_r} \int_0^\infty h_{ij}(r)\, r dr \tag{2.94}$$

where the electrostatic component of the total correlation function in the Wiener-Hopf factorization is given by:

$$\int_0^\infty h_{ij}^{\#}(r)\, r dr = \frac{J}{2\pi} = -\frac{\left(1 + \kappa_D a - \sqrt{1 + 2\kappa_D a}\right)}{2\pi\kappa_D \rho a^2} \tag{2.95}$$

The script $J$ corresponds to a value obtained as a result from the factorization method as described in the literature.[25,53] The resulting capacitance is:[53]

$$C^{MSA} = \varepsilon_0\varepsilon_r \left(\frac{a}{2} + \frac{1}{2\Gamma}\right) \tag{2.96}$$

with the definition of a renormalized screening parameter $\Gamma$ calculated in terms of the Debye screening parameter as follows:[53]

$$\Gamma = (2a)^{-1}\left(\sqrt{1+2\kappa_D a}-1\right) \tag{2.97}$$

Inserting the result in equation (2.94) at infinite dilution to isolate the electrostatic term yields the coulombic component to the excess internal energy. The corresponding chemical potential of electrostatic origin for the restricted primitive case is given by:[53]

$$\mu_i^{el} = k_B T ln\left(\gamma_i^{el}\right) = -\frac{q_i^2}{8\pi\varepsilon_0\varepsilon_r}\left(\frac{2\Gamma a}{1+\Gamma a}\right) \tag{2.98}$$

which has a similar form to the DH result from equation (2.31) and corresponds to the restricted primitive case of the MSA (RP-MSA). The value $\Gamma$ is a renormalized screening length that excludes a spherical dielectric occupied by the hard spherical ions. As shown further ahead, RP-MSA and MDE-DH have a remarkable qualitative agreement.

### 2.2.6 The Mean Ionic Activity Coefficient

For the purpose of calculating phase equilibria of a salt from the ionic activity coefficient of electrostatic origin $\gamma_i^{el}$ of the ions the assumption of full dissociation is first defined:

$$C_{v_+}A_{v_-} \rightleftharpoons v_+ C^{z_+} + v_- A^{z-} \tag{2.99}$$

where $v_+$ and $v_-$ are the stoichiometric coefficients of the dissociation reaction.

The mean ionic activity coefficient (MIAC) of the salt, denoted by $\mu_\pm$, is introduced as a theoretical value, given that single ion properties are controversial.[4] Thus, applying equation (2.13) and assuming infinitely diluted salt as the reference state results in:

$$\frac{\mu_{\pm Total}}{RT} = \frac{\mu_\pm^{ideal} + \mu_\pm^E}{RT} = \frac{v_+}{v}\ln(x_+) + \frac{v_-}{v}\ln(x_-) + \frac{v_+}{v}\ln(\gamma_+) + \frac{v_-}{v}\ln(\gamma_-)$$

$$\gamma_\pm = \left(\gamma_+^{v_+}\gamma_-^{v_-}\right)^{\frac{1}{v}} \quad \text{mean ionic excess contribution} \tag{2.100}$$

$$x_\pm = \left(x_+^{v_+}x_-^{v_-}\right)^{\frac{1}{v}} \quad \text{mean ionic ideal contribution}$$

with $v = v_+ + v_-$. Equation (2.100) is presented with the mole fraction $x$ as concentration scale, but one may use other concentration scales as basis (e.g. molality, molarity). The conversion between concentration scales can be found in the literature.[4,25,60] The ionic and mean ionic activity coefficients have infinite dilution as the standard state i.e. they are treated as solutes. Thus, as $c_\pm \to 0$ one should obtain $\gamma_\pm^{(c)} \to 1$.

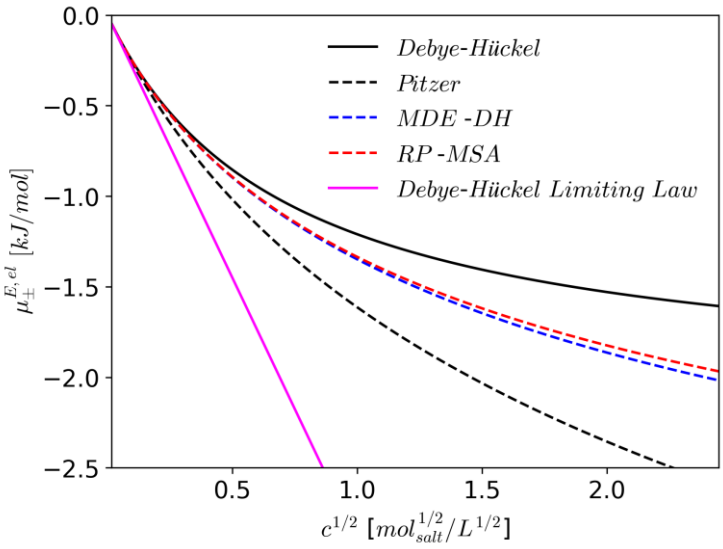


**Figure 6. Excess chemical potential of electrostatic origin calculated in molar concentration by the DHLL, DH theory, Pitzer's extension of the DH theory, the MDE-DH theory and the RP-MSA: equations (2.31), (2.35), (2.83)-(2.86) and (2.98), respectively for $a = 4.25$ Å, $\varepsilon_r = 78.65$ and $T = 298.15$ K.**

Figure 6 shows the excess chemical potential of electrostatic origin $\mu_\pm^{E,el} = RT \ln(\gamma_\pm^{el})$, as calculated with diverse theories. Compared to the more advanced MDE-DH and RP-MSA, DH theory inherently carries an overestimation of $\mu_\pm^E$ due to a fundamentally incomplete description of ion-ion correlations and neglecting the excluded dielectric volume of the cloud ions. In contrast, Pitzer's re-derivation of the DH theory underestimates the value of $\mu_\pm^E$ when compared to the more advanced MDE-DH and RP-MSA theories.

### 2.2.7 Effects of Ions in Solution

Water is the most abundant liquid solvent on our planet and an efficient solvent for ions due to its small molecular size, its high dipole moment and its donor-acceptor properties along with its structured hydrogen bonding network.[61] Unsurprisingly, the most abundantly studied electrolyte systems are aqueous and the effects of ions in pure water have been widely characterized,[60–66] whereas data from non-aqueous systems is limited.

### *Relative Permittivity and the Dielectric Decrement*

As described previously, the relative permittivity is the only property that describes the solvent in the PM. Determining the relative permittivity of a liquid, e.g. water, requires the study of the orientation of its molecules under the influence of an external electric field and how this orientation can be affected by other factors.[67]

At a macroscopic level, the relative permittivity denotes the capacity of a polarizable medium to distribute its internal charge in presence of an external electric field. At the microscopic level, it is related to the re-orientation of the molecules and their internal charge distribution in the presence of an electric field. This is illustrated in Figure 7.

The PM considers the macroscopic definition for a medium surrounding the ions. Thus, even though the PM remains the basis for the most widespread electrostatic solvation models,[6,25,68] it is evidently missing structural effects from the solvent molecules. The simplest relation to describe this is on the macroscopic level is given by:[25]

$$\mathbf{P} = \varepsilon_0(\varepsilon_r - 1)\mathbf{E} \tag{2.101}$$

where $\mathbf{P}$ is the polarization of the medium in presence of the electric field $\mathbf{E}$, $\varepsilon_r$ is the relative permittivity of the medium and $\varepsilon_0$ is vacuum permittivity. At the molecular (microscopic) level, $\mathbf{P}$ has an orientational component from the molecular dipole moment $\mu_0$, and a component from the induced polarization (the electric field can deform the electron distribution of a molecule depending on its polarizability tensor $\alpha_0$).

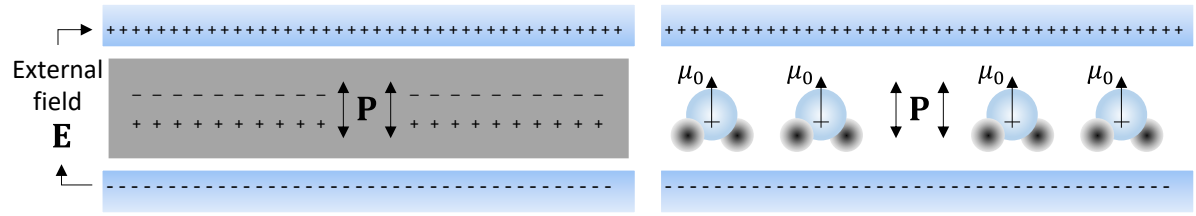


**Figure 7. The relative permittivity of a material under the influence of an external electric field. Left: macroscopic perspective, applicable to the PM. Right: the microscopic perspective.**

Thus, many efforts were invested[50,69–71] and still are currently invested,[72–74] in order to describe the relative permittivity of a fluid in terms of its molecular dipole moment and polarizability. An equation that is commonly applied for this purpose was derived from statistical mechanics for spherical molecules by Onsager:[69]

$$\frac{(\varepsilon_r - n_D^2)(2\varepsilon_r + n_D^2)}{\varepsilon_r(2 + n_D^2)^2} = \frac{\rho\mu_0^2}{9\varepsilon_0 k_B T} \tag{2.102}$$

where $n_D^2$ is the refractive index of the pure component in question. The generalized expression assumes ideal packing and an equivalent spherical radius, reducing equation (2.102) to the following for pure compounds:

$$\frac{(\varepsilon_r - n_D^2)(2\varepsilon_r + n_D^2)}{\varepsilon_r(2 + n_D^2)^2} = \frac{N_A\mu_0^2}{9\varepsilon_0 k_B T \mathrm{v}}\mathrm{g}_i \tag{2.103}$$

where v denotes molar volume and further corrections[75] to Onsager's equation lead to the introduction of the Kirkwood g-factor ( $\mathrm{g}_i$ ), which accounts for the geometrical configuration of highly structured molecular fluids like water. The Kirkwood g-factor assumes that the macroscopic relative permittivity is approximated by evaluating a region around a molecule and the orientation of its nearest neighbors as follows:[75]

$$\mathrm{g}_i = (1 + z < \cos\theta >) \tag{2.104}$$

being $z$ the coordination number of the molecule with its nearest neighbors and $\theta$ the angle between the dipoles. To calculate $\varepsilon_r$ in a non-electrolyte mixture, the concept is generalized[76] in equation (2.105) for $j$ neutral entities:

$$\frac{(\varepsilon_r - n_D^2)(2\varepsilon_r + n_D^2)}{\varepsilon_r(2 + n_D^2)^2} = \frac{N_A}{9\varepsilon_0 k_B T \mathrm{v}}\sum_j x_j \mathrm{g}_j \mu_{j,0}^2 \tag{2.105}$$

Equation (2.105) is derived for neutral, spherical dipoles. Electrolyte mixtures behave differently due to the electric fields of the ions penetrating further into the medium when compared to a dipole. The electric field of an ion disrupts the orientation and structure of the solvent molecules and tends to re-arrange these around the ions forming a solvation shell. This is dependent on the dipole moment of the solvent molecules and the surface charge density of the ions, among other factors. The resulting effect is that the permittivity of the liquid medium tends to decrease as ion concentration rises and this is commonly known as the dielectric decrement.[61] These microscopic, structural aspects (depicted in Figure 8), are not represented in the PM.

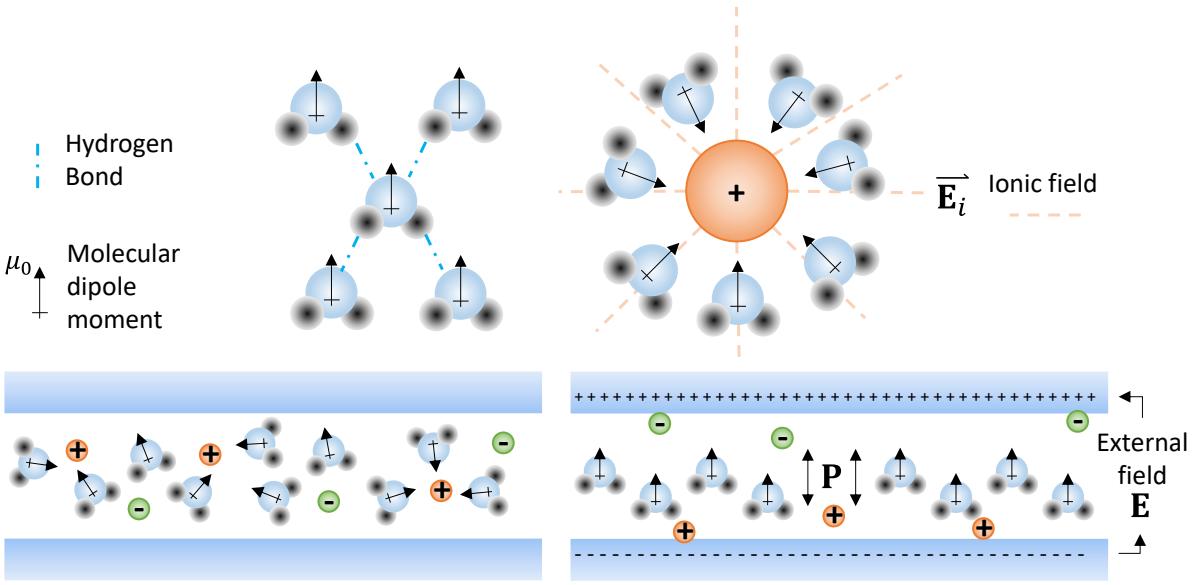


**Figure 8. The structure of water as a hydrogen-bonding network of molecules (upper-left) and the rearrangement of water molecules around a cation (upper-right). An electrolyte solution with no influence of an external field (lower-left) and its response in presence of an external electric field (lower-right).**

To determine the relative permittivity of a liquid, its dielectric response (Debye dielectric relaxation time $\tau_D$ or simply: relaxation time) is experimentally evaluated under the influence of an external electric field at varying frequencies to apply the Debye equation for complex permittivity.[67] In the case of electrolytes, there is a dynamic contribution due to the movement of the ions in the presence of an external electric field: as shown in Figure 8 (lower-left to lower-right), ions will move and tend to deposit in the walls with a counter-charge. According to Hubbard and Onsager,[77,78] in order to obtain the relative permittivity of the mixture $\varepsilon_m$, this dynamic contribution $\Delta\varepsilon_k$ must be removed from the experimentally measured value $\varepsilon_{ex}$ by means of the following equation:

$$\Delta\varepsilon_k = \left(1 - \frac{n_D^2}{\varepsilon_{ex}}\right)\frac{\tau_D \Lambda_{\mathrm{el}}}{\varepsilon_0} \tag{2.106}$$

where $\Lambda_{\mathrm{el}}$ is the conductivity of the electrolyte and $n_D^2 \equiv \varepsilon_\infty$ is the infinite frequency permittivity of the salt-free medium (pure solvent). Depending on the assumptions taken, $\Delta\varepsilon_k$ can be scaled by a factor of 2/3 (perfect slip condition) or left as calculated with equation (2.106) (no slip condition).[79]

For use of $\varepsilon_r = \varepsilon_m$ in the PM, the phenomenon of dielectric decrement is accounted for empirically. A non-exhaustive list of common examples is presented in Table 2.

**Table 2. Several empirical equations to account for the dielectric decrement in electrolyte solutions.**

| Equation | Details |
|---|---|
| $\varepsilon_m(c_i) = \varepsilon_s - \delta_s(c_i)$ | Linear regime of the dielectric decrement; $\boldsymbol{\varepsilon_s}$ is the permittivity of the solvent; $\boldsymbol{c_i}$ is molar concentration of the salt, $\delta_s$ is an empirical parameter<br>Source: E. Hückel[80] |
| $\varepsilon_m(c_i) = \varepsilon_s - \delta_s(c_i) + \beta_s(c_i)^{3/2}$ | Linear regime of the dielectric decrement. $\delta_s, \beta_s$ are empirical parameters, $\boldsymbol{c_i}$ is salt molar concentration.<br>Source: Tikanen A.C. and Fawcett W.R.[81] |
| $f = \frac{2\varepsilon_s + \varepsilon_e}{(\varepsilon_s + \varepsilon_e)} \frac{\varepsilon_s - \varepsilon_m}{(2\varepsilon_s + \varepsilon_m)}$ | Assumes volume fraction $f$ of solvated ions in terms of $\varepsilon_s$, with $\varepsilon_e$ being the permittivity of a solvated ion (taken as a value of 2). $f$ is used to estimate the number of water molecules that do not contribute to the structure of water and applied in the Debye equation for complex permittivity. Commonly termed the "Pottel" model.<br>Source: Giese K, Kaatze U. and Pottel R.[82] |
| $\varepsilon_m = \frac{\varepsilon_s}{1 + \sum_i \alpha_i x_i}$ | Phenomenological model where subscript $i$ denotes "ions", being $\boldsymbol{\alpha_i}$ an ion specific parameter and $x_i$ is the mole fraction of the ion.<br>Source: Simonin P., Bernard O., Blum L.[83] |
| $\varepsilon_m = \frac{\varepsilon_s}{1 + \sum_i A_i x_i \ln\left(1 + B_i\sqrt{I_x}\right)}$ | Phenomenological model where subscript $i$ denotes "ions", being $\boldsymbol{A_i}$ and $B_i$ temperature dependent ion specific parameters and $x_i$ is the mole fraction of the ion. $I_x$ is the ionic strength (equation (2.47))<br>Source: Wang P., Anderko A.[84] |
| $\varepsilon_m = \frac{\sum_i x_i \varepsilon_i \mathrm{v}_i}{\sum_i x_i \mathrm{v}_i}$ | Additive by volume fraction with $\mathrm{v}_i$, $\varepsilon_i$ and $x_i$ being the molar volume, pure compound relative permittivity and mole fraction of any arbitrary species $i$, respectively. Applied to an aqueous IL mixture.<br>Source: Koeberg M. et al.[85] |

Finally, due to the aforementioned dynamic effects, and considering that molten salts are highly conductive and hygroscopic, the experimental methods of the relative permittivity of molten salts and room temperature ionic liquids (RTILs) require care, extrapolations and assumptions.[86] There is a large discrepancy between the values reported with different measurement techniques in the literature, sometimes even with contradicting and unexpected trends.[86,87] Furthermore, a molten salt is a highly polar fluid, but the assumptions and models developed for highly polar, neutral species are not applicable.[88] So far, one can only assume that these molten salt/IL permittivity values are expected to be low (e.g. $\varepsilon_{melt} \approx 8$ or lower, in spite of them being polar) and tend to decrease with increasing molar mass.[86,87]

### *Molar Volume and Electrostriction*

The size of an isolated ion is not a well-defined concept, e.g. the lithium cation is a small spherical entity, and the largest portion of its volume is an electron cloud. In solution, the lithium ion has passed an electron over to the anion. This pulls the remaining electrons towards the inner nucleus of the cation and reduces its polarizability: it is a hard ion. In contrast, a spherical anion has an extra electron in its cloud. Therefore, it can shift its internal charge distribution under influence of an electric field more easily and has a higher polarizability: it is a soft ion. The hardness and softness the ions influence their behavior in solution and their capability to participate in donor-acceptor interactions.[61]

Furthermore, the ions affect the molar volume of water in an aqueous solution, resulting in an apparent molar volume. For instance, water molecules rearrange around an ion and have donor-acceptor interactions with it. In addition to these donor-acceptor interactions, the electric field of the ion pulls the water molecules of its solvation shell towards its center and the water molecules are said to be electrostricted.[61] Therefore, the density of electrolyte solutions, especially aqueous electrolyte solutions, can be expected to have a non-ideal behavior and that is not easily predicted from first principles nor from theoretical considerations.[89,90] Thus, in the same fashion as with the dielectric decrement, the density of electrolyte solutions is usually handled empirically.[6,61,91] Experimental measurements of the electrolyte density are commonly applied to estimate the apparent molar volume of an electrolyte $\mathrm{v}_{el}$ by means of the Marignac expression:[90]

$$\mathrm{v}_{el} = \frac{n_T \mathrm{v}_T - n_s \mathrm{v}_\mathrm{s}}{n_{el}} = \frac{M_{el}}{d} - \frac{d_s - d}{m_{el} d d_s} \tag{2.107}$$

where $n_{el}$ is moles of electrolyte, $n_T \mathrm{v}_T$ is the volume of the solution, $n_s \mathrm{v}_\mathrm{s}$ is the volume of the solvent. In the reformulation, $M_{el}$ and $m_{el}$ are the molar mass and molality of the salt, respectively; $d$ and $d_s$ are the densities of the solution and the pure solvent, respectively.

The partial molar volume of an ion can be divided into three contributions:[90] its crystallographic molar volume (which would be pure, single ion property and thus not measurable), the electrostricted solvent molecules in the solvation shell and a disorder factor contribution to the solvent molecules outside of the solvation shell.

For the specific case of large polyatomic ions with delocalized charges, like ILs, the pure compound and concentration dependent densities are more easily correlated. The

abundant measurements of pure IL densities and negligible electrostriction allow for a more straightforward calculation of a concentration dependent density in IL mixtures with less parameters and higher precision.[87,92,93]

### *Ion Pairing*

At low salt concentrations, one may already observe positive deviations of the $\gamma_{\pm}$ values calculated with conventional electrolyte theories with respect to the experimentally measured mean ionic activity coefficient. The most commonly invoked explanation for these positive deviations is the formation of ion pairs in the solution.[89] Ion pairing is a strongly attractive interaction, expected to decrease the value of $\gamma_{\pm}$.

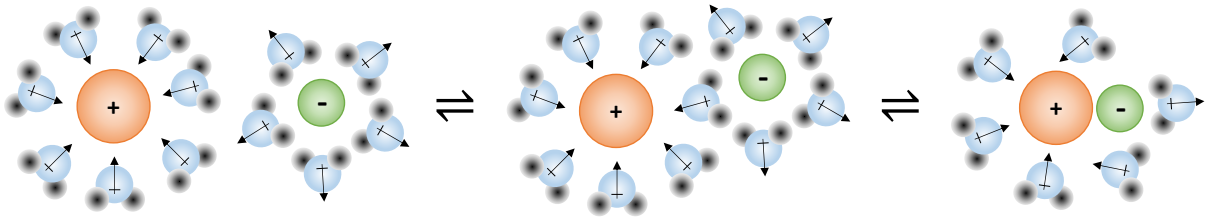


**Figure 9. From left to right: a hypothetical depiction of a solvent-solvent separated ion pair, a solvent separated ion pair and a direct contact pair. Contact pairs could lose some of the solvent molecules in the outer solvation shell.**

Conventionally,[25,94] the Bjerrum treatment is applied as a semi-empirical method to determine the degree of dissociation in an electrolyte. The approach was proposed by Niels Bjerrum[95] and consists of a rather straightforward procedure. It is first hypothesized that a fraction $1 - \alpha$ of the ions in a solution consists of free (subscript $f$), solvated ions, and the remaining α fraction consists of partially solvated pairs according to the chemical dissociation reaction from equation (2.99), depicted in Figure 9.

It must be stressed that, strictly speaking, the concept of "ion pairing" in the RPM is implicit in the higher order terms of the Poisson-Boltzmann approach and in the higher order pair correlations. Thus, from the theoretical physics standpoint, a more complete electrolyte theory would dispense with ion pairing at the McMillan-Mayer level.[94,96,97] This was already suggested in 1934 by Kirkwood,[50] and even earlier by others.[98,99] But, in the absence of a more complete theory, Bjerrum correctly asserted that higher order corrections to the Debye-Hückel electrostatic potential $\psi_i^{DH}(r)$ translate into apparent reductions of the effective ion concentration (the ions that take part in the shielding of

electrostatic forces).[95,97] Bjerrum proposed a chemical model based on an association constant to approximate these reductions:

$$v_+C^{z_+} + v_-A^{z-} \overset{\mathrm{K_A}}{\rightleftarrows} C_{v_+}A_{v_-}$$

$$\mathrm{K_{assoc}} = \frac{[\mathrm{a}_{CA}]}{[\mathrm{a}_+]^{v_+}[\mathrm{a}_-]^{v_-}} = \frac{\left[c_{AC}\gamma_{AC}^{(c)}\right]}{\left[c_{f+}\gamma_{f+}^{(c)}\right]^{v_+}\left[c_{f-}\gamma_{f-}^{(c)}\right]^{v_-}} \tag{2.108}$$

where $\mathrm{a}_{f+}$, $\mathrm{a}_{f-}$ and $\mathrm{a}_{CA}$ are the activities of the free cations, free anions and paired entities, respectively. The observable mean ionic activity coefficient of the salt is then defined as $\gamma_{\pm}^{(c)} = (1-\alpha)\gamma_{f\pm}^{(c)}$. The total ion concentration is $\sum_j v_j c_{salt} = v c_{salt}$ and the concentration of the free cations and free anions is $c_{f+} = (1-\alpha)v_+c_{salt}$ and $c_{f-} = (1-\alpha)v_-c_{salt}$, respectively. The fraction of the ions that are not free is $\alpha\sum_j v_j c_{salt}$ and therefore the concentration of paired entities is $c_{AC} = \alpha v^{-1}\sum_j v_j c_{salt}$. Furthermore, for the restricted primitive charge symmetric electrolyte it is valid that $c_{salt} = c_+ = c_- = c_\pm$ and $\gamma_+ = \gamma_- = \gamma_\pm$. Thus, is it commonly assumed that $\gamma_{AC}^{(c)} = 1$ to reduce equation (2.108) to a very simple expression for the 1:1 electrolyte in the PM.[94]

With known concentrations the remaining task is to calculate α with a known $\mathrm{K_A}$. Bjerrum suggested[95] a theoretical $\mathrm{K_A}$ value based on the RPM. It is a commonly neglected fact that Bjerrum's treatment was originally conceived as a correction to DH theory. Consequently, in practice the theoretical $\mathrm{K_A}$ from the PM is scaled based on known ion dissociation degrees from conductivity measurements and estimating a distance of closest approach for the solvated ionic species.[25,94,100–102] The reason for empirical adjustment of Bjerrum's $\mathrm{K_A}$ and similar expressions, is that already at very low concentrations the PM does not represent non-Coulombic interaction related effects (e.g. ion aggregation).[94] Thus, Bjerrum's treatment in some methodologies has even degenerated from a PM correction to a method that fits out a model's deficiencies by means of an additional, fully empirical parameter $\mathrm{K_A}$ of arguable physical meaning. Nonetheless, these non-Coulombic effects have been characterized in water and observable trends have been identified.[62,103,104]

*Other Effects of Electrolytes and Ionic Liquids in Solution*

An electrolyte is a conductive mixture: it can facilitate charge transport when compared to the pure solvent. The conductivity of electrolytes is reduced by ion-ion interactions. This causes a direct relationship with ion pairing theories and higher order corrections to the PB equation. Furthermore, the presence of ions affects the dynamic viscosity of the liquid phase, in some cases enhancing it and in other cases diminishing it. The enhancement of the dynamic viscosity of an aqueous mixture upon addition of ILs with decreasing molar volume is an exemplary case.[61,87]

In very general terms, the conductivity of an IL solution tends to be lower than that of a conventional salt-based electrolyte[105] and the dynamic viscosity of the IL solution tends to be higher than that of a conventional salt electrolyte. Other additional effects of no particular significance to the present work are described in the literature[61,87]

# 2.3 The COSMO-RS Model

Basic principles for ionic interactions have been laid out in section 2.2. Moving on to short-ranged contact forces (e.g. dipole – dipole, hydrogen bonding, interatomic repulsion, etc.), a robust, predictive method for the thermodynamics of neutral molecules is the Conductor-like Screening Model for Realistic Solvation (COSMO-RS).

## 2.3.1 The Conductor-like Screening Model

The Conductor-like Screening Model (COSMO) from Klamt and Schüürmann[106] is a dielectric continuum model: a molecule is embedded into a dielectric continuum. The response of the dielectric results in an outer surface screening charge distribution i.e. the surface charge is screened by the dielectric at the surface of the molecular cavity.

The screening charge density $\sigma$ at a given point $(r)$ on the molecular surface is a function of the dielectric continuum permittivity $\varepsilon$ and the local electric field $\mathbf{E}$ at the inner boundary of the surface. This is described by the following relationship:[106]

$$4\pi\sigma(r) = (\varepsilon - 1)\mathrm{n(r)}\mathbf{E}(r) \tag{2.109}$$

where n(r) is the normal vector. In order to solve equation (2.109), the molecular cavity is divided into $m$ segments. A condition is that the interaction energy when approaching the inner boundary equals the interaction energy when approaching the outer boundary of the molecular cavity. The former relates to the internal surface charge distribution and the latter to the polarization response of the dielectric medium.[106,107] Apparent surface charge models were introduced to approximate a solution.[107] A well known model is the polarizable continuum model (PCM) which couples the self-consistent quantum chemical field with the polarizable dielectric boundary.

Klamt and Schüürmann[106] proposed applying an ideal conductor ($\varepsilon = \infty$) at the boundary instead of a dielectric, which reduces the computational costs of calculating the charge density at the surface of the molecular cavity. An ideal conductor fully screens the charge density at the surface of the molecular cavity, as depicted in Figure 10, with the boundary condition that the potential vanishes at the outer contact between the grounded conductor and the molecule. The relation between the screening energies using a real dielectric ($\varepsilon = \varepsilon_m$) and the screening energies using a grounded conductor ($\varepsilon = \infty$) are well approximated by the following scaling function from electrostatics:[107]

$$f(\varepsilon_m) = \frac{\varepsilon_m - 1}{\varepsilon_m + x} \tag{2.110}$$

where $x$ takes a value of 0.5. The interaction energy is calculated in a single step as:[106,107]

$$E^{\mathrm{X}} = -f(\varepsilon_m)\Phi^{\mathrm{X}}\mathbf{A}^{-1}\Phi^{\mathrm{X}} = \mathrm{Q}^{\mathrm{X}}\mathbf{D}\mathrm{Q}^{\mathrm{X}} \tag{2.111}$$

where $\Phi^{\mathrm{X}}$ is the surface potential given by the internal charge distribution and $\mathbf{A}^{-1}$ is the inverse Coulomb interaction matrix of the $m$ surface segments. This is reformulated in terms of a charge-density representation $\mathrm{Q}^{\mathrm{X}}$ and $\mathbf{D}$ is a matrix representation of Green's function. The free energy gain is $\frac{1}{2}E^{\mathrm{X}}$ in an apparent surface charge model.[107]

The key information from the screening energy of a molecule results from its internal charge distribution. This is dependent on the position of sub-atomic particles at a given instant, which is fundamentally described by Schrödinger's equation in its time-independent form:[22,108]

$$\hat{H}(\Psi(r)) = \hat{E}(\Psi(r)) \tag{2.112}$$

where $\hat{H}$ is the Hamiltonian operator applied on the wave function $\Psi(r)$ and $\hat{E}$ is the energy of the subatomic particle. Equation (2.112) states that, with a stationary solution to its wave function, the kinetic and potential energies of a particle can only be obtained from quantum mechanical operators.[108] The direct implication of this is that calculating a charge-density representation $Q^X$ requires computational quantum chemistry tools.

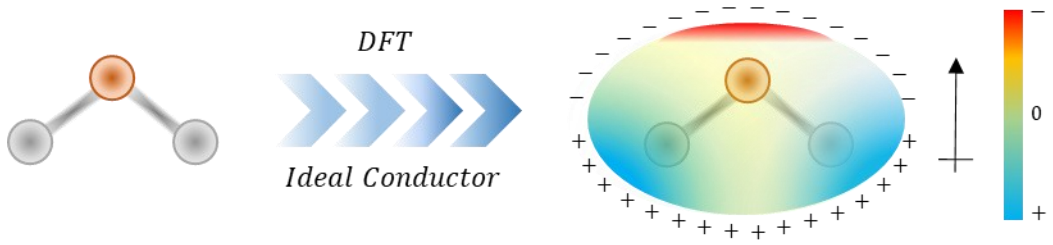


**Figure 10. Conceptual dielectric screening of the molecular cavity for a water molecule.**

Density Functional Theory (DFT) is the most commonly applied tool for the integration of continuum solvation models with estimates of the internal charge distribution (electronic structure) of a molecule with any arbitrary geometry.[109] DFT calculations estimate the energy of the electrons as a functional of electron density instead of the wave function and is considered a reliable and computationally efficient method.[107]

COSMO was implemented in several quantum chemical packages and its combination with TURBOMOLE® (Turbomole GmbH)[110] provided the fastest gas phase DFT calculations.[107]

### 2.3.2 The Conductor-like Screening Model for Realistic Solvation

COSMO is a fast methodology with a robust quantum chemical backbone to estimate solvation energies in a dielectric continuum. This works well for non-polar molecules (e.g. alkanes) but is nevertheless inadequate for mixtures and polar solvents.[107] For instance, the reorientation of water molecules due to hydrogen bonding around a solute is not captured by homogeneous dielectric screening. For this problem, the Conductor-like Screening Model for Realistic Solvation (COSMO-RS) is introduced. COSMO-RS applies the screened molecular surfaces from COSMO in the context of statistical thermodynamics of pairwise interacting surface segments.[107] Thus, COSMO-RS is an excess Gibbs-free energy model ($g^E$-model) for the prediction of solvation and phase equilibria.

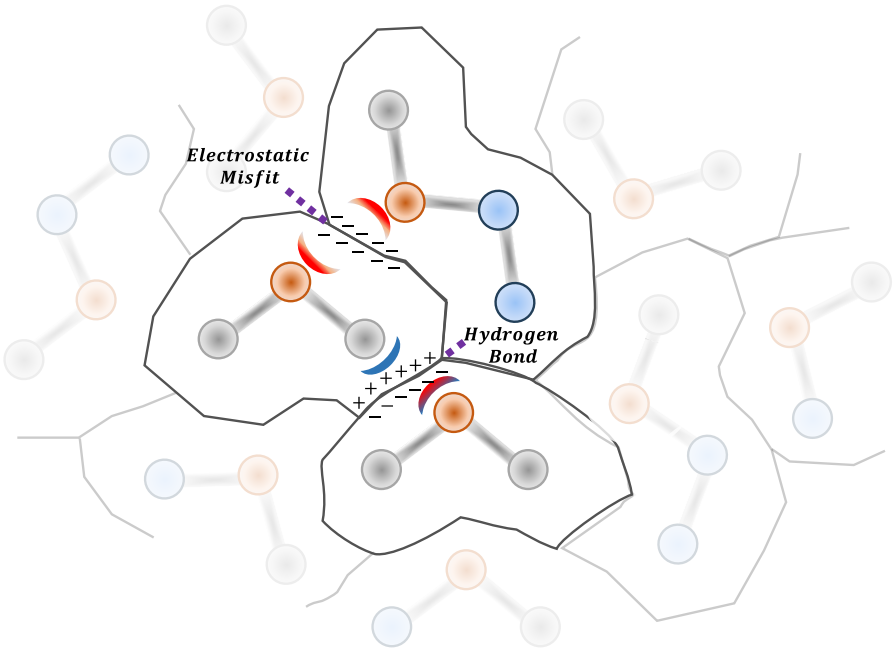


**Figure 11. Ideally screened molecules in close contact as graphically conceptualized by Klamt.[107] Exemplified here for a water + alcohol system.**

The COSMO-RS method is based on the idea of the ideally screened molecular surfaces coming in contact, as graphically represented in Figure 11 for a binary mixture. An ideally screened molecule (i.e. a molecule that undergoes the process show in Figure 10) is placed in the vicinity of other molecules that have also been screened by the ideal conductor. If the molecules are packed together and the ideal conductor is removed, the charged molecular surfaces are allowed to interact with each other.[8,107,111]

To estimate an averaged energy, one would require sampling a very large number of configurations like Figure 11. If the molecular surfaces are divided into small surface segments that are allowed to interact, then statistical thermodynamics can be applied to estimate averaged interaction energies. Thus, a preliminary step is dividing the molecular surfaces into $m$ segments of surface charge $\sigma_m = q_m^{COSMO}/s_m^{COSMO}$ where $q_m^{COSMO}$ and $s_m^{COSMO}$ are the charge and surface of a surface segment in COSMO. A local average for each segment is calculated as:[107]

$$\sigma_I = \frac{\sum_J \frac{q_J^{COSMO}}{s_J^{COSMO} + s_{av}} \exp(-d_{IJ}^2/r_{av}^2)}{\sum_J \frac{s_J^{COSMO}}{s_J^{COSMO} + s_{av}} \exp(-d_{IJ}^2/r_{av}^2)} \tag{2.113}$$

where $s_{av} = \pi r_{av}^2$ with $r_{av}$ being an averaging radius and $d_{IJ}$ the euclidean distance between the segments $I$ and $J$ in the COSMO cavity.

Subsequently, if a surface segment $I$ from one molecule contacts a surface segment $J$ from another molecule, the energy cost with respect to the ideal conductor is:[7,8]

$$E_{IJ}^{mf} = \frac{a_{eff}}{2} \alpha \left(\sigma_I + \sigma_J\right)^2 \tag{2.114}$$

where an ideal contact happens when the surface charge of a segment equals the opposite surface charge of the other ($\sigma_J = -\sigma_I \therefore E_{IJ}^{mf} = 0$). Essentially, equation (2.114) represents the electrostatic energy penalty of deviating from the ideal conductor screening state. A favorable electrostatic misfit is therefore found when $\sigma_J \approx -\sigma_I$ and $E_{IJ}^{mf}$ is very small. However, as exemplified in Figure 11, if two highly charged surface segments of the same sign, like that of an oxygen atom in water and that of an oxygen atom from an R-OH group come in contact, then the electrostatic misfit is strongly repulsive in nature. In equation (2.114), $a_{eff}$ stands for the effective area of contact between the two surface and α is a universal empirical energy parameter. Equation (2.114) is called the misfit energy.[8]

A relevant refinement[7] to the misfit energy is the introduction of a new descriptor that accounts for the polarization charge density in the vicinity of an interacting surface. The averaged polarization charge density surrounding a segment $I$ is denoted by $\sigma_I^{\circ}$ and calculated with equation (2.113) applying twice the averaging radius. The averaged polarization charge density of the surface segment and the averaged polarization charge density of its surroundings strongly correlate. For this reason, the orthogonal component of the polarization charge density is introduced and given by:[7,107]

$$\sigma_I^{\perp} = \sigma_I^{\circ} - 0.816\sigma_I \tag{2.115}$$

and applied to the refined misfit energy as follows:[7,107]

$$E_{IJ}^{mf,\perp} = \frac{a_{eff}}{2} \alpha \left(\sigma_I + \sigma_J\right)\left(\sigma_I + \sigma_J + f^{\perp}\left(\sigma_I^{\perp} + \sigma_J^{\perp}\right)\right) = a_{eff} \cdot e_{mf}(\sigma_I, \sigma_J) \tag{2.116}$$

which replaces equation (2.114) and with a parameter $f^{\perp}$ typically in the range of 2.

In addition to the electrostatic misfit, a surface with a strong positive charge (i.e. $\sigma_I \ll 0$ where the sigma is negative because it is the counter-charge of the screening conductor)

may act as a hydrogen bond donor and a surface with a strong negative charge as a hydrogen bond acceptor. This type of interaction is attractive in nature and results in a free energy gain.[107] Hydrogen bonding is accounted for empirically in the COSMO-RS method by means of the following equation:[7,8]

$$G_{IJ}^{hb} = \begin{cases} a_{eff} \cdot c_{hb}(T) \cdot \max(0, \sigma_I - \sigma_{hb}) \cdot \min\left(0, \sigma_J + \sigma_{hb}\right) & \forall\ \sigma_J < 0 < \sigma_I \\ a_{eff} \cdot c_{hb}(T) \cdot \max\left(0, \sigma_J - \sigma_{hb}\right) \cdot \min(0, \sigma_I + \sigma_{hb}) & \forall\ \sigma_I < 0 < \sigma_J \end{cases} \quad (2.117)$$

where $\sigma_{hb}$ is a hydrogen bonding threshold of $0.0085\,\frac{e}{\text{Å}^2}$, e.g. a surface segment with a surface charge smaller than $-\sigma_{hb}$ acts as a hydrogen bond donor. For simplicity, we express $G_{IJ}^{hb}$ in a generalized form as $G_{IJ}^{hb} = a_{eff} \cdot e_{hb}(\sigma_I, \sigma_J, T)$. Temperature dependency is introduced in the hydrogen bonding energy term by means of a parameter:[107]

$$c_{hb}(T) = c_{hb}\left[1 - c_{hb}^{T} + c_{hb}^{T}\left(\frac{298.15}{T}\right)\right] \quad (2.118)$$

where $c_{hb}$ and $c_{hb}^{T}$ are universal empirical parameters. The resulting full interaction is:

$$A_{IJ} = E_{IJ}^{mf,\perp} + G_{IJ}^{hb} = a_{eff} \cdot \left(e_{mf}(\sigma_I, \sigma_J) + e_{hb}(\sigma_I, \sigma_J, T)\right) \quad (2.119)$$

Once the interaction energies between two surface segments in contact are known, a statistical thermodynamics framework is necessary to estimate the averaged interaction energies between molecules based on the pairwise interactions of their surface segments.

For this purpose, we first assume that there is an ensemble containing all surface segments of the molecules of a component or mixture and that these surface segments have been screened by an ideal conductor. We also assume that all surfaces have pairwise interactions and found an interaction partner. Finally, we introduce here the partition function $Z$ from statistical mechanics. The partition function is defined as the sum of the Boltzmann factor of all interaction energies from all possible configurations of the ensemble. The partition function contains all statistical information of the ensemble and is used to calculate its thermodynamic properties.[23] For instance, the residual Gibbs-free energy relates to the residual partition function as follows:[107]

$$G^{R} = -k_B T \ln Z^{R} \quad (2.120)$$

To obtain $G^{R}$ from the partition function of an ensemble of pairwise interacting surfaces, one would require probing a sufficiently large enough number of configurations.

Given that geometrical constraints have been neglected, the statistical thermodynamics become less intensive and probing a large amount of configurations (e.g. via a Monte-Carlo method) is not necessary. Instead, one may choose a segment $i$ of nature $I$ and a segment $j$ of nature $J$ and remove them from the ensemble. A new ensemble results from this procedure with a partition function denoted by $Z^R_{-i,-j}$. The original partition function $Z^R$ would then be given by the reintroduction of all $ij$ pair interactions as follows:[8]

$$Z^R = \sum_j N \exp\left(-\beta E_{ij}\right) Z^R_{-i,-j} \tag{2.121}$$

For a sufficiently large ensemble and in accordance with equation (2.120), one may propose the following approximation:[8,107]

$$\ln\left(\frac{Z^R_{-i,-j}}{Z^R}\right) \approx -\frac{\partial}{\partial N_i}\ln(Z^R) - \frac{\partial}{\partial N_j}\ln(Z^R) = \beta\mu'_i + \beta\mu'_j \tag{2.122}$$

which is reintroduced in equation (2.121) to yield the following:

$$\sum_j N \cdot exp\left(\beta(-E'_{ij} + \mu'_i + \mu'_j\right) = 1 \tag{2.123}$$

where $\mu'_i$ and $\mu'_j$ are the chemical potentials of surface segments $i$ and $j$, respectively. Solving for $\mu'_i$ yields a self-consistent expression:

$$\mu'_i = -k_B T \ln \sum_j N\, exp\left(-\beta E'_{ij} + \beta\mu'_j\right) \tag{2.124}$$

Thus, for any surface $I$ in an ensemble of pairwise interacting surfaces where the pair interaction energy $E'_{ij}$ is known from equation (2.119), we can write:

$$\mu_I = -k_B T \ln \sum_J N\, exp\left(-\beta A_{IJ} + \beta\mu_J\right) \tag{2.125}$$

Equation (2.125) lies as the heart of the COSMO-RS method and must be solved iteratively,[8,112] since the sigma potential $\mu_I$ of surface of type $I$ is a function of the sigma potentials of all other paired surfaces $\mu_J$. Thus, in the first iteration loop $\mu_J = 0\ \forall\ J \neq I$ is assumed when approximating $\mu_I$.[8] The chemical potential of all surface segments is approximated in this fashion and the corresponding values inserted in the second

iteration loop. Equation (2.125) is self-consistent and must be iterated until convergence. Its more elegant integral form is commonly found in the literature.[7,8,111,112]

By defining the activity coefficient $\Gamma_I$ and mole fraction $\Theta_I$ of any surface segment $I$ in the ensemble and introducing the definition $\beta\mu_I = \ln(\Gamma_I\Theta_I)$ in equation (2.125) one obtains:

$$\Gamma_I = \left(\sum_J \Theta_J \Gamma_J \tau_{IJ}\right)^{-1} \tag{2.126}$$

with an ideal conductor reference state and $\tau_{IJ}$ as interaction energy parameter given by:

$$\tau_{IJ} = \exp(-\beta A_{IJ}) \tag{2.127}$$

Equation (2.126) is analogous to equation (2.125) and is also calculated iteratively until convergence for all surface segment types in the ensemble. Summation over the molecular surface yields the activity coefficient of a molecule $i$ with the ideal conductor screening of the surface segments ensemble as the reference state:[107,113]

$$\ln\left(\gamma_i^{\#}(x_i)\right) = \sum_J \frac{A_J^i}{a_{eff}} \ln(\Gamma_J) \tag{2.128}$$

where $A_J^i$ is the area of the surface segments of type $J$ in molecule $i$. The subscript # here stands for grounded conductor reference state. The conventional residual activity coefficient can then be calculated with a change of reference state to pure compound and the ideal conductor screening reference state cancels out:

$$\ln(\gamma_i^R(x_i)) = \ln\left(\gamma_i^{\#}(x_i)\right) - \ln\left(\gamma_i^{\#}(x_i = 1)\right) \tag{2.129}$$

The residual contribution from COSMO-RS is complemented with a combinatorial term like e.g. the Staverman-Guggenheim or similar terms[107,114] that account for the entropic contribution arising from the differences in molecular size and geometry.

The COSMO-RS methodology constitutes a robust, widespread tool for the prediction of phase equilibria and solvation energies with applications in chemical engineering, physical chemistry and the pharmaceutical industry, among others.[2,112,114–117] There are several COSMO-RS based methods (e.g. COSMO-SAC[118,119]) where some refinements of the theory are lost, as well as alternative COSMO-RS implementations[114] available. The most advanced and refined version is provided as the commercial software COSMOtherm.[120]

## 2.4 The COSMO-RS-ES model

The COSMO-RS method alone cannot handle electrolyte systems due to several reasons; being two of them of central relevance: firstly, the COSMO-RS methodology has no expression for strong electrostatic interactions occurring with ions. Secondly, the COSMO-RS methodology only considers direct surface contacts.

The COSMO-RS-ES model is an electrolyte specific reimplementation of COSMO-RS from Gerlach et al.[14] that includes descriptors in order to distinguish specific surface segment interactions that involve surface segments from an ionic compound.

This facilitates a distinction between the conventional COSMO-RS equations that apply to neutral molecules, described in the previous subchapter, and new, empirical equations that handle ion-ion and ion-solvent interactions. The missing long-range coulombic interactions where accounted for with the PDH term (equation (2.51)) assuming full dissociation, with a distance of closest approach of $b_{constant}^{(x)} = 14.9$ for all systems and applying a salt-free reference state for electrolytes with mixed solvents. In the later, a mass fraction mixing rule was applied for the density and a volume fraction mixing rule was applied for the relative permittivity of the salt-free state.[14]

**Table 3. Parameters applied by Gerlach et al.[14] for the COSMO-RS residual term and for the combinatorial term (Staverman-Guggenheim, see Appendix).**

| Model | Parameter | Value |
|---|---|---|
| COSMO-RS (Residual) | $a_{eff}$ [Å$^2$] | 6.25 |
| | α [kJ Å$^2$ mol$^{-1}$ $e^{-2}$] | 5950 |
| | $c_{hb}$ [kJ Å$^2$ mol$^{-1}$ $e^{-2}$] | 36700 |
| | $c_{hb}^T$ [−] | 1.5 |
| | $\sigma_{hb}$ [$e$ Å$^{-2}$] | 0.0085 |
| | $r_{av}$ [Å] | 0.5 |
| | $f^{\perp}$ | 2.4 |
| Staverman-Guggenheim (Combinatorial) | $A_{std}$ [Å$^2$] | 79.53 |
| | $z$ [−] | 10 |

The COSMO-RS parameters applied by Gerlach et al.[14] for interactions between neutral molecules are shown in Table 3. As stated in Table 3, the Staverman-Guggenheim equation

was selected as the combinatorial term applying molecular surfaces and volumes from the COSMO molecular cavity. The COSMO-RS-ES model applies the refined misfit interaction energy from equation (2.116) for all neutral-to-neutral molecule interactions i.e. for all solvent to solvent interactions.

For ion-ion and ion-solvent contacts, the misfit interaction energy expression from equation (2.114) is applied replacing α for an interaction specific misfit factor $A_I$ for each interaction type $I$. The hydrogen bonding energy contribution from equation (2.117) is replaced by empirical interaction energy equations. These are shown in Table 4. Furthermore, the radii of the cations are also applied as fitting parameters in the model.

**Table 4. COSMO-RS-ES ion specific interaction equations from Gerlach et al.[14]**

| Interaction | Misfit Factor | Ion Interaction Energy Term |
|---|---|---|
| MC - $H_2O$ | $A_1$ | $E^{ion}_{cat-H_2O} = \frac{a_{eff}}{2} B_1 \sigma_{cat}\, max\left(0, \sigma_{H_2O}\right)$ |
| MC – Organic solv. | $A_2$ | $E^{ion}_{cat-om} = \frac{a_{eff}}{2} B_2 \sigma_{cat}\, max(0, \sigma_{om})$ |
| MC – MA | 0 | $E^{ion}_{cat-hal} = \frac{a_{eff}}{2} B_3\, min\left(0, \sigma_{cat}(1 - D_1\lvert\sigma_{cat}\rvert^{E_1})\right)\ \sigma_{hal}$ |
| MC - PA | 0 | $E^{ion}_{cat-pa} = \frac{a_{eff}}{2} B_4\, min\left(0, \sigma_{cat}(1 - D_1\lvert\sigma_{cat}\rvert^{E_1})\right) max\left(0, \sigma_{pa}\right)^{E_2}$ |
| MA – $H_2O$ | $A_3$ | $E^{ion}_{hal-H_2O} = \frac{a_{eff}}{2} B_5\, min\left(0, \sigma_{H_2O}\right) max(0, \sigma_{hal} - C_1)$ |
| MA – Organic solv. | $A_4$ | $E^{ion}_{hal-om} = \frac{a_{eff}}{2} B_6\, min(0, \sigma_{om})\, max(0, \sigma_{hal} - C_2)^{E_3}$ |
| PA – $H_2O$ | $A_5$ | $E^{ion}_{pa-H_2O} = \frac{a_{eff}}{2} B_7\, min\left(0, \sigma_{H_2O}\right) max\left(0, \sigma_{pa}\right)$ |
| PA – Organic solv. | $A_6$ | $E^{ion}_{pa-om} = \frac{a_{eff}}{2} B_8\, min(0, \sigma_{om})\, max\left(0, \sigma_{pa} - C_3\right)$ |

MC: Monoatomic Cation, MA: Monoatomic Anion, PA: Polyatomic Anion

The first parameterization[14] of the COSMO-RS-ES model was performed with a database of aqueous mean ionic activity coefficient data at room temperature for salts from alkali cations, the ammonium cation and calcium and magnesium cations with halides as monoatomic anions as and $SO_3^{2-}$, $SO_4^{2-}$, $NO_3^-$, $ClO_4^-$, $H_2PO_4^-$, $HPO_4^{2-}$ and $S_2O_3^{2-}$ as polyatomic anions. In addition to the mean ionic activity coefficient data, a liquid-liquid equilibrium (LLE) database of aqueous systems was also included.

The original COSMO-RS-ES model underwent a re-parameterization which included Gibbs free energies of transfer of ions reported in the literature[121–123] as part of the training set. The inclusion of these data provided an improvement in the performance of the model, providing evidence that the parameterization procedures may be prone to local minima,

which can be improved by the introduction of new types of data in the training set. The corresponding parameters, applicable to Table 4, can be consulted in the literature,[15] along with the fitted cationic radii.

Müller et al.[16] modified the empirical interaction energy equations, as shown in Table 5 and re-parameterized the model including the concept of effective ionic strength in the PDH term. For this purpose, a fraction of the ions was assumed not to partake in LR electrostatics. This fraction of the ions in turn was estimated by means of the ion association constant from Bjerrum.[95] The applied strategy was not an explicit Bjerrum ion pair treatment, given that ion-ion attractive interactions are present in the short-range COSMO-RS energy interactions. The considerations for an effective ionic strength that is proportional to the relative permittivity of the solvent yielded marked improvements in the prediction of salt solubility and liquid-liquid partitioning. The resulting parameters, along with the fitted cationic radii, can be consulted in the literature.[16] Systematic deviations and areas of opportunity of the model were observed for highly concentrated, non-aqueous electrolytes.[16,17]

**Table 5. Modified COSMO-RS-ES ion specific interaction equations from Müller et al.[16]**

| Interaction | Misfit Factor | Ion Interaction Energy Term |
|---|---|---|
| MC - $H_2O$ | $A_1$ | $E^{ion}_{cat-H_2O} = \frac{a_{eff}}{2} B_1 \sigma_{cat}\, max\left(0, \sigma_{H_2O} - \sigma_{hb}\right)$ |
| MC – Organic solv. | $A_2$ | $E^{ion}_{cat-om} = \frac{a_{eff}}{2} B_2 \sigma_{cat}\, max(0, \sigma_{om})$ |
| MC – MA | 0 | $E^{ion}_{cat-hal} = \frac{a_{eff}}{2} B_3\, min\left(0, \sigma_{cat}(1 - D_1\lvert\sigma_{cat}\rvert^{E_1})\right)\ \sigma_{hal}$ |
| MC - PA | 0 | $E^{ion}_{cat-pa} = \frac{a_{eff}}{2} B_4\, min\left(0, \sigma_{cat}(1 - D_1\lvert\sigma_{cat}\rvert^{E_1})\right) max\left(0, \sigma_{pa}\right)^{E_2}$ |
| MA – $H_2O$ | $A_3$ | $E^{ion}_{hal-H_2O} = \frac{a_{eff}}{2} B_5\, min\left(0, \sigma_{H_2O} + \sigma_{hb}\right) max(0, \sigma_{hal})$ |
| MA – Organic solv. | $A_4$ | $E^{ion}_{hal-om} = \frac{a_{eff}}{2} B_6\, min(0, \sigma_{om} + C_1)\, max(0, \sigma_{hal} - C_2)^{E_3}$ |
| PA – $H_2O$ | $A_5$ | $E^{ion}_{pa-H_2O} = \frac{a_{eff}}{2} B_7\, min\left(0, \sigma_{H_2O} + \sigma_{hb}\right) max\left(0, \sigma_{pa}\right)$ |
| PA – Organic solv. | $A_6$ | $E^{ion}_{pa-om} = \frac{a_{eff}}{2} B_8\, min(0, \sigma_{om} + C_1)\, max\left(0, \sigma_{pa}\right)$ |

MC: Monoatomic Cation, MA: Monoatomic Anion, PA: Polyatomic Anion

# 3 State of the Art

The present chapter summarizes the latest efforts in modelling electrolyte systems for practical applications. In spite of continuous developments the topic remains a challenge in chemical engineering and practical industrial application.[1,2,6,124] In most models, coulombic forces are accounted for with conventional DH or MSA based expressions.[3] Nevertheless, the growing interest in non-aqueous and mixed solvent electrolytes,[5,125] including ILs and salt-based deep eutectic solvents,[126–128] presents a need for revision and extension of electrolyte modelling strategies. Furthermore, the growing digitalization in the industry demands more standardized, predictive, consistent models.[2] Some recent advances in electrolyte modelling are emphasized.

For the sake of brevity, non-primitive LR approaches are omitted. A non-primitive approach considers coulombic interactions with explicit solvent molecules as dipoles, instead of a dielectric medium. For these, the works of Simonin,[129] Martínez Borquez et al.,[130] and Theiss and Gross[131] are representative examples of recent progress.

## 3.1 Strong Electrolytes

### 3.1.1 EoS for Electrolytes

The first Equations of State (EoS) for electrolytes were based on well-established cubic EoS combined conventional LR terms like DH theory or MSA.[132,133] These approaches continued to develop over time but mostly focused on aqueous systems.[134–137] EoS operate at the Helmholtz free energy level with the summation of a series of free energy contributions[6] like an EoS-based term that can be further divided into subgroups of attractive and repulsive contributions (e.g. Wertheim theory based terms). A Born term is usually included for ion energy transfer from vacuum to the liquid phase.

The cubic plus association EoS (CPA-EoS) combines cubic EoS like Redlich-Kwong-Soave or Peng-Robinson with an association term from the Statistical Associating Fluid Theory (SAFT)[138] to better represent hydrogen bonding interactions. With the work from Wu and Prausnitz[139] as background, Inchekel et al.[140] proposed an extension of the CPA-EoS for

electrolytes with the MSA as LR term including a concentration dependent permittivity. In their work, the models from Giese et al.[82] and Simonin et al.[83] (corresponding to the expressions in lines 3 and 4 from Table 2) were tested for the ion concentration dependent relative permittivity. Another electrolyte implementation of the CPA-EoS was published by Maribo-Mogensen et al.[141,142] The latter also included a concentration dependent relative permittivity of the mixture by means of equation (2.105) where the probability of association required for the Kirkwood g-factor was calculated from the Wertheim association term. This e-CPA was successfully applied for solubility, vapor-liquid equilibrium (VLE) and LLE in salt-based electrolyte systems, has been extended for ion-specific interaction parameters[143,144] and re-parameterized to correctly reproduce the trends of single ion activity coefficients.[145] Recently, the e-CPA EoS was modified by Roosta and Rezaei[146] to include specific ion-ion and ion-water association cites, which enabled the EoS to predict the conductivity of aqueous electrolytes with higher accuracy.

Fully SAFT- and group contribution SAFT-based EoS for electrolytes have gained attention in recent years.[147] Some of the first electrolyte implementations were SAFT2 for ions from Ji and Adidharma[148] and the SAFT-VR EoS[149] extension by Galindo et al.[150] The latter (SAFT-VRE) was applied for the calculation of aqueous MIAC values[151] and salting-out effects in aqueous systems.[152] Schreckenberg et al.[153] published a reformulation of the SAFT-VRE EoS with the non-restricted MSA as LR term, introducing the Born term in the model and a method to calculate the concentration dependency of the relative permittivity with respect to the solvent molecules. The model was able to describe MIAC values, VLE and salting-out effects in aqueous alcohol mixed solvent electrolytes.

The SAFT-VR Mie EoS[154–156] was extended by Eriksen et al.[157] with the primitive non-restricted MSA as electrostatic term, applied to calculate MIAC values of aqueous electrolytes up to the solubility limit and later applied to aqueous choline chloride mixtures.[158] Another extension by Selam et al.[159] applies DH theory as the LR electrostatic term. Both apply the Born contribution. The eSAFT-VR Mie EoS from Selam et al.[159] was successfully applied to the calculation of aqueous MIAC values, osmotic coefficients and the density of multiple salt solutions. Novak et al.[160] applied the eSAFT-VR Mie EoS for the estimation of gas solubility in concentrated aqueous electrolytes and rigorous isothermal flash calculations.[161] Walker et al.[162] systematically evaluated the eSAFT-VR Mie model for the aqueous NaCl case applying DH theory and MSA as electrostatic terms including a

solvent, salt and temperature concentration dependency of the relative permittivity. For the solvent related dependency, the method from Schreckenberg et al.[153] was taken; for the salt concentration dependency, the empirical expression used by Valiskó and Boda[163] was applied; and for the temperature dependency of the dielectric constant of pure water, the expression from Zuo and Fürst was taken.[134] Walker et al.[162] concluded that application of MSA or DH theories yield similar results, which is in agreement with the findings of Maribo-Mogensen et al.[164] More importantly, the authors demonstrated that concentration and temperature dependencies of the relative permittivity play a major role in the performance of the model. Subsequently, eSAFT-VR Mie EoS was extended by Novak et al.[125] for non-aqueous electrolytes by introducing a concentration dependent relative permittivity tested with two mixing rules and ultimately introduced in the model as a mole fraction mixing rule. The extended eSAFT-VR Mie EoS successfully reproduced the MIAC values and densities of non-aqueous single salt electrolytes. Furthermore, the working group of Kontogeorgis has documented considerations on the consistency of ion and mixed solvent concentration dependencies of the relative permittivity and its application in DH theory and EoS based approaches.[165–168]

The extension of SAFT with a perturbed chain contribution (PC-SAFT[169,170]) was first extended by Cameretti et al.[171] with DH theory and the Born term and applied to VLE and liquid densities in aqueous electrolytes. A later ePC-SAFT implementation with the primitive MSA as electrostatic term is reported by Lee and Kim.[172] The ePC-SAFT EoS from Cameretti et al.[171] was applied by Held et al.[173] for the MIAC of aqueous electrolytes, extended[174,175] for weak electrolytes by means of association/dissociation equilibrium and applied for the calculation of osmotic and activity coefficients of single salts in alcohols,[176] in aqueous amino acids,[177] and for the estimation of salting-out effects in aqueous two-phase systems.[178–180] The revised ePC-SAFT EoS included dispersion interactions between cations and anions to improve its accuracy at higher ion concentrations.[181] A concentration dependent relative permittivity was first incorporated in ePC-SAFT by Bülow et al.[182] and reformulated as ePS-SAFT *advanced*.[183] The latter was applied by Ascani and Held[184] to evaluate its impact in the modelling of electrolyte LLE systems. Ascani et al.[185] applied ePC-SAFT *advanced* for the calculation of multiphase equilibria with mixed solvents and mixed electrolytes. The ePC-SAFT *advanced* EoS was applied by Schick et al.[186] in combination with the correlative Pitzer equations for the estimation of the temperature dependent solubility of salts in organic solvents and the

framework has also been applied to model the extraction of lithium from magnesium-rich brines using ILs as extractants.[187] Schick et al.[188] also successfully predicted $CO_2$ solubility in aqueous and organic electrolyte mixtures and Ascani et al.[189] successfully predicted the pH of multiphase, multicomponent mixtures containing electrolytes.

The polar PC-SAFT EoS was extended for electrolytes by Rozmus et al.[190] as e-PPC-SAFT with MSA as the electrostatic term and a Born contribution. It was successfully applied to calculate MIAC values of salts in water, aqueous electrolyte densities and the temperature dependent solubility of gases in aqueous electrolyte. Yang et al.[191] provided ion specific parameter sets for the e-PPC-SAFT EoS for 15 aqueous alkali halide solutions and found that dispersion terms become increasingly relevant for lithium to water interactions. Ahmed et al.[192] introduced a concentration dependent relative permittivity in the e-PPC-SAFT EoS using the model from Giese et al.[82] and concluded that an ion concentration dependent relative permittivity is beneficial for model performance. A good account of other CPA and SAFT based EoS for electrolytes can be found in Ahmed et al.[192] and recent reviews of EoS for electrolytes in general can be found in Kontogeorgis et al.[6] and Held.[5]

Olsen et al.[193] compared e-CPA and e-PPC-SAFT by correlating densities, osmotic coefficients and MIACs of NaCl in water in a wide range of temperatures and pressures. Scenarios with and without dispersion and association forces for the ions were evaluated and several dependencies of the relative permittivity were also considered ($T$, v, $n$). While both EoS performed similarly, it was found that the dependencies of the relative permittivity, inclusion of both dispersion and association, and a temperature dependency of the binary interaction parameters all have a positive impact on model performance.

Naseri Boroujeni et al.[105] recently introduced a binding DH theory (BiDH) which combines DH theory with Wertheim's theory and the reference cavity approximation. BiDH is accurate compared to Monte-Carlo results for symmetric and asymmetric electrolytes due to the introduction of explicit ion-ion association sites. While further studies are pending, future EoS approaches with BiDH could provide considerable qualitative and quantitative corrections for both salt and IL systems in practical application.

In general, salt-based electrolyte EoS focus their application on mean ionic and osmotic coefficients, vapor pressures, densities and gas solubility in salt-based aqueous electrolytes. Salt solubility, LLE, apparent molar volumes and single ion activity coefficients are not so commonly studied.[6] Systematic extension to non-aqueous

electrolytes remains a challenge[5] increasingly addressed in recent years.[125,182,183] Finally, there is a lack of standardization in electrolyte EoS approaches, the use of the Born term, methods of validation and selection of a LR contribution.[6,167,168]

### 3.1.2 $g^E$-models for Electrolytes

In practical application, $g^E$-models like UNIFAC and COSMO-RS have a strong presence when it comes to (semi-)predictive power and $g^E$-models like UNIQUAC and NRTL have a strong presence when it comes to accurate system specific correlation. The fully correlative NRTL[194] model is a well-established standard in academic and industrial application. This extends to the electrolyte e-NRTL model[1,195,196] and is an indicator of the lack of predictive power in established, standardized EoS and $g^E$-models for electrolytes, as clearly stated in surveys about present industrial needs and requirements.[2,124]

Diverse electrolyte NRTL formulations can be found in the literature. The first e-NRTL from Chen and Evans[195,196] consists of a NRTL based contribution and the PDH term with a fixed $b_{constant}^{(x)} = 14.9$. An alternative electrolyte NRTL reformulation by Liu et al.[197] modified the model to account for more transferable ion specific parameters instead of salt specific parameters and introduced the use of the Born term and a modification of the DH theory. The e-NRTL model from Chen and Evans[195,196] is widespread and has undergone changes and modifications. The most relevant are a generalized extension for multicomponent mixtures by Chen and Song,[198] and a reformulation of the generalized extension to apply the symmetric reference state by Song and Chen.[199] In the same fashion, the NRTL-SAC model from Chen and Song[200] has also been extended for electrolytes[201] with an asymmetric and symmetric[202] reference states for the ions. Another electrolyte NRTL implementation including a Born and PDH terms can be found in Olaya et al.[203]

The first electrolyte extensions of UNIQUAC with DH theory and the third term of a virial expansion with system specific parameters are reported by Christensen et al.[204] and Sander et al.[205,206] who successfully correlated the SLE, VLE and LLE of several electrolyte systems. The virial term was dropped off in later implementations and the method extended to multiple solvent electrolytes.[207–209] Further electrolyte UNIQUAC implementations can be found in the literature, including the LIQUAC[210,211] model, which

kept the use of a virial term and has been applied and has been extended for multiple solvent electrolytes[212–215] and undergone revisions and extensions.[216] Overall, the LIQUAC model has also proven to be successful in the correlation of phase equilibria in electrolyte systems. A similar implementation is that of Anderko et al.[217] which exhibits comparable capabilities.[218–220] The latter at some point introduced a concentration dependent relative permittivity in the LR electrostatic term via a model developed by Wang and Anderko.[84] This was however dropped in later applications of the model.

In a similar fashion, UNIFAC based approaches, which provide a higher semi-predictive nature compared to UNIQUAC, have been extended for electrolyte systems. Most notably, the LIFAC model[216,221] (analogous to the LIQUAC model) and the AIOMFAC model[222] have undergone extensions to successfully correlate and predict MIACs and phase equilibria (LLE, VLE, SLE) in (mostly mixed aqueous) electrolyte systems.[216,223–225]

The first COSMO-RS based model for electrolytes was proposed by Hsieh and Lin[10] who combined the COSMO-SAC model[118,226] with the PDH term and tailored COSMO-SAC-based short-range equations for the ionic interactions which were trained with MIAC values at room temperature. The model proved capable of predicting VLEs, osmotic coefficients and mixed solvent MIACs in aqueous electrolytes. In the same year, Wang et al.[13] suggested a different approach applying combined electrolyte sigma profiles instead of single ion sigma profiles with COSMO-SAC and the PDH term. The latter approach was only tested for sodium chloride in water and water-ethanol mixtures and was not developed further. Ingram et al.[9] suggested a different approach by scaling the hydrogen bonding interaction energies of ion specific interactions in COSMO-RS and adding the PDH term for LR electrostatics. The latter model was systematically tested with a broad LLE database of mixed aqueous electrolytes. The COSMO-RS-ES model from Gerlach et al.[14] followed as continuation of the efforts from Ingram et al.[9] The COSMO-RS-ES model is capable of accurately reproducing aqueous MIACs and predicting phase equilibria in mixed aqueous electrolytes[14,15,227] at room temperature and has already been detailed in section 2.4.

Toure et al.[11,228] combined the COSMO-RS model with the PDH term for LR electrostatics to estimate the MIAC of salts in pure water. In their approach, no modifications to COSMO-RS were performed. Instead, COSMO calculations were performed for explicitly solvated ions. These ion-solvent clusters were then introduced in the calculation and treated with

the conventional COSMO-RS misfit and hydrogen bonding energy interactions. Chemical equilibrium between the diverse solvated clusters down to the bare ions was applied. The method was later applied to a mixed solvent electrolyte.[12] The method requires building explicit solvation clusters, which hinders its transferability to more complex mixtures, but provides a sound proof of principle for simple electrolytes in pure water.

Recent approaches[229] also modelled ionic systems applying explicit solvated ion clusters with equilibrium reactions. Silva et al.[230] also modelled the SLE of several choline chloride based deep eutectic solvents with a tailored COSMO-RS approach (4 parameters). These approaches neglected coulombic LR interactions and were fitted to small datasets.

The electrolyte COSMO-SAC, the COSMO-RS-PDHS and the COSMO-RS-ES models apply the PDH term with a fixed parameter of closest approach ($b_{constant}^{(x)} = 14.9$: a choice possibly attributed to the e-NRTL convention trickling down to other models) and have not been systematically extended for non-aqueous single solvent and mixed solvent electrolytes.

## 3.2 State of the Art Modelling of Ionic Liquids

ILs are considered as designer solvents due to the simple fact that the number of possible cation/anion combinations is virtually endless. The are commonly modelled with little to no consideration for their electrolytic nature; efforts have focused on predictive screening based on COSMO-RS, group contribution methods, Quantitative Structure Property Relationship (QSPRS) methods, lattice models and SAFT-based EoS.[231–234]

Consequently, abundant literature that neglects coulombic ion-ion interactions can be found.[128,231] Lubben et al.[235] compared the performance of NRTL and PC-SAFT correlations, and COSMO-RS and COSMO-SAC predictions, in the calculation of LLEs in systems with $NTf_2$-based ILs. The authors considered NRTL and PC-SAFT as applicable methods. COSMO-RS methods are qualitatively reliable but present systematic quantitative inaccuracies that cannot be properly characterized based on the nature of the cation and anion due to the fact that a large amount of the available data corresponds to imidazolium-based cations with a bistriflimide ($NTf_2$) anion. Thangarajoo et al.[236,237] developed a group contribution method for the prediction of the IDAC of alcohols in pure ILs with an average absolute relative deviation (AARD) of 11.97% for methanol, 7.49%

for ethanol and 9.91% for 1-propanol. Lee et al.[238] developed a machine learning model for the prediction of IDACs of neutral molecules in pure ILs using artificial neural networks. In their comparison, the resulting model is 10 to 50% more accurate than COSMO-RS, UNIFAC and Abraham solvation parameters. Li et al.[239] trained a factorization machine based neural network with over 50,000 IDAC data points in a temperature range of 288.15 to 428.15 K. The reported AARD was lower than 8% for all solvent classes. Benimam et al.[240] applied a support vector machine regression (SVMr) algorithm trained with 2666 data points to calculate the IDAC of diverse solutes in pure ILs. The regression included sigma profile descriptors from COSMO calculations. The reported root mean square error (RMSE) of 0.18 was compared to an RMSE of 1.12 reported for COSMO-RS. Dong et al.[241] applied the UNIFAC method for the calculation of binary and ternary VLEs and gas solubility in IL systems. The missing UNIFAC chemical group binary interaction parameters were estimated from COSMO-RS based calculations (the so-called integrated COSMO-UNIFAC approach). The authors concluded that the model provides "moderate" quantitative predictions when the UNIFAC parameters are vacant and consequently estimated via COSMO-RS.

The COSMO-RS method is well established for IL screening,[242–245] VLE calculations[244,246] and qualitative estimates of LLE in binary and ternary IL-containing systems.[247–250] It has even been applied in systems with mixed salt and IL electrolytes.[251] In spite of the fact that the coulombic nature of ILs is omitted, it is the standard to model their activity coefficient as a mean ionic property assuming full dissociation (also known as the "electroneutral approach"), as described by Diedenhofen and Klamt.[252]

Thorough, systematic evaluations of the COSMO-RS methodology applied to IL systems have been performed. Paduszyński[116] evaluated the capabilities of COSMO-RS in the prediction of infinite dilution activity coefficients of neutral molecules in pure ILs and an AARD of 84.6% was reported for COSMO-RS (at the TZVP parameterization level) for 41868 data points from 8554 binary systems. Paduszyński[115] also evaluated the capabilities of the model in predicting the liquid-liquid phase equilibria of binary and ternary systems containing ILs. This evaluation was updated a couple of years later by Paduszyński and Królikowska,[253] reporting a RMSE of 0.142 and 0.136 for COSMO-RS (TZVP parameterization level) with the lowest energy conformer and all conformer sets, respectively. These, and other studies,[245,248,248,254] conclude that the COSMO-RS method

alone is promising and qualitatively reliable for qualitative prediction. Nevertheless, the model presents notable quantitative deviations and, in some cases, fails to predict an LLE split or considerably deviates from experimental $\gamma_i$ and $\gamma_i^{\infty}$ values depending on the nature of the species involved.[115,116,253] The COSMO-RS model was also evaluated by Fernandez et al.[255] for the estimation of fusion properties of choline chloride through in silico prediction of the SLE of choline chloride combined with other ionic compounds.

Han et al.[256] performed an IL specific parameterization of ADF-COSMO-RS (a COSMO-RS implementation) with a training set of 2283 neutral molecule IDAC values and 1433 experimental solubility values of CO2 in diverse ILs. Essentially, the misfit parameter and effective surface contact area were parameterized to the experimental solubility data. The quantitative accuracy of the predictions improved for IL systems (ARD of 32.2%), further demonstrating the potential of the method for IL applications. Schneider et al.[257] extended the F-SAC model (a combination of group contribution and COSMO-RS based calculations) for ionic liquids introducing 25 new IL parameters fitted to 1332 IDAC data points. Predictions were then performed for VLE and LLE systems containing ILs.

Considerable efforts to address the electrolytic nature of ILs have been performed with the COSMO-SAC model.[118] Lee and Lin[258] combined COSMO-SAC with the PDH term to estimate MIAC values, IDAC values of neutral compounds and VLE in IL systems. It was found that the full dissociation assumption in the PDH term results in large systematic deviations. The use of an effective ionic strength with reduced IL dissociation provided systematic corrections to this issue. The corrections applied by Müller et al.[16] to the COSMO-RS-ES model for salt-based electrolyte systems are conceptually similar. Lee and Lin[259–261] further explored the concept of partial dissociation in ionic liquid systems with the COSMO-SAC + PDH model. The dissociation constant between the ions was estimated based on an assumed dissociation degree of 35% for all ionic liquids at the molecular-solvent-free limit, thereby providing successful predictions with a set of 9857 data points consisting of IDAC values, VLE and LLE measurements as well as osmotic and activity coefficients from the literature. Chang and Lin[262] proceeded to extend the PDH term by introducing the compositional derivatives of the relative permittivity, density and molar mass into equation (2.49), thereby developing an extended PDH term (E-PDH. This extension improved the performance of the model for the prediction of phase equilibria and activity coefficients in ionic liquid systems and was later applied to an improved

COSMO-SAC + E-PDH model that considers differentiated hydrogen bonding at the interacting surface level based on the chemical groups.[263] The reported RMSE for 3555 IDAC datapoints was 0.71 assuming full association (no LR), 0.77 with 35% dissociation and 0.93 with full dissociation. Thus, considerable literature confirms that tailoring[264] a COSMO-RS based contribution and extending LR electrostatics[262] can be consistently performed and systematically evaluated.[263] Nevertheless, the COSMO-SAC + E-PDH result remains best for IDAC calculations when the LR electrostatic term is fully neglected, which contradicts theoretical evidence of electrostatic forces present in pure ILs.[96,265,266]

Efforts to model ILs with EoS omitting LR electrostatics are also abundant in the literature and include PR, RKS, CPA, Group Contribution EoS, Lattice Model EoS and SAFT-type EoS.[267] These approaches consider an IL as a fully associated entity (an exception is the he-SAFT model from Ji and Adidharma[268] for dissociated ions but no LR electrostatics).

Paduszyński and Domańska[269] evaluated the performance of PC-SAFT for IL systems with a methodology for the estimation of binary SLE, LLE, VLE, surface tension, critical properties, among other properties. Temperature dependent parameters and adjustment of binary interaction parameters to IDAC values were required. Missing binary interactions were estimated based on UNIFAC. Various thermodynamic properties could sometimes be reproduced with excellent accuracy, particularly when the interaction parameters were fitted to reliable experimental data. Gharehzadeh Shirazi et al.[270] modelled thermodynamic properties of mixtures containing an IL with PC-SAFT and compared results fitting the model to experimental data and to COSMO DFT estimates. Maia et al.[267] applied the CPA EoS for the calculation of LLE and VLE of systems with ILs. The CPA model performed satisfactorily for VLE calculations, but LLE calculations presented larger deviations when reproducing the experimental data. The authors concluded that additional work is needed in order to define a standardized approach.

Andreu and Vega[271] introduced the modelling of $CO_2$ solubility in ILs with soft-SAFT (a SAFT version that applies a Lennard-Jones fluid as the reference state, instead of hard spheres). More recently, Crespo et al.[272] developed a robust soft-SAFT implementation parameterized with high pressure density of ILs to estimate pure compound properties.

Notable efforts for the treatment of ILs as dissociated electrolytes have been reported with SAFT-type EoS. Guzmán et al.[273] compared the soft-SAFT implementation from Andreu and Vega[271] with an electrolyte SAFT implementation with MSA for the

correlation of Monte-Carlo calculated orthobaric IL densities. The electrolyte SAFT-MSA equation consistently outperformed soft-SAFT. Ji et al.,[274,275] Ji and Held[276] and Shen et al.[277] used the ePC-SAFT model to estimate the solubility of gases in IL systems, the density of ILs and their second order thermodynamic derivative properties (e.g. isothermal compressibility) with reliability in a wide temperature and pressure range (0°C to 140°C and 0.1 to 150 MPa). Shen et al.[278] applied ePC-SAFT to describe the behavior of $CO_2$/IL mixtures confined in nanopores. Sun et al.[279] described a method to detect fictitious liquid-liquid critical lines due to possible unstable solutions to ePC-SAFT when describing pure IL properties. Subsequently, Dai et al.[280] applied the published parameters to perform IL screening with ePC-SAFT for $CO_2$ separation technologies.

ePC-SAFT *advanced* has also been applied to IL systems by Bülow et al.[182] to describe the LLE of binary systems containing water and an IL. Results were compared with ePC-SAFT from Ji et al.[274] and the authors concluded that ePC-SAFT *advanced* had a better performance due to the introduction of a concentration dependent relative permittivity.

Jiřiště and Klajmon[281] compared PC-SAFT and COSMO-RS based approaches for the calculation of isobaric heat capacity, vapor pressure, enthalpy of vaporization and solubility of $CO_2$ in ILs. PC-SAFT was applied as the original model from Gross and Sadowski[169,170] and the ePC-SAFT model from Cameretti et al.,[171] whereas COSMO-RS was applied with molecular (fully associated) and electroneutral (fully dissociated) approaches, but with no contribution for LR coulombic forces. While results were mixed depending on the desired property, ePC-SAFT and COSMO-RS (both approaches) were recommended for $CO_2$ solubility estimation. The authors commented on the molecular IL approach being better with COSMO-RS for pure IL property predictions and the electroneutral approach being better for mixtures. The authors recommend COSMO-RS and ePC-SAFT as the candidates for further improvement.

Finally, studies where IDAC and phase equilibria in IL systems are correlated can be found in the literature with electrolyte UNIQUAC implementations.[282,283] Shariatmadar Tehrani and Haghtalab[284] compared the performance of UNIQUAC, electrolyte UNIQUAC and electrolyte NRTL implementations in correlating aqueous two phase systems containing salts and ILs. The authors concluded that the electrolyte versions outperformed the non-electrolyte model. Notably, Ganguly et al.[285] were the first to combine an electrolyte UNIQUAC implementation with the E-PDH term from Chang and Lin.[262] Ganguly et al.[285]

concluded that introduction of the thermodynamically consistent E-PDH term enhanced the performance of the UNIQUAC model when describing the LLE of IL-containing biphasic mixtures. The e-NRTL model has also been recently applied to model dissociation of ILs in the work of Lin et al.[286] with the symmetric PDH term for LR electrostatics.

A large number of studies have correlated phase equilibria of IL containing systems with non-electrolyte NRTL, UNIQUAC and UNIFAC implementations. These are not reported here for the sake of brevity and arguable state-of-the-art modelling.

# 4 Objectives

There exists a wide variety of modelling approaches to describe phase equilibria in electrolyte systems. However, most have an applicability that reduces to aqueous systems and small ions. Some of these models have been specifically tailored to describe more complex systems in special applications. Nevertheless, universal applicability is lost as different model versions with different parameters and approaches are documented. The objective of the present work is to provide a consistent extension of the COSMO-RS-ES model that can describe activity and phase equilibria in a broad range of electrolytes spanning from the simplest aqueous salt systems to multicomponent non-aqueous systems and the ionic liquid state with the same basis and parameters for species.

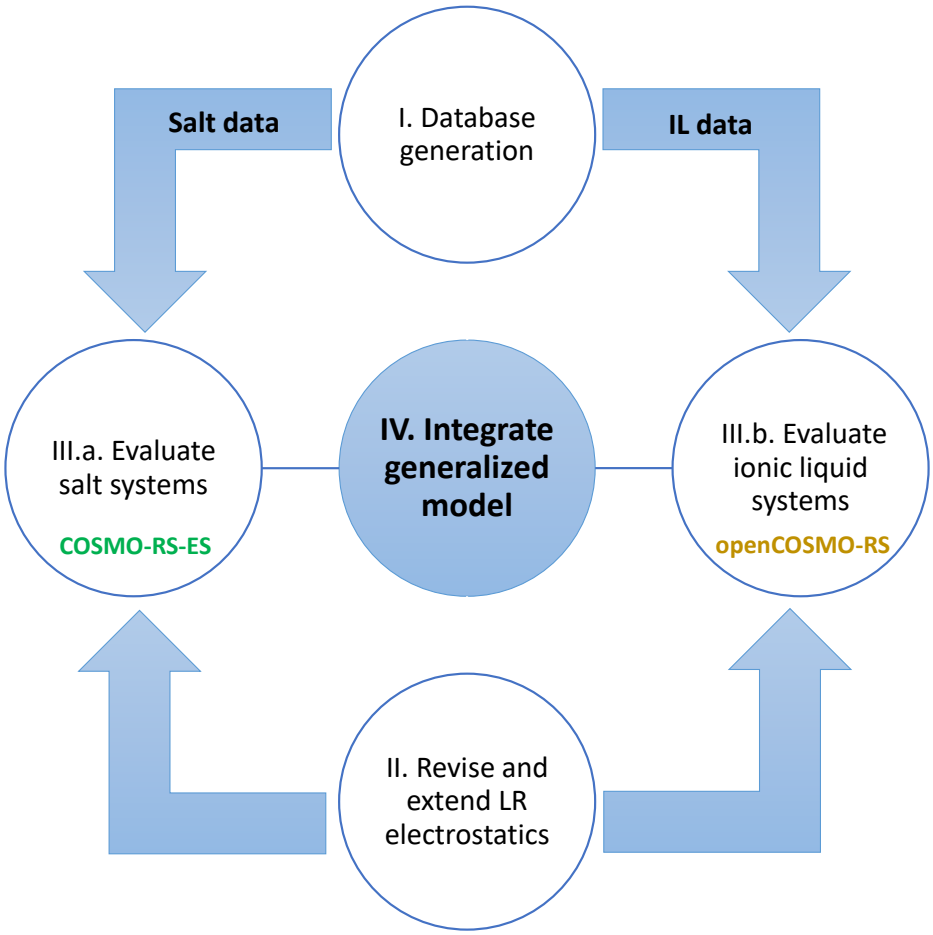


**Figure 12. General overview of the present work to integrate a fully extended COSMO-RS-ES model which improves the modelling of IL systems by treating them as electrolytes while retaining precision and predictive power for conventional salt-based electrolytes.**

The structure of the present work is shown in Figure 12 with the following milestones:

I. Database generation: Enlarging and curating the database applied for the parameterizations of the COSMO-RS-ES model has always been a continuous process. The present work seeks to include new datasets focused on LLE data of systems containing ILs and IDAC of neutral solvents in pure ILs. The search includes the recent literature and publicly available databases.

II. Revise and extend long-range electrostatics: As previously stated in section 3, recent systematic modelling approaches of non-aqueous electrolyte and IL systems have emphasized the need for extensions of the conventional electrostatic theory. An electrostatic term that can be simultaneously applied with the same basis to both conventional salts and ILs is non-existent. For this reason, a literature review regarding the potential considerations for non-aqueous electrolytes is conducted. These include both theoretical and empirical approaches to the modelling of non-aqueous electrolytes to seek or develop an appropriate LR term that replaces the PDH term in the COSMO-RS-ES model to improve and extend its reach.

III. Application to electrolyte systems: The present work aims to support the hypothesis that it is more convenient to treat ILs as electrolytes. A LR electrostatics term that is consistently applicable to both salts and ILs can be tested in separate settings:

a) Application to conventional salt systems. Changes to the COSMO-RS-ES model are introduced with focus on improving its performance for highly concentrated non-aqueous systems by means of modified LR electrostatics and re-parameterization of the SR interactions.
b) Application to IL systems. It is relevant to evaluate the same developments for LR electrostatics in a COSMO-RS-ES-independent setting (i.e. with the basic, unmodified COSMO-RS theory) at the molecular-solvent-free limit. This provides insights into the physical significance of LR electrostatics when combined with an established predictive method: COSMO-RS alone provides mixed to satisfactory results in IL systems, then this should be built upon, not disregarded.

IV. Integration into a single model: the central objective is to integrate COSMO-RS based approaches for salts and ILs into a generalized model. Of central relevance is the proof of principle that ILs and salts can be treated predictively and with the same basis.

# 5 Database and Computational Methods

## 5.1 Database

In previous studies, the COSMO-RS-ES model has been parameterized with extensive datasets comprising MIACs, LLEs and free energies of transfer of ions.[14–16] However, the specific number of selected data points and systems employed in each parameterization has varied slightly due to continuous data curation and introduction of new systems from the literature. In the present work, a systematically updated and curated database was generated with special focus on ionic-liquid systems. The characterization presented in the following pages corresponds to the latest available dataset before completion of this manuscript and was applied for parameterization in the concluding section 6.4.3.

### 5.1.1 Salt-Based Electrolytes and Single Ion Energies of Transfer

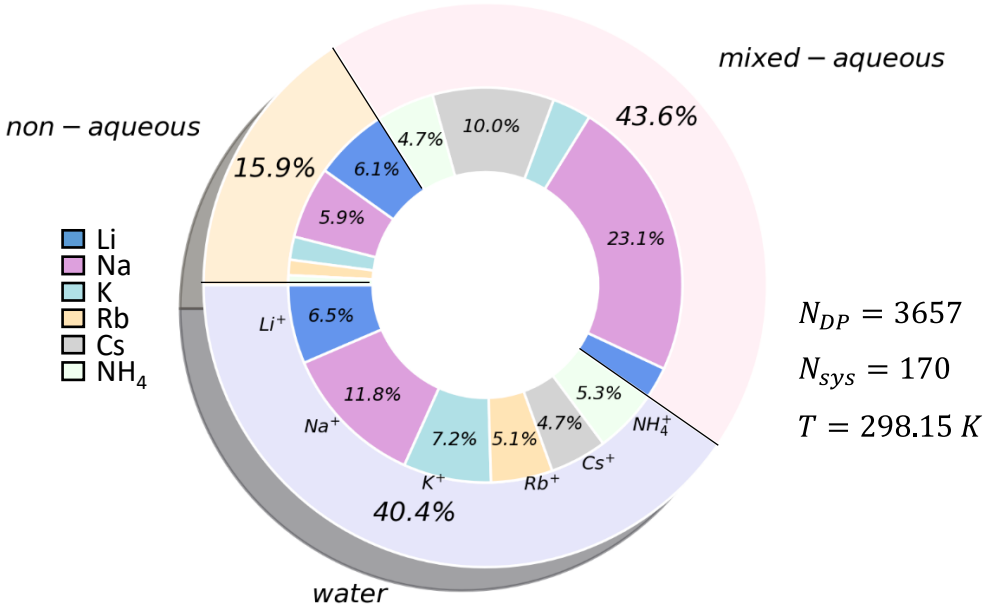


**Figure 13. Characterization of the mean ionic activity coefficient database of salt systems at room temperature; 59.9% of all data points correspond to alkali halides.**

Figure 13 shows a brief characterization of the room temperature MIAC database applied in the present work. Most of the data corresponds to aqueous systems (either pure water

as solvent or a mixed aqueous solvent). Non-aqueous systems are not direct experimental measurements but correlations from experimental osmotic coefficients with the Pitzer-Mayorga equations or numerical conversions via the Gibbs-Duhem relation. For this reason, their contribution to the total objective function (section 5.2) is lower than that of the aqueous systems, which are considered more reliable. Literature sources for the salt + water systems at room temperature have been described elsewhere.[14] Literature sources for the mixed- and non-aqueous systems are included in the Appendix.

In addition to previously available data, this work incorporates temperature dependent MIAC datasets for a range of salts in water from the Joint Expert Speciation System (JESS) database,[287–291] namely from the curated thermo-physical database JESS-FIZ. While these data are not part of the training set, they are integrated as pseudo-experimental data generated from a Pitzer-Mayorga fit to test the model in section 6.4.3. Due to licensing restrictions, the JESS-FIZ data is neither shared nor characterized. Broadly, it corresponds to the MIAC of alkali halide salts in a temperature range from 0 to 210°C in pure water.

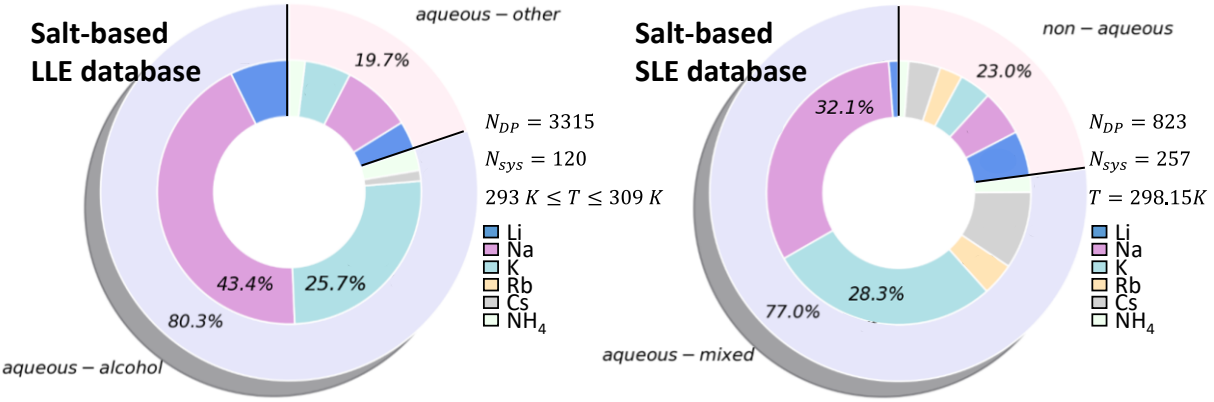


**Figure 14. Left: Characterization of the experimental salt-based LLE database. Of the 3315 datapoints, 1056 correspond to salt partitioning (69.97% are alkali halides) and the remaining 2259 correspond to solvent partitioning. Right: Characterization of the experimental SLE database.**

Characterization of the LLE database is shown in Figure 14 – left. The experimental LLE database of conventional salt systems remains the same as in previous publications and its literature sources have been described elsewhere.[14] In the present work alkali earth ions were excluded. Of the 3315 available datapoints for partitioning coefficients, 1056 correspond to the partitioning coefficients of the salts and are part of the training set. The partitioning coefficients of the neutral species are not used in the training set. Characterization of the solid-liquid equilibria (SLE) of salt containing systems is shown in

Figure 14 – right. The sources of this database have also been characterized in previous works.[16] The SLE database is used for validation and is not part of the training set.

Global remarks regarding the available MIAC, LLE and SLE data can be made. Firstly, the most common anion is, unsurprisingly, chloride and consequently the most common salts are NaCl and KCl. In contrast, data for systems with cesium salts is scarce and even more so for rubidium salts. Secondly, most mixed aqueous systems involve an alcohol as co-solvent and the most common co-solvent family in the data for single ion energies of transfer (Figure 15) are alcohols as well.

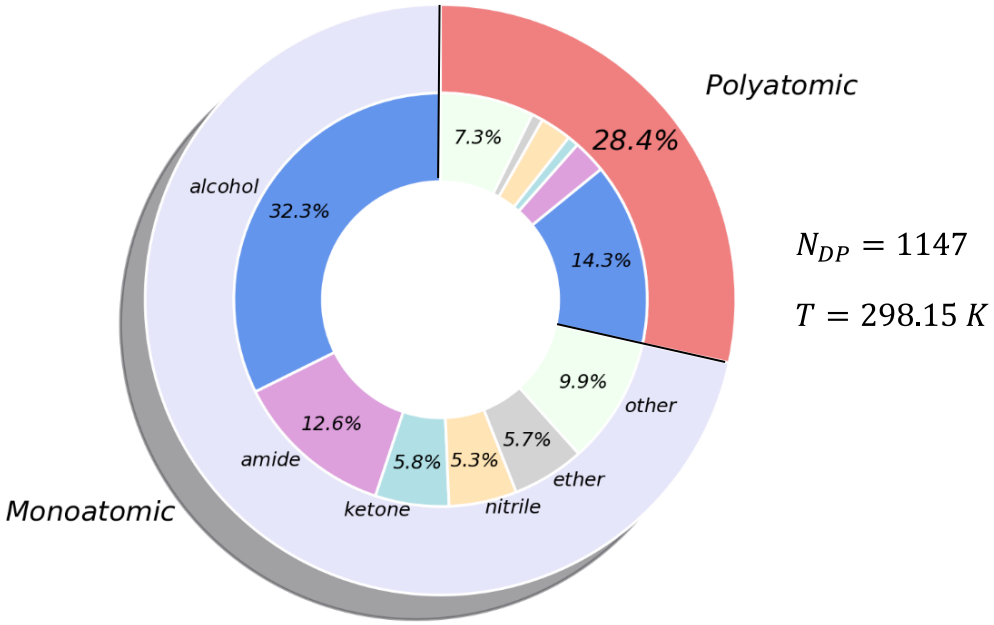


**Figure 15. Characterization of the database for Gibbs-free energies of transfer of single ions from water to single and mixed organic solvents.**

Figure 15 provides visual characterization of the single ion free energies of transfer extracted from Kalidas et al.[121], Marcus[123], Gulaboski et al.[292], Olaya et al.[293], Marcus,[294] Osakai et al.[122] and Kihara et al.[295] Roughly 87% of all data points belong to the first two of the aforementioned publications. Most data belong to monoatomic ions. The most abundant data for polyatomic ions found in ILs corresponds to tetra-alkylammonium ions (183 data points, from which 67% are transfer from water to three solvents: acetonitrile, ethanol and methanol). Gibbs free energies of transfer are used as part of the training set in the final parameterization of this work.

### 5.1.2 Ionic Liquid Systems Database

Ionic liquid data acquired during this work are the latest addition to the dataset and represent a significant growth of its scope. The largest IL subset consists of infinite dilution activity coefficients (IDACs) of neutral species in pure ILs and IL mixtures. These were extracted from the publicly available IL-Thermo database.[296,297] In total, 46,158 datapoints were retrieved. Of these, binary systems (neutral molecule + IL) for which the relative permittivity of the neutral solvent is known, were selected. The resulting 21,634 datapoints are characterized in the upper frames of Figure 16 and were used in the training set of the final parameterization. Further details are provided in the Appendix.

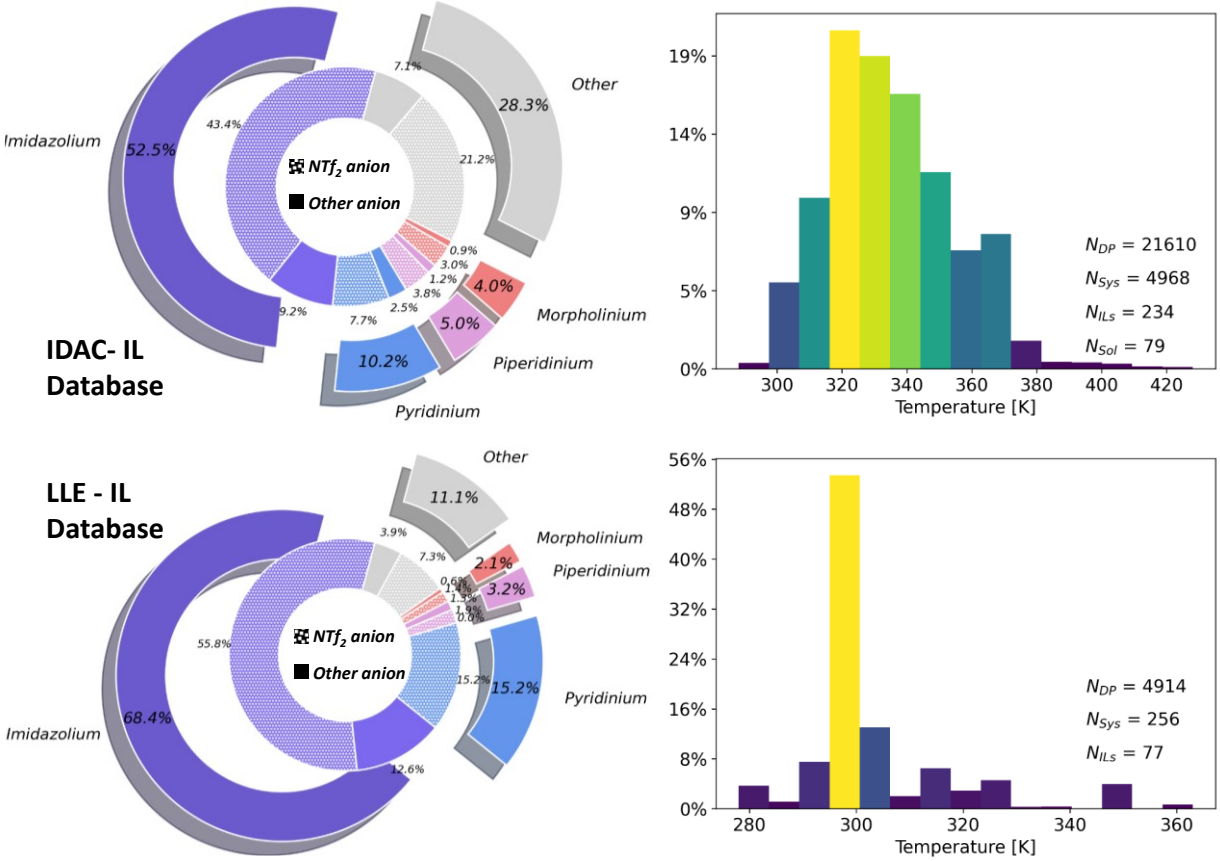


**Figure 16. Characterization of the IDACs database taken from IL-Thermo[296,297] and IL ternary LLE systems taken from Paduszyński.[115] From the 4914 datapoints of the LLE systems, 1637 correspond to the partitioning of the IL and the rest to the partitioning of the neutral compounds. Both datasets predominantly involve imidazolium and pyridinium based ILs with a bistriflimide ($NTf_2$) anion.**

Finally, 4914 experimental partitioning coefficients from ternary LLE systems containing an IL were taken from the work of Paduszyński.[115] These are characterized in Figure 16 (lower frames). Only 1637 of the total datapoints correspond to the partitioning of the IL

and were used in the training set of the final parameterization. A tabular summary of these can be found in Appendix Table 3.

## 5.2 Computational Methods

All COSMO-RS-ES and openCOSMO-RS calculations performed in the present work make use of the parameters shown in Table 3 for interactions between neutral compounds. Parameters for ion-specific equations are described further down in the corresponding chapters. Activity coefficient calculations for all species include the Staverman-Guggenheim equation as combinatorial term.

COSMO files for all neutral and ionic species were generated with COSMOconf 3.0 and Turbomole 6.6 software at the def-TZVP basis using DFT with the BP-86 functional.[110,298] Calculations are performed with the lowest energy conformer for each species given that COSMO-RS-ES does not handle multiple conformers.

The following objective functions to minimize the difference between calculated and experimental values were applied during the parameterization procedures:

a) For the mean ionic activity coefficients:

$$\mathrm{OF_{MIAC}} = \mathrm{W_{MIAC}} \sum_{i=1}^{N_{DP}} \left(\ln\left(\gamma_{\pm,i}^{calc}\right) - \ln\left(\gamma_{\pm,i}^{exp}\right)\right)^2 \tag{5.1}$$

b) For LLE systems:

$$\mathrm{OF_{LLE}} = \mathrm{W_{LLE}} \sum_{i=1}^{N_{DP}} \left(\ln\left(K_{salt/IL,i}^{OS,calc}\right) - \ln\left(K_{salt/IL,i}^{OS,exp}\right)\right)^2 \tag{5.2}$$

where the partition coefficient $K_{salt,i}^{OS}$ relates to the partitioning of the salt (or IL) between the ion-rich phase and the ion-poor phase:

$$K_{salt,i}^{OS} = \frac{\gamma_{\pm}^{S}}{\gamma_{\pm}^{O}} = \gamma_{\pm,O\rightarrow S} \tag{5.3}$$

c) For Gibbs free energies of transfer of single ions:

$$\mathrm{OF_{GT}} = \mathrm{W_{GT}} \sum_{i=1}^{N_{DP}} \left(\ln\left(\gamma_{w\to o,i}^{calc}\right) - \ln\left(\gamma_{w\to o,i}^{exp}\right)\right)^2 \tag{5.4}$$

where, as denoted by the subscript $w \to o$, all free energies relate to single ion transfer from water to some organic or mixed solvent.

d) For infinite dilution activity coefficients of neutral molecules in ILs:

$$\mathrm{OF_{IDAC}} = \mathrm{W_{IDAC}} \sum_{i=1}^{N_{DP}} \left(\ln\left(\gamma_{s,i}^{\infty,calc}\right) - \ln\left(\gamma_{s,i}^{\infty,exp}\right)\right)^2 \tag{5.5}$$

The total objective function is the weighted sum of the objective functions of the different system types (ST):

$$\mathrm{OF_{tot}} = \sum_{\mathrm{ST}} \mathrm{OF_{ST}} \tag{5.6}$$

The objective functions are weighted by a factor W, which is chosen in order to give the diverse system types a total objective function of roughly the same order of magnitude at the initial point of the parameterization.

For aqueous MIAC values, $\mathrm{W_{MIAC}} = 60$; for mixed solvent $\mathrm{W_{MIAC}} = 40$ and for single-solvent non-aqueous MIAC values, $\mathrm{W_{MIAC}} = 15$. For LLE systems with salts $\mathrm{W_{LLE}} = 3$ and for LLE systems with ILs $\mathrm{W_{LLE}} = 2$. Gibbs free energies of transfer of ions are the least reliable dataset, given their extra-thermodynamic assumptions[299] based on ion size, therefore a low value of $\mathrm{W}_{GT} = 0.3$ was chosen, so that the objective function of these data is roughly half of the objective functions of the other datasets. Finally, a value of $\mathrm{W_{IDAC}} = 0.7$ was selected for the infinite dilution activity coefficients, which provided an objective function equal to that of the combined LLE databases at the starting point.

The selected quantitative and qualitative measures for evaluation are the average absolute deviation (AAD) and the average relative deviation (ARD) for the logarithmic properties applied in the objective functions:

$$\mathrm{AAD} = \frac{1}{N_{DP}} \sum_{i=1}^{N_{DP}} \left|\mathcal{P}_i^{calc} - \mathcal{P}_i^{exp}\right| \tag{5.7}$$

$$\mathrm{ARD} = \frac{1}{N_{DP}} \sum_{i=1}^{N_{DP}} \left( \mathcal{P}_i^{exp} - \mathcal{P}_i^{calc} \right) \tag{5.8}$$

where the corresponding property $\mathcal{P}$ is the calculated and expected logarithmic solubility products in the case of salt solubility data, the logarithmic partitioning coefficient in the case of LLE data, the logarithmic MIAC and the logarithmic activity coefficients for IDAC and single ion free energy of transfer data, unless explicitly stated otherwise. In some representative cases the distribution of the relative deviation and an appropriate probability density function (PDF) are also presented for further evaluation.

The algorithms applied in the different parameterizations were Nelder-Mead, Levenberg-Marquardt and differential evolution. Any calculations of data types that belong to the training set (e.g. ternary LLE, IDAC, MIAC) are correlations. Any calculations that do not belong to the training set (e.g. binary LLE, salt solubility) are considered pure predictions.

# 6 Results and Discussion

## 6.1 The Modified PDH Term

In the following section the systematic deviation of linear electrolyte theories for low permittivity systems is addressed. To qualitatively correct this deviation without the need for iterative speciation approaches, a modified PDH term (M-PDH) is proposed with a new parameter of closest approach. This electrostatic term is applied to the COSMO-RS-ES model for the calculation of MIAC values and phase equilibria in salt systems. Its use yields an improvement of the calculations and predictions for liquid phases with a low relative permittivity. Some results of this section were published by González de Castilla, et al. *J Mol Liq.* 2021; 326, 115204.[17]

### 6.1.1 Semi-Empirical Development

Linearized theories, namely the RP-MSA (equation (2.98)) and DH theory (equation (2.31) or the PDH term from equation (2.51)), remain the most widely used contributions applied for electrolyte modelling (with $g^E$-models and EoS) in chemical engineering.[1–3,6] In some specific applications, ion-pairing theories combined with these terms are invoked as a correction.[16,184] In general, the choice between MSA-based and DH theory-based approaches seems arbitrary. The differences and advantages or disadvantages between both theories are blurred in practice by parameterization and the choice between them remains a topic of discussion in the literature.[3,5] Maribo-Mogensen et al.,[164] analyzed the trends of the volume, composition and temperature derivatives of $\Delta A^{el}$ (the Helmholz free energy of electrostatic origin) from DH theory and MSA (non-restricted primitive) concluding that both theories yield qualitatively similar results. This work found that scaling the distance of closest approach in DH theory $a_{DH}$ as $^5/_6$ of the distance of closest approach used in MSA (hard-sphere diameter $\sigma_{MSA}$) makes the theories behave very similarly. Thus, a major finding of their work is that, when $a$ is an adjusted parameter, the difference between MSA and DH theory is blurred during parameterization with chemical

engineering models. Nevertheless, there are some open questions of interest for this work:

1) Does the impact of scaling $a_{DH} = \frac{5}{6} a_{MSA}$ extend to solvents other than water?
2) Why does a factor $a_{DH} = \frac{5}{6} a_{MSA}$ make the theories behave similarly?
3) Does this have any additional implications in practical modelling?

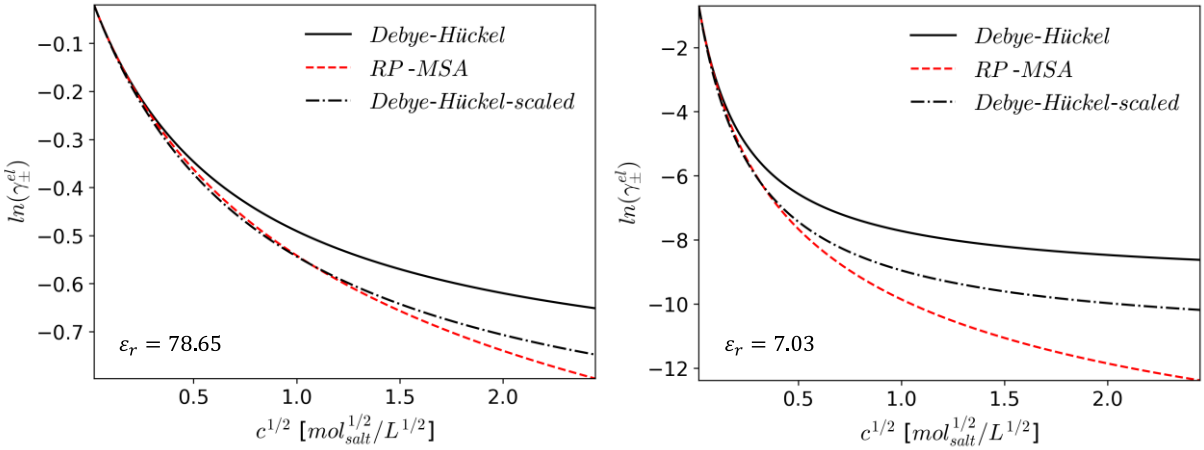


**Figure 17. Logarithmic mean ionic activity coefficients of electrostatic origin calculated with the RP-MSA and DH theory, where the dash-dotted black line is DH theory with $a_{scaled} = \frac{5}{6} a$. Calculations for $a = 4.25$ Å at room temperature with $\varepsilon_r = 78.65$ (left) and $\varepsilon_r = 7.03$ (right).**

The first question can be answered by testing calculations with different dielectric constant values, as shown in Figure 17, which compares calculations of the mean ionic activity coefficient of electrostatic origin as calculated with RP-MSA and with DH theory. Two calculations for DH theory are shown: one with the selected distance of closest approach $a$ and one where this distance of closest approach is replaced by the scaled value $a_{scaled} = \frac{5}{6} a$. Qualitatively, similar trends are observed. This is an expected result, given that the screening lengths $\Gamma$ and $\kappa_D$ in the linearized MSA and DH theory, respectively, are both functions with the same dependency $\propto \varepsilon_r^{-1/2}$. Thus, the qualitative trends for $\Delta A^{el}$ and its derivatives with respect to volume, composition and temperature, hold accordingly. Nevertheless, it is also observed that the numerical similarity between both theories require a different scaling factor for the low relative permittivity case.

For RP-MSA and DH theory to have a better numerical agreement in Figure 17 (right) that is comparable to Figure 17 (left), one would require a scaling factor that is closer to $^2/_3$ instead of $^5/_6$. Thus Maribo-Mogensen et al.[164] correctly assert that the choice between

theories loses significance when $a$ is an adjustable parameter; but fixing $a_{DH} = \frac{5}{6} a_{MSA}$ leads to systematic numerical deviations when one is interested in modelling non-aqueous systems. If achieving quantitative similarity between DH theory and MSA at different relative permittivity values requires a different scaling $f_{sc}$, then one can propose using a function $f_{sc}(a, \varepsilon_r, T, \rho_j)$ instead. This function should be $\approx {}^{5}/_{6}$ for water and, for instance, $\approx {}^{2}/_{3}$ for dimethoxyethane (DME, with $\varepsilon_r = 7.03$).

One may indirectly find an expression by use of the spherical capacitor analogy from Lesser Blum. Blum proposed[53] that in the MSA theory the total electrostatic energy of the electrolyte takes the form of the quotient between the total squared charge of the system ($\sum_j \rho_j q_j^2$) and the capacitance $C^{MSA}$ resulting from the collection of spherical capacitors, as previously shown in equation (2.94). This capacitance in turn is given in RP-MSA by equation (2.96), from which one can identify the following:

$$\varepsilon_0 \varepsilon_r C^{MSA} = \varepsilon_0 \varepsilon_r \left( \frac{a}{2} + \frac{1}{2\Gamma} \right) = C_a + C_\Gamma \tag{6.1}$$

where the total capacitance is given by the additive contributions of the individual capacitance from the central sphere $C_a$ and the capacitance from the screening parameter $C_\Gamma$. Additive capacitances correspond to a capacitor circuit in parallel. It can then be proposed[17,53] that linearized electrolyte theories can be represented as capacitor circuits with the following generalized form:

$$\frac{\mu_i^{el}}{RT} = \ln\left(\gamma_i^{el}\right) = -\frac{z_i^2 e^2}{8\pi} \cdot \left(\varepsilon_0 \varepsilon_r C^X\right)^{-1} \tag{6.2}$$

where $\varepsilon_0 \varepsilon_r C^X$ corresponds to the capacitance from electrolyte theory $X$ in a medium of relative permittivity $\varepsilon_r$. This representation was described by Blum[53] for the RP-MSA and DH theory, and can be extended[17] to other linearized theories.

The easiest representation of the concept is provided by the Debye-Hückel limiting law (DHLL), which corresponds to solving the inexact LPB equation with no volume excluded for the central ion. The well-known result is:

$$\frac{\mu_i^{el,DHLL}}{RT} = \ln\left(\gamma_i^{el}\right) = -\frac{z_i^2 e^2}{8\pi} \cdot \left(\varepsilon_0 \varepsilon_r C^{DHLL}\right)^{-1} = -\frac{z_i^2 e^2}{8\pi} \cdot \frac{\kappa_D}{\varepsilon_0 \varepsilon_r} \tag{6.3}$$

where the capacitance is given by a collection of point charges and $C^{DHLL} = \kappa_D^{-1}$. The circuit representation of the DH theory, Pitzer's extension of the DH theory, MDE-DH and the RP-MSA are shown in Table 6, where the form of $(C^X)^{-1}$ is included for each case. It can then be stated that, for all forms of $(C^X)^{-1}$ in Table 6, scaling the distance of closest approach $(a)$ results in scaling total the capacitance.[17]

**Table 6. Capacitor circuit representations of diverse electrolyte theories.**

| Theory | Circuit Representation | $(C^X)^{-1}$ | Inserting in equation (6.2) |
|---|---|---|---|
| **DH theory[1]** | 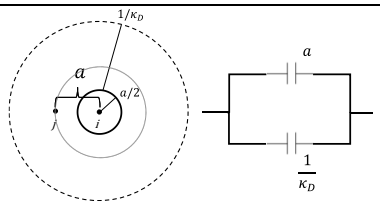  | $\left(a+\frac{1}{\kappa_D}\right)^{-1}$ | Yields equation (2.30) |
| **Pitzer[2]** | 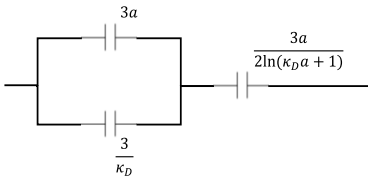  | $\left(3a+\frac{3}{\kappa_D}\right)^{-1} + \left(\frac{3a}{2\ln(\kappa_D a+1)}\right)^{-1}$ | Yields equation (2.35) |
| **MDE-DH** | 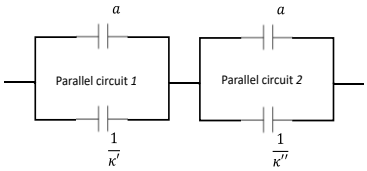  | $\left(a\mathcal{E}'+\frac{\mathcal{E}'}{\kappa'}\right)^{-1} + \left(a\mathcal{E}''+\frac{\mathcal{E}''}{\kappa''}\right)^{-1}$ | Yields equation (2.83) |
| **RP-MSA** | 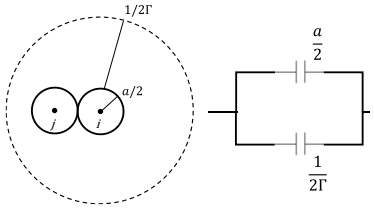  | $\left(\frac{1}{2\Gamma}+\frac{a}{2}\right)^{-1}$ | Yields equation (2.98) |

[1]DH theory via the charging processes; [2]DH theory via the pressure equation.

Thus, when DH theory is applied in water with $a_{DH} = \frac{5}{6}a_{MSA}$, it is not the distance of closest approach what is being scaled, but the capacitance of the whole arrangement due to the additive nature of capacitors in parallel. As argued by Maribo-Mogensen et al.,[164] scaling the distance of closest approach in DH theory accounts for missing volume exclusion effects (overscreening) in the ion cloud. These are formally accounted for by the renormalized $\Gamma$ in the RP-MSA, as already described in section 2.2. Therefore, if scaling of the distance of closest approach in DH theory roughly mimics the effect of the

renormalized $\Gamma$ in MSA theory, one may propose[17] that the exact scaling function $f_{sc}(a, \varepsilon_r, T, \rho_j)$ between them is nothing more than the dimensionless scaling factor required by $a_{DH}$ to make the capacitances $C^{DH}$ and $C^{MSA}$ equal. The result is:

$$f_{sc,(1)} = f_{sc}^{DH,RP-MSA}(a, \varepsilon_r, T, \rho_j) = \frac{a_{MSA}}{2a_{DH}} + \frac{1}{a_{DH}}\left(\frac{1}{2\Gamma} - \frac{1}{\kappa_D}\right) \tag{6.4}$$

Unsurprisingly, replacing $\kappa_D a$ by $\kappa_D a f_{sc,(1)}$ in the excess chemical potential of electrostatic origin from DH theory yields equation (2.98) from the RP-MSA. Thus, one can argue that the factor $5/6$ from Maribo-Mogensen et al.[164] actually stands for an averaged value of $f_{sc,(1)}$ in water. It is worthwhile to explore the concept of scaling the distance of closest approach a bit further.

In the same fashion that the scaling factor $a_{DH} = \frac{5}{6} a_{MSA}$ provides a similar performance between DH theory and the RP-MSA, one may evaluate whether scaling the distance of closest approach in equation (2.25) from Pitzer provides some form of qualitative agreement. This is indeed the case,[17] as shown in Figure 18.

Compared to DH theory, the qualitative behavior of Pitzer's electrostatic term has a closer qualitative resemblance to the more advanced theories (RP-MSA, MDE-DH) when the distance of closest approach is $a_{PDH} = \frac{3}{2} a_{MDE-DH}$. This similarity holds with less systematic deviations as the fluid specification $\lambda_B/a$ changes (i.e. use of different values for $\varepsilon_r$), when compared to the similarity between DH theory and more advanced theories. However, the central conclusion from Maribo-Mogensen et al.[164] remains valid: applying any of the four electrostatic models and letting $a$ vary as a parameter will lead to very similar results for the excess mean ionic chemical potential of electrostatic origin and the thermodynamic properties that can be extracted from it.

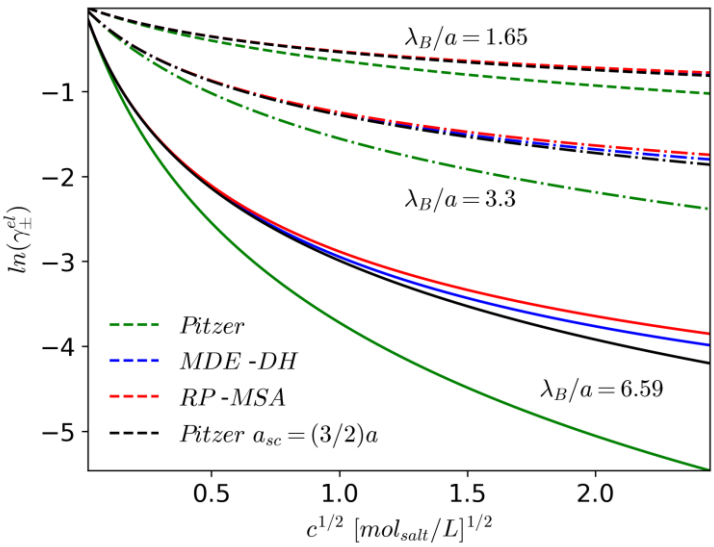


**Figure 18. Comparison between MDE-DH, RP-MSA and Pitzer's extension of the DH theory. All calculations apply $a = 4.25$ Å, being the black dash-dotted line Pitzer's extension with the scaling of $1.5a$ replacing the distance of closest approach. For room temperature, these fluid specifications $\lambda_B/a$ correspond to relative permittivities of 80, 40 and 20 (from top to bottom). One may observe that the scaled Pitzer extension has a good qualitative agreement with the more advanced theories.**

The analysis presented so far is not productive, unless the third question at the beginning of this chapter is addressed: does this principle have any additional practical implications? To answer this question, a central hypothesis of the present work is introduced: if empirically scaling the distance of closest approach in DH theory qualitatively compensates for overscreening[164] (missing volume effects) to some degree, then it can also compensate for underscreening to some degree.[17]

Underscreening, as its name implies, relates to a strong positive deviation of the shielding of electrostatic forces from the conventional linearized theories: the ions are not being screened as described by the ideal Debye length $\lambda_D$ and the realistic, experimentally measured screening length is considerably larger.[265,300,301] Furthermore, underscreening is directly given by ion-ion correlations and is therefore close to the concept of ion pairing.[96,265,302] The electric fields of the ions penetrate the medium with a distance that is considerably longer than the Debye length $\lambda_D = \kappa_D^{-1}$. This implies that the experimentally measured screening parameter $\kappa$ is smaller than $\kappa_D$. As customary with deviations observed with DH theory, ion pairing is invoked as explanation for $\kappa < \kappa_D$.[265]

There are many reasons why underscreening occurs. The three most commonly analyzed situations are:[265,300,302,303] very high ion concentrations, the presence of polyvalent ions and a low relative permittivity of the medium. Thus, while the Bjerrum ion pair treatment

offers a relatable explanation, the chemical model for ion pairing is only a tool to address one or perhaps two dimensions of a more complex issue.[25,304]

Setting the cases of acids (actual chemical speciation) and ionic surfactants (non-coulombic aggregation) aside, the ion pairing chemical model makes use of ion pairs as chemical species to represent the global average of ion pairs behaving as short-lived entities with half-lives of picoseconds.[94,305] Furthermore, the chemical model for ion pairing as such is a two-body correlation and will not capture effects of higher order.[304] Finally, as argued by Nordness and Brennecke,[305] a fluid is dynamic and labeling ion pairs as static entities is more a modelling tool than an accepted convention. In the words of Kirkwood in 1934: "*Bjerrum also makes use of a special hypothesis concerning ionic association which, though intuitively attractive, is in some respects arbitrary*".[50]

Efforts in the literature to go beyond the Bjerrum ion pair treatment of DH theory focused on attempts to provide solutions to the PB equation beyond the linearized regime. For instance, in 1927 LaMer and Mason sought to derive equations for the asymmetric electrolytes by means of estimating new electrostatic potentials that included two terms of the total correlation function.[98] In 1933, Onsager provided further considerations to correct the PB equation, acknowledging the complexity of estimating higher order effects.[99] In 1964, Onsager reviewed the approach from LaMer and Mason demonstrating that the Poisson-Boltzmann equation required corrections in the mean electrostatic potential given by expansions in terms of $\kappa_D$, $\lambda_B$ and $\eta$, the latter defined as:[97]

$$\eta_1 = \frac{\sum_j q_j^3 \rho_j}{\sum_j q_j^2 \rho_j} \tag{6.5}$$

for the charge asymmetrical case, and:

$$\eta_2 = \frac{\sum_j q_j^4 \rho_j}{\sum_j q_j^2 \rho_j} \tag{6.6}$$

for the charge symmetrical case. Other approaches and modifications to the PB equation and DH theory can be found in the literature,[306–311] though a full list of all works related to the topic would be very extensive.

Reformulation of the exact PB by the DIT from Kjellander and Mitchell[42] leads to the limiting law described in equation (2.74), where one may readily observe that the

corrections $\eta_1$ and $\eta_2$ to the mean electrostatic potential from Onsager are implicit in the second and third terms on the right hand side. Equation (2.74) is repeated here for direct comparison:

$$\left(\frac{\kappa}{\kappa_D}\right)^2 = 1 + \frac{\Lambda \ln(3)}{4}\left(\frac{\sum_j z_j^3 v_j}{\sum_j z_j^2 v_j}\right)^2 + \frac{\Lambda^2 \ln(\Lambda)}{6}\left(\frac{\sum_j z_j^4 v_j}{\sum_j z_j^2 v_j}\right)^2 + \mathcal{O}(\Lambda^2)$$

Interestingly, Onsager suggested at the end of his publication[97] that the trends of his lengthy analytical result for asymmetric electrolytes could be well-approximated simply by replacing $\kappa_D^2$ with $\kappa_D^2\left(1 + \frac{\kappa_D \eta_1^2}{12\pi\varepsilon_0\varepsilon_r k_B T}\right)$ in DH theory. This approximation lies close to the first two terms of the DIT's limiting law (a formally exact solution at infinite dilution), the total difference being only the factor of $\frac{\ln(3)}{4}$ which is $\frac{1}{3}$ in Onsager's suggestion.

Smith et al.[302] analyzed the deviations of the observed experimental decay length $\lambda = \kappa^{-1}$ with respect to the Debye length $\lambda_D = \kappa_D^{-1}$ by means of the DIT. In the low concentration regime, the DIT provides a good description.[49,302,303] Furthermore the authors suggested a correlation between the conventional ion pair equilibrium and the concept of an effective screening length given by the following expression:[302]

$$\frac{\kappa}{\kappa_D} = \sqrt{1 - \alpha_1 \Lambda^2}$$
$$\alpha_1 = \frac{K_{assoc}(T, \varepsilon_r, a)}{8\pi z^2 N_A \lambda_B^3} \tag{6.7}$$

where $K_{assoc}^{(c)}(T, \varepsilon_r, a)$ is an association constant and equation (6.7) can be considered as a lower order approximation/correction that emulates the first and quadratic (third) terms of the limiting law from the DIT.

Thus, the concept of scaling the sum of $a + \kappa_D^{-1}$, either by tweaking the value of $a$,[164] or by (more fundamentally[32,97]) scaling $\kappa_D$ with an expansion that represents corrections to the mean electrostatic potential, are valuable tools to correct DH theory and approximate a large diversity of both computational and experimental observations.

With these considerations, and in direct analogy to the equivalency obtained in equation (6.4), one can suggest[17] a hypothetical scaling factor $f_{sc}^H(a, \varepsilon_r, T, \rho_j)$ applied to the DH theory at a very dilute regime with high ion coupling that scales the distance of closest

approach in order to make its capacitance approximate the DIT limiting law. The function therefore seems to be scaling $a$ applied in DH theory in order to mimic the effect of $\kappa$. This is the same principle as scaling $a$ to mimic the effect of $\Gamma$ from equation (6.4). The result from equating the capacitances has a form similar to $f_{sc,(1)}$ given by:

$$f_{sc(2)} = f_{sc}^{H}\left(a, \varepsilon_r, T, \rho_j\right) = 1 + \frac{1}{\kappa_D a}\left(\frac{\kappa_D}{\kappa} - 1\right) \tag{6.8}$$

To apply the scaling function $f_{sc(2)}$, one requires to know the values of the quotient $\frac{\kappa_D}{\kappa}$. The limiting law given by equation (2.74) has validity in the dilute regime and provides a correction for the initial slope of $\ln\left(\gamma_{\pm}^{el}\right)$ that describes both positive and negative deviations from the DH theory depending on the permittivity of the medium and the valence of the ions, but it does not fully describe strong ion pairing in 1:1 electrolytes, for which the missing term $\mathcal{O}(\Lambda^2)$ would be necessary. Equation (6.7), on the other hand, is specifically designed to approximate negative deviations from $\kappa_D$ , mimicking the qualitative behavior of the limiting law from the DIT with $\mathcal{O}(\Lambda^2)$ for the case of strong ion coupling.[302] It is nevertheless only mathematically meaningful for concentrations at which $\alpha_1\Lambda^2 \ll 1$.

Equation (6.7) can be (semi-)linearly extrapolated at infinite dilution by a very simple relation valid at infinite dilution (further details provided in Appendix 8.2):[17]

$$\frac{\kappa^{\infty}}{\kappa_D^{\infty}} = \frac{1}{\sqrt{1 + \alpha_1(\Lambda^{\infty})^2}} \tag{6.9}$$

This approximation assumes that the largest correction applied to the screening length occurs in the low concentration regime and then retains linear behavior at higher concentrations. This is exemplified for a fluid specification of $\frac{\lambda_B}{a} = 9.34$ in Figure 19, where a calculation using Bjerrum's theory is also included for reference. The advantage of equation (6.9) is that it does not become complex valued, unlike equation (6.7). Furthermore, it has a decaying asymptotic behavior as concentration rises in a similar fashion to Bjerrum's theory while avoiding the necessity of invoking a concentration of ion pairs in chemical equilibrium.

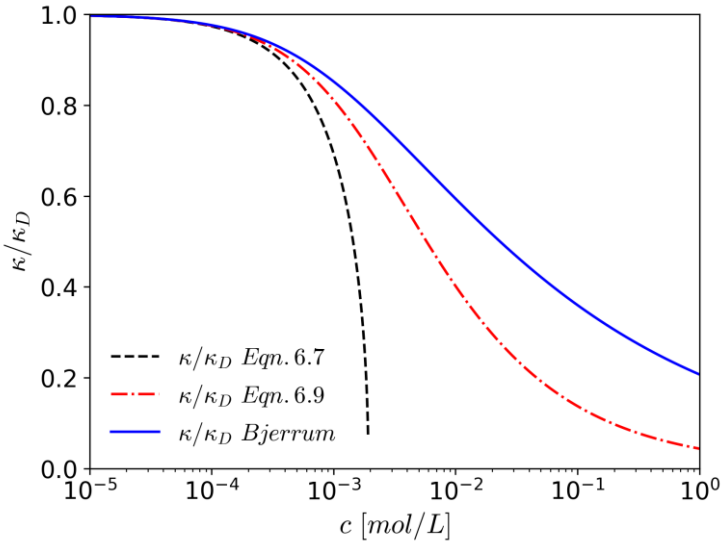


**Figure 19. Calculation of the ratio $\kappa/\kappa_D$ as approximated by equation (6.7) and its semi-linear extrapolation given by equation (6.9). A calculation with Bjerrum's theory is included for reference. Calculations at room temperature with $a = 3$ Å and $\varepsilon_r = 20$ for a 1:1 electrolyte.**

Insertion of equation (6.9) in equation (6.8) leads to the following scaling function:

$$f_{sc(2)} = f_{sc}^{H}(a, \varepsilon_r, T, \rho_j) = 1 + \frac{1}{\kappa_D a}\left(\sqrt{1 + \alpha_1 \Lambda^2} - 1\right) \tag{6.10}$$

Smith et al.[302] suggested Bjerrum's integral as an input to estimate $\alpha_1$. It is the writing author's choice to apply the association constant derived by Ebeling from cluster theory,[312] which can also be derived by a different pathway in DH theory,[313] given that it provides more straightforward, simpler expressions in the upcoming sections. The association constant from Ebeling for a concentration in $m^3/mol$ is given by:[312]

$$K_{assoc}(T, \varepsilon_r, a) = 8\pi N_A (a)^3 \sum_{n=1}^{\infty} \frac{(\lambda_B/(a))^{2n+2}}{(2n+2)! \cdot (2n-1)} \tag{6.11}$$

Having proposed a function to scale the distance of closest approach to account for underscreening (low permittivity case), one requires a thorough justification. Validation in a practical setting with experimental data, is performed in section 6.1.3 in combination with the COSMO-RS-ES model. The thermodynamic consistency of the approach, as well as its assumptions and limits are briefly discussed in section 6.2, which includes an extension of the approach for concentration dependent density, molar mass and relative permittivity. Finally, the limits of the approach are tested in sections 6.3 and 6.4 when considering the molten salt state by means of experimental IL data.

Firstly, and as historical referent, a good example of an involuntarily direct application of the concepts behind equation (6.10) are the empirical Pitzer equations, where the electrostatic term is given by equation (2.36) and a so-called parameter of closest approach $b^{(m)}$ (molal basis) replaces the distance of closest approach $a$, due to the convenience of defining the ionic strength.[27,36] The parameter of closest approach in the molality convention is given by equation (2.42), repeated here:

$$b^{(m)} = \frac{\kappa_D^{(m)} a}{\sqrt{I^{(m)}}} = a\sqrt{8\pi\lambda_B N_A d_s} \tag{2.42}$$

In practice, the physical value expressed by equation (2.42), and in general all linearized theories, lead to considerable underestimations of the experimentally observed mean ionic activity coefficient when ion coupling is strong due to a low dielectric constant. This is exemplified for dimethoxyethane in Figure 20.

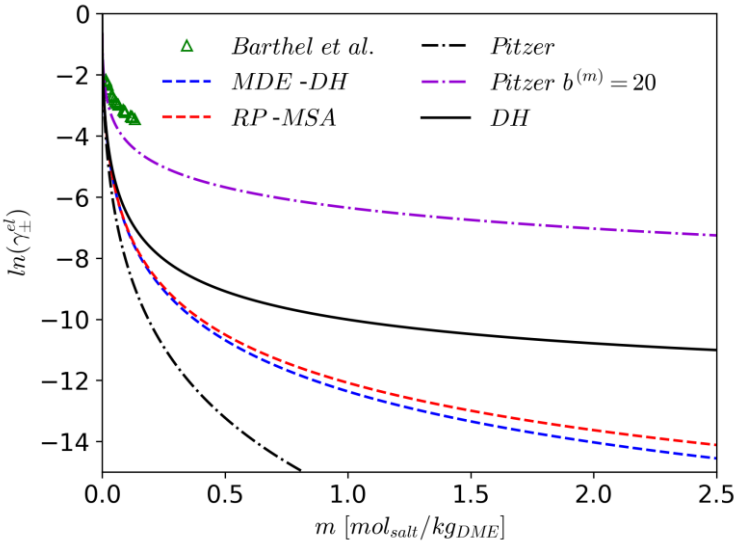


**Figure 20. MIAC values (1:1) for DME ($\varepsilon_r = 7.03$) at room temperature. Calculations with $a = 3$ Å for DH theory, the electrostatic term from the Pitzer equations, MDE-DH and RP-MSA. The purple line shows the empirical strategy of the Pitzer equations: applying an empirically recommended value of $b^{(m)} = 20$, which corresponds to a scaling of $4.36 \cdot a$ in equation (2.42). The green triangles are logarithmic MIAC correlated data from Barthel et al.[304] for $LiClO_4$ in DME.**

As shown in Figure 20, the physical value of the distance of closest approach can be scaled by an empirical constant in order to provide a qualitative correction, thereby scaling the parameter of closest approach $b^{(m)}$. Consequently, one finds empirically recommended values for $b^{(m)}$, which effectively replace the physical value described by equation (2.42). A trend of these recommended values is identified: the empirical value replacing $b^{(m)}$

increases as the solvent relative permittivity decreases. This was already an established fact in the reviewed literature,[25,304,314] as shown in the first two columns of Table 7.

For direct comparison with the recommended values, equation (6.10) is reformulated as follows:

$$\kappa_D a \cdot f_{sc(2)} = \kappa_D a + \left(\sqrt{1 + \alpha_1 \Lambda^2} - 1\right) \tag{6.12}$$

and directly introduced into the definition of $b^{(m)}$, thereby yielding the following expression:[17]

$$b_{mod}^{(m)} = \frac{1}{\sqrt{I^{(m)}}} \cdot \kappa_D a \cdot f_{sc(2)} \tag{6.13}$$

where the subscript "*mod*" stands for modified. When ion coupling is low, i.e. high relative permittivity, the second term on the right-hand side of equation (6.13) tends to zero. Thus, one can apply the scaling of 1.5 to the distance of closest approach in the first term, in accordance with the observations discussed for Figure 18.

**Table 7. Values for the parameter of closest approach used in the electrostatic term of the Pitzer equations: empirical values from the literature, values calculated with equation (2.42) and values calculated with the modified parameter of closest approach from equation (6.15).**

| Solvent | Empirical literature[25] value for $b^{(m)}$ | Calculated with eqn. (2.42) for $a = 3$ Å | Calculated with eqn. (6.15) for $a = 3$ Å and $\alpha_{sc} = 30$ |
|---|---|---|---|
| Water: $\varepsilon_s = 78.34$ | 1.2 or 2.0* | 0.99 | 1.61 |
| Acetonitrile: $\varepsilon_s = 32.63$ | 3.2 | 1.26 | 2.42 |
| Ethanol: $\varepsilon_s = 24.35$ | 3.2 | 1.57 | 3.57 |
| Dimethoxyethane: $\varepsilon_s = 7.08$ | 20 | 3.03 | 19.40 |
| Dimethyl Carbonate: $\varepsilon_s = 3.09$ | 95 | 5.14 | 97.21 |

* Depending on the source: Pitzer applied a value of 2.0 for water in eutectic molten salt mixtures.[40] The value 14.9 (the mole fraction equivalent of 2.0 for water) was adopted by various electrolyte models as the standard parameter of closest approach for the PDH term.[11,13–15,195,198,218,228,284,315,316]

As ion coupling due to lower permittivity values becomes more relevant, the second term comes into play. Firstly, introduction of the ionic strength as part of the numerator and

use of equation (6.11) reformulates the second term of the right hand side of equation (6.13) into the following:

$$\frac{\left(\sqrt{1-\alpha_1\Lambda^2}-1\right)}{\sqrt{I^{(m)}}} = \sqrt{\frac{1}{I^{(m)}} + d_s \cdot 8\pi N_A (a)^3 \sum_{n=1}^{\infty} \frac{(\lambda_B/(a))^{2n+2}}{(2n+2)! \cdot (2n-1)}} - \frac{1}{\sqrt{I^{(m)}}} \qquad (6.14)$$

Subsequently, in order to reproduce the empirical values from the literature, the term inside the square root that corresponds to the association constant is applied with a scaling factor $\alpha_{sc}$ that adjusts the behavior of equation (6.11) in the same fashion as if one were fitting the association constant to experimental data. With all these considerations, the preliminary expression for the modified parameter of closest approach is:[17]

$$b_{mod}^{(m)} = \frac{3}{2} b^{(m)} + \sqrt{\frac{1}{I^{(m)}} + d_s \cdot 8\pi N_A (\alpha_{sc} a)^3 \sum_{n=1}^{\infty} \frac{(\lambda_B/(\alpha_{sc} a))^{2n+2}}{(2n+2)! \cdot (2n-1)}} - \frac{1}{\sqrt{I^{(m)}}} \qquad (6.15)$$

Replacing $b^{(m)}$ with $b_{mod}^{(m)}$ in the electrostatic term of the Pitzer equations can then be applied to accurately reproduce the recommended values from the literature with a smooth trend, as shown in Table 7. The final, simplified and fully consistent form of equation (6.15) is given further ahead (see equations (6.17) and (6.18) and the appendix). The parameter of closest approach applied to equation (2.36) is directly transferable to the PDH term from equation (2.51) by accounting for the molar mass of the solvent.[17,40]

### 6.1.2 M-PDH: Brief Perspective from Statistical Mechanics

At the time in which the concept of scaling the parameter of closest approach in the PDH term via equation (6.15) was published,[17] it was interpreted as a crude correlation for practical use in the PDH term. Therefore, the deeper connection between DIT-based approximations and the empirically recommended values for the parameter of closest approach merit further clarification.

A central question regarding equation (6.15) is that the value required by $\alpha_{sc}$ must be large in order to reproduce the empirical values of $b^{(m)}$. Evidently, a distance of closest approach that is roughly nineteen times larger than the theoretical value for the case of

dimethylcarbonate in Table 7 cannot be taken as a physically meaningful value. It only provides a qualitative correction for the calculation of $\ln\left(\gamma_{\pm}^{el}\right)$ in the case of very strong ion-ion coupling due to a low permittivity of the medium, as exemplified in Figure 20.

In the molarity scale, $b^{(c)}$ contains the product $\kappa_D a$ and, accordingly, the modified parameter of closest approach contains the product $\kappa_D a f_{sc(2)}$. Due to historical reasons,[36] this product is divided by the square root of the ionic strength to calculate $b^{(c)}$, leaving the distance of closest approach and some constants. Thus, for $b_{mod}^{(c)}$ one could wrongfully assume that $f_{sc(2)}$ empirically scales $a$ with no further significance.

However, applying $f_{sc(2)}$ from equation (6.10) to the total correlation function in the inexact LPB formulation does provide a correction to DH theory. One can numerically estimate osmotic coefficients of electrostatic origin via the pressure equation. With this simple exercise, it can be demonstrated that $f_{sc(2)}$ is not scaling the distance of closest approach (which leads to erroneous results) but actually scaling the screening length $\kappa_D$. The attempted correction to the total correlation function is then given by equation (6.16):

$$h_{ij}^{\#,mod}(r) = \frac{-\beta q_i q_j}{4\pi\varepsilon_0\varepsilon_r r}\left(\frac{\exp\left(-f_{sc(2)}\kappa_D(r-a)\right)}{f_{sc(2)}\kappa_D a + 1}\right) \quad \forall \quad r > a \tag{6.16}$$

Figure 21 provides a comparison between osmotic coefficients of electrostatic origin (no hard core) from several expressions and two samples of their linearized radial distribution functions for a system at room temperature with $a = 4.25$ Å and a very low permittivity value of $\varepsilon_r = 4$. On the upper-left and lower-left frames (A and C), the black lines represent DH theory and the red lines represent DH theory with the scaling function $f_{sc(2)}$ applied to the electrostatic term of equation (2.33). The blue squares in frame C are a numerical approximation from the radial distribution of the DIT (limiting law) applied to the pressure equation and the red squares are a numerical approximation from equation (6.16) applied to the pressure equation. On the upper-right and lower-right frames (B and D), the black lines correspond to DH theory, the thick red lines correspond to calculations via equation (6.16) and the blue lines correspond to the radial distribution from the DIT (limiting law).

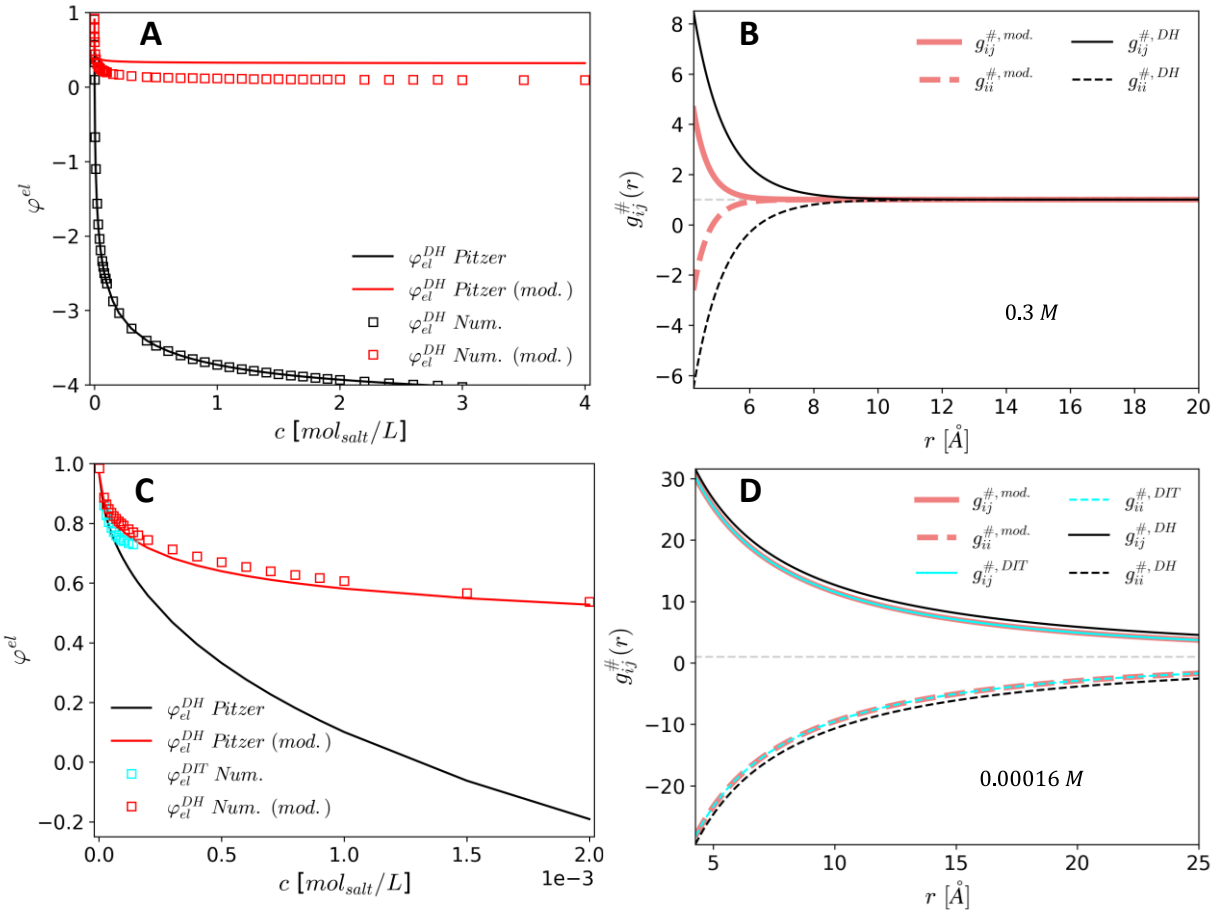


**Figure 21. Calculations of the osmotic coefficient of electrostatic origin $\varphi_{el}$ (1:1) and radial distribution functions (two term expansion of $g_{ij}^{\#}(r)$) for $a = 4.25$ Å, $T = 298.15\ K$ and $\varepsilon_r = 4$. (A): Comparison between DH theory (numerically and the electrostatic component of equation (2.33)) and M-PDH ($f_{sc(2)}$ with $\alpha_{sc} = 30$ applied to the electrostatic component of equation (2.33) and the numerical result via equation (6.16)). (B): $g_{ij}^{\#}(r)$ given via equation (6.16) compared to DH theory at $c = 3$ molar. (C): A close-up of the calculations for $\varphi_{el}$ in the diluted regime including the numerical result via equations (2.64) and (2.74) from the DIT within limits of its applicability. (D): $g_{ij}^{\#}(r)$ given by equation (6.16), DH theory and the DIT at $c = 16 \cdot 10^{-5}$ molar. Numerical results correspond to the electrostatic component of the pressure equation (equation (2.32)) and $g_{ij}^{\#}(r)$ for each case.**

In Figure 21-A, the numerical calculation of the radial distribution function from DH theory applied to the pressure equation (black squares) is included as a validation. In such an evaluation with a very low relative permittivity, one may once again observe the pronounced systematic underestimation given by DH theory. It is of several orders of magnitude for the MIAC. The scaling $af_{sc(2)}$ in the parameter of closest approach, which stands for the empirical $b^{(m)}$ values from the literature, provides a rough but desirable qualitative correction. The scaling $\kappa_D f_{sc(2)}$ applied to the total correlation function and to the pressure equation yields a very similar correction. Both strategies are qualitatively

equivalent when adjusting the values for $\alpha_{sc}$ in each case (i.e. $\alpha_{sc} = 30$ for the $af_{sc(2)}$ case and $\alpha_{sc} \approx 15$ for the $\kappa_D f_{sc(2)}$ case).

One may observe in Figure 21-B that the correction is principally given by a reduction of the counter-ion concentration in the vicinity of the central ion. The reduction of counter-ions in the vicinity of the central ion can be explained in terms of the DIT: some counter-ions will strongly correlate and couple with other ions in their vicinity and exhibit a decreased effective charge, thereby decreasing their attraction towards the central ion $i$ being analyzed in the pair correlation. This effect is naturally absent in DH theory. In the dilute regime, one may observe that the qualitative correction applied by equation (6.16) agrees with the correction applied by the DIT, as shown in Figure 21-C. It is relevant to clarify that the inconsistency $g_{ii}^{\#} < 0$ is present in the linearized regime. This inconsistency is left here because DH theory and its extensions are in the linearized regime; hence, it is retained for direct comparison. In an advanced, non-linear theory, one would observe notable, successive charge inversions for this case.

While the formal correction of the extrapolated $\frac{\kappa}{\kappa_D}$ should be applied via the pressure equation, this brief exercise demonstrates that its practical effect in the calculation of osmotic and activity coefficients is very well approximated simply by scaling $\kappa_D a$ in DH theory for the case of strong ion-ion coupling due to a low relative permittivity. Consequently, the recommended literature values of $b^{(m)}$ used in the electrostatic term of the Pitzer equations and their inverse proportionality to $\varepsilon_r$ represent, in essence, a blunt correction to the pair correlations. Furthermore, given that derivation with $\kappa_D f_{sc(2)}$ would lead to lengthier, unorthodox expressions and the effect of scaling the distance of closest approach provides the same qualitative effect, it is also a sensible, pragmatic decision to keep $af_{sc(2)}$ as the modelling strategy.

Though systematic proof of concept is provided in the following sections, Figure 22 is also included here for reference and shows the full result of the pressure equation from the linearized DH theory and the application of the scaling $af_{sc(2)}$ in the electrostatic term (the scaling does not apply to the hard-core term), compared to data from Barthel et al.[304] for a salt in a solvent with a low relative permittivity. One may observe that the applied correction delivers meaningful trends in an experimental setting.

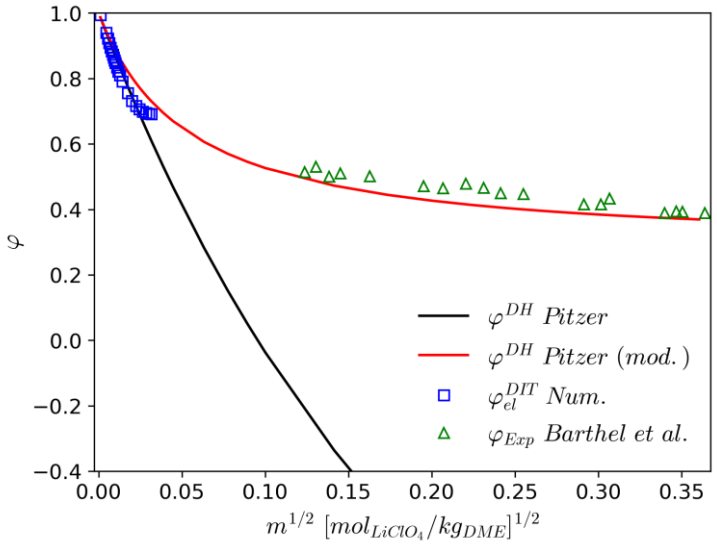


**Figure 22. Osmotic coefficient in DME ($\varepsilon_s = 7.03$) at room temperature with $a = 3$ Å as calculated with equation (2.33) in the molality convention including the hard-core term. Black: conventional DH result from Pitzer; Red: equation (2.33) with a scaled distance of closest approach $f_{sc(2)} \cdot a$ in the electrostatic term; Blue squares: numerical result of the electrostatic contribution from the DIT (for reference); Green triangles: experimental data from Barthel et al.[304] for $LiClO_4$ in DME.**

Onsager suggested[97] that crudely multiplying $\kappa_D^2$ in DH theory by an expansion in terms of $\Lambda$, $\eta_1$ and $\eta_2$ could lead to some qualitative improvements that reflect the results of more formal approaches. In the same fashion, one may suggest that some qualitative improvements can be effectively introduced by directly multiplying the distance of closest approach by functions of $\Lambda$, $\eta_1$ and $\eta_2$. This semi-empirical approach is evidently not suitable for the case of negative deviations from DH theory attributed to charge asymmetry (e.g. 3:3 charge asymmetric electrolytes). However, it is well-suited for a rough qualitative correction to the large negative deviations of the linear DH theory found in low relative permittivity media. The correction is best therefore suited for combination with correlative and (semi-)predictive models that omit explicit association (e.g. eNRTL, COSMO-RS-ES, eUNIQUAC).

### 6.1.3 Application of M-PDH to COSMO-RS-ES for Conventional Salts

For systematic validation, the modified parameter of closest approach can be combined with the PDH term in electrolyte models. Combination with the COSMO-RS-ES model serves both as validation of M-PDH as a good systematic improvement for correlative

approaches as well as an improvement to the COSMO-RS-ES model itself. The modified parameter of closest approach is reformulated in the mole fraction scale as follows:

$$b_{mod}^{(x)} = \frac{3}{2} b^{(x)} + \sqrt{\frac{1}{I^{(x)}} + \frac{d_s}{M_s} \cdot 8\pi N_A (\alpha_{sc} a)^3 \sum_{n=1}^{\infty} \frac{(\lambda_B/(\alpha_{sc} a))^{2n+2}}{(2n+2)! \cdot (2n-1)}} - \frac{1}{\sqrt{I^{(x)}}} \quad (6.17)$$

Gibbs-Duhem consistency requires that the parameter of closest approach in equation (2.51) remains constant. Therefore, keeping $b_{mod}^{(x)}$ with a scaling function $f_{sc(2)}$ that scales the distance of closest approach yields a small Gibbs-Duhem inconsistency (see Appendix). The fully Gibbs-Duhem consistent equivalent of equation (6.17), expressed in terms of the conventional $b^{(x)}$ from Pitzer, is given by:

$$b_{mod}^{(x)} = \frac{3}{2} b^{(x)} + b^{(x)} \left( \frac{\lambda_B}{a \, (4! \, \alpha_{sc})^{1/3}} \right)^{3/2} \quad (6.18)$$

where $a = F_a(r_+^{COSMO} + r_-^{COSMO})$ and $F_a$ is a fitting parameter. The path from equation (6.17) to the simpler equation (6.18) is discussed further ahead in section 6.2 and with more detail in Appendix section 8.2. Both equations yield the same results with negligible differences in the low concentration regime, but equation (6.18) provides strict thermodynamic consistency in the PDH term. The systematic correction for low permittivity is primarily led by the second term on the right-hand side of equation (6.18).

With these definitions, the explicit M-PDH for application in $g^E$-models is given by directly replacing $b^{(x)}$ with $b_{mod}^{(x)}$ in equation (2.51) to yield the following:[17]

$$\ln\left(\gamma_i^{M-PDH(x)}\right) = -A_\phi^{(x)} \left[ \frac{2 z_i^2}{b_{mod}^{(x)}} \ln\left(1 + b_{mod}^{(x)} \sqrt{I_x}\right) + \frac{z_i^2 \sqrt{I_x} - 2 I_x^{3/2}}{1 + b_{mod}^{(x)} \sqrt{I_x}} \right] \quad (6.19)$$

Estimation of the salt-free density in mixed solvents was performed with a mass fraction mixing rule and with a volume fraction mixing rule for the salt-free relative permittivity, in the same fashion as previous works.[14–16]

The COSMO-RS-ES model with the short-ranged COSMO-RS based equations for ions from Müller et al.[16] (Table 5) can then be applied and the short-ranged COSMO-RS-ES parameters reparametrized using $\ln\left(\gamma_i^{M-PDH(x)}\right)$ instead of $\ln\left(\gamma_i^{PDH(x)}\right)$ as the LR

contribution. The results[17,317] from diverse COSMO-RS-ES parameterizations applying different strategies for the LR coulombic interactions are summarized in Table 8.

**Table 8. Average Absolute Deviation (AAD) of various datasets evaluated[17,317] with the COSMO-RS-ES model applying different strategies for LR electrostatics.**

| Dataset ($N_{DP}$) | COSMO-RS-ES original version[14] LR electrostatics: equation (2.51) with fixed $b_{constant}^{(x)} = 14.9$ | COSMO-RS-ES with corrections*** for low permittivity[16] LR electrostatics: equation (2.51) with fixed $b_{constant}^{(x)} = 14.9$ | COSMO-RS-ES + M-PDH LR electrostatics: equation (6.19); parameters are published[17] |
|---|---|---|---|
| | SR interaction energy equations | | |
| | Table 4 | Table 5 | Table 5 |
| MIAC aq.* (1206) | 0.043 | 0.043 | 0.042 |
| LLE aq.* (1056) | 0.675 | 0.518 | 0.524 |
| GT* (992) | 3.158 | 3.768 | 3.865 |
| SLE** (836) | 1.000 | 0.896 | 0.903 |
| MIAC org.** (980) | 2.679 | 1.274 | 0.892 |

* Dataset is part of the training set. ** Dataset is not part of the training set (prediction). *** Applies a Bjerrum-treatment-like adjustment for the effective ionic strength. MIAC aq.: aqueous mean ionic activity coefficients (pure water, room temperature). LLE aq.: aqueous mixed solvent electrolytes with salting out effects. GT: Gibbs free energies of transfer of ions from water to organic solvents. SLE: solid-liquid equilibria in aqueous, mixed and non-aqueous systems. MIAC org.: non-aqueous mean ionic activity coefficients (room temperature).

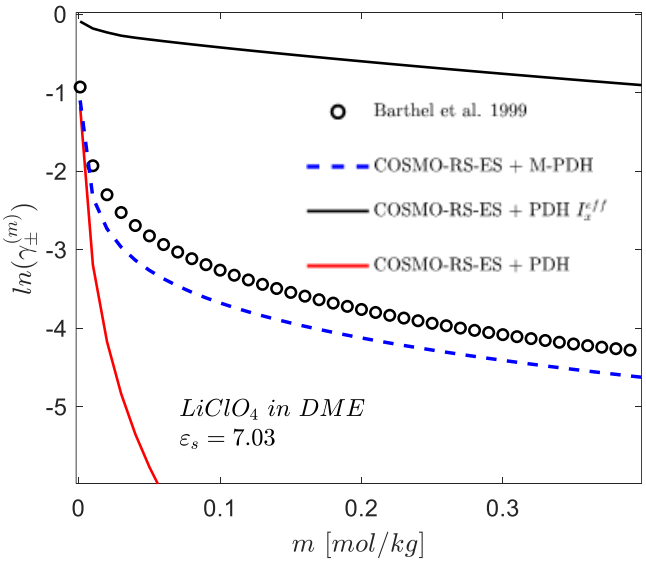


**Figure 23. Results for the logarithmic MIAC of LiClO4 in dimethoxyethane (DME) as calculated by the three different strategies shown in Table 8. This system is the same as the example used in Figure 20 and in Figure 22. The red line corresponds to the result with the parameters from Gerlach et al.[14] (applicable to Table 4); the black line corresponds to the result from Müller et al.[16] and the dashed blue line corresponds to the present work[17] (both using the COSMO-RS-ES version from Table 5).**

Historically, the COSMO-RS-ES model has had systematic problems when calculating non-aqueous electrolyte systems.[16] This problem is not unique to the COSMO-RS-ES model. In

general, electrolyte models run into systematic deviations and require corrections when calculating non-aqueous electrolytes, particularly when ion coupling becomes more relevant (i.e. in lower permittivity media and/or in presence of polyvalent ions).[3,5,125,304] In this and other regards, the need for pragmatic and easily applicable electrolyte models in the industry remains present.[1,2]

In this section a modification to the PDH term has been achieved, which improves model performance in non-aqueous electrolytes without the need of invoking speciation. The overall results shown in Table 8 validates M-PDH as an easily applicable alternative that provides systematic improvement when compared to the commonly applied PDH term. The modification presented here leads to the largest corrections for non-aqueous systems, particularly for the mean ionic activity coefficient calculations of salts in organic solvents. Additional details regarding the application of the M-PDH term in combination with the COSMO-RS-ES model can be found in the original publication.[17,317]

A few words regarding the use of $b^{(x)}_{\text{constant}} = 14.9$ in the PDH term from equation (2.51) adopted by various electrolyte models,[11,13–15,195,198,218,228,284,315,316] are necessary. Although parameterization with a $g^E$-model will frequently blur its consequences, the customary choice of $b^{(x)}_{\text{constant}} = 14.9$ is unfortunate. The systematic deviations exemplified in Figure 20 are more pronounced for the PDH term when $b^{(x)}_{\text{constant}} = 14.9$ is applied. These deviations are present even in water when including a relative permittivity that depends on salt concentration. The definition $b^{(x)} = a(8\pi\lambda_B N_A d_s)^{1/2}(M_s)^{-1/2}$ (with an averaged value $a \approx 4.5$ Å) as well as $b^{(x)}_{mod}$ (with an averaged value $a \approx 3$ Å and $\alpha_{sc} = 30$) are both better choices. Further details on this discussion are not included here for the sake of brevity, but can be consulted in the original publication.[17] Any semi-predictive electrolyte model applied to a broad dataset of electrolyte systems with mixed and non-aqueous solvents that applies $b^{(x)}_{\text{constant}} = 14.9$, could be re-parameterized with the physical $b^{(x)}$ or with $b^{(x)}_{mod}$ instead and mild systematic improvements should ensue.

## 6.2 Extended Long-Range Electrostatics

In this section, equation (6.19) is extended via the differentiate down method[262,318–320] with a concentration dependency for the density, relative permittivity, and molar mass.

Subsequently, Gibbs-Duhem consistency is tested with direct application of equation (2.11). The modified-extended PDH term (ME-PDH) is applied by means of mixing rules for mixture properties in combination with the COSMO-RS model (openCOSMO-RS) for IL systems and with the COSMO-RS-ES model for salt systems for validation, providing further evidence that extended LR electrostatics improve the results for highly concentrated, non-aqueous electrolytes. Partial results of this section were published by González de Castilla, et al. *J Mol Liq.* 2022; 360, 119398.[18]

The present sub-chapter makes use of the subscripts $i, j, k, s$ with specific definitions (unless stated otherwise):

- $i$ and $k$ stand for any arbitrary species
- $j$ stands for ionic species
- $s$ stands for the dielectric medium (single solvent or multiple solvents)

### 6.2.1 Theoretical Development, Gibbs-Duhem Consistency and the McMillan-Mayer Framework

One of the central objectives of the present work is improving the modelling of non-aqueous systems, which is partially achieved in section 6.1. This goal is intertwined with achieving precision at very high salt concentrations which is a well documented[15,16] area of opportunity for the COSMO-RS-ES model. To achieve this, it is proposed to extend the LR electrostatics with concentration dependent properties, in line with the recent literature.[125,184,262,285,321,322] Performing this requires addressing several issues, namely thermodynamic consistency and appropriate mixing rules for multiple solvent systems.

#### *The Extended PDH Term (E-PDH)*

A relevant hurdle is the fact that explicitly handling the dielectric medium as its constituents is in violation of the McMillan-Mayer framework. To address this issue, one can first proceed to the derivation of some expressions to be discussed and evaluated.

To the best of the author's knowledge, the first attempt to extend the PDH term for concentration dependent properties is found in van Bochove et al.[320] In their work, the expression for the Gibbs free energy of electrostatic origin derived by Pitzer (equation

(2.49)) is differentiated with solvent concentration dependent salt-free properties. Consequently, the expression derived by van Bochove et al.[320] accounts for the derivative of the relative permittivity, density and molar mass with respect to moles of solvent in mixed solvents; but does not account for ion concentration dependent effects.

Several years later, Chang and Lin proposed[262] performing the full derivative of equation (2.49) for all species (ions and solvent) resulting in the extended PDH term (E-PDH):

$$\frac{G^{E-DH(x)}}{RT} = -\frac{4A_\phi^{(x)} n_T I_x}{b^{(x)}} \ln\left(1 + b^{(x)}\sqrt{I_x}\right) \tag{6.20}$$

In contrast to the conventional derivation where only $I_x$ is concentration dependent, the relative permittivity, molar mass, and density are now also concentration dependent. The compositional derivatives of the Debye-Hückel slope $A_\phi^{(x)}$ and of the parameter of closest approach $b^{(x)}$ are included leading to equation (6.21) (details found in the Appendix):

$$\begin{aligned}\ln\left(\gamma_i^{E-PDH(x)}\right) &= \left(\frac{\partial G^{E-DH(x)}}{RT\partial n_i}\right)_{T,P,n_j} \\ &= -A_\phi^{(x)}\left\{\frac{2z_i^2}{b^{(x)}}\ln\left(1 + b^{(x)}\sqrt{I_x}\right) + \frac{z_i^2 I_x^{1/2} - 2I_x^{3/2}\left(\frac{M_i}{M_m}\right)}{\left(1 + b^{(x)}\sqrt{I_x}\right)}\right. \\ &- \frac{2I_x^{3/2} n_T}{\left(1 + b^{(x)}\sqrt{I_x}\right)}\left[\frac{1}{\varepsilon_m}\frac{\partial \varepsilon_m}{\partial n_i} - \frac{1}{d_m}\frac{\partial d_m}{\partial n_i}\right] \\ &\left. - \frac{4I_x \ln\left(1 + b^{(x)} I_x^{1/2}\right) n_T}{b^{(x)}}\frac{1}{\varepsilon_m}\frac{\partial \varepsilon_m}{\partial n_i}\right\}\end{aligned} \tag{6.21}$$

where the subscript $m$ denotes mixture properties and with the following reformulated definitions for the Debye-Hückel slope and the parameter of closest approach:

$$A_\phi^{(x)} = \frac{1}{3}\left(\frac{2\pi N_A d_m}{M_m}\right)^{0.5}\left(\frac{e^2}{4\pi\varepsilon_0\varepsilon_m k_B T}\right)^{1.5} \tag{6.22}$$

$$b^{(x)} = a \cdot \sqrt{\frac{2N_A e^2 d_m}{M_m \varepsilon_0 \varepsilon_m k_B T}} \tag{6.23}$$

The molar mass $M_m$ is defined in terms of pure compound properties as follows:

$$M_m = \sum_i x_i M_i \tag{6.24}$$

There are no standard definitions for the density $d_m$ and relative permittivity of the mixture $\varepsilon_m$. Therefore, mixing rules and/or additional physical property models with their corresponding compositional derivatives $\frac{\partial \varepsilon_m}{\partial n_i}$ and $\frac{\partial d_m}{\partial n_i}$ are required. Chang and Lin[262] chose a mole fraction based mixing rule for the density of the mixture:

$$\begin{gathered} \frac{1}{d_m} = \sum_i \frac{x_i}{d_i} \\ \frac{\partial d_m}{\partial n_i} = \frac{\partial}{\partial n_i}\left(\sum_i \frac{n_i}{d_i n_T}\right)^{-1} = \frac{-d_m^2(d_i^{-1} - d_m^{-1})}{n_T} \end{gathered} \tag{6.25}$$

and a mass fraction ($\mathrm{w}_i$) based mixing rule for the relative permittivity of the mixture:

$$\begin{gathered} \varepsilon_m = \sum_i \mathrm{w}_i \varepsilon_i \\ \frac{\partial \varepsilon_m}{\partial n_i} = \frac{\partial}{\partial n_i}\left(\sum_i \mathrm{w}_i \varepsilon_i\right) = \frac{\partial}{\partial n_i}\left(\sum_i \frac{x_i M_i \varepsilon_i}{\sum_i x_i M_i}\right) = \frac{M_i}{M_m n_T}(\varepsilon_i - \varepsilon_r) \end{gathered} \tag{6.26}$$

To reduce the systematic deviations exemplified in Figure 20, Chang and Lin[262] introduced an empirical scaling of the parameter of closest approach by a factor of 2.5. Thus, the final expression from Chang and Lin[262] is given by:

$$\begin{aligned} \ln\left(\gamma_i^{CL(x)}\right) = -A_\phi^{(x)} \Bigg\{ & \frac{2z_i^2}{2.5b^{(x)}} \ln\left(1 + 2.5b^{(x)}\sqrt{I_x}\right) + \frac{z_i^2 I_x^{1/2} - 2I_x^{3/2}\left(\frac{M_i}{M_m}\right)}{\left(1 + 2.5b^{(x)}\sqrt{I_x}\right)} \\ & - \frac{2I_x^{3/2}}{\left(1 + 2.5b^{(x)}\sqrt{I_x}\right)}\left[\left(\frac{M_i}{M_m}\right)\left(\frac{\varepsilon_i}{\varepsilon_m} - 1\right) + \frac{d_i^{-1} - d_m^{-1}}{d_m^{-1}}\right] \\ & - \frac{4I_x \ln\left(1 + 2.5b^{(x)} I_x^{1/2}\right)}{2.5b^{(x)}}\left(\frac{M_i}{M_m}\right)\left(\frac{\varepsilon_i}{\varepsilon_m} - 1\right) \Bigg\} \end{aligned} \tag{6.27}$$

which is applied in the literature with averaged properties for neutral species only, assuming a fixed dissociation degree.[262] In the present work, full dissociation is applied and the mixture average is calculated with all the species present (ions and solvents).

Having obtained some initial expressions as described in the literature, the procedure can be repeated with the modified parameter of closest approach $b_{mod}^{(x)}$.

### *The Modified-Extended PDH Term (ME-PDH)*

Evaluation of $b_{mod}^{(x)}$ in the form given by equation (6.14) can show that the term $\frac{1}{I^{(m)}}$ inside of the square root and the term $-\frac{1}{\sqrt{I^{(m)}}}$ have a negligible impact on the overall value of the function. Furthermore, Gibbs-Duhem consistency would require derivation of the excess Gibbs free energy introducing equation (6.15) into equation (6.20) to obtain the chemical potential. This results in the derivation of several unnecessary expressions that are unconventional and negligible. Thus, a pragmatic choice was to apply a simpler expression given in equation (6.18) which expresses $b_{mod}^{(x)}$ reformulated in terms of the conventional $b^{(x)}$ as follows:

$$\begin{aligned} b_{mod}^{(x)} &= b_{(0)}^{(x)} + b_{(1)}^{(x)} \\ b_{(0)}^{(x)} &= \omega_{(0)} b^{(x)} \\ b_{(1)}^{(x)} &= \left(\omega_{(1)} \frac{\lambda_B}{a}\right)^{3/2} b^{(x)} \end{aligned} \tag{6.28}$$

where $\omega_{(0)}$ and $\omega_{(1)}$ can be considered fitting parameters. The current recommendation is to keep $\omega_{(0)} = 3/2$ and $\omega_{(1)} = (24\,\alpha_{sc})^{-\frac{1}{3}} \approx 1/9$ as fixed values.

The modified extension then follows the same pathway from E-PDH but replacing $b^{(x)}$ with $b_{mod}^{(x)}$ from equation (6.28) to introduce a systematic correction for very low relative permittivity values without the need to invoke ion pairing procedures. The partial derivatives of $b^{(x)}$, $b_{mod}^{(x)}$ and $A_{\phi}^{(x)}$ can be found in the Appendix, along with the detailed derivation. Introduction of a concentration dependent $b_{mod}^{(x)}$ and $A_{\phi}^{(x)}$ into the full derivative of equation (6.20) leads to the modified-extended PDH term (ME-PDH):[18]

$$\begin{aligned} ln\left(\gamma_i^{ME-PDH(x)}\right) = & -A_{\phi}^{(x)} \left\{ \frac{2z_i^2}{b_{mod}^{(x)}} \ln\left(1 + b_{mod}^{(x)} \sqrt{I_x}\right) + \frac{z_i^2 I_x^{1/2} - 2I_x^{3/2}\left(\frac{M_i}{M_m}\right)}{\left(1 + b_{mod}^{(x)} \sqrt{I_x}\right)} \right. \\ & - \frac{2I_x^{3/2} n_T}{\left(1 + b_{mod}^{(x)} \sqrt{I_x}\right)} \left[ \left(1 + \frac{3b_{(1)}^{(x)}}{b_{mod}^{(x)}}\right) \frac{1}{\varepsilon_m} \frac{\partial \varepsilon_m}{\partial n_i} - \frac{1}{d_m} \frac{\partial d_m}{\partial n_i} \right] \\ & \left. - \frac{2I_x \ln\left(1 + b_{mod}^{(x)} I_x^{1/2}\right) n_T}{b_{mod}^{(x)}} \left(2 - \frac{3b_{(1)}^{(x)}}{b_{mod}^{(x)}}\right) \frac{1}{\varepsilon_m} \frac{\partial \varepsilon_m}{\partial n_i} \right\} \end{aligned} \tag{6.29}$$

which can be directly compared to equation (6.21). As a matter of fact, setting $\omega_{(0)} = 1$ and $\omega_{(1)} = 0$, reduces the ME-PDH term to the E-PDH term. Equation (6.29) is a central result of the present work.

One may test thermodynamic consistency by means of the Gibbs-Duhem relation from equation (2.11), which is rewritten for the isothermal-isobaric case as follows:

$$\sum_j x_j \frac{\partial \ln\left(\gamma_j^{el}\right)}{\partial x_i} + \sum_s x_s \frac{\partial \ln(\gamma_s^{el})}{\partial x_i} = 0 \tag{6.30}$$

where subscripts $j$ and $s$ stand for ions and solvent(s), respectively, and can be numerically evaluated with small concentration steps $\Delta x_i$ of any species $i$.

Sample calculations can be performed with the diverse extended terms for an aqueous IL (e.g. [BMIM][$BF_4$] with $d_{IL} = 1202\frac{g}{L}, M_{IL} = 226.03\frac{g}{mol}$ ). Literature values of the experimental $\varepsilon_{IL}$ span in a range from 6.7 to 13.9.[85,86,323,324] It is documented that these values are in strong disagreement with each other due to differences in the experimental techniques and the possible presence of water in some measurements.[86] It is also documented that the concentration dependency of $\varepsilon_m$ for the water – [BMIM][$BF_4$] system can be accurately described with a simple volume fraction $\phi$ mixing rule.[85]

The calculation is performed with full dissociation as the basis for the ionic strength and with the following assumptions for the cation and anion properties:

$$d_{IL} = d_+ = d_- \tag{6.31}$$

$$\varepsilon_{IL} = \varepsilon_+ = \varepsilon_- \tag{6.32}$$

$$M_{IL}/v = \bar{M}_j \tag{6.33}$$

A volume fraction mixing rule can be applied to any property $\mathcal{P}$ (i.e. density and relative permittivity of the mixture) according to the following generalized form:

$$\begin{gathered} \mathcal{P}_m = \sum_i \phi_i \mathcal{P}_i \\ \frac{\partial \mathcal{P}_m}{\partial n_i} = \frac{\partial}{\partial n_i}\left(\sum_i \phi_i \mathcal{P}_i\right) = \frac{\partial}{\partial n_i}\left(\sum_i \frac{x_i \mathrm{v}_i \mathcal{P}_i}{\sum_i x_i \mathrm{v}_i}\right) = \frac{\mathrm{v}_i}{\mathrm{v}_T n_T}(\mathcal{P}_i - \mathcal{P}_m) \end{gathered} \tag{6.34}$$

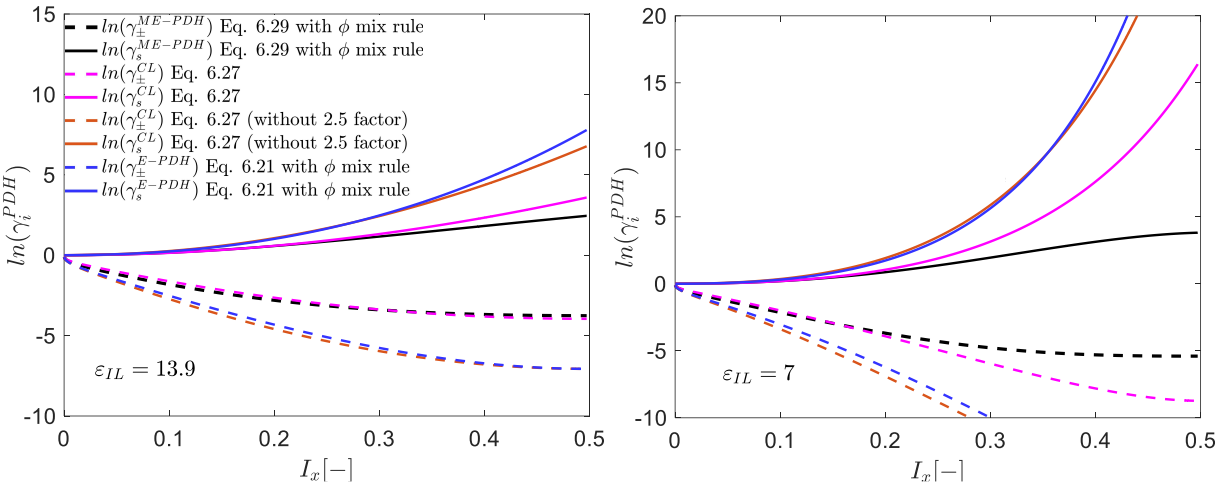


**Figure 24. Sample calculations (T=25°C) with PDH extensions for the water – [BMIM][$BF_4$] system using relative permittivity values of $\varepsilon_{IL} = 13.9$ (left) and $\varepsilon_{IL} = 7$ (right) for the IL. $a = 4$ Å.**

where the molar volume of the mixture is $v_m = \sum_i v_i x_i$. The pure compound molar volumes are calculated from the corresponding pure compound densities and molar masses. One may note that mass fraction and volume fraction based mixing rules are directly interchangeable with the use of either molar mass or molar volume. It is necessary to state that volume fraction is a more physically meaningful mixing rule.

Figure 24 shows diverse evaluations using the E-PDH term from equation (6.21) applying the volume fraction mixing rule for $d_m$ and $\varepsilon_m$; results using the expression from Chang and Lin[262] (equation (6.27) with and without the empirical scaling factor of 2.5); and results using the ME-PDH term from equation (6.29) applying the volume fraction mixing rule for $d_m$ and $\varepsilon_m$. In all cases, a distance of closest approach of $a = 4$ Å was assumed.

Figure 24 (right) applies a value of 13.9 for the relative permittivity of the pure IL. One can observe that, for both the solvent and the ion contributions, the choice of mixing rules has a minor impact (e.g. E-PDH with $\phi$ based mixing rule vs. the result from Chang and Lin without the scaling factor of 2.5). Furthermore, the expression from Chang and Lin is in good qualitative agreement with the results from ME-PDH.

In contrast, in Figure 24 (left), a value of 7 has been applied for the relative permittivity of the pure IL. As the calculations approach this lower value in the high concentration range, one may observe that equations (6.21) and (6.27) have a systematic deviation that results in overestimation of the solvent contribution and underestimation of the mean ionic contribution to the activity coefficient. These deviations, which can be of several

logarithmic units, become rather pronounced as the relative permittivity of the mixture attains lower values and have the same origins as the deviations previously discussed for Figure 20. The introduction of $b_{mod}^{(x)}$ applies a correction to these systematic deviations and one can observe that the result for ME-PDH (equation (6.29)) retains a more expected trend. This correction is led primarily by the component $b_{(1)}^{(x)}$ in $b_{mod}^{(x)}$, as discussed previously, and exemplified in Figure 25. The direct, practical advantage of this fact is systematically validated further ahead in section 6.3.2 where the E-PDH and ME-PDH terms are combined with the basic COSMO-RS model.

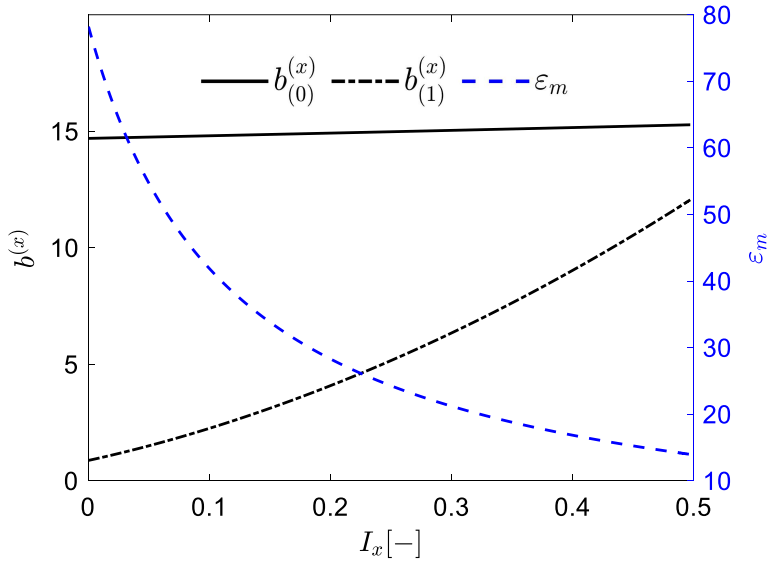


**Figure 25. Calculated values of the components of $b_{mod}^{(x)}$ as a function of IL concentration compared to the value of $\varepsilon_m$ as a function of IL concentration for the case of Figure 24 (right).**

The Gibbs-Duhem consistency of the present approach is expected due to mathematical reasons. The differentiate down method of an excess Gibbs free energy should lead to consistent expressions when the appropriate partial derivatives are applied.[318] Thus, numerical evaluation of equation (6.30) applying equation (6.29) to estimate the pertaining activity coefficients is both a test for mathematical correctness and for thermodynamic consistency. This numerical evaluation is shown in Figure 26.

In the same fashion, one may perform a Gibbs-Duhem consistency test for the E-PDH term with volume fraction (or other) mixing rules and for the extended PDH term from Chang and Lin,[262] both of which are also Gibbs-Duhem consistent expressions, as expected.

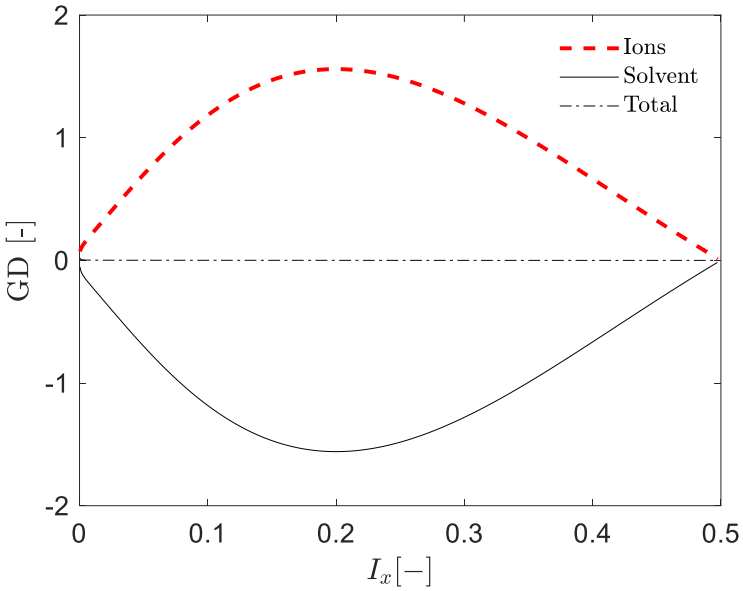


**Figure 26. Gibbs-Duhem consistency test of the ME-PDH term. The red dashed line represents the first term on the left hand side of equation (6.30), the full black line represents the second term on the left hand side of equation (6.30). The sum of both (black dashed line) should be equal to zero in the entire concentration range. Calculation corresponds to the case shown in Figure 24 (right).**

All pertaining calculations related to Figure 24, as well as the proposed derivation, involve a single solvent system. The case of multiple solvent systems must be addressed, as well as its relationship with the choice of an appropriate, fixed reference state.

### *PDH-Based-Extensions and the McMillan-Mayer Framework*

Having obtained some initial expressions, one can now address the desirable situation that introducing concentration dependent properties for multiple solvent systems should remain thermodynamically consistent and retain its physical background.

Inclusion of concentration dependent properties $(\varepsilon_r, d, M)$ in RPM based electrostatic models remains a controversial topic in the literature.[35,167,168,325] As argued by Novak et al.[167] there is no clear consensus even for the modelling of mixed solvent electrolytes, let alone ion concentration dependent properties. Furthermore, as argued by Cardoso and O'Connell,[325] the traditional DH theory neglects pressure effects. The excess energy from the McMillan-Mayer state function $B^E(T, V, N, \mu_s)$ is equivalent to the excess Gibbs free energy, but the partial derivatives are different,[325,326] due to the definition $G^E(P, T, N)$. Thus, several conversions and considerations are necessary to obtain physically meaningful derivatives that do not result in spurious terms and unphysical trends.

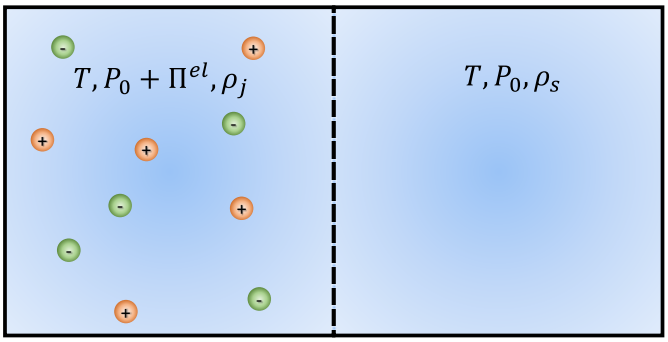


**Figure 27. The McMillan-Mayer osmotic setup. The osmotic pressure of the medium arising from the presence of charged hard spheres is described in the context of DH theory by Pitzer's formalism.**

Regarding multiple solvents, Sander et al.[205] proposed applying a generalization for LR electrostatics in mixed solvent systems as follows:

$$\frac{G^{E-DH(x)}}{RT} = -\sum_s x_s G_s^{E-DH(x)} \tag{6.35}$$

where $G_s^{E-DH(x)}$ is calculated with pure solvent properties for each solvent in the mixture. The authors reported that doing so results in seemingly spurious expressions that contradict expected physical trends.[205,325] The McMillan-Mayer level (Figure 27) deals with a single macroscopic dielectric continuum and hard spherical ions. With this in mind, it seems that partial derivation of DH theory based expressions that attempt discretizing the system (as done with equation (6.35)) may lead to systematic errors.[206,325] Furthermore, the thermodynamic relations that lead to equation (2.44) imply the use of a dielectric continuum of constant molar volume at fixed composition,[35,325] which underlines the statement that the dielectric continuum is not to be discretized.

In contrast, no unexpected trends were observed when including the partial compositional derivation of the density, molar mass and relative permittivity of the mixed solvents within the calculation of $G^{E-DH(x)}$, as done by van Bochove et al.[320] for the PDH term. While no unexpected trends were identified in the LLE calculations of their work, the compositional derivatives did not include the ions. Therefore, the resulting expression was not Gibbs-Duhem consistent. This was corrected in the extension of the PDH term from Chang and Lin,[262] which includes the ions in the compositional derivatives but no further clarifications regarding the use of an averaged global solvent compared to the use of single solvent properties is provided.

Regarding this use of ion concentration dependent properties, Breil and Mollerup[167,327] suggest that the constrain of having fixed dielectric medium properties can be relaxed, given that in an electrolyte "*neither is the solvent a continuous medium, nor the relative permittivity constant".* While some authors disagree with this view, others suggest that a consistent approach that improves practical modelling is achievable when the relative permittivity of the mixture and its compositional derivatives account for all species.[142,167]

With this discussion as a background, one may propose a constrained dependency of the mixture properties (Figure 28) that considers a dielectric continuum characterized by a fixed global average of the solvents. Alternatively, one may also propose a more relaxed dependency (Figure 29) that considers all solvents separately.

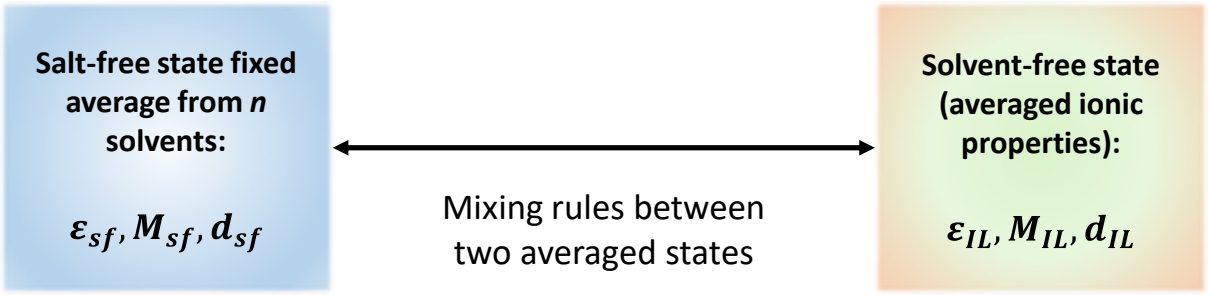


**Figure 28. Proposed approximation (I) for the extension with ion-concentration-dependent properties in a PDH-term-based extension. A concentration dependent path between the salt-free and the solvent-free averaged states (no single ion properties).**

Alternatively, one may also propose a more relaxed dependency (Figure 29) that considers all solvents explicitly. This changes the electrostatic contribution to the activity coefficient of the solvents, making it solvent-specific.

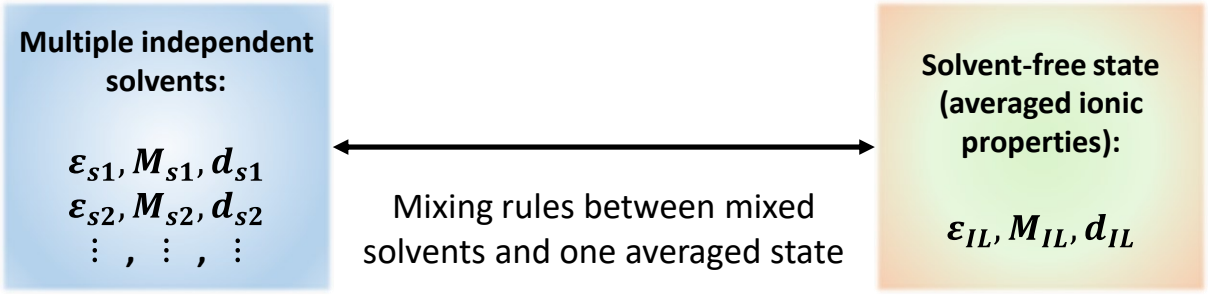


**Figure 29. Proposed approximation (II) for the extension with ion-concentration-dependent properties in a PDH-term-based extension. Multiple solvents with single solvent properties and an averaged solvent-free state (no single ion properties).**

In Figure 28, salt-free averaged properties are kept constant throughout the ion concentration range. The main drawback in Figure 28 is that all solvents in a mixed

solvent electrolyte system are treated with the same averaged properties (salt-free state average) and all have the same averaged contribution of electrostatic origin $\ln(\gamma_s^{el})$, which makes them (from the LR electrostatics perspective) indistinguishable. This is essentially the same drawback found in the application of the conventional PDH term and DH theory in mixed solvent systems;[14,224,225] it is the inevitable cost of a more conservative approach that remains true to the concept of a homogeneous dielectric medium used in the PM. Parameterization procedures are expected to absorb some systematic deviations.[167,168]

Partial derivation with equation (6.34) for all solvents in a mixed solvent electrolyte corresponds to the use of volume fraction mixing rules in the context of Figure 29. An exemplary use of volume fraction mixing between two states with averaged properties $\bar{\mathcal{P}}$ (Figure 28) in a mixed solvent electrolyte reformulates equation (6.34) as follows:

$$\begin{aligned} \mathcal{P}_m &= \sum_i \phi_i \bar{\mathcal{P}}_i = \sum_s \phi_s \bar{\mathcal{P}}_{sf} + \sum_j \phi_j \bar{\mathcal{P}}_j \\ \frac{\partial \mathcal{P}_m}{\partial n_s} &= \frac{\partial}{\partial n_s}(\mathcal{P}_m) = \frac{\bar{\mathrm{v}}_{sf}}{\mathrm{v}_m n_T}\left(\bar{\mathcal{P}}_{sf} - \mathcal{P}_m\right) \\ \frac{\partial \mathcal{P}_m}{\partial n_j} &= \frac{\partial}{\partial n_j}(\mathcal{P}_m) = \frac{\bar{\mathrm{v}}_j}{\mathrm{v}_m n_T}\left(\bar{\mathcal{P}}_j - \mathcal{P}_m\right) \end{aligned} \tag{6.36}$$

and the concentration dependency of the molar mass of the mixture as follows:

$$\begin{aligned} M_m &= \sum_s x_s \bar{M}_{sf} + \sum_j x_j \bar{M}_j \\ \frac{\partial M_m}{\partial n_s} &= \frac{\bar{M}_{sf}}{n_T} - \frac{M_m}{n_T} \\ \frac{\partial M_m}{\partial n_j} &= \frac{\bar{M}_j}{n_T} - \frac{M_m}{n_T} \end{aligned} \tag{6.37}$$

for all *s* solvents and *j* ions present in a multi-component electrolyte, where subscript *sf* stands for salt-free average of the mixed solvents and subscript *j* for the ions with the solvent-free average molar mass of the ions. Thus, ions are indistinguishable from each other (except for charge) and solvents are also indistinguishable from each other. This is consistent with DH theory. The subtle effects of applying averaged states compared to applying explicit properties for each solvent, i.e. applying equation (6.36) instead of equation (6.34) in a mixed solvent system, is exemplified in section 6.3.2.

The concept of a salt-free state includes additional considerations regarding its use as the reference state in mixed solvents, where the convention is that the reference state in the calculation of the chemical potential should be infinite dilution in the most abundant solvent. This is not done in this[18] nor in previous works[14–16] with the COSMO-RS-ES model. For an LLE, it is argued[167] that use of a reference state for the ions at infinite dilution in an averaged, salt-free solvent implies that the reference state is different in each of the two phases (e.g. $\alpha$ and $\beta$) and therefore, the condition $x_i^\alpha \gamma_i^\alpha = x_i^\beta \gamma_i^\beta$ is not met unless the difference between reference states is accounted for. For instance, Chen and Song[198] select infinite dilution in water as the reference state for all calculations and introduce a Born term for transfer energetics between water each of the mixed solvent liquid phases.

Selecting infinite dilution in the most abundant solvent for both phases is indeed correct. However, the definition of a salt-free reference state remains a helpful tool that does not necessarily run into inconsistencies depending on how it is applied. In an LLE, one may choose infinite dilution in one of the two liquid phases as the reference state for both, thereby circumventing any further complications if this chosen reference state is accessible and free energies of transfer at infinite dilution are accounted for. An interesting subtlety is that this is perfectly possible and easily done with a COSMO-RS based model, where the grounded conductor is the initial state and any arbitrary pure compound or mixture can be selected as the reference state for the calculation of the residual activity coefficient according to equation (2.129). Furthermore, LR electrostatic terms do not account for single ion solvation but for ion-ion interactions, which are absent for single ion transfer in the salt-free state. Therefore, choosing infinite dilution in one phase as the reference state for the other implies transfer in the absence of ion-ion interactions and no LR term is involved.

COSMO-RS based electrolyte models describe the partitioning of ions[15] and the use of free energies of transfer of ions as part of the training set improves the prediction of species partitioning in liquid-liquid systems.[15,16] Thus, it seems that COSMO-RS based electrolyte models can effectively describe these systems without the need for a Born term. This does not exclude the fact that the Born term could be tested as a complement in the future.

Finally, in the RPM the only variables that characterize the solvent are the relative permittivity and density. The presence of the density and the molar mass in the partial derivatives in equations (6.21), (6.27) and (6.29) comes, as described in section 2.2.3, from

concentration scale conversions of the charge density valid at low concentrations. In the DH theory (Poisson-Boltzmann based), a hard spherical ion is approximated by means of excluded dielectric volume with a point charge at the center (refer to Figure 2 and Figure 3). This implies that the excluded volume at $r < a$ retains the properties of the medium.[22] The proposed approach in Figure 28 for concentration dependency does not assign a different density to the excluded volume; it represents concentration dependent changes of the whole dielectric continuum. In this sense the framework is still respected. However, variable density and molar mass do violate the constant molar volume assumption. Thorough derivation may include concentration dependencies in the fundamental calculation of the averaged electrostatic potential $\psi_i^{av}(r)$, but such approaches can quickly lead to equations with no analytical solution.[33] Furthermore, non-trivial $\Delta(\Pi^{el}V)$ corrections due to the $\Delta G^{el} \equiv \Delta A^{el}$ assumption are necessary to introduce the effect of pressure (including the electrostatic contribution) on the volume of the mixture.[325,328–330] Assuming and incompressible liquid, the COSMO-RS-ES model neglects these[14–17] and the present work assumes that their effects are small and can be absorbed into the adjusted parameters. Setting aside the premise that systematic deviations remain acceptable after parameterization, one can still assess the effects of considering molar mass and density as concentration dependent properties from the perspective of practical application.

### *Symmetric and Asymmetric Conventions*

The conventional PDH term from equation (2.51) is the derivative of the excess Gibbs free energy expression from equation (2.49) and has the pure solvent as the reference state. The overall electrostatic contributions to the activity coefficients have a reference state in the symmetric convention for the solvent ($\gamma_s^{PDH} \to 1, x_s \to 1$) and in the asymmetric convention for the ions ($\gamma_j^{PDH} \to 1, x_j \to 0$). If one were to formulate a term that is also symmetric for the ions (strictly speaking "pseudo-symmetric": here the reference state of a single ion, regardless of its charge and nature, is a stochiometric undercooled melt of ions and counter-ions), then one requires to subtract the value of $G^{DH}$ at the pure IL / hypothetical molten state in equation (2.49) as follows:

$$\frac{G^{DH(x)}}{RT} = -\frac{4A_\phi^{(x)} n_T I_x}{b^{(x)}} \ln\left(1 + b^{(x)}\sqrt{I_x}\right) + \frac{4A_\phi^{(x)} n_{IL} I_x^{IL}}{b^{(x)}} \ln\left(1 + b^{(x)}\sqrt{I_x^{IL}}\right) \qquad (6.38)$$

where the ionic strength of the molten salt/IL can be easily calculated as $I_x^{IL} = \frac{1}{2}\sum_j \frac{z_j^2 v_j}{v}$, but formally it equates to the following definition:

$$I_x^{IL} = \frac{\delta_{z_i}}{2}\sum_j z_j^2 x_j^{IL} \qquad \delta_{z_i} = \begin{cases} 0, & i = s \\ 1, & i = j \end{cases} \tag{6.39}$$

where $x_j^{IL} = n_j/n_{IL}$ and a delta $\delta_{z_i}$ is introduced because the ionic strength of the melt is independent of the solvent, but not of the ions. For instance, a mole fraction of 0.2 NaCl in an aqueous electrolyte will keep a 1:1 cation to anion ratio, regardless of any changes in the concentration of water. The ionic strength $I_x$ depends on the concentrations of all the species in the mixture, but $I_x^{IL}$ depends exclusively on the ion to counter-ion ratio. Thus, the derivative of equation (6.39), also solvent independent, is expressed as follows:

$$\frac{\partial I_x^{IL}}{\partial n_i} = \frac{\delta_{z_i} z_i^2}{2n_{IL}} - \frac{\delta_{z_i} I_x^{IL}}{n_{IL}} \qquad \delta_{z_i} = \begin{cases} 0, & i = s \\ 1, & i = j \end{cases} \tag{6.40}$$

which is evidently not zero despite $I_x^{IL}$ being a constant in practical calculations. At the fused salt state $n_T \to n_{IL}$ and partial derivation of equation (6.38) leads to:

$$\ln\left(\gamma_{i,\ symm}^{PDH}\right) = -A_\phi^{(x)}\left[\frac{2z_i^2}{b^{(x)}}\ln\left(\frac{1+b^{(x)}\sqrt{I_x}}{1+b^{(x)}\sqrt{I_x^{IL}}}\right) + \frac{z_i^2\sqrt{I_x} - 2I_x^{1.5}}{1+b^{(x)}\sqrt{I_x}} - \frac{z_i^2\sqrt{I_x^{IL}} - 2(I_x^{IL})^{1.5}}{1+b^{(x)}\sqrt{I_x^{IL}}}\right] \tag{6.41}$$

which differs from the commonly referenced equation (2.53). The latter is missing the third term, which was most likely omitted by Pitzer[40] given that, strictly speaking, the DH derivation is for the charge symmetric 1:1 case ($I_x^{IL} = 0.5$) where the third term vanishes:

$$\frac{z_i^2\sqrt{I_x^{IL}} - 2(I_x^{IL})^{1.5}}{1+b^{(x)}\sqrt{I_x^{IL}}} = 0 \quad \forall \ \ z_+ = |z_-| = 1$$

The case is different in practical calculations when DH theory is applied to other $z_+, z_-$ charge configurations where the third term is no longer zero. Thus, as correctly noted by Chen and Song,[199] the derivative of $I_x^{IL}$ with respect to the ion to counter-ion ratio in the ionic melt is to be accounted for. Therefore, the fully correct expression for the symmetric PDH term is equation (6.41), not the commonly cited equation (2.53).

In line with this discussion, the full forms of the symmetric E-PDH and ME-PDH terms are straightforward, both stemming from equation (6.38) but including the corresponding

concentration dependencies to the Debye-Hückel slope $A_{\phi}^{(x)}$ and the parameter of closest approach ($b^{(x)}$ or $b_{mod}^{(x)}$, when applicable):[18]

$$ln\left(\gamma_{i,\ symm}^{E-PDH(x)}\right) = ln\left(\gamma_{i}^{E-PDH(x)}\right) + A_{\phi_{IL}}^{(x)}\left\{\frac{2z_i^2\ ln\left(1 + b_{IL}^{(x)}\sqrt{I_x^{IL}}\right)}{b_{IL}^{(x)}} + \frac{z_i^2\sqrt{I_x^{IL}} - 2(I_x^{IL})^{1.5}}{1 + b_{IL}^{(x)}\sqrt{I_x^{IL}}}\right\} \quad (6.42)$$

$$ln\left(\gamma_{i,\ symm}^{ME-PDH(x)}\right) = ln\left(\gamma_{i}^{ME-PDH(x)}\right) + A_{\phi_{IL}}^{(x)}\left\{\frac{2z_i^2\ ln\left(1 + b_{mod_{IL}}^{(x)}\sqrt{I_x^{IL}}\right)}{b_{mod_{IL}}^{(x)}} + \frac{z_i^2\sqrt{I_x^{IL}} - 2(I_x^{IL})^{1.5}}{1 + b_{mod_{IL}}^{(x)}\sqrt{I_x^{IL}}}\right\} \quad (6.43)$$

where the superscript/subscript $IL$ stand for fixed averaged solvent-free properties.

A last comment on the solvent-free state properties is necessary. The fused salt state is calculated with averaged ionic properties, as already implied in Figure 28 and Figure 29. Multiple salt, multiple IL or salt + IL systems should also apply averaged molten salt properties to handle a fixed, averaged solvent-free state. The disadvantages of this procedure are that all ions, regardless of their size, are treated with the same properties (except charge). Unfortunately, this is how the RPM is formulated and attributing more properties to the ions implies using a different approach. The RPM is limited in this sense.

Derivation of a PDH term in the mole fraction convention with corrections for size and charge asymmetries of the ions is possible[166,331,332] and an option that could be explored in the future in order to have some level of distinction between diverse ions in a mixed salt/IL system. Ionic size asymmetries have a negligible impact in the dilute region,[17] however, ionic charge asymmetries do have an impact in the entire concentration range.[48,97] The impact of ionic size asymmetries is yet to be evaluated in the highly concentrated regime and could provide a direction for future research.

### 6.2.2 Application of ME-PDH to COSMO-RS-ES for Conventional Salts

In the same fashion as described in section 6.2.2, equation (6.29) is combined with the COSMO-RS-ES model and the corresponding SR parameters from Table 5 are re-parameterized, in order to systematically evaluate the benefits and drawbacks of including extended LR electrostatics within the modelling of electrolyte systems.

In order to apply the ME-PDH term from equation (6.29), the more conservative approach from Figure 28 was selected. Thus, the following mass fraction based mixing applied for

density was kept from previous versions of the COSMO-RS-ES model,[14–16] but now including a hypothetical extrapolation for the highly concentrated salt:

$$d_m = \sum_j \frac{x_j \bar{M}_j \bar{d}_{salt}}{\sum_i x_i \bar{M}_i} + \sum_s \frac{x_s \bar{M}_{sf} \bar{d}_{sf}}{\sum_i x_i \bar{M}_i} \tag{6.44}$$

where averaged properties between the salt-free and solvent-free states are applied, in line with Figure 28.

The extrapolated density of the highly concentrated salt $\bar{d}_{salt}$ is estimated according to the following correlation:

$$\bar{d}_{salt} = 1076.48004 \cdot M_{salt}^{0.1553} \tag{6.45}$$

and the averaged salt-free value $\bar{d}_{sf}$ is estimated based on the mass fraction average in the case of mixed solvents.

The relative permittivity of the mixture was estimated with the following mixing rule:

$$\varepsilon_m = \left[\frac{\bar{\varepsilon}_{sf}}{1 + \alpha_{salt} \sum_j x_j}\right]\left(\sum_s x_s\right) + \varepsilon_{salt}\left(\sum_j x_j\right) \tag{6.46}$$

where $\bar{\varepsilon}_{sf}$ is the salt-free volume fraction based average of the solvents and $\alpha_{salt}$ is a fitting parameter. Equation (6.46) provided more satisfactory results when compared to mass or volume fraction based mixing rules and is based upon a combination of the mixing rules reported by Inchekel et al.[83,140] and Ascani and Held.[184] The chosen value for $\varepsilon_{salt}$ was 13, based on averaged values for molten salts and ILs.[86,87]

The qualitative behavior of equation (6.49) matches the qualitative behavior of the volume fraction mixing rule when $\alpha_{salt}$ is fitted to do so. For instance, the experimental relative permittivity of the water + [BMIM][$BF_4$] system reported by Koeberg et al.[85] is virtually equivalent to the volume fraction mixing rule and satisfactorily described with equation (6.49) using $\alpha_{salt} = 3.62$ ($AAD = 0.319$ $R^2 = 0.9998$ for $\varepsilon_w = 78.34$ and $\varepsilon_{IL} = 6.7$). Thus, for salt systems, a general deviation from volume fraction is expected to be captured by $\alpha_{salt}$ if left as an open parameter.

The distance of closest approach $a$ applied in equations (6.23) and (6.28) for use in the ME-PDH term is estimated in the same manner as performed in section 6.1.3 where $a = F_a(r_+^{COSMO} + r_-^{COSMO})$ and $F_a$ is a fitting parameter.

Re-parameterizations of the COSMO-RS-ES model with E-PDH (for comparison) and ME-PDH are presented in Table 9. Several conclusions can be drawn from the results shown in Table 9. Firstly, the use of a PDH-term-based extension results in overall enhanced performance when the modified parameter of closest approach is applied instead of the conventional parameter of closest approach. This finding agrees with the results discussed for Table 8. This is expected based on the observations made for Figure 24 and provides further, consistent evidence that modifications to the conventional theory are required to provide more reliable modelling results.

**Table 9. Results of diverse parameterizations with the COSMO-RS-ES model (energy interaction equations from Table 5; parameters are published[18]) applying extended LR electrostatics.**

| **Parameterization** | **I. COSMO-RS-ES +E-PDH eq. (6.21)** | **II. COSMO-RS-ES +ME-PDH eq. (6.29)** | **III. COSMO-RS-ES +ME-PDH eq. (6.29)** |
|---|---|---|---|
| Permittivity Model (optimized $\alpha_{salt}$) | Eq. (6.46) with $\alpha_{salt} = 1.82$ $\varepsilon_{salt} = 13$ | Eq. (6.46) with $\alpha_{salt} = 2.39$ $\varepsilon_{salt} = 13$ | Eq. (6.46) with $\alpha_{salt} = 2.38$ $\varepsilon_{salt} = 30.8$ |
| Dataset ($N_{DP}$) | Average Absolute Deviation (AAD) | | |
| MIAC aqueous + mixed aqueous ($m_{max} = 15\,\frac{mol}{kg}$) (2889) | 0.111 | 0.076 | 0.069 |
| MIAC non-aqueous (976) | 0.835 | 0.434 | 0.497 |
| LLE (1056) | 0.781 | 0.718 | 0.660 |
| Dielectric decrement (259) | 6.281 | 5.201 | 5.918 |
| SLE (836) | 0.905 | 1.027 | 0.948 |
| **Total (5757)** | 0.473 | 0.392 | 0.375 |

Results from datasets that are no included in the training set can be considered pure predictions. The results of parameterization III included $\varepsilon_{salt}$ as an optimizable parameter. The results from parameterizations I and II kept $\varepsilon_{salt} = 13$ as a constant. **Color:** not part of the training set.

Model performance is satisfactory for aqueous systems, as in previous versions of the model.[14] Thus, the central goal, as can be inferred from the results from Table 8 and Table 9, is a continuous improvement with focus on non-aqueous systems while keeping the already achieved precision for aqueous systems. While consistent reduction of the AAD

for non-aqueous MIACs can be observed in the historical model development from Table 8 to Table 9, a more relatable illustration is the direct prediction of salt solubility in diverse solvents.

Figure 30 provides predictions of this type of data for several aqueous and non-aqueous systems performed with parameterization III from Table 9. The corresponding parameters are shown in Table 10.

**Table 10. Parameters for the COSMO-RS-ES model (version corresponds to Table 5) combined with the ME-PDH term applying the mixing rules from equations (6.44) and (6.46).**

| **Cation Radii [Å]** | | **Parameters A, B** $\left[\frac{\mathbf{kJ\ Å^2}}{\mathbf{mol\ e^2}}\right]$ | | **Threshold Parameters** $\left[\frac{\mathbf{e}}{\mathbf{Å^2}}\right]$ | | **parameters D, E** $[-]$ | |
|---|---|---|---|---|---|---|---|
| $Li^+$ | 1.589 | $A_1$ | 7249 | $C_1$ | 0.0102 | $D_1$ | 33.149 |
| $Na^+$ | 1.874 | $A_2$ | 0 | $C_2$ | 0.0009 | $E_1$ | 1.1253 |
| $K^+$ | 2.016 | $A_3$ | 1537 | $C_3$ | 0 | $E_2$ | 0.2362 |
| $Rb^+$ | 2.108 | $A_4$ | 4653 | | | $E_3$ | 0.0634 |
| $Cs^+$ | 2.174 | $A_5$ | 184 | | | | |
| | | $A_6$ | 3918 | | | | |
| **Supplementary LR parameters** | | $B_1$ | 24068 | | | | |
| $F_a$ | 0.562 | $B_2$ | 8528 | | | | |
| $\alpha_{salt}$ | 2.384 | $B_3$ | 8805 | | | | |
| $\varepsilon_{salt}$ | 30.8 | $B_4$ | 413 | | | | |
| | | $B_5$ | 25685 | | | | |
| | | $B_6$ | 1035 | | | | |
| | | $B_7$ | 16596 | | | | |
| | | $B_8$ | 3E-4 | | | | |

The corresponding parameters for parameterizations I and II of Table 9 can be consulted in the original publication.[18] In the best performing parameterization, one may observe that several of the parameters shown in Table 10 have attained comparably large values, whereas a couple (including a misfit term) have practically vanished. This could be indicative of a local minimum, which would not be surprising. As suggested by Müller et al.[15] the COSMO-RS-ES model may present multiple minima in the solution space and

these can sometimes be overcome by introducing additional data types into the training set. Furthermore, unexpected parameters that nevertheless yield good results can be found in virtually all published COSMO-RS-ES parameterizations (e.g. exponentials that tend to zero,[14,15] negligible interaction energy parameters[16,18]). These types of observations sometimes lost attention but point to the flexibility of the model, the non-triviality of the optimization problem and the need to introduce the widest possible training set. They also encourage to explore areas of opportunity in the short-range contribution (section 6.4.3). Within the context of this discussion, the resulting predictions of the model are remarkable but have required a careful balance of the short- and LR contributions via systemic parameterization procedures.

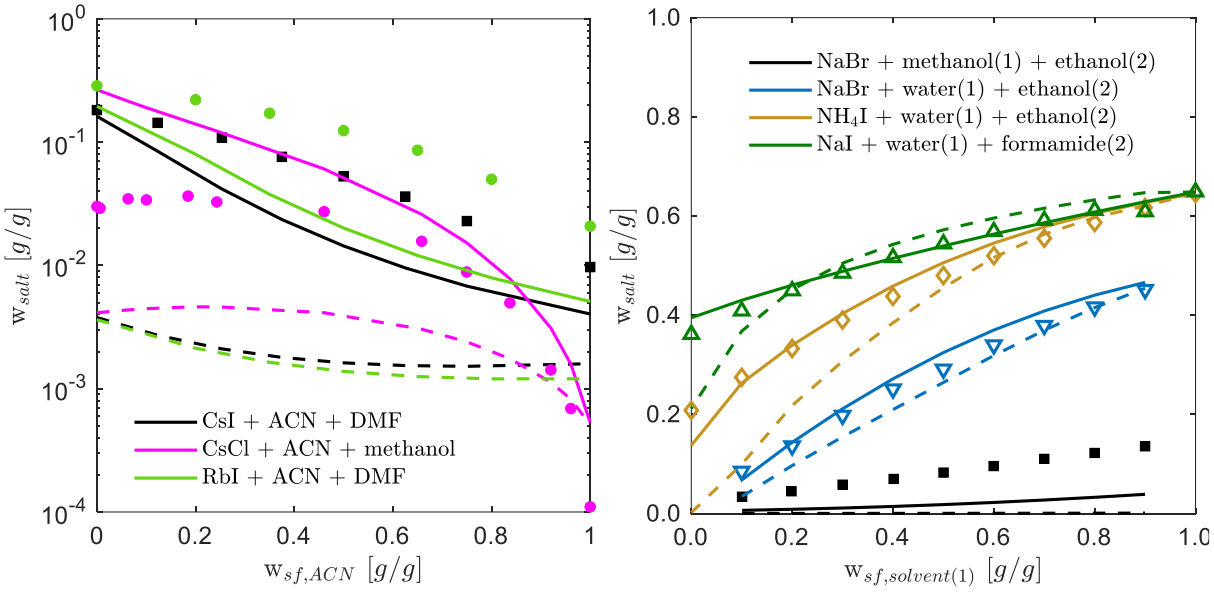


**Figure 30. Predictions of the solubility of diverse salts in aqueous mixed and non-aqueous mixed solvents. Salt solubility is displayed as a function of the mass fraction of one of the solvents in the salt-free mixture. Full lines are predictions performed with the COSMO-RS-ES model + ME-PDH as the LR term (parameterization III from Table 9; parameters from Table 10). The dashed lines are predictions from the COSMO-RS-ES model + PDH from Müller et al.[16] The solubility on the left side is presented in logarithmic scale to facilitate visual comparison. Experimental data from the IUPAC-NIST Solubility Data Series[333] for the left pane. The NaBr systems are taken from Pinho and Macedo,[334] the NaI system from Hernández-Luis et al.,[335] and the $NH_4I$ system from Seidell.[336] ACN = acetonitrile; DMF = N,N-dimethylformamide; T = 298.15 K.**

In general, qualitative improvement can be observed for the solubility predictions performed with the present parameterization which applies modified and extended LR electrostatics. In Figure 30 (left), the predicted solubility of cesium iodide and rubidium iodide in the acetonitrile + N,N-dimethylformamide mixture has a correction of roughly one order of magnitude for both salts when compared to previous works. Furthermore, the qualitative trend is also corrected, and the predicted solubility of rubidium iodide is

higher than that of cesium iodide, which is in agreement with the corresponding experimental data. In contrast, one may observe that the predicted solubility of cesium chloride in the acetonitrile + methanol mixture is in agreement with previous works for the limit of pure acetonitrile (both parameterizations overestimate the result) and overestimates the solubility with increasing methanol concentration. An overestimation of the solubility comes from an underestimation of the corresponding mean ionic activity coefficient values with respect to expectation. This could be indicative of solvation effects of the ions that are not being correctly accounted for and/or of overestimated ion to counter-ion interaction energies.

Interestingly, the solubility of CsCl should be the lowest of all the datasets presented in Figure 30 (left), yet both parameterizations predict it as the highest. This provides further evidence that, while extended LR electrostatics improve the overall results, the systematic errors from both the short-range empirical equations (Table 5) and the Debye-Hückel linearized derivation are carried to newer versions of the COSMO-RS-ES model. Nevertheless, model performance remains quite satisfactory, given that solubility data are not part of the training set, and these have been predicted (in some cases with high precision) without invoking any system specific or group contribution parameters. This is evidenced in Figure 30 (right), which shows the predicted solubility of several salts in mixed aqueous systems and a mixed alcohol system. It is noteworthy to point out that the sodium iodide + water + formamide system may have co-crystallization near the 80% mass water concentration of the salt-free solvent. This behavior in the diagram may also be due to experimental error, given that the resulting sodium iodide crystals presented some anomalies possibly due to oxidation according to Hernández-Luis et al.[335]

Regarding the concentration dependent properties, it can be observed in Table 9 that excluding the dielectric decrement data from the training set yields a slightly better optimum by reducing the effects of the ions on the relative permittivity of the solution. The generalized increase of the AAD of the dielectric decrement dataset is due to an overestimation with respect to raw experimental values. This is clearly exemplified in Figure 31 for aqueous lithium bromide.

Figure 31 includes the experimental values and a correction for the kinetic depolarization, as described in section 2.2.7. One may observe that the calculated value lies in the upper limit of the corrected dielectric decrement. Thus, results from parameterization III seem

to support the concept that raw experimental values of the dielectric decrement should not be applied to a thermodynamic model without any considerations, as discussed by Maribo-Mogensen et al.[141] Lacking experimental data for the conductivity of mixed and non-aqueous electrolytes, the concentration dependent relative permittivity is left as an open prediction with no contribution to the objective function. Experimental data for the density of salt and IL systems could be considered in the future as part of the training set.

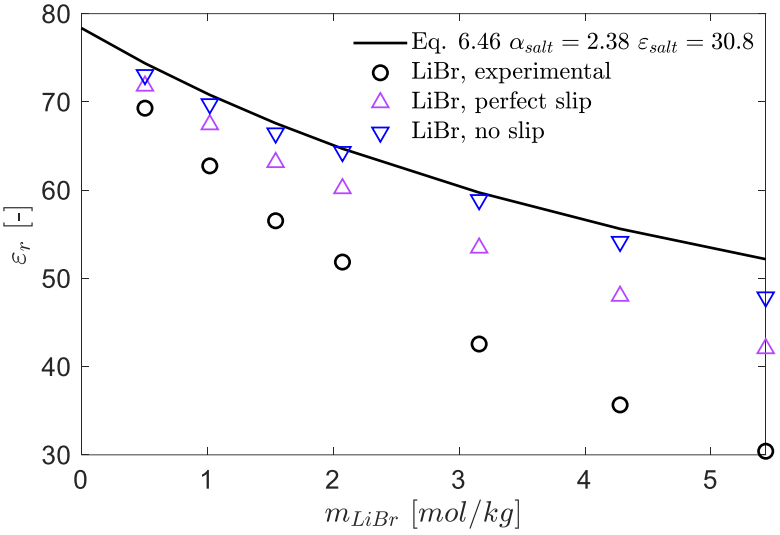


**Figure 31. Dielectric decrement of aqueous LiBr at room temperature. Experimental data from Barthel et al.[337] The perfect slip and no slip conditions were applied with equation (2.106) using a response time of $\tau = 7.4$ [ps] for water and correlated conductivity data from Wu et al.[338] Similar examples can be consulted in the original publication.[18]**

Finally, while correlations and predictions of non-aqueous systems benefit considerably in the parameterizations presented in section 6.1.3 and even more so in the present section, there is an evident tradeoff. The precision of the partitioning of salts in aqueous liquid-liquid equilibria in salt systems has an AAD of 0.66 for parameterization III in Table 9, which is comparable to the AAD of 0.69 reported by Gerlach et al.[14] But the lowest reported AAD for these systems is 0.52 from Müller et al.[16] Describing solvation in neat organic solvents reduces precision for LLE systems. In spite of this tradeoff, corrections towards the concentrated, non-aqueous regime are achieved and one may begin to consider IL systems.

Before introducing IL systems directly into a COSMO-RS-ES-based approach (section 6.4), an attempt to assess these types of systems with the normal COSMO-RS is performed (section 6.3). The central reason for this being that some IL data are acceptably described by the normal COSMO-RS model without the need for any electrolyte considerations other

than using an electroneutral, fully dissociated mixture.[252] This modelling approach with no LR electrostatics represents a considerable gap between COSMO-RS-ES approach and the widespread use of the normal COSMO-RS as a tool for IL screening and modelling.

## 6.3 Assessing openCOSMO-RS for Ionic Liquids

It is commonly assumed that ILs behave like neutral molecules in a liquid phase and that no additional complexities are required in their modelling. In chemical engineering, it is indeed known[115,116,252,269] that the COSMO-RS model performs rather well when estimating infinite dilution activity coefficients of neutral substances diluted in pure ILs. Furthermore, the COSMO-RS model has been widely applied and reviewed[115,243,244,339–341] for solvent screening as well as the estimation of liquid-liquid equilibria in IL systems and salt-based deep eutectic mixtures. The results for LLE are, in several cases, not satisfactory.[115,247,253] This begs the question of whether a correction with LR electrostatics is physically meaningful or whether attempting this is, in plain terms, trying to fix a non-existent problem. In essence: is a short-range contribution good enough for all practical purposes when modelling ILs?

The experience with the COSMO-SAC + E-PDH model is that IDAC calculations are best when LR forces are completely absent.[263] Equation (6.29) provides a unique opportunity to reassess the prospective performance of a COSMO-RS model for IL systems and test whether LR electrostatics do play some role in systematic improvement at the molecular-solvent-free limit. If the COSMO-RS model already performs satisfactorily, one may hypothesize that physically meaningful LR electrostatics should only provide some form of minor correction. Thus, the present subchapter tests this hypothesis by comparing calculations with openCOSMO-RS[114] and performing IL-dedicated COSMO-RS parameterizations with and without the inclusion of extended LR electrostatics.

In the present section, IDACs of neutral molecules in pure ILs and ternary LLE data of single IL-containing systems (refer to section 5.1.2 for database description) are used for initial validation and subsequent parameterizations to assess the impact of extended LR electrostatics.

### 6.3.1 Brief Validation of openCOSMO-RS at the Pure Ionic Liquid Limit

Paduszyński[116] has performed a thorough systematic evaluation of the commercially available COSMO-RS model (COSMOtherm) applied to the prediction of the activity coefficients of molecular solvents infinitely diluted in pure ILs. The accuracy of the model is then assessed both qualitatively and quantitatively. At the TZVP parameterization level, the evaluations performed in his work yield an AAD of 0.595 for the logarithmic infinite dilution activity coefficients from a total of 41868 data points.

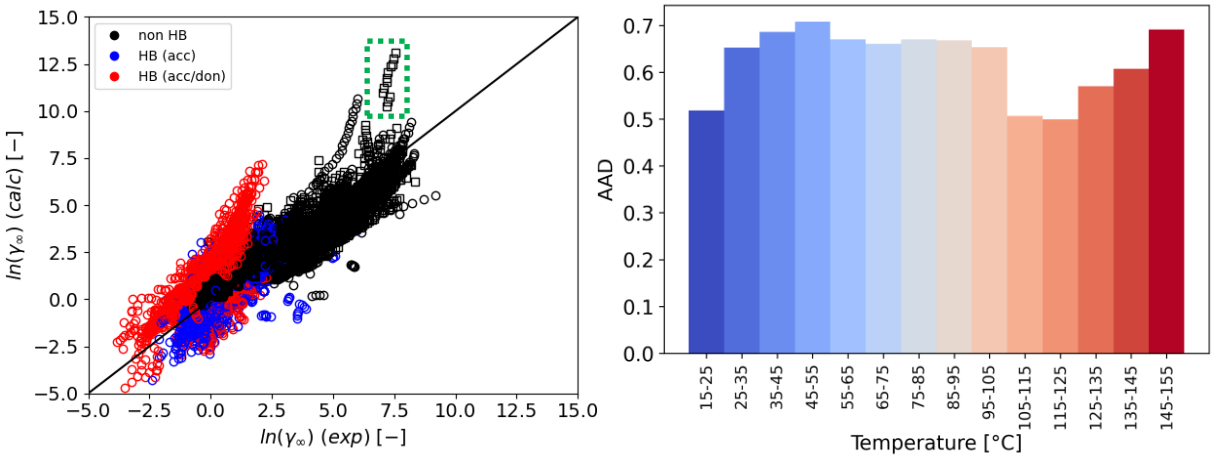


**Figure 32. Right: parity plot of the logarithmic IDAC values of neutral components in pure ILs extracted from the IL-Thermo database[296,297] vs. openCOSMO-RS[114] predictions with the parameters given in section 2.4. Left: AAD broken down by temperature range.**

The COSMO-RS implementation[114] applied in the present work has several drawbacks when compared to the commercially available version. Namely, and as previously stated in section 2.4, Van der Waals parameters have not yet been introduced and the use of averaged conformer weights for a compound have also not been introduced. Nevertheless, one should expect to obtain averaged deviations of the same order of magnitude as those observed in the work of Paduszyński.[116]

Figure 32 shows a parity plot of experimental and predicted logarithmic IDAC values with the openCOSMO-RS[114] implementation using the parameters described in section 2.4. The resulting AAD is 0.673 for 21634 data points, which is higher than the 0.588 value reported for the commercial COSMO-RS version reported by Paduszyński,[116] but in the same order of magnitude and with a clearly general qualitative trend, as expected.

In Figure 32 the neutral molecules infinitely diluted in pure ILs have been classified as non-polar/non-hydrogen bonding (black), hydrogen bond acceptors/donors (red) and

hydrogen bond acceptors (blue). Some systematic deviations are observable for the donor/acceptor group, which are mostly overestimated, and the non-polar group that tends to skew towards overestimation for the larger values. In the present work, the largest outliers in the non-polar group (green rectangle) correspond to an imidazolium hydrogen-sulfate based IL. The second largest outlier in the nonpolar group corresponds to measurements in an imidazolium tris(dicyanoazanide) based IL. These observations are in agreement with what is reported by Paduszyński.[116] Roughly, 80% of the predicted values have an absolute deviation that is below one logarithmic unit and over 97% of the predicted values fall below a deviation of 2 logarithmic units.

Further characterization of the results are beyond the scope of the present work and thorough details regarding the efficiency of the COSMO-RS methodology for this type of data can be consulted in literature.[116] For the presently addressed purposes, the results from Figure 32 constitute a validation of both the database and the COSMO-RS implementation being applied. The central question pertaining to the present work is testing whether these predictions can improve upon addition of LR electrostatics.

### 6.3.2 Extended Long-Range Electrostatics at the Pure Ionic Liquid Limit

The IDAC values are useful to evaluate and refine the impact of LR electrostatics on neutral compounds. This was not performed for conventional salts due to very limited access to actual experimental data of solvents diluted in the fused salt state. The molten state of conventional salts (with a few exceptions, e.g. several post-transition metal halides or some eutectic salt mixtures) is commonly expected at temperatures of 200°C or (considerably) higher. Thus, not only is the data scarce, but it is also more resource intensive. The case is different for ILs, which are commonly in a molten state at temperatures below 100°C.

The present subchapter tests LR electrostatic terms in combination with openCOSMO-RS as published,[114] with the COSMO-RS parameters from Gerlach et al.[14] shown in Table 4. The required physical properties are the density of the pure IL, a value for the relative permittivity of the pure IL and the molar mass of the ions in question. In line with findings and discussions from previous sections, the following assumptions are kept for the ions in an IL:

$$d_{IL} = d_+ = d_- \tag{6.47}$$

$$\varepsilon_{IL} = \varepsilon_+ = \varepsilon_- \tag{6.48}$$

$$M_{IL}/v = M_j \tag{6.49}$$

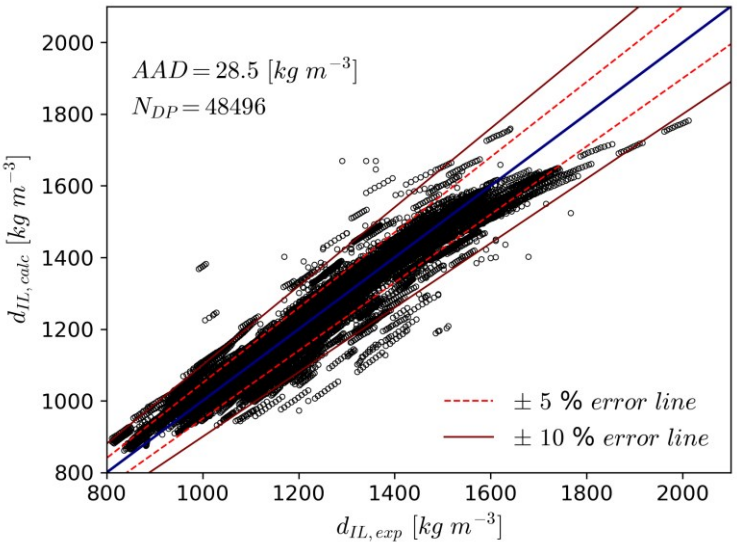


**Figure 33. Density of diverse ILs as calculated with equation (6.50) compared to 48496 experimental data points extracted from IL-Thermo.[296,297] Over 90% of the calculated values lie below the ±5% error threshold. The AAD of 28.5 g/L corresponds to an absolute deviation of 2.33%.**

The density of pure ILs obtained from the IL-Thermo database[296,297] can be correlated with a simple four parameter expression given by:

$$d_{IL}\,[g \cdot L^{-1}] = A \cdot \left(\frac{M_{IL}\ [g \cdot mol^{-1}]}{V_{IL}^{vdw}\ [\text{Å}^3]}\right)^B - C \cdot T\,[K] + D \cdot P\,[MPa] \tag{6.50}$$

where $V_{IL}^{vdw}$ stands for the sum of the individual Van der Waals volumes of all the atoms in an IL. The corresponding parameters are: $A = 2033.324, B = 0.6909, C = 0.6717$ and $D = 4.52 \cdot 10^{-4}$. The molecular Van der Waals volumes applied where taken from the RDkit package[342] for Python. This correlation results in an AAD of 28.5 g/L and its results can be observed in Figure 33. To evaluate the density of the mixture and its compositional partial derivatives, volume fraction mixing rules were selected. Equation (6.50) is based on the expression proposed by Slattery et al.[343,344]

Measurements of the relative permittivity of pure ionic liquids was also extracted from the IL-Thermo database.[296,297] These remain controversial because they are based on

extrapolations of adjusted models.[87] High values (e.g. $\varepsilon_{IL} > 15$) could be subjected to experimental error e.g. due the presence of water or other impurities.[86,87] Still, some high values for specific cases like (2-hydroxyethyl)ammonium nitrate are consistently found.[86,323] Furthermore, an apparent increase in the relative permittivity of an electrolyte is typically attributed to instantaneous dipoles from ion-pairing.[345] In an IL, instantaneous pairs may be present but as well as ions that are themselves dipoles, which introduces further complications.[87] Conflicting literature sources can be found, like the reported $\varepsilon_{IL}$ value of 8.3 for (2-hydroxyethyl)ammonium lactate in the work of Bennett et al.[86] in contrast to the value of 85.6 reported by Huang et al.[323] Thus, the experimentally measured relative permittivity of pure ILs may be biased in many regards and should be treated with reserve.

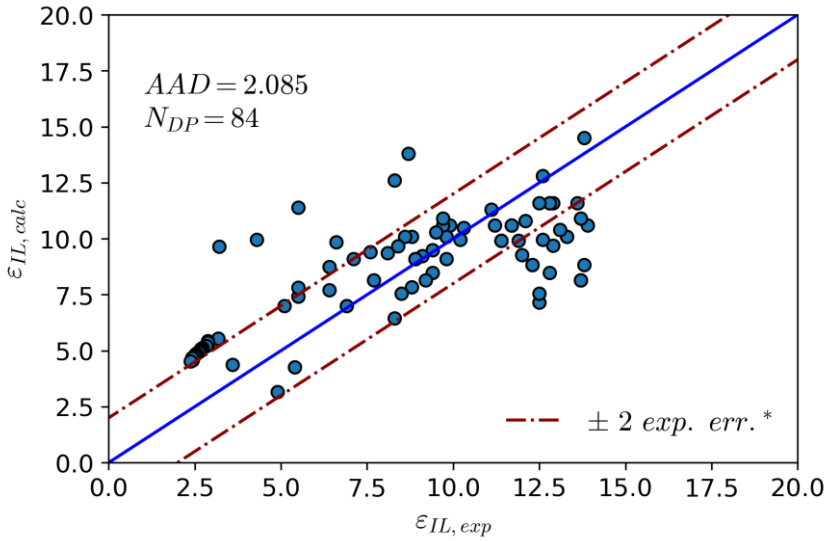


**Figure 34. Relative permittivity of several ILs calculated with equation (6.51) compared to 84 extrapolations from experimental measurements extracted from IL-Thermo.[296,297] *±2 is the largest experimental error reported for values below 15. As a reference, the two parameter correlation for $\varepsilon_{IL}$ provided by Chang and Lin[262] yields an AAD of 2.604 for the same dataset.**

Arbitrarily selecting values below 15, the experimental measurements of $\varepsilon_{IL}$ extracted from IL-Thermo can be acceptably correlated as a function of molar volume as follows:

$$\varepsilon_{IL} = 1 - A \cdot \ln(\mathrm{v}_{IL}\ [L\ mol^{-1}]) \left(1 + \frac{298.15K}{T\ [K]}\right) \tag{6.51}$$

with $A = 2.867$. The results of this expression are shown in Figure 34. Molar volumes are calculated with the molar mass and the density results from equation (6.50). High $\varepsilon_{IL}$ values cannot be discarded in extraordinary cases[86,323,346] (e.g. ethylammonium nitrate,

(2-hydroxyethyl)ammonium formate) are not included and cannot be reproduced with equation (6.51).

**Table 11. Diverse volume fraction based mixing rules that can be applied (e.g. with extended LR electrostatics) for the permittivity of an arbitrary liquid mixture.**

| Mixture Permittivity | Partial Compositional Derivative |
|---|---|
| Linear<br>$\varepsilon_m = \sum_i \phi_i \varepsilon_i = \sum_i \frac{x_i \mathrm{v}_i \varepsilon_i}{\sum_i x_i V_i}$ | $\frac{\partial \varepsilon_m}{\partial n_k} = \frac{\partial}{\partial n_k}\left(\sum_i \frac{x_i \mathrm{v}_i \varepsilon_i}{\sum_i x_i \mathrm{v}_i}\right) = \frac{\mathrm{v}_k}{\mathrm{v}_T n_T}(\varepsilon_k - \varepsilon_m)$ |
| Quadractic<br>$\varepsilon_m = \frac{1}{2}\sum_i \sum_j (\varepsilon_i + \varepsilon_j)(1 + k_{ij})\phi_i \phi_j$ | $\frac{\partial \varepsilon_m}{\partial n_k} = \frac{1}{2}\sum_i \sum_j \frac{\partial \varepsilon_m^{ij}}{\partial n_k}$<br>$\frac{\partial \varepsilon_m^{ij}}{\partial n_k} = (\varepsilon_i + \varepsilon_j)(1 + k_{ij})\left(\phi_i \frac{\partial \phi_j}{\partial n_k} + \phi_j \frac{\partial \phi_i}{\partial n_k}\right)$ |
| Cubic<br>$\varepsilon_m = \frac{1}{3}\sum_i \sum_j \sum_l (\varepsilon_i + \varepsilon_j + \varepsilon_l)(1 + k_{ijl})\phi_i \phi_j \phi_l$ | $\frac{\partial \varepsilon_m}{\partial n_k} = \frac{1}{3}\sum_i \sum_j \sum_l \frac{\partial \varepsilon_m^{ijl}}{\partial n_k}$<br>$\frac{\partial \varepsilon_m^{ijl}}{\partial n_k} = (\varepsilon_i + \varepsilon_j + \varepsilon_l)(1 + k_{ijl})\left(\phi_i \phi_l \frac{\partial \phi_j}{\partial n_k} + \phi_j \phi_l \frac{\partial \phi_i}{\partial n_k} + \phi_i \phi_j \frac{\partial \phi_l}{\partial n_k}\right)$<br>$\frac{\partial \phi_i}{\partial n_k} = \frac{\mathrm{v}_i}{\mathrm{v}_T n_T}(\delta_{ki} - x_i) - \frac{\phi_i}{\mathrm{v}_T n_T}(\mathrm{v}_k - \mathrm{v}_T)$ |

$\delta_{ki}$ stands for Kronecker delta: $(1 \,\forall\, k = i\,;\, 0 \,\forall\, k \neq i)$. Note that quadratic and cubic volume fraction mixing rules reduce to the conventional volume fraction mixing rule when all $k_{ij} = 0$. The same applies to the mole fraction equivalents. In this table all $i, j, k, l$ subscripts stand for any arbitrary species. Consistency requires that $k_{iii} = 0$ for all species.

The derivation pathways and mixing rules or property models for the concentration dependent relative permittivity of an electrolyte are widely discussed topics in the recent literature[125,165,184,262,311] and an issue that was already addressed in section 6.2. Additional extended volume fraction based mixing rules that can be directly applied to the E-PDH and ME-PDH terms are provided in Table 11.

The quadratic and cubic volume fraction mixing rules provide a degree of non-linearity that is highly flexible for systems with both positive and negative deviations from the linear behavior. In order to reproduce these behaviors, one requires to fit binary/ternary interaction parameters. For instance, the experimentally measured relative permittivity values of the water (1) + tert-butanol (2) system reported by Kaatze et al.[347] can be

decently reproduced by the cubic volume fraction mixing rule with the following $k_{ijl}$ parameters: $k_{112} = k_{121} = k_{211} = 0.184$ and $k_{221} = k_{212} = k_{122} = -0.463$. The mixing rule yields an AAD of 0.31 units. The strongly non-linear nature of the relative permittivity of simple water + tert-butanol mixtures is a humbling reminder that one cannot expect mixing rules to represent complex electrolyte systems properly. Furthermore, relative permittivity measurements of electrolytes and ILs are scarce and controversial.[61,87] Therefore, in the absence of data to reasonably fit or predict $k_{ij(l)}$ interaction parameters for such a broad space of salt, IL and solvent combinations, one is left with the conventional linear volume fraction (equation (6.34)) as an educated guess to estimate the relative permittivity of the mixture and its compositional derivatives.

**Table 12. Average absolute deviation (AAD) and average relative deviation (ARD) of the logarithmic IDAC from simple openCOSMO-RS predictions and their combination with a LR contribution.**

| Short-Range Term | Long-Range Term | Mixing Rule for $\varepsilon_m$ | Value of $\varepsilon_{IL}$ | AAD $ln(\gamma^{\infty}_{solv})$ | ARD $ln(\gamma^{\infty}_{solv})$ |
|---|---|---|---|---|---|
| openCOSMO-RS | N/A | N/A | N/A | 0.673 | 0.121 |
| | ME-PDH: Equation (6.29) * | Volume fraction: Equation (6.34) | Equation (6.51) | 0.965 | 0.260 |
| | | | $\varepsilon_{IL} = 4.75$ | 0.784 | 0.567 |
| | | | ** $\varepsilon_{IL} = 1 + 4.35\left(\frac{298.15}{T}\right)^{1.339}$ | 0.757 | 0.556 |
| | | Equation (6.46) | Equation (6.51) | 0.718 | 0.099 |
| | | | $\varepsilon_{IL} = 7.88$ | 0.671 | 0.079 |
| | | | ** $\varepsilon_{IL} = 1 + 7.99\left(\frac{298.15}{T}\right)^{1.339}$ | 0.663 | 0.088 |

All pure IL densities are calculated with equation (6.50) and the compositional derivative of the density is estimated based on the conventional volume fraction mixing rule. * $a = 3$ Å was applied for all calculations. ** Temperature exponential fitted to the data from Kottummal et al.[348]

Table 12 shows diverse calculations of the logarithmic IDACs applying the conventional COSMO-RS method and adding an LR contribution (ME-PDH with two different mixing rules) with several estimations for the relative permittivity of the IL phase. The correlation obtained from experimental delivers the largest deviations. Regarding the other estimations of $\varepsilon_{IL}$, three main observations can be pointed out. Firstly, the empirical mixing rule given by equation (6.46) seems to provide better approximations than the volume fraction mixing rule. Secondly, including a weak temperature dependency in the

estimation of $\varepsilon_{IL}$ provides a mild but additional improvement in the approximations. Thirdly, and most importantly, qualitative corrections are obtainable upon addition of extended LR electrostatics to basic COSMO-RS estimations of the logarithmic IDAC of neutral molecules in pure ILs. It must be pointed out that these results are possible with ME-PDH and not with E-PDH due to the reasons previously discussed for Figure 24: namely, due to the low $\varepsilon_{IL}$ values. Use of these low $\varepsilon_{IL}$ in E-PDH result in unrealistic, high $\ln(\gamma_s)$ values. Hence its results are not included in Table 12. Once again, this partially explains the use of the empirical 2.5 factor in equation (6.27) among other assumptions from Chang and Lin[262] which counter-balance the effect of the low $\varepsilon_{IL}$ values to a certain extent. Results with the conventional PDH term show an even larger overestimation of $\ln(\gamma_s)$ with the physical closest approach parameter. The worst results are observed with the PDH term using a constant $b^{(x)} = 14.9$.

There are several possible reasons to why the equation fitted to experimental values (equation (6.51)) is not providing good approximations. The IDAC database used in the present work is predominantly constituted by imidazolium, pyridinium, piperidinium and morpholinium cation based ILs and over half of them have bistriflimide as an anion. Thus, most ILs in the database are highly likely to correspond to a low value of $\varepsilon_{IL}$. Furthermore, even the experimental values $\varepsilon_{IL} \leq 15$ could be biased: for instance, [BMIM][$BF_4$] can be found with reported[85,86,323] values in a range of 9.7 to 13.9 and [BMIM][$NTf_2$] in a range of 9.2 to 13.7. Limiting the selected experimental values to $\varepsilon_{IL} \leq 10$ reduces the dataset to 52 experimental data points with a parameter $A = 2.231$ leading to an AAD of 1.532 (27% improvement). Thus, future correlations could involve a term based on the molar volume plus fitted chemical group contributions particularly relevant for hydrogen atoms that act as donors and for strongly dipolar ions like formate. For the present purposes, a single value of $\varepsilon_{IL}$ (with or without temperature dependency) is kept for all ILs. Finally, one may observe that the optimized $\varepsilon_{IL}$ values strongly depend on the applied mixing rule, and one cannot discard the possibility that other empirical mixing rules could work better using the correlated experimental values.

The previous analysis (Table 12) yields ambiguous results regarding the use of two mixing rules for the relative permittivity of the mixture. Interestingly, the empirical mixing rule from equation (6.46), which was originally conceived to reproduce a deviation from the linear volume fraction mixing rule for small ions via a single parameter, seems

to work best. Furthermore, one may observe that if $\alpha_{salt} = 0$ in equation (6.46), it reduces to the volume fraction equivalent of the mixing rule recommended by Ascani and Held.[184] This result supports proposing the development of phenomenological volume fraction based mixing rules.

**Table 13. Energy interaction matrix for IL dedicated parameterizations with openCOSMO-RS using the COSMO-RS parameters from Table 3.**

| | PC | PA | MA | $H_2O$ | Org. |
|---|---|---|---|---|---|
| PC | | X | X | X | X |
| PA | | | | X | X |
| MA | | | | X | X |
| H2O | | | | | |
| Org. | | | | | |

X Optimized*
Apply misfit (eq. 2.114)
Apply orthogonal misfit (eq. 2.116)

PC: polyatomic cation
PA: polyatomic anion
MA: monoatomic anion
Org.: organic solvent

Hydrogen Bonding term is equation (2.117) in all cases.

Having briefly analyzed some expressions to apply extended LR electrostatics at the solvent-free limit, a stronger argument in favor of extended LR electrostatics is made by performing IL dedicated parameterizations with and without the ME-PDH term. These are performed by scaling the misfit interaction and hydrogen bonding interaction (scaling factors $F_{IJ}^{mf}$ and $F_{IJ}^{hb}$, respectively) for all specific cation-water, anion-water, cation-organic, anion-organic and cation-anion interactions according to the interaction matrix shown in Table 13. This procedure yields two parameters per interaction, as shown in the upper equation from equation set (6.52), giving 16 optimizable scaling factors in total. In line with the COSMO-RS-ES model,[14] the misfit interaction $E_{IJ}^{mf}$ with no orthogonal component is applied for all ionic related interactions.

$$A_{IJ} = F_{IJ}^{mf} \cdot E_{IJ}^{mf} + F_{IJ}^{hb} \cdot G_{IJ}^{hb} \quad \text{optimized ionic interactions (X)}$$

$$A_{IJ} = E_{IJ}^{mf} + G_{IJ}^{hb} \quad \text{other ionic interactions (■)} \tag{6.52}$$

$$A_{IJ} = E_{IJ}^{mf,\perp} + G_{IJ}^{hb} \quad \text{neutral – neutral interactions (■)}$$

Furthermore, in spite of the fact that equation (6.46) performs well in the calculations from Table 12 for the IDAC systems, volume fraction remains the selected mixing rule for the IL dedicated parameterizations. There is a good reason for this choice: volume fraction can be implemented in the form of equation (6.34) with single solvent properties, or in the form of equation (6.36) with an averaged salt-free state for all neutral solvents. This brief exercise provides insights for the discussion regarding the use of single molecular solvent properties or averaged salt-free properties for multiple solvent systems, i.e. whether substantial difference is observable by comparing the concentration dependencies shown previously in Figure 28 and Figure 29. Furthermore, equation (6.46) is an empirical expression for salt systems, whereas volume fraction mixing rules seem to provide an educated guess for both the density and relative permittivity of IL systems.

By optimizing parameters for the ion related interactions, it is expected that the prediction of the salting-out effects should also improve indirectly in a Gibbs-Duhem consistent model. Consequently, increasingly systematic errors in the partitioning of neutral molecules can be partially attributed to the LR term and the corresponding mixing rules being applied, thereby providing insights into the consistency of the approach.

Regarding other inputs for the LR electrostatic term, the value of the distance of closest approach $a$ is estimated as a sum of the ionic radii (spherical volume equivalent radii from the COSMO cavity), which in turn are preliminary estimated as follows:

$$r_{ion} = F_a \cdot r_{COSMO} \cdot \Psi_{ion}^{COSMO} \tag{6.53}$$

where $\Psi_{ion}^{COSMO}$ is the sphericity of the ion calculated from the COSMO surface and volume and $F_a$ is a scaling parameter. This approximation yields values close to $4\ \text{Å} < a < 8\ \text{Å}$ for a wide variety ILs. The choice is rather rough and arbitrary, but facilitates generalized application yielding values that lie close to the distances of closest approach applied to diverse ILs in experimental electrostatic force interaction measurements.[49,265,300,301]

The hypothetical values of the relative permittivity of the IL (molten solvent-free state) are estimated with a simple temperature dependency as follows:

$$\varepsilon_{IL} = 1 + \varepsilon_A \left(\frac{298.15\ K}{T}\right)^{\varepsilon_B} \tag{6.54}$$

where $\varepsilon_A, \varepsilon_B$ are open parameters. IL densities are calculated by equation (6.50).

The parameterization includes both the IL IDAC values for which density and permittivity values for the molecular solvent are available and the ternary LLE systems. The results are summarized in Table 14 for comparison:

**Table 14. Average absolute deviation (AAD) of the logarithmic IDACs in pure ILs and the logarithmic partition coefficients of solvent and IL species in LLEs systems. Results with diverse parameterizations of openCOSMO-RS according to the interaction matrix shown in Table 13. Parameters and additional information are included in the Appendix.**

| Short-Range Term | Long-Range Term | Mixing Rule for the Relative Permittivity * | AAD (IDAC) $ln(\gamma_{solv}^{\infty})$ | AAD (LLE) $log(K_{IL}^{OS})$ | AAD (LLE) $log(K_{solv}^{OS})$** |
|---|---|---|---|---|---|
| openCOSMO-RS | N/A | N/A | 0.673 | 2.162 | 0.702 |
| openCOSMO-RS IL-dedicated parametrization (Table 13) | N/A | N/A | 0.760 | 1.751 | 0.594 |
| | ME-PDH: Equation (6.29) | Equation (6.36) | 0.697 | 1.089 | 0.646 |
| | | Equation (6.34) | 0.697 | 1.089 | 0.695 |

*If $\varepsilon_m$ is calculated with the averaged salt-free state, then also molar mass and density are calculated for all neutral compounds according to Figure 28. Calculation with single neutral solvent properties with equation (6.34) applies according to Figure 29. In both cases cations and anions are applied with equal, averaged properties. **Partitioning of the neutral species is not part of the training set.

In Table 14 it can be observed that optimizing openCOSMO-RS for IL systems without any LR electrostatic contribution implies a tradeoff between IDAC and LLE systems: the partitioning of the compounds in the ternary LLEs is improved at a minor expense of some precision for the IDAC calculations. Given that the optimized objective functions are weighted so that their contribution to the global objective function remains similar (see section 5.2), this imbalance could suggest that some physics are unaccounted for, among other possible reasons. Thereby a plausible explanation is provided by the parameterizations performed with equation (6.29), which indicate that LR electrostatics do play a relevant role in the qualitative description of IL systems. A marked improvement is obtained in the calculation of both IDAC values and the partitioning of all compounds in the ternary LLE systems. The only additional optimizable parameters are $\varepsilon_A$ and $\varepsilon_B$ from equation (6.54). Furthermore, the IDAC calculations provide a limiting case at the solvent-free limit, where any unexpected departures from the basic COSMO-RS prediction can be directly attributed to the LR contribution. This type of evaluation is therefore more

meaningful for ILs than for salt systems and was discarded in section 6.2.2. Nevertheless, the resulting conclusions remain applicable to conventional salt systems as well.

While results for the IDAC calculations and the partitioning of the IL in the LLE systems have a marked improvement, a difference is observed for the partitioning of the neutral molecular solvents. Namely, the partitioning of these improves in all cases with respect to the basic COSMO-RS prediction, but a significant difference is observed between the modelling strategies from Figure 29 and Figure 28 i.e. the volume fraction mixing rule using equation (6.34) or equation (6.36), respectively. This result seems counter-intuitive: the use of averaged salt-free state properties provided superior performance to the use of single solvent properties. Given that the partitioning of neutral molecules is not part of the training set, then any notable deviations may be attributed to the thermodynamic consistency of the approach. This in turn suggests that respecting the framework of the PM (the LR term can only see a global homogeneous dielectric) is a better choice when including compositional derivatives into the derivation.

As concluding remarks to the present subchapter, the results presented here firmly support the hypothesis that extending LR electrostatics with considerations for strong coupling in the low permittivity range provides further systematic corrections to COSMO-RS based predictions. Concisely for the case of ILs: evidence is provided to suggest that a tailored COSMO-RS model combined with appropriate LR electrostatics performs better than a tailored COSMO-RS model on its own. Furthermore, it is demonstrated that the full dissociation basis at the molecular-solvent-free limit remains applicable when corrections to the LR term are applied. Ionicity (dissociation degree) remains a qualitative correction that cannot be avoided in the future for salts and ILs and might be of particular relevance when actual chemical speciation takes place (e.g. acids). However, the writing author supports the views of Onsager:[97,331] corrections to the PB equation and use of its higher order terms in the radial distribution functions of electrostatic origin should be explored as a rigorous and more correct alternative to the traditional Bjerrum treatment. This implies that actual chemical speciation should be treated separately as a supplement to, but not a part of, applied theoretical corrections to the linearized electrostatic theory.

## 6.4 A Fully Extended COSMO-RS-ES Model

The ultimate goal of the present work is summarized in the last subchapter, which deals with the integration of the observations from sections 6.2 and 6.3 to obtain a revised and extended COSMO-RS-ES model, called COSMO-RS-ES+. This extension consistently treats simple salts and ILs in a range from infinite dilution to the molten ionic liquid state. The major insight of this final chapter demonstrates that satisfactory predictions of phase equilibria in single salt and single IL systems can be performed with all ions sharing the same basis and universal parameters. The method currently excludes the need to invoke any ionicity/ion-pairing related procedures. Results presented here support the use of single solvent properties instead of the salt-free average as reference state in the LR term. New possibilities for future research and further model development are identified.

### 6.4.1 Revised Short-Range Interaction Equations

Section 6.3 provides proof that the basic COSMO-RS equations (the electrostatic misfit term from equation (2.114) and the hydrogen bonding term (2.117)) yield qualitatively reliable predictions for the activity coefficient of molecular solvents that are infinitely diluted in a pure IL. Results are not satisfactory for the partitioning in liquid-liquid equilibria with an IL compound. These findings are in agreement with systematic evaluations from the literature.[115,253] However, the performance of the model improves considerably upon scaling specific ion interactions. Further improvements are visible when an appropriate LR contribution is applied as a complement. Thus, a connection between modelling ILs with COSMO-RS and with COSMO-RS-ES is feasible.

The COSMO-RS-ES equations from Table 4 and Table 5 were tailored for conventional salt systems[14] and apply several considerations with a certain degree of empiricism for the ion-ion energy interactions. An alternative is dealing with explicit ion solvation clusters as described by Toure et al.[11,12] Nevertheless, such an approach is not practicable for a broad and varied database with multiple systems, solvents and ions, given that one would have to guess the concentration dependent structure of all possible solvation shells. For this reason, the pragmatic choice is to further develop the COSMO-RS-ES model as an electrolyte-dedicated $g^E$-model with potential for robust predictive capability.

**Table 15. Revised short-range interaction equations for the extended COSMO-RS-ES+ model. $E_{IJ}^{mf}$, $E_{IJ}^{mf,\perp}$ and $G_{IJ}^{hb}$ correspond to equations (2.114), (2.116) and (2.117), respectively.**

| Interaction | Misfit Factors | Attractive contact interaction energies |
|---|---|---|
| Neut. – Neut. | $E_{IJ}^{mf,\perp}$ | $G_{IJ}^{hb}$ |
| MC – org. mol. | $E_{IJ}^{mf}$ | $a_{eff} \cdot B_1 \cdot c_{hb} \cdot \max(0, \sigma_{om} - C_1) \cdot \sigma_{MC}$ |
| PC – org. mol. | $A_1 \cdot E_{IJ}^{mf}$ | $\begin{cases} a_{eff} \cdot B_2 \cdot c_{hb} \cdot \max(0, \sigma_{om} - \sigma_{hb}) \cdot \min(0, \sigma_{PC} + \sigma_{hb}) \;\; if\ \sigma_{PC}\ from\ Group\ 1 \\ G_{IJ}^{hb}\ for\ all\ other\ surface\ contacts \end{cases}$ |
| MA – org. mol. | $A_2 \cdot E_{IJ}^{mf}$ | $a_{eff} \cdot B_3 \cdot c_{hb} \cdot \min(0, \sigma_{om} + \sigma_{hb}) \cdot \sigma_{MA}$ |
| PA – org. mol. | $A_3 \cdot E_{IJ}^{mf}$ | $\begin{cases} a_{eff} \cdot B_4 \cdot c_{hb} \cdot \min(0, \sigma_{om} + \sigma_{hb}) \cdot \max(0, \sigma_{PC} + \sigma_{hb}) \;\; Interaction\ type\ 1 \\ a_{eff} \cdot B_5 \cdot c_{hb}(T) \cdot \min(0, \sigma_{om} + \sigma_{hb}) \cdot \max(0, \sigma_{PC} + \sigma_{hb}) \;\; if\ \sigma_{om}\ from\ Group\ 2 \\ G_{IJ}^{hb}\ for\ all\ other\ remaining\ surface\ contacts \end{cases}$ |
| MC – $H_2O$ | $A_4 \cdot E_{IJ}^{mf}$ | $a_{eff} \cdot B_6 \cdot c_{hb} \cdot \max\left(0, \sigma_{H_2O} - \sigma_{hb}\right) \cdot \sigma_{MC} \cdot (1 + D_0 \lvert\sigma_{MC}\rvert)$ |
| PC – $H_2O$ | $A_5 \cdot E_{IJ}^{mf}$ | $\begin{cases} a_{eff} \cdot B_7 \cdot c_{hb} \cdot \max\left(0, \sigma_{H_2O} - \sigma_{hb}\right) \cdot \sigma_{PC} \;\; \forall\ \sigma_{PC}\ from\ Group\ 2\ and\ \sigma_{PC} < \sigma_{hb} \\ G_{IJ}^{hb}\ for\ all\ other\ surface\ contacts \end{cases}$ |
| MA – $H_2O$ | $E_{IJ}^{mf}$ | $a_{eff} \cdot B_8 \cdot c_{hb} \cdot \min\left(0, \sigma_{H_2O} + \sigma_{hb}\right) \cdot \max(0, \sigma_{MA} - \sigma_{hb})$ |
| PA – $H_2O$ | $A_6 \cdot E_{IJ}^{mf}$ | $\begin{cases} a_{eff} \cdot B_9 \cdot c_{hb} \cdot \min(0, \sigma_{om} + \sigma_{hb}) \cdot \max(0, \sigma_{PC} + \sigma_{hb}) \;\; \forall\ \sigma_{PC}\ from\ O\ atoms \\ a_{eff} \cdot B_{10} \cdot c_{hb}(T) \cdot \min(0, \sigma_{om} + \sigma_{hb}) \cdot \max(0, \sigma_{PC} + \sigma_{hb}) \;\; \forall\ other\ acceptor\ \sigma_{PC} \\ G_{IJ}^{hb}\ for\ all\ other\ remaining\ surface\ contacts \end{cases}$ |
| MC – MC | $E_{IJ}^{mf}$ | 0 |
| MC – MA | $E_{IJ}^{mf}$ | $a_{eff} \cdot B_{11} \cdot c_{hb} \cdot \sigma_{MC} \cdot \sigma_{MA} \cdot \max(0, 1 - D(\lvert\sigma_{MC}\rvert)^E)$ |
| MC – PA | $A_7 \cdot E_{IJ}^{mf}$ | $a_{eff} \cdot B_{12} \cdot c_{hb} \cdot \sigma_{MC} \cdot \max(0, \sigma_{PA}) \cdot \max(0, 1 - D(\lvert\sigma_{MC}\rvert)^E) \quad \forall\ \sigma_{PA} > \sigma_{HB}$ |
| PC – PC | $E_{IJ}^{mf}$ | $B_{13} \cdot G_{IJ}^{hb}$ |
| PC – MA | $A_8 \cdot E_{IJ}^{mf}$ | $a_{eff} \cdot B_{14} \cdot c_{hb} \cdot \sigma_{PC} \cdot \sigma_{MA} \cdot \max(0, 1 - D\lvert\sigma_{PC}\rvert^E)$ |
| PC – PA | $A_9 \cdot E_{IJ}^{mf}$ | $\begin{cases} a_{eff} \cdot B_{15} \cdot c_{hb} \cdot \sigma_{PC} \cdot \sigma_{PA} \cdot \max(0, 1 - D\lvert\sigma_{PC}\rvert^E) \\ G_{IJ}^{hb} \quad \forall \quad \sigma_{PC} > 0, \sigma_{PA} < 0 \end{cases}$ |
| MA – MA | $E_{IJ}^{mf}$ | 0 |
| PA – PA | $E_{IJ}^{mf}$ | $B_{13} \cdot G_{IJ}^{hb}$ |

MC – monoatomic cation; PC – polyatomic cation; MA – monoatomic anion; PA – polyatomic anion; Group 1 are polarized donor surface segments belonging to N, P and S atoms as well as all hydrogen donor surface segments except those from alcohol groups; Group 2 corresponds to hydrogen donor surface segments from polarized alkyl groups; Interaction type 1 refers to any polarized hydrogen donor surfaces segments (except alkyl groups) interacting with any anionic oxygen acceptor surface segments.

Development of the COSMO-RS-ES+ short-ranged contribution has been achieved by combination of the equations from Table 5 and Table 13 with some additional adjustments, leading to the ion-specific interaction energy equations shown in Table 15. Some general comments on the development of these heuristic equations can be made.

Firstly, the largest deviations of basic COSMO-RS calculations from experimental electrolyte data arise from the ion to counter-ion interactions in which localized cationic charges are involved (e.g. mono-, di-, tri-alkyl azanium ions, ammonium ion, spherical cations). In an explicitly solvated ion cluster approach, the strong positive charge of these cationic surfaces is unavailable for contact interactions because they are blocked by a solvation shell. This explains the absence of pronounced negative deviations in the values

of $\gamma_{\pm}$ from Toure et al.[11,12] These large deviations would otherwise appear if only bare monoatomic cations are used. The COSMO-RS-ES model overcomes this issue by introducing an empirical penalty to strong ion-ion interactions via an empirical factor $(1 - D|\sigma_+|^E)$, with $D$ and $E$ as global parameters. In this regard, one may test different approaches, including a Gaussian distribution of the interaction energy around $\sigma_+$. Nevertheless, only marginal improvements can be achieved given that the largest areas of opportunity lie elsewhere, as discussed further ahead. Consequently, the original COSMO-RS-ES penalty for ion to counter-ion interaction energies was kept, thereby prioritizing a reduced number of universal parameters.

The COSMO-RS-ES model had minor questionable details like absent electrostatic misfit terms for ion to counter-ion interactions and no attractive like-ion interactions between polyatomic ions. These have been included in Table 15 and they do play a beneficial role in specific cases. For example, in the presence of attractive interactions between polyatomic anions with polarized hydrogen donor surfaces (e.g. dihydrogen phosphate) or the case of hydrogen bonding between the -OH groups of two choline cations.

Most of the equations in Table 15 retain a similar form to that of the original COSMO-RS equations and target specific segment interactions. All other remaining surface segment contacts are treated with the conventional COSMO-RS hydrogen bonding energy. Emphasis was placed on retaining the latter whenever possible, given that the conventional COSMO-RS hydrogen bonding energy equation provides good results and keeps the structure of the model more normalized. This is acknowledged in the thermodynamics community and demonstrated in Figure 32. A small particularity is introduced for the specific case of the interaction of acceptor surfaces from a polyatomic anion and donor surfaces from an organic molecule. The factor $B_4$ scales the interaction energy between the polyatomic anion and polarized hydrogen atom donor surfaces in the organic molecule. Polarized hydrogen atom donor surfaces belonging to an alkyl chain were excluded. This choice provides further improvements in performance for the ternary liquid-liquid systems with an IL compound.

Lastly, both the COSMO-RS-ES equations from Table 4, Table 5, and the new equations from Table 15, were developed with systematic trials focused on reducing the amount of scaling parameters used for the electrostatic misfit and attractive terms. In this sense, some of the short-range contributions (ion to counter-ion interactions in particular) of

the COSMO-RS-ES and COSMO-RS-ES+ models are empirical. Furthermore, it should be noted that local minima in the parameterization strategy also depend on the size of the spherical ions and the form of the ion to counter-ion interaction energy equations. Careful modification of the short-range energy interaction equations is advised in the future.

### 6.4.2 Revised Long-Range Interaction Equations

The selected LR interaction for COSMO-RS-ES+ is the ME-PDH term from equation (6.29) with $\omega_{(0)} = 1$ instead of $\omega_{(0)} = 3/2$ in equation (6.28). The choice of ME-PDH is justified based the improved performance it yields when combined with openCOSMO-RS for IL systems (section 6.3.2) as well as with COSMO-RS-ES model for salt systems (section 6.2.2). The distance of closest approach was calculated based on geometrical COSMO data from the cation and the anion according to:

$$a = \sum_i (F_i \Psi_+^{COSMO} r_+^{COSMO} + F_i \Psi_-^{COSMO} r_-^{COSMO}) \tag{6.55}$$

where the radius of the charge is given by the equivalent spherical radius of the COSMO cavity in Å penalized by the sphericity Ψ (calculated from the COSMO cavity). $F_i$ is a global scaling parameter for monoatomic ions ($F_M$) and polyatomic ions ($F_P$).

#### *Selected Pure Compound Properties*

The pure compound densities and relative permittivity data of neutral, molecular solvents (with temperature dependency when available) was taken from the DIPPR,[349] Landolt-Börnstein[350] and CRC[351] pure compound databases. To have a broad temperature range in the specific case of pure water, the correlation provided by Maribo-Mogensen et al.,[164] was used for the temperature dependent density and the correlation provided by Pátek et al.[352] was re-parameterized with data from the literature and applied for the temperature dependent relative permittivity (see Appendix).

Pure compound densities of IL were calculated with equation (6.50) as given in section 6.3.2. The densities of conventional salts in solution were approximated with the following correlation which reproduces the general equation from Nguyen et al. when combined with volume fraction as the mixing rule:

$$d_{salt} = 973.349 \cdot (M_{salt})^{0.1536} \tag{6.56}$$

The hypothetical (or hypothetical subcooled liquid) relative permittivity of any molten state for salts and ionic liquids was calculated by means of equation (6.54), which provided the best results in section 6.3.2. For consistency, the molar volume of all ions is an averaged property by means of the averaged molar mass of the salt or IL ($M_{salt}/v$ or $M_{IL}/v$) and the assumptions $d_+ = d_- = d_{IL/salt}$ and $\varepsilon_+ = \varepsilon_- = \varepsilon_{IL/salt}$ are kept.

### *Selected Mixing Rules*

The molar mass of the mixture and its compositional derivatives are known by definition. Mixture density can be modelled with pure compound properties and a mixing rule that can be mass fraction based, or volume fraction based on equation (6.25). One may perform different comparisons and demonstrate that these do not substantially deviate from each other. In the present case, volume fraction was selected as the more coherent choice.

The relative permittivity of a mixture depends on pressure, temperature and composition. It is a highly structural and, in essence, a fundamentally thermodynamic property. Literature data on the relative permittivity of binary mixtures like water + tert-butanol[347] or isopropanol + benzene[353] present non-linear behaviors that cannot be easily predicted. The present work deals with multi-component mixtures. Thus, linear volume fraction is kept as an educated guess for mixtures of molecular solvents. While it hardly captures all the complexity of electrolyte systems, it provides a reasonably value for salt and IL systems.[82,85] The linear volume fraction mixing rule is calculated according to equation (6.34), where single solvent properties are used and an averaged ionic molar volume with a single $\varepsilon_{IL}$ value is used for all salts and ILs. The choice of equation (6.34) over equation (6.36) will be justified further down. This choice is carried over to molar mass and density (i.e. the chosen standard is the approach depicted in Figure 29 with linear volume fraction mixing rules for the density and relative permittivity).

## 6.4.3 COSMO-RS-ES+: From Infinite Dilution to the Fused Salt State

The training set for the present parameterization includes 5909 systems that amount to a total of 29131 datapoints. These are broken down into 184 MIAC systems with 3657

datapoints for salt systems (1479 with pure water as solvent, 1595 with aqueous mixed solvents, 583 with non-aqueous organic solvents). A total of 389 datasets with 2693 datapoints for LLE systems (1637 from IL containing systems and 1056 from salt containing systems). A total of 368 datasets with 1147 datapoints from Gibbs free energies of transfer (950 from ions involved in salt systems and 197 from polyatomic organic ions), and 4968 systems with 21634 datapoints from the IDAC systems of molecular solvents infinitely diluted in pure ILs. In the latter, only 3.3% of all datapoints have monoatomic anions, thus the IDAC dataset is predominantly representative of systems with large polyatomic ions. The resulting values for the parameters from Table 15, the monoatomic ion radii, equation (6.54) and equation (6.55) obtained after the parameterization shown in Table 16:

**Table 16. Parameters for the COSMO-RS-ES+ model (version corresponds to Table 15) combined with the ME-PDH term applying the mixing rules from equations (6.44) and (6.46).**

| **Monoatomic ion radii [Å]** | | **Misfit scaling parameters A** [−] | | **Interaction energy scaling parameters B** [−] | | **Thresholds C** $\left[\frac{\mathbf{e}}{\mathbf{Å^2}}\right]$ **and parameters D, E** [−] | |
|---|---|---|---|---|---|---|---|
| $Li^+$ | 1.552 | $A_1$ | 0.7282 | $B_1$ | 0.0622 | $C_1$ | 0.0100 |
| $Na^+$ | 1.752 | $A_2$ | 0.7034 | $B_2$ | 0.3056 | $D_1$ | 269.94 |
| $K^+$ | 1.940 | $A_3$ | 0.2436 | $B_3$ | 0.3560 | $E_1$ | 1.44 |
| $Rb^+$ | 2.029 | $A_4$ | 0.5417 | $B_4$ | 0.5556 | $D_2$ | 166.64 |
| $Cs^+$ | 2.186 | $A_5$ | 0.2122 | $B_5$ | 1.0001 | $E_2$ | 1.48 |
| $F^-$ | 1.860 | $A_6$ | 0.0884 | $B_6$ | 0.1461 | | |
| $Cl^-$ | 2.000 | $A_7$ | 0.3880 | $B_7$ | 0.2513 | | |
| $Br^-$ | 2.117 | $A_8$ | 0.3159 | $B_8$ | 0.4192 | | |
| $I^-$ | 2.186 | $A_9$ | 0.1525 | $B_9$ | 0.4444 | | |
| **Supplementary LR Parameters** | | | | $B_{10}$ | 0.7463 | | |
| $F_M$ | 1 | | | $B_{11}$ | 0.0397 | | |
| $F_P$ | 0.614 | | | $B_{12}$ | 0.0476 | | |
| $\varepsilon_A$ | 4.137 | | | $B_{13}$ | 0.8255 | | |
| $\varepsilon_B$ | 1.259 | | | $B_{14}$ | 0.0702 | | |
| | | | | $B_{15}$ | 0.1070 | | |

The initial values for the cationic radii were taken from section 6.2.2. The initial values for the anionic were the fixed values from the COSMO-RS-ES model: 1.72 Å, 2.05 Å, 2.16 Å and 2.32 Å for fluorine, chlorine, bromide and iodide, respectively. Parameterizations with total average deviations that are comparable to the COSMO-RS-ES predecessor for salt systems and superior to openCOSMO-RS for IL systems can be obtained, when leaving the monoatomic anion radii constant. Presently, the monoatomic anion radii were parameterized as a second step refinement. All resulting monoatomic radii are shown in Figure 35 in contrast to the bare ion values reported by Marcus.[30]

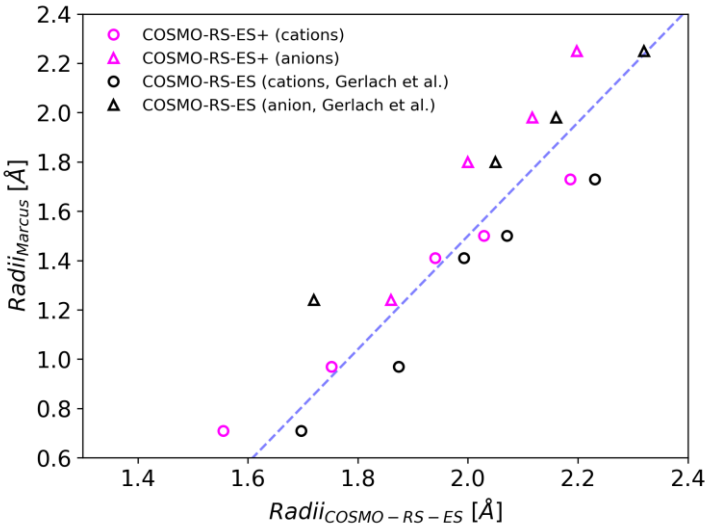


**Figure 35. Monoatomic radii from the present COSMO-RS-ES+ parameterization compared to the monoatomic radii ion values reported by Marcus.[30] The monoatomic radii applied by the first COSMO-RS-ES parameterization from Gerlach et al.[14] are included for reference. The dashed blue line is for visual aid only.**

A comparative summary of the performance of the present COSMO-RS-ES+ model using the equations from Table 15, and the ME-PDH term with the parameters from Table 16, is presented in Table 17. For the comparison of IL systems, the openCOSMO-RS results from section 6.3 are used. As a comparison for the salt systems, the best reported values from all available COSMO-RS-ES parameterizations are included. To evaluate the temperature effect in salt systems, the AAD of the predictions of temperature dependent MIAC values of salts in pure water are included when compared to the JESS database.[287–291] The latter are not part of the training set. Therefore, these calculations constitute pure predictions. The same can be said for the binary LLE systems with an IL compound and the SLE calculations for salts in pure and mixed solvents. The latter remain a standard indicator of predictive capability in the same fashion as in previous works.[15–18]

In general, the COSMO-RS-ES+ model retains an accuracy that is comparable to that if its COSMO-RS-ES for salt systems. Additionally, the COSMO-RS-ES+ model can also describe IL systems and outperform openCOMO-RS in their description. The largest improvement for IL systems can be observed in the calculation of liquid-liquid equilibria. These data yield an AAD of 2.162 with openCOSMO-RS, 1.089 with a tailored openCOSMO-RS and 1.025 with the present parameterization for the logarithmic partitioning coefficients of the IL. This represents a 51.3% reduction of the averaged absolute deviation with respect to a non-electrolyte COSMO-RS reference.

**Table 17. Performance comparison between diverse COSMO-RS-ES parameterizations, openCOSMO-RS and the extended COSMO-RS-ES+ models for a broad range of datasets.**

| Average Absolute Deviation (AAD) | | | |
|---|---|---|---|
| s- (salt) and IL - Datasets ($N_{DP}$) | Benchmark 1: COSMO-RS-ES (reported or calculated values) | Benchmark 2: openCOSMO-RS, (section 6.3) | COSMO-RS-ES+ (present parameterization) |
| s-MIAC aq. A (1190) | 0.042[a] | N/A | 0.059 |
| s-MIAC aq. B (1479) | 0.090[b] | N/A | 0.063 |
| s-MIAC aq. mix. (1595) | 0.045[b] | N/A | 0.050 |
| s-MIAC aq. T (4141) | 0.112[b] | N/A | 0.071 |
| s-MIAC org. (583) | 0.510[b] | N/A | 0.416 |
| s-LLE (1056) | 0.68[a] - 0.520[c] | N/A | 0.649 |
| s-SLE (823) | 0.89[c] | N/A | 0.753 |
| GT (1147) | 3.158[d] (salt ions) | 10.011 (organic ions) | 3.052 (all ions) |
| IL-LLE (1637) | N/A | 2.162 | 1.025 |
| Binary IL-LLE (113) | N/A | 1.915 | 0.992 |
| IL-IDAC (21634) | N/A | 0.673 | 0.655 |

[a] COSMO-RS-ES from Gerlach et al.[14]; [b]COSMO-RS-ES from section 6.2; [c]COSMO-RS-ES from Müller et al.[16]; [d]COSMO-RS-ES from Müller et al.[15]; s-MIAC aq. Salts A and B: two datasets of aqueous mean ionic activity coefficients (pure water, 25°C and up to 6 and 20 molal, respectively); s-MIAC aq. T: aqueous mean ionic activity coefficients from the JESS database (salts in pure water, from 0°C to 200°C, $m_{max}$ = 6 mol/kg); s-MIAC aq. mix.: mean ionic activity coefficients of salts in mixed aqueous solvents at room temperature up to 15 mol/kg. s-MIAC org.: non-aqueous mean ionic activity coefficients (room temperature) up to 15 mol/kg. LLE aq.: aqueous mixed solvent electrolytes with salting out effects. GT: Gibbs free energies of transfer of ions from water to organic solvents with 992 datapoints for inorganic (salt) ions and 155 datapoints for organic and IL ions. SLE: solid-liquid equilibria in aqueous, mixed and non-aqueous systems. **Color:** Pure predictions, not part of the training set in any parameterization of COSMO-RS-ES+.

Table 17 includes two aqueous MIAC datasets for salts in water at room temperature. Dataset A has salts of alkali and $NH_4^+$ cations with halides and $SO_4^{-2}$, $SO_3^{-2}$, $S_2O_3^{-2}$, $NO_3^-$, $ClO_4^-$, $H_2PO_4^-$ and $HPO_4^{-2}$ as anions up to a molal concentration of 6 mol/kg. This dataset corresponds to the COSMO-RS-ES parameterizations from Gerlach et al.,[14] Müller et al.,[15,16] and the COSMO-RS-ES parameterization from section 6.1.3. For section 6.2.2 this dataset was extended to a maximum concentration of 15 mol/kg. In the present COSMO-RS-ES+ parameterization, dataset B is used in the training set. Dataset B further extends

dataset A to a maximum concentration of 20 mol/kg and additionally includes salts with the anions $ClO_3^-$, $CNS^-$ and $BrO_3^-$. Furthermore, COSMO-RS-ES included dataset A up to 6 mol/kg (or 15 mol/kg in section 6.2.2) as the aqueous MIAC training set, whereas the present parameterization for COSMO-RS-ES+ applies dataset B as the training set. Thus, while it is sufficient to argue that both versions of the model have a comparable performance, the fairest contrast is the temperature dependent MIAC dataset obtained from JESS,[287–291] which is not part of any training set.

As additional context to the values presented in Table 17, the parameterization for the MIAC systems in organic solvents was performed with 976 datapoints in section 6.2 and with 583 datapoints in the present parameterization. The reason is that systems with unreliable data were removed during continuous data curation. The organic solvent MIAC systems deemed unreliable presented no values in the low concentration range (and thus absent confirmation of agreement with the Debye-Hückel Limiting Law), or values in the low concentration range that deviated from the DHLL.

In the following pages, the comparison summarized in Table 17 will be broken down into groups and analyzed with more detail.

### *Single-Ion Free Energies of Transfer and Infinite Dilution Activity Coefficients*

The simultaneous evaluation of single ion free energies of transfer (water to organic solvents) and the evaluation of the IDACs of molecular solvents in pure ILs is a relevant milestone for the objectives described previously in section 4. One dataset describes ions infinitely diluted in mixed and pure molecular solvents and the other describes molecular solvents infinitely diluted in ions: the two limits of the entire concentration range.

Figure 36 shows parity plots of the results for Gibbs free energies of transfer (left) and IDAC values of molecular solvents in pure ILs (right) calculated with the resulting parameterization of the extended COSMO-RS-ES+ model. The free energies of transfer include ions involved in salt systems (950 datapoints) where the model results in an AAD of 3.045. This result is comparable to previously reported values with its COSMO-RS-ES predecessor. The remaining 197 datapoints correspond to polyatomic organic ions and the resulting AAD is 2.852, which lies well below the AAD of 10.011 calculated with the IL-tailored openCOSMO-RS from section 6.3.2.

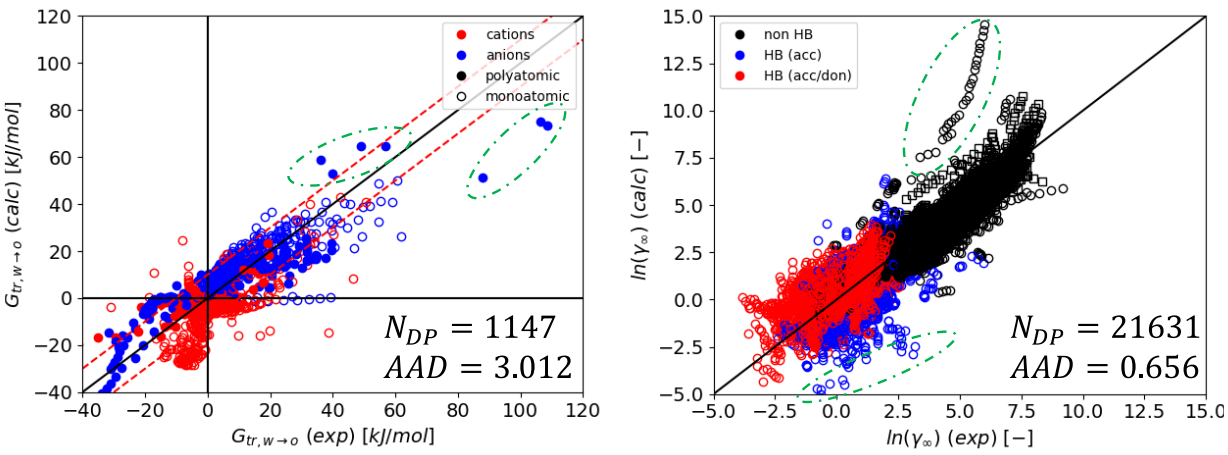


**Figure 36. Left: Gibbs-free energies of transfer of ions from water to diverse organic solvents (experimental vs. calculated values). Right: Infinite dilution activity coefficients of diverse molecular solvents in pure ionic liquids (experimental vs. calculated values).**

Figure 37 shows the probability density function of the relative error for the IDAC systems included in the parameterization, compared to the distribution function of the relative error from IDAC calculations with openCOSMO-RS (corresponding to Figure 32). Due to the amount of datapoints in the IDAC parity plots and the marginal difference in AAD, distributions of the relative errors are presented to facilitate a more objective contrast.

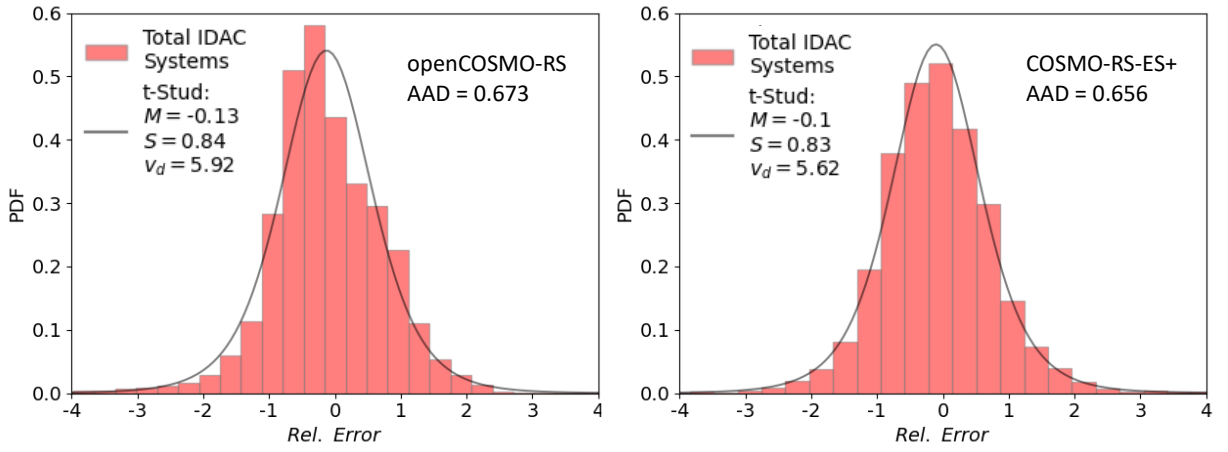


**Figure 37. Left: probability density function (PDF) of the relative error for all IDAC datapoints corresponding to Figure 32 (openCOSMO-RS[114]). Right: PDF of the relative error for all IDAC datapoints corresponding to COSMO-RS-ES+. In this plot: *M* = median of the fitted distribution, *S* = scaling factor of the fitted distribution, $v_d$ = degrees of freedom of the fitted distribution.**

In general, a systematic underestimation of the $\gamma_i^\infty$ of molecular solvents in pure ILs is observable with both methodologies. While the AAD of the present parameterization (COSMO-RS-ES+) shows a marginal improvement when compared to openCOSMO-RS, it is the density distribution of the relative error with COSMO-RS-ES+ what demonstrates

that these systematic deviations have been improved. The relative error of the IDAC systems from the present parameterization presents a narrower distribution of the relative error, when compared to the relative error distribution of the calculations with openCOSMO-RS (*M* = -0.09 vs *M* = -0.13, from the fitted t-Student distributions in Figure 37). Finally, a couple of outlying datapoints have become more notable. These are highlighted with dashed green ellipsoids in the left panel in Figure 36 and correspond to IL systems with cations and/or anions that are rich in polarized nitrogen surfaces with a negative charge (e.g. tris(dicyanoazanide)).

Regarding the free energies of transfer of single ions, a marked improvement with the present model is achieved. In contrast to previous approaches,[15–17] these data were kept in the training set. It is of interest to point out that the systematic deviations observed in Figure 36-left for all monoatomic cations are closely similar to previous works[15] regardless of the use of new ion-specific equations in COSMO-RS-ES+. This could indicate a limit of COSMO-RS-based models to describe the solvation of monoatomic cations in organic solvents unless additional phenomenology (e.g. polarizability of solvent molecules) is accounted for. Some polyatomic ions lie on the upper right side of the parity plot in Figure 36 (left). These are highlighted with dashed green ellipsoids and correspond to sulfate and thiosulfate ions.

### *Mean Ionic Activity Coefficients*

As previously discussed, aqueous MIAC datasets A and B are part of the training set of the COSMO-RS-ES and COSMO-RS-ES+ models, respectively. Consequently, COSMO-RS-ES shows a better performance for dataset A and COSMO-RS-ES+ shows a better performance for dataset B. Furthermore, the weighting factors of the objective functions have also changed for the latter, due to the introduction of large amounts of new IL datasets. Therefore, the temperature dependent aqueous MIAC values extracted from the JESS[287–291] database provide a more just comparison between COSMO-RS-ES+ and its predecessor, given that the JESS dataset is not included in their training sets.

Predictions of temperature dependent MIAC for diverse salts in water are compared to data from the JESS dataset in Figure 38 as a parity plot. The effect of temperature in the MIAC of salts in pure water is more accurately captured (lowest AAD value) in the present

parameterization without the need for any additional temperature dependent parameters. The calculations shown in Figure 38-right are purely predictive.

Parameterization of the COSMO-RS-ES predecessor model with no extensions in the long-range term requires additional temperature-dependent parameters at the COSMO-RS level to improve modelling results with the JESS dataset. If no ion-specific temperature dependent parameters are included at the COSMO-RS level, the COSMO-RS-ES+ model provides a better performance when compared to its predecessor. This finding suggests that the temperature dependent density and permittivity of the solvent (water in this case) is not the only factor to be accounted for.

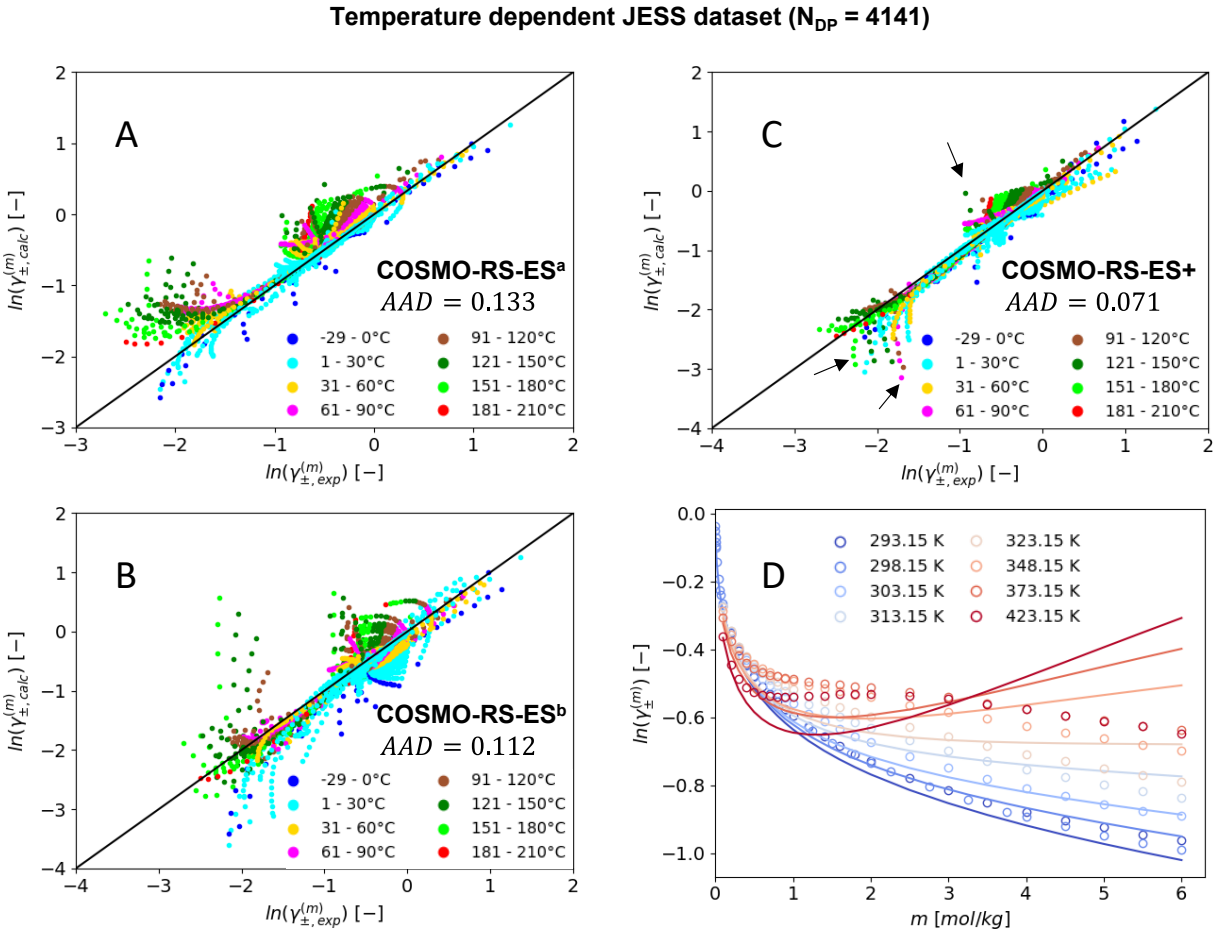


**Figure 38. Predictions of the MIACs of salts in aqueous systems from the temperature dependent dataset generated from JESS[287,288] with pure water as solvent. A: COSMO-RS-ES from Gerlach et al.[14] B: [b]COSMO-RS-ES from section 6.2.2. C: COSMO-RS-ES+ in the present parameterization. D: A closer look into the temperature dependency of the aqueous $NaNO_3$ as described by the COSMO-RS-ES+ model compared to experimental data from Pramanik and Das.[354] Calculated values constitute pure predictions: this dataset is not included in any of the training sets.**

The compositional derivatives of the selected mixing rules also have an impact. Application of equation (6.46) as mixing rule for the relative permittivity of the mixture

(COSMO-RS-ES from section 6.2.2, corresponding to Figure 38 - B) seems to have a detrimental effect for the prediction temperature dependent trends. This small but relevant observation points towards the use of volume fraction-based mixing rule as a more physically meaningful option. Nevertheless, it must be clarified that ion pairing and ion solvation in water may increase or decrease depending on the type of salt and this phenomenon cannot be captured by the current model and mixing rules. Such phenomenon may even be present in the same system, as exemplified by aqueous $NaNO_3$ shown in Figure 38 – D. In this system, ln ($\gamma_{\pm}$) decreases with increasing temperature at low concentrations, but the trend is inverted at higher concentrations.

Finally, it must be pointed out that, with rising temperatures, the MIAC of some salts in water may exhibit a non-monotonic behavior. This provides an explanation for some outlying data points at higher temperatures like the ones highlighted by the arrows in Figure 38-right. Non-monotonic behavior cannot be fully captured by the empirical parameters at the COSMO-RS level alone. Further modification is recommended for future model development with either a methodology for explicit speciation or additional temperature dependent parameters.

### *Liquid-Liquid Equilibria*

Figure 39 shows several parity plots of the logarithmic partitioning coefficients (experimental vs. calculated) for all ternary/quaternary LLE systems in the training set. These are divided into salt systems (all aqueous, upper frames) and IL systems (aqueous and non-aqueous, lower frames). The performance of the COSMO-RS-ES+ model for salt systems is compared to the equivalent calculation with COSMO-RS-ES from section 6.2.2. The performance of the COSMO-RS-ES+ model for IL systems is compared to the equivalent calculation with openCOSMO-RS from section 6.3.2.

The reported AAD for the logarithmic partitioning coefficients of salts in LLE systems in the work of Gerlach et al.[14] is 0.68 and the best reported value is 0.520 in the parameterization of Müller et al.[16] The COSMO-RS-ES+ model retains the same qualitative performance with an AAD that lies in the aforementioned range. In the case of IL systems, the AAD of the calculated logarithmic partitioning coefficients of the ILs is 2.162 for openCOSMO-RS and 1.089 for the tailored openCOSMO-RS that was parameterized with the ME-PDH term for IL systems in section 6.3.2. The best performance for IL systems

(AAD = 1.026) is found with COSMO-RS-ES+ in the present section. Thus, it can be stated that the COSMO-RS-ES+ model provides a highly competitive performance when compared to a COSMO-RS benchmark with the advantage of being able to handle salts and ILs with the same basis and parameters. This should be exploited and further developed to meet the industrial requirements[1,2] for more standardized, predictive models that handle electrolyte systems in a broad spectrum of compositions and nature.

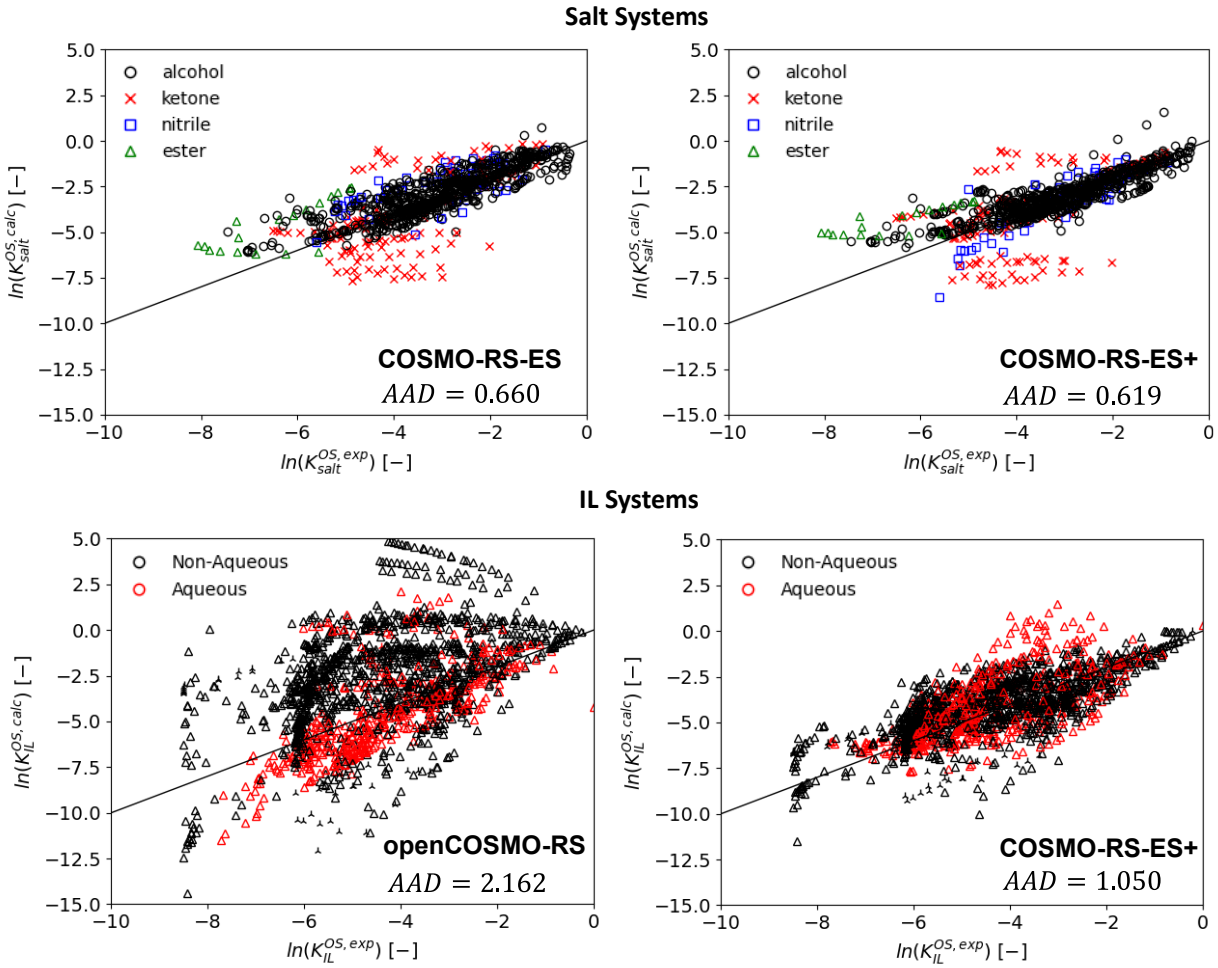


**Figure 39. Experimental vs. calculated logarithmic partition coefficients of salts (upper frames, all aqueous) and ILs (lower frames) in liquid-liquid equilibrium systems with diverse COSMO-RS based models. The COSMO-RS-ES calculation corresponds to the parameterization from section 6.2.2,[18] and the COSMO-RS-ES+ calculations correspond to the present parameterization. Complementary symbols (lower frames): Δ - ILs with polyatomic anions; ⅄ - ILs with monoatomic anions. $K^{OS}_{salt/IL}$ stands for the partition coefficient of the salt or IL between organic and salt-rich phase.**

Regarding the qualitative trends in biphasic mixtures with ILs (Figure 39 – lower frames), systematic deviations are present for aqueous systems in particular. These correspond to mixtures where the hydrophobic effect of polyatomic cations (e.g. tetrabutylammonium) and anions (e.g. hexafluorophosphate) presents an area of opportunity for future work.

Furthermore, strong aggregation and even micelle formation in aqueous media may occur with ions containing long aliphatic chains. The COSMO-RS-ES+ model cannot account for this behavior. This phenomenon is expressed with strong non-linear behavior of the activity coefficients. Examples of strong non-Coulombic ion aggregation (hydrophobic nature of one ion + hydrophilic counter-ion) are documented in the literature.[103,104]

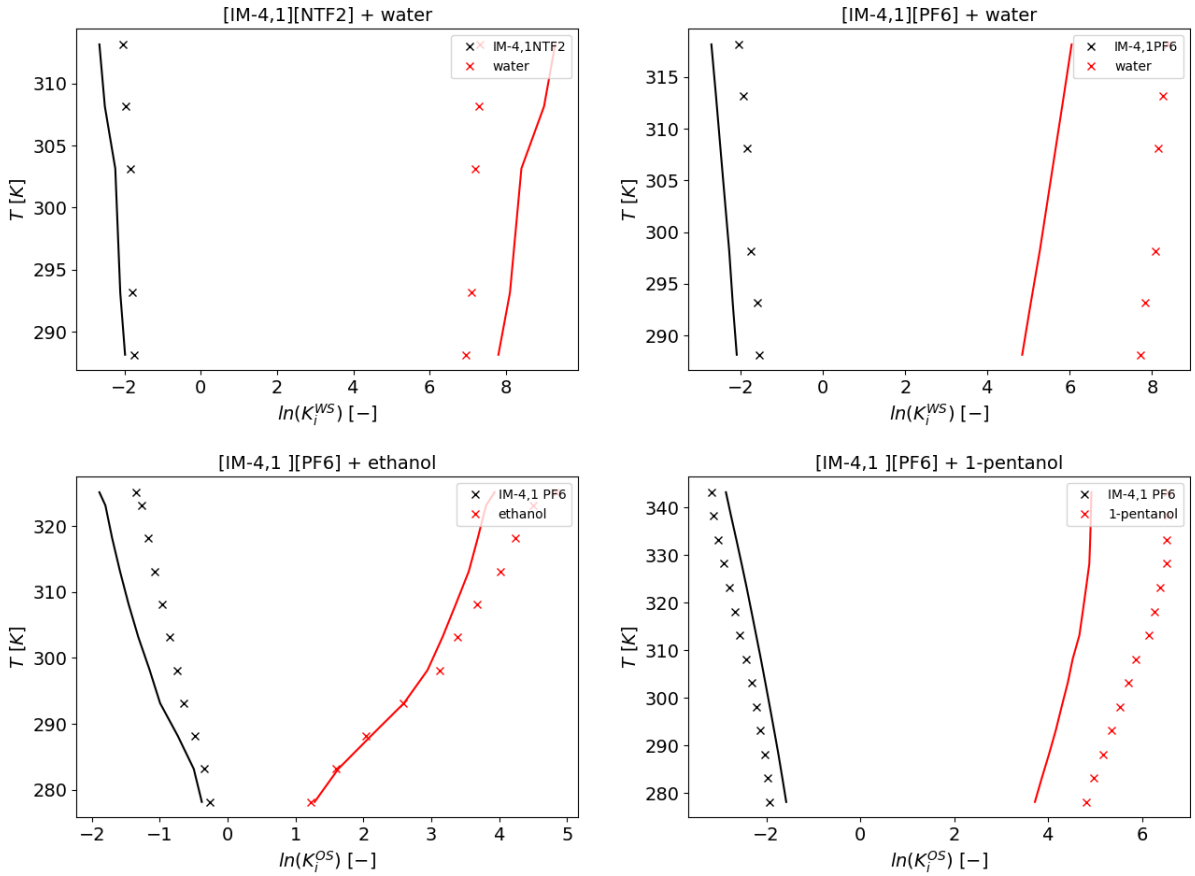


**Figure 40. Predictions with COSMO-RS-ES+ (lines) of the temperature effect on the logarithmic partition coefficients of binary 1-butyl-3-methyl imidazolium (IM-4,1) based IL binary systems compared to experimental data (x) reported by Freire et al.[355] (upper frames) and by Pereiro and Rodríguez[356,357] (lower frames). These binary LLE data are not included in the training set. $K_i^{O(W)S}$ is the partition coefficient of species *i* between the IL-poor and IL-rich phase.**

For instance, Figure 40 provides pure predictions with COSMO-RS-ES+ compared to experimental data of the temperature effect on the logarithmic partition coefficients of biphasic binary IL systems. This encouraging, brief example nevertheless shows the largest deviation (over two logarithmic units) for the partitioning of water in the 1-butyl-3-methylimidazolium hexafluorophosphate + water system. In contrast, the predicted miscibility of the same IL in alcohols has a closer resemblance to experimental data, as well as the predictions of an IL + water system with the same cation but combined with

the less hydrophobic bistriflimide [NTf2] anion (Figure 40 – upper left). Additional examples could be shown but, as previously discussed for Figure 39, capturing the hydrophobic effect of large ions in water will require further refinement.

An analysis of the partitioning of the neutral compounds in all LLE systems is of particular interest. Historically, objective functions used to parameterize the COSMO-RS-ES model focus exclusively on activity and partition coefficients of salts and transfer of single ions. Presently, the IDAC database applied to the extended COSMO-RS-ES+ model is the first type of data where focus is given to neutral compounds as part of the global objective function. However, binary IDAC calculations are not affected by the application of single solvent properties or averaged salt-free solvent properties in the mixing rules applied to the extended long-range electrostatics term. The case is different for neutral solvents in ternary or quaternary LLE systems where a consistent approach should provide an acceptable prediction of neutral compound partitioning.

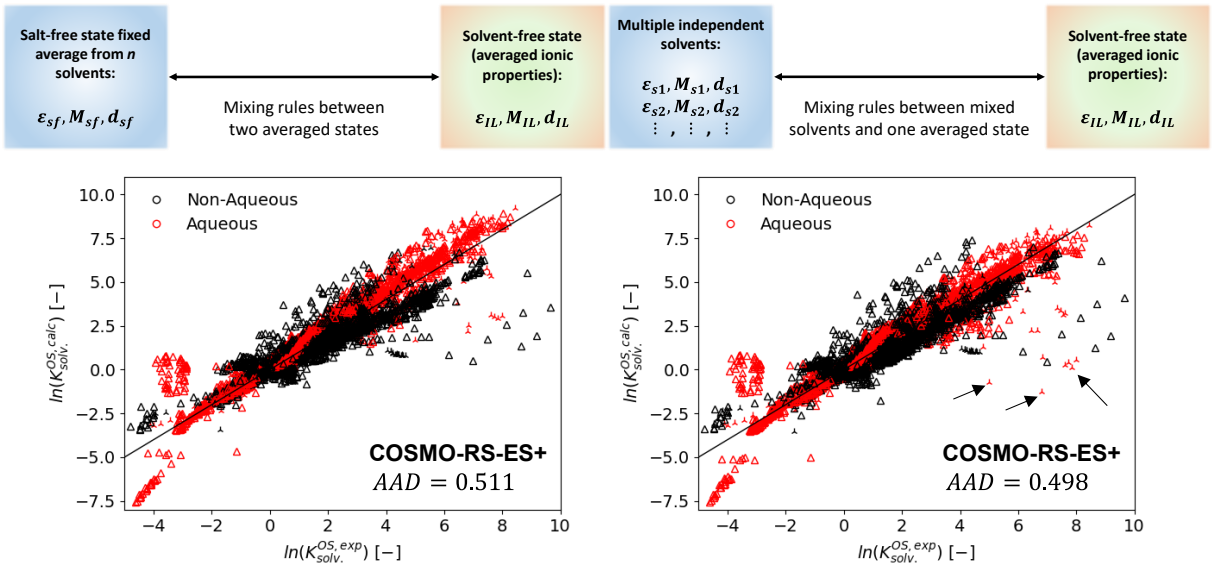


**Figure 41. Logarithmic partition coefficients (experimental vs calculated) of all neutral compounds in all ternary/quaternary LLE systems present in the training set. Left: COSMO-RS-ES+ applying an average salt-free state for the compositional derivatives. Right: COSMO-RS-ES+ applying single solvent properties for the compositional derivatives. In total, 5533 datapoints for the partitioning of neutral compounds are available. Of these, 3274 correspond to IL systems and 2259 to salt systems. Complementary symbols: Δ - Systems with polyatomic anions; ⅄ - Systems with monoatomic anions.**

The solvent-free limit is fixed as an average of the corresponding ions. The subtlety is that the molar mass, density, and relative permittivity of the salt-free limit in mixed solvent systems can be modelled with a global salt-free average of the solvents involved or with explicit single solvent properties. The calculated value of a property $\mathcal{P}$ of the mixed

solvent is the same at a given concentration, regardless of the chosen strategy, but the partial derivatives are different.

The direct consequence is that one can effectively parameterize the model using the approach from Figure 28 or the approach from Figure 29 for the compositional derivatives of the extended long-range term and end up with the same result for the MIAC, LLE, IDAC and Gibbs-free energies of transfer. It is only in the partitioning of the neutral compounds where one can observe the impact of the selected convention for the mixing rules. Figure 41 shows this comparison, where the use of single solvent properties provides a slightly better prediction than the use of the averaged salt-free state.

A delicate issue is worth discussing. The primitive model is indeed not formulated for mixed solvents and theoretical discussions remain active in the recent literature.[167,168] However, including the compositional derivatives with explicit solvents in a Gibbs-Duhem consistent manner yields a (slightly) better result in the current evaluation. This contradicts the results from section 6.3.2, where better results were obtained using the salt-free averaged state for mixed solvent LLE systems. While the evaluation performed in this section applies a broader dataset and application of explicit, individual solvent properties provides higher accuracy, the more advantageous choice remains unclear.

Lastly, one may observe a few unexpected salting-in effects that are more pronounced in Figure 41 – right. These have been pointed out with black arrows and correspond to LiCl systems in biphasic water n-pentanol (or n-butanol) systems. The notable deviations in the partitioning of salts that have been described in previous works[14,16] also correspond in a large majority to systems with lithium salts (e.g. LiCl in a water + 2-methyl-2-butanol biphasic system, or $Li_2SO_4$ in a water + methyl-isobutyl ketone biphasic system). The most plausible explanation for these deviations is that the model does not properly capture the effect of attractive interactions (strong negative deviations from the DH theory) arising from the presence of stabilized ion pairs in the organic phase. In diluted salt systems, these can be appropriately captured by a Bjerrum treatment-based approach. However, traditional ion pairing is inappropriate for IL systems[358,359] and incompatible with extended long-range electrostatics unless speciation is accounted for in the mixing rules.

In a general electrostatic theory, ion pairing is not an actual association, but rather a probabilistic question pertaining the distance between the ions in terms of the radial distribution function and the charge-charge correlations.[96] Thus, if the same basis for all

ions is to be retained, future model development will most likely require further innovation and perhaps modern re-derivations of long-range electrostatic theories that either formally or empirically account for higher order terms.

The present chapter constitutes an initial and powerful demonstration that salt- and IL-based systems can be systematically modelled in a predictive fashion with the same basis and parameters. Nevertheless, the beneficial impact of extended LR electrostatics is closely related to a careful selection of appropriate mixing rules or surrogate models.

## *Solid-Liquid Equilibria*

In the closing evaluation of the present manuscript, the predictive capacity of the novel COSMO-RS-ES+ model in the calculation of the solid-liquid equilibria of salts in mixed and non-aqueous solvents is validated. The salt solubility dataset has been taken as validation of predictive capability in previous works[15,16] with COSMO-RS-ES. The case is not different for COSMO-RS-ES+, where performance in salt solubility prediction is kept as a qualitative indicator for overall predictive capacity.

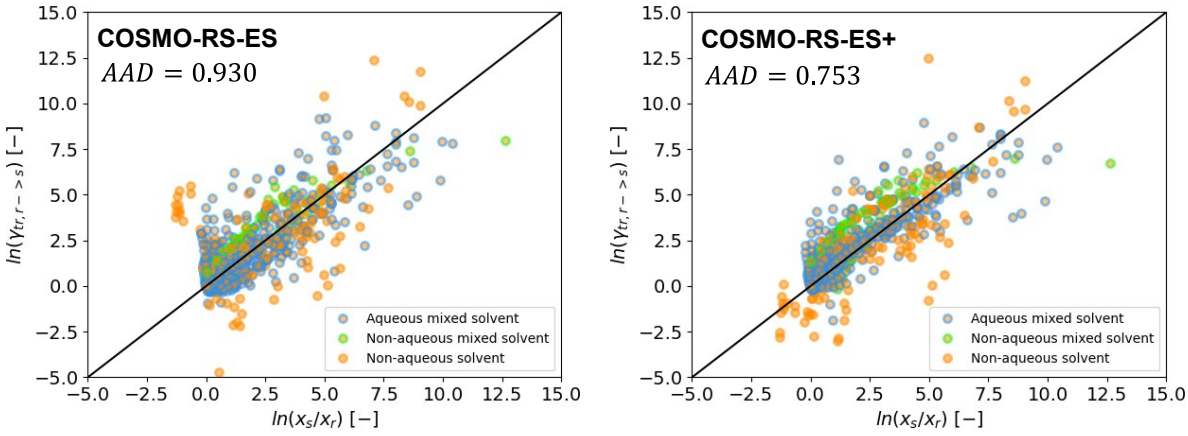


**Figure 42. Predicted solubility of diverse salts in aqueous and non-aqueous solvents applying pure water as the reference solvent. Solubility data are not part of the training set. Left: predictions with COSMO-RS-ES from section 6.2.2. Right: current predictions with COSMO-RS-ES+.**

The SLE dataset from Table 9, corresponding to the evaluation of COSMO-RS-ES combined with the ME-PDH term in section 6.2.2 contains 836 datapoints, whereas the presently evaluated SLE dataset from Table 17 contains 823 datapoints. The missing datapoints correspond to a $Cs_2SO_4$ + water + ethanol system that was eliminated from the database during continuous data curation.

A direct comparison between the predictive capacity of the COSMO-RS-ES+ model and its predecessor is shown in Figure 42, which provides compares salt solubility predictions of the COSMO-RS-ES model (as parameterized in section 6.2.2) and the new COSMO-RS-ES+ model from the present section. Figure 42 is a parity plot between the expected value using a reference solvent and the activity coefficient of transfer from the reference solvent according to equation (6.57):

$$\ln\left(\gamma_{tr,r\to s}\right) = \ln\left(\frac{x_{\pm,s}}{x_{\pm,r}}\right) \tag{6.57}$$

where $\gamma_{tr,r\to s}$ is the transfer activity coefficient from the reference solvent to the solvent of the system being calculated and the ratio $x_{\pm,s}/x_{\pm,r}$ is the solubility of the salt in the solvent of interest normalized by the solubility of the salt in the reference solvent. Further details regarding this calculation can be found in the Appendix.

With an AAD of 0.753, the COSMO-RS-ES+ model comes with a 19% improvement in the solubility calculations with respect to its predecessor as parameterized in section 6.2.2. In addition, the best reported AAD values for this type of evaluation is 0.89 in the work of Müller et al.[16] Given that the salt solubility dataset constitutes the largest validation for salt systems, one can state that the fully extended COSMO-RS-ES+ model represents a step forward in predictive capacity. The model has the solid foundation from its predecessor and is enhanced by a combination with thermodynamically consistent, extended long-range electrostatics. This step is accompanied by the novel introduction of IL systems, fully handled as electrolytes in the dataset and an improved performance for temperature dependent phase equilibria.

# 7 Conclusions

Electrolytes can be found everywhere in nature and are often used in industrial processes. Their impact on phase equilibria remains challenging to describe for practical application in extraction or distillation processes, due to the inherent complexity of electrolyte thermodynamics and the need for more experimental data, particularly for non-aqueous systems. Furthermore, there is an increasing demand for more standardized, transferable methodologies and more predictive power to model electrolyte systems. A promising method is the COSMO-RS-ES model, which was the first COSMO-RS based predictive electrolyte model to be systematically tested with broad datasets of aqueous liquid-liquid equilibria, mean ionic activity coefficients of salts in water, free energies of transfer of ions and salt solubility data in mixed solvents. The ultimate objective of this thesis was to extend the scope of the COSMO-RS-ES model towards a generalized application in aqueous, non-aqueous and highly concentrated electrolytes including ionic liquid systems. Several steps were taken to achieve this goal.

Initially, efforts were invested in developing a correlation between literature values of the parameter of closest approach used in the empirical Pitzer equations and advanced electrolyte theory. The literature values were found to correlate with the slope of the Limiting Law of the Dressed Ion Theory. Based on this observation, the Pitzer-Debye-Hückel term was first adapted by the introduction of a modified parameter of closest approach to correct the large systematic deviations found in the description of ions in low relative permittivity media. This modification scales the original parameter of closest approach with the Bjerrum length and indirectly represents the effects of correcting the magnitude of the radial distribution function in the linearized Debye-Hückel theory. This modification is empirical and intended avoid iterative ion pairing procedures, thereby providing a straightforward approach for correlative electrolyte models in chemical engineering when phase equilibria is the phenomenon of interest.

The modified parameter of closest approach was tested with the COSMO-RS-ES model resulting in considerable improvements for the mean ionic activity coefficients of salts in organic solvents. The corresponding average absolute deviation of these shows a reduction of 66.7% with respect to the original COSMO-RS-ES and of 30.0% with respect

to the COSMO-RS-ES model with ion-pairing based corrections for low permittivity. Minor improvements were observed in all other aqueous systems.

Subsequently, the Pitzer-Debye-Hückel term, is extended by introducing the compositional derivatives of the molar mass, relative permittivity and density of the mixture. In contrast to similar derivations of Pitzer-Debye-Hückel-based extensions found in the literature, the derivation in this work was performed with the modified parameter of closest approach and introducing minor corrections to the overall derivation pathway. The Gibbs-Duhem consistency of the resulting expression is confirmed in this work via numerical evaluation with the Gibbs-Duhem relation.

The COSMO-RS-ES model was re-parameterized applying the new modified extension of the Pitzer-Debye-Hückel term as electrostatic term and compared to analogous parameterizations that apply the unmodified extension of the Pitzer-Debye-Hückel term. The COSMO-RS-ES model is found to have a superior performance in the description of electrolyte systems when combined with the modified extension. In addition, improved performance in the calculation of mean ionic activity coefficients of salts in non-aqueous electrolytes was observed. Nevertheless, no further improvements are obtained for the calculation of salt partitioning in salt-based liquid-liquid equilibrium systems when compared to previous parameterizations of the model.

In a separate setting, the modified extension of the Pitzer-Debye-Hückel term was combined with conventional COSMO-RS theory using openCOSMO-RS to calculate activity coefficients and phase equilibria in ionic liquid systems. These systems consist of activity coefficients of molecular solvents infinitely diluted in pure ionic liquids and partitioning in ternary liquid-liquid equilibria with one ionic liquid compound. It is demonstrated that a tailored parameterization of openCOSMO-RS combined with the modified extension of the Pitzer-Debye-Hückel term outperforms a tailored parameterization of openCOSMO-RS alone in the description of ionic liquid systems. This result agrees with the recent literature and provides further evidence in favor of accounting for long-range electrostatics in the modelling of ionic liquid systems to improve model performance.

With the insights obtained from salt and ionic liquid systems, the COSMO-RS-ES+ model is developed and introduced. This novel extension of the COSMO-RS-ES model integrates the approach of its predecessor for salt-based electrolyte systems with the conventional openCOSMO-RS approach for ionic liquid systems, while applying the same basis and

energy interaction parameters for all ions. The COSMO-RS-ES+ model consists of revised ion-ion and ion-solvent short-ranged COSMO-RS based energy interaction equations combined with the modified extension of the Pitzer-Debye-Hückel term using volume fraction based mixing rules for the density and relative permittivity of the mixture.

The performance of the COSMO-RS-ES+ model is overall superior to that of its predecessor while retaining a similar performance for the description of liquid-liquid equilibria in ternary and quaternary salt-water-organic(s) systems. The prediction of salt solubility in mixed solvents with COSMO-RS-ES+ is also considerably improved. Moreover, the extended model demonstrates a superior performance when compared to openCOSMO-RS in the description of ionic liquid systems, particularly for partitioning in liquid-liquid equilibria, where an AAD has a value of 2.162 with openCOSMO-RS and of 1.025 with COSMO-RS-ES+, representing a 53% reduction of the averaged absolute deviation.

The results and observations from this work as well as the recent literature, firmly support considering the electrolytic nature of ILs to boost model performance and predictive capabilities for practical phase equilibria calculations. A consistent introduction of the compositional derivatives of the molar mass, density and relative permittivity of the mixture in the long-range electrostatics term plays a central role in achieving this goal. Furthermore, while theoretical discussions in the recent literature remain inconclusive, treating solvents as independent entities instead of an averaged dielectric medium provided a better performance for the partitioning of neutral compounds in ternary and quaternary liquid-liquid equilibria.

Advancements were made towards developing a correlative, Gibbs-Duhem consistent representation of long-range electrostatics that provides an educated guess for the electrostatic contribution to $\gamma_{\pm}$ under difficult conditions (high concentration, low relative permittivity) where the Debye-Hückel theory incurs into large underestimations. Other systematic deviations inherent to Debye-Hückel theory related to polyvalent charge symmetric electrolytes and size asymmetric ions have not been considered. Further developments in this direction for more accurate long-range electrostatics are required if COSMO-RS-ES+ is to be successfully extended for increasingly more complex systems with polyvalent ions (e.g. valence $|z| \geq 3$).

One of the largest simplifications presented here involves the use of correlations and mixing rules to describe pure compound properties and concentration dependent properties for long-range electrostatics. While these correlations and mixing rules are a valuable tool to enhance model performance, particularly in the case of ionic liquid systems, their application to concentration dependent density and relative permittivity of non-aqueous salt systems is an area of opportunity for future model development. The introduction of phenomenological, volume fraction based mixing rules, or a similar surrogate model, for the description of the relative permittivity of the mixture may further enhance model performance. Finally, the results presented in this thesis demonstrate that the full dissociation basis is feasible for a broad space of electrolyte systems when appropriate and general qualitative corrections are used. Nevertheless, ion speciation is to be considered in the future if the model is to be extended to describe acidity. Further qualitative improvements can be considered by the introduction of the effects from non-coulombic aggregation, particularly for the case of ionic liquids in water.

The COSMO-RS-ES+ model developed in this work is the first predictive model to systematically describe the phase equilibria and activities of a broad spectrum of salt and ionic liquid systems in mixed aqueous and non-aqueous solvents using the same basis and parameters for all ions in a Gibbs-Duhem consistent manner. The temperature effect on the activity coefficients is partially captured without the need for any additional temperature-dependent parameters at the COSMO-RS level. The development and results of the COSMO-RS-ES+ model firmly support the beneficial impact of consistently introducing compositional derivatives in long-range electrostatics as a strategy to improve and extend model performance and realm of application.

# 8 Appendix

## 8.1 Supplement to Debye-Hückel Theory Related Derivations

The amount of information presented in section 2.2 is rather condensed and, for the sake of brevity, several fundamental details were taken for granted. These are presented here for the interested reader.

### *Supplement to Debye-Hückel Theory and the Canonical Ensemble*

A formal estimation of the chemical potential in statistical mechanics applies the pair interaction potential and the radial distribution. In section 2.2.2 this form was introduced without any further comments. It is now briefly presented here for the excess chemical potential in an NVT ensemble with ideal, equally sized hard spheres of radius $\frac{a}{2}$ and ideal osmotic pressure:[22]

$$\mu_i^{ex} = V_{sphere} k_B T \rho_j + \sum_j \int_0^1 \mathrm{d}\xi \int_a^\infty 4\pi r^2 \, u_{ij}(r) \rho_j g_{ij}^{DH}(r;\xi) dr \tag{8.1}$$

where $V_{sphere} k_B T \rho_j = \frac{4\pi}{3} k_B T \rho_j a^3$ comes from the work ($\Delta PV$) of opening a cavity in the medium (excluded volume) in terms of the ideal pressure of the solution. Rigorously, the second integral on the right hand should go from 0 to infinity.[22] The consideration that $g_{ij}^{\#}(r) \equiv g_{ij}^{DH}(r) = 0$ inside the hard core diameter $a$ has already been factored in to change the limits of the integral.

The following definitions are known from DH theory (section 2.2.2):

$$g_{ij}^{DH}(r) = 1 + h_{ij}^{DH} = 1 - \beta q_j \psi_i^{DH}(r) \quad \forall \quad r > a$$

$$u_{ij}(r) = \begin{cases} 0 & \xi = 0 \\ \dfrac{q_i q_j}{4\pi\varepsilon_0\varepsilon_r r} & \xi = 1 \end{cases}$$

$$\psi_i^{DH}(r) = \frac{q_i}{4\pi\varepsilon_0\varepsilon_r r}\left(\frac{\exp\big(-\kappa_D(r-a)\big)}{\kappa_D a + 1}\right)$$

It then follows that:

$$\mu_i^{el} = \sum_j \int_0^1 \mathrm{d}\xi \int_a^\infty 4\pi r^2\, u_{ij}(r)\rho_j\, g_{ij}^{DH}(r;\xi)dr$$

$$= \int_0^1 \mathrm{d}\xi \int_a^\infty \frac{4\pi r^2 q_i}{4\pi\varepsilon_0\varepsilon_r r}\left(\sum_j \rho_j\, q_j\right)\left(1-\beta q_j \psi_i^{DH}(r)\right)dr$$

$$= \int_0^1 \mathrm{d}\xi \int_a^\infty \frac{r q_i}{\varepsilon_0\varepsilon_r}\left(\beta\sum_j \rho_j\, q_j^2\right)\left(\frac{-q_i}{4\pi\varepsilon_0\varepsilon_r r}\left(\frac{\exp\left(-\kappa_D(r-a)\right)}{\kappa_D a+1}\right)\right)dr$$

$$= -\int_0^1 \mathrm{d}\xi \int_a^\infty \frac{q_i^2}{4\pi\varepsilon_0\varepsilon_r}\left(\frac{\beta\sum_j \rho_j\, q_j^2}{\varepsilon_0\varepsilon_r}\right)\left(\frac{\exp\left(-\kappa_D(r-a)\right)}{\kappa_D a+1}\right)dr$$

$$= -\int_0^1 \mathrm{d}\xi \int_a^\infty \frac{q_i^2}{4\pi\varepsilon_0\varepsilon_r}(\kappa_D^2)\left(\frac{\exp\left(-\kappa_D(r-a)\right)}{\kappa_D a+1}\right)dr$$

$$= -\frac{q_i^2\kappa_D^2}{4\pi\varepsilon_0\varepsilon_r}\int_0^1 \mathrm{d}\xi \int_a^\infty \left(\frac{\exp\left(-\kappa_D(r-a)\right)}{\kappa_D a+1}\right)dr$$

$$= -\frac{q_i^2\kappa_D^2}{8\pi\varepsilon_0\varepsilon_r}\frac{\exp(\kappa_D a)}{(\kappa_D a+1)}\int_a^\infty \exp(-\kappa_D r)\,dr = -\frac{q_i^2}{8\pi\varepsilon_0\varepsilon_r}\frac{\kappa_D}{(\kappa_D a+1)}$$

which is the form applied in equation (2.30) and the contributions of (2.83) and (2.86). Thus, the more complete form of the excess chemical potential in DH theory is:

$$\mu_i^{DH+HC} = \frac{4\pi}{3}k_B T\rho_j a^3 - \frac{q_i^2}{8\pi\varepsilon_0\varepsilon_r}\frac{\kappa_D}{(\kappa_D a+1)} \tag{8.2}$$

from which the electrostatic term is isolated in the dilute regime: $\mu_i^{el} = -\frac{q_i^2}{8\pi\varepsilon_0\varepsilon_r}\frac{\kappa_D}{(\kappa_D a+1)}$.

### *Derivation of the Debye-Hückel theory via the Debye charging process*

The Debye charging process considers the charging the whole system: all ions of nature $i$, thereby calculating the Helmholtz free energy of electrostatic origin.[23] It therefore considers the internal charge distribution of the central sphere and its immediate vicinity at the boundary $r = a$ which is exactly at the distance $\frac{a}{2}$ from the assumed ionic surface. Firstly, let us reconsider equation (2.19), rewritten in the Appendix as equation (8.3):

$$\nabla^2\psi_i^{DH}(r) = 0 \quad \forall \quad r \le a \tag{8.3}$$

$$\nabla^2\psi_i^{DH}(r) = \frac{-1}{\varepsilon_0\varepsilon_r}\left(\sum_j q_j\rho_j\left[1-\beta q_j\psi_i^{DH}(r)\right]\right) = \kappa_D^2\psi_i^{DH}(r) \;\; \forall \quad r > a$$

where the solution outside of the excluded volume that corresponds to the central ion has been described in section 2.2.2 (equation (2.54)) and repeated here:

$$\psi_i^{DH}(r) = \frac{q_i}{4\pi\varepsilon_0\varepsilon_r r}\left(\frac{\exp\left(-\kappa_D(r-a)\right)}{\kappa_D a+1}\right) \quad \forall \;\; r > a$$

The Debye charging process considers the charge distribution inside the volume excluded for the central ion, which corresponds in the inexact LPB to:

$$\nabla^2\psi_i^{DH}(r) = \frac{1}{r^2}\frac{\partial}{\partial r}\left(r^2\frac{\partial\psi_i^{DH}(r)}{\partial r}\right) = 0 \quad \forall \;\; r \le a \tag{8.4}$$

The easiest boundary condition for this ordinary differential equation is a point charge at $r = 0$, which should reduce the mean DH potential $\psi_i^{DH}(r=0)$ to Coulomb's law:

$$\psi_i^{DH}(r=0) = \frac{q_i}{4\pi\varepsilon_0\varepsilon_r r} \tag{8.5}$$

As a second boundary condition, one can readily assume that the potential is a smooth function, such that $\psi_{i,r\le a}^{DH}(r\to a) + \psi_{i,r=a}^{DH}(r=a)) = \psi_{i,r>a}^{DH}(r\to a)$ to fulfill Gauss' Law. In other words, the potential of the central ion and its immediate vicinity at $r = a$ equals to the potential at $r \to a$ when approached from $r > a$. Thus, one can write the following:

$$\psi_i^{DH}(r=a) = \frac{q_i}{4\pi\varepsilon_0\varepsilon_r a}\left(\frac{1}{\kappa_D a+1}\right) - \frac{q_i}{4\pi\varepsilon_0\varepsilon_r\, a} = -\frac{q_i}{4\pi\varepsilon_0\varepsilon_r}\left(\frac{\kappa_D}{\kappa_D a+1}\right) \tag{8.6}$$

The excess Helmholtz free energy of electrostatic origin of the system is then calculated through charging all entities in the mixture with their corresponding internal potential $\psi_i^{DH}(r=a)$:[23]

$$\Delta A^{el} = \sum_i N_i q_i \int_0^{q_i} \psi_i^{DH}(r=a)dq \tag{8.7}$$

where $q_i$ is implicit in $\kappa_D$. Thus, one can propose[23,31] charging the ions from a state of no charge $\lambda q_i = 0$ to a state of full charge $\lambda q_i = q_i$ to define $\kappa_D(\lambda) = \sqrt{\beta\varepsilon_0^{-1}\varepsilon_r^{-1}\sum_i \lambda^2 q_i q_i\rho_i} = \lambda\kappa_D$ , thereby rewriting the integral as shown in equation (8.8) followed by its straightforward solution:

$$\Delta A^{el} = -\frac{\sum_i N_i q_i^2}{4\pi\varepsilon_0\varepsilon_r}\int_0^1\left(\frac{\lambda^2\kappa_D}{\lambda\kappa_D a+1}\right)d\lambda \tag{8.8}$$

$$\begin{aligned}\Delta A^{el} &= -\frac{\sum_i N_i q_i^2}{4\pi\varepsilon_0\varepsilon_r}\int_0^1\left(\frac{\lambda^2\kappa_D}{\lambda\kappa_D a+1}\right)d\lambda = -\frac{\sum_i N_i q_i^2}{4\pi\varepsilon_0\varepsilon_r}\frac{1}{a}\int_0^1\left(\frac{\lambda^2\kappa_D a}{\lambda\kappa_D a+1}\right)d\lambda\\ &= -\frac{\sum_i N_i q_i^2}{4\pi\varepsilon_0\varepsilon_r a}\int_0^1\left(\frac{\lambda^2\kappa_D a+\lambda-\lambda}{\lambda\kappa_D a+1}\right)d\lambda = -\frac{\sum_i N_i q_i^2}{4\pi\varepsilon_0\varepsilon_r a}\left[\frac{\lambda^2}{2}-\int_0^1\left(\frac{\lambda}{\lambda\kappa_D a+1}\right)d\lambda\right]\\ &= -\frac{\sum_i N_i q_i^2}{4\pi\varepsilon_0\varepsilon_r a}\left[\frac{(\lambda^2)|_0^1}{2}-\frac{1}{\kappa_D a}\int_0^1\left(\frac{\lambda\kappa_D a+1-1}{\lambda\kappa_D a+1}\right)d\lambda\right]\\ &= -\frac{\sum_i N_i q_i^2}{4\pi\varepsilon_0\varepsilon_r a}\left[\frac{1}{2}-\frac{\lambda|_0^1}{\kappa_D a}+\frac{1}{\kappa_D a}\int_0^1\left(\frac{1}{\lambda\kappa_D a+1}\right)d\lambda\right]\\ &= -\frac{\sum_i N_i q_i^2}{4\pi\varepsilon_0\varepsilon_r a}\left[\frac{1}{2}-\frac{1}{\kappa_D a}+\frac{1}{\kappa_D^2 a^2}\ln(\kappa_D a+1)\right]\end{aligned}$$

which can be reformulated to the more conventional form:

$$\begin{aligned}\frac{\Delta A^{el}\beta}{V} &= -\frac{\mathcal{X}_0}{4\pi}\\ \mathcal{X}_0 &= \frac{1}{a^3}\left(\frac{\kappa_D^2 a^2}{2}-\kappa_D a+\ln(1+\kappa_D a)\right)\end{aligned} \tag{8.9}$$

In the canonical ensemble the chemical potential is given by:[23]

$$\mu_i^{el} = \left(\frac{\partial(\Delta A^{el})}{\partial N_i}\right)_{T,V} = \frac{\partial}{\partial N_i}\left[-\frac{\sum_i N_i q_i^2}{4\pi\varepsilon_0\varepsilon_r}\frac{\mathcal{X}_0}{\kappa_D^2}\right]_{T,V} = \left(\frac{V}{\beta}\right)\frac{\partial}{\partial N_i}\left[-\frac{\mathcal{X}_0}{4\pi}\right]_{T,V} \tag{8.10}$$

It then follows that:

$$\begin{aligned}\mu_i^{el} &= \left(\frac{V}{\beta}\right)\frac{\partial}{\partial N_i}\left[-\frac{\mathcal{X}_0}{4\pi}\right]_{T,V} = \left(\frac{-V}{4\pi\beta a^3}\right)\frac{\partial}{\partial N_i}\left(\frac{\kappa_D^2 a^2}{2}-\kappa_D a+\ln(1+\kappa_D a)\right)\\ &= \left(\frac{-V}{4\pi\beta a^3}\right)\left(\kappa_D a^2-a+\frac{a}{1+\kappa_D a}\right)\left(\frac{\partial\kappa_D}{\partial N_i}\right) = \left(\frac{-V}{4\pi\beta a^3}\right)\left(\frac{\kappa_D^2 a^3}{1+\kappa_D a}\right)\left(\frac{\partial\kappa_D}{\partial N_i}\right)\\ &= \left(\frac{-V}{4\pi\beta a^3}\right)\left(\frac{\kappa_D^2 a^3}{1+\kappa_D a}\right)\left(\frac{\beta q_i^2}{2V\varepsilon_0\varepsilon_r\kappa_D}\right) = -\frac{q_i^2}{8\pi\varepsilon_0\varepsilon_r}\left(\frac{\kappa_D}{1+\kappa_D a}\right)\end{aligned}$$

Thus, the Debye charging process leads to an expression for $\mu_i^{el}$ that is exactly equal to equation (2.30) from statistical mechanics and equation (2.31) from the Güntelberg charging process, both shown in section 2.2.2.

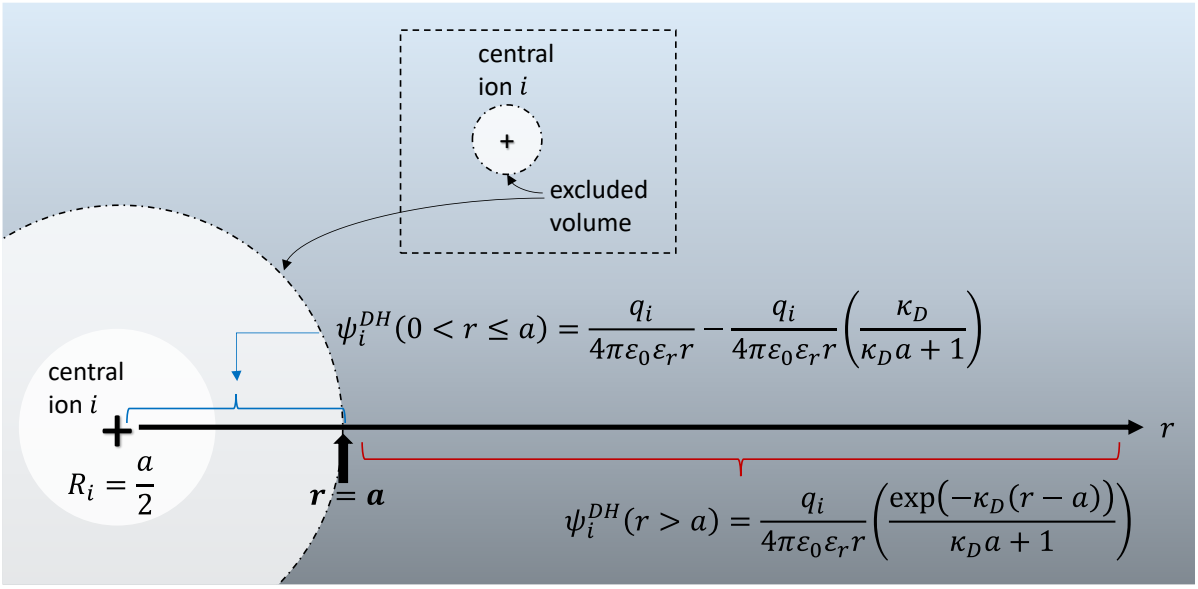


**Appendix Figure 1. Schematic representation of the different domains of the electrostatic potential in DH theory.**

## *Supplement to the Dressed Ion Theory and its Approximations*

Some details for the DIT and one of its approximations (MDE-DH) are briefly included here as a supplement. For further details, the reader is referred to the original works of Kjellander and Mitchell[41,42] and Kjellander.[32,48,49]

### *Supplement to the Dressed Ion Theory Limiting Law*

The central concept of the DIT is to reformulate the pair correlation functions in a shorter-ranged term (denoted by 0) and a longer-range term (denoted by #) and apply this in the context of the PB formulation. By splitting the pair correlation functions, one is also splitting the density distribution. Thus, the exact PB equation takes the form of equation (2.60), repeated here:

$$-\varepsilon_0\varepsilon_r\nabla^2\psi_i^{av}(r) = \rho_{E,i}^0(r) + \rho_{E,i}^{\#}(r) = \rho_{E,i}^0(r) - \int \alpha(|r-r'|)\psi_i^{av}(r')dr'$$

The sum $\rho_{E,i}^0 + \rho_{E,i}^{\#} = \rho_{E,i}^{tot}$ is the total charge density of the system distributed around the origin of ion $i$: the charge density $\rho_{E,i}^0$ of the central ion and its dress (ions in its immediate vicinity) plus the charge density of the ion cloud $\rho_{E,i}^{\#}$.

The unitary charge distribution $\rho_{E,i}^0$ (equivalent to $\rho_i^0(r)$ in Kjellander and Mitchell's notation[42] where $n_i$ was used to denote number density) from the OZ equation has the following definition:

$$\rho_{E,i}^{0} = q_i \delta^{(3)}(r) + \sum_j q_j \rho_j h_{ij}^{0}(r) \tag{8.11}$$

which is equivalent with the present notation and symbols to equation (20) of the original publication.[42] The source charge $q_i\delta^{(3)}(r)$ is commonly ignored in the conventional DH derivation.[32] Thus, one can note that the charge distribution of ion $i$ has its self-charge at the limit $q_i\delta^{(3)}(r) = q_i \;\; \forall \;\; r = 0$, plus the $ij$ correlated charges in its immediate vicinity (the dress). In the same fashion an ion $j$ in the vicinity has a charge density distribution $\rho_{E,j}^{0}$ around it which is also its self-charge plus a function of $h_{ji}^{0}$. This is a result of the OZ equation: the correlation of $i$ and $j$ in the vicinitiy of $i$ is affected by the presence of other $j$ ions.

Another relevant result from splitting the total pair correlation function $h_{ij}(r) = h_{ij}^{0}(r) + h_{ij}^{\#}(r)$ is the following relationship obtained from the OZ equation in combination with the coulombic pair potential:[42]

$$h_{ij}(r) = h_{ij}^{0}(r) - \beta \int \rho_{E,j}^{0}(|r - r'|)\psi_i^{av}(r')dr' \tag{8.12}$$

Thus, by means of the definition shown in equation (8.11) the following is found:

$$\begin{aligned} h_{ij}(r) &= h_{ij}^{0}(r) - \beta \int \rho_{E,j}^{0}(r - r')\psi_i^{av}(r')dr' \\ &= h_{ij}^{0}(r) - \beta \int \left( q_j \delta^{(3)}(|r - r'|)\psi_i^{av}(r') + \sum_i q_i \rho_i h_{ij}^{0}\,(|r - r'|)\psi_i^{av}(r') \right) dr' \\ &= h_{ij}^{0}(r) - \beta q_j \psi_i^{av}(r) - \beta \int \left( \sum_k q_k \rho_k h_{kj}^{0}\,\psi_i^{av}(r') \right) dr' \end{aligned}$$

and one can observe in the linearized regime that $h_{ij}(r)_{trunc} = h_{ij}^{0}(r) - \beta q_j \psi_i^{av}(r')$ and therefore $h_{ij}^{\#}(r)_{trunc} = -\beta q_j \psi_i^{av}(r)$. This corresponds in the DH theory formulation to $h_{ij}^{DH}(r) = -\beta q_j \psi_i^{DH}(r)$. This definition was introduced in the main text directly after equation (2.62). In the non-linear regime the full expression applies:

$$h_{ij}^{\#}(r) = -\beta \int \rho_{E,j}^{0}(|r - r'|)\psi_i^{av}(r')dr' \tag{8.13}$$

which was introduced in the main text as equation (2.67). Thus, for the region outside of the volume excluded for the central ion $i$ and its dress (at $r > a$) the electrostatic "cloud" component $\rho_{E,i}^{\#}(r)$ is:

$$\rho_{E,i}^{\#} = \sum_j \rho_j \, q_j g_{ij}^{\#}(r) = -\beta \sum_j \rho_j \, q_j \int \rho_{E,j}^{0}(|r - r'|)\psi_i^{av}(r')dr' \tag{8.14}$$

where electroneutrality is invoked for $\sum_j \rho_j \, q_j g_{ij}^{\#}(r) = \sum_j \rho_j \, q_j h_{ij}^{\#}(r)$. In combination with the definition introduced in equation (8.11), the following is obtained:

$$\sum_j \rho_j \, q_j h_{ij}^{\#}(r) = -\beta \sum_j \rho_j \, q_j \int \left[ q_j \delta^{(3)}(|r - r'|) + \sum_i q_i \rho_i h_{ji}^{0}(|r - r'|) \right] \psi_i^{av}(r')dr'$$

$$= -\left[ \beta \sum_j \rho_j \, q_j^2 + \beta \sum_{ij} \rho_i \rho_j q_i q_j h_{ji}^{0}(r) \right] \psi_i^{av}(r) = -\alpha(r)\psi_i^{av}(r)$$

The polarization response function $\alpha(r)$ was introduced in equation (2.61) of the main text as a part of the exact PB formulation.

The polarization of a medium in presence of an external electric field was introduced in the main text as equation (2.101) repeated here:

$$\mathbf{P} = \varepsilon_0(\varepsilon_r - 1)\mathbf{E}$$

The dielectric constant $\varepsilon_r$ (in modern convention called the relative permittivity), is the capacitance of the medium with respect to vacuum: $C/C_0$. The dielectric flux density (the permeation of the electric field through an arbitrary perpendicular surface segment of the medium) is facilitated in the measure that $\varepsilon_r$ attains lower values. An increase in flux density caused by an additional external charge is called a dielectric displacement $\mathbf{D}$, which is by definition:[67]

$$\mathbf{D}(r) = \varepsilon_0 \mathbf{E}^{\mathbf{Ext}}(r) \tag{8.15}$$

One can now assume that the medium is a conducting electrolyte. The averaged potential of the electrolyte at an arbitrary point is $\psi_i^{av}(r)$. By introducing a test charge in this point $r$ the dielectric displacement is then given by:[42]

$$\mathbf{D}(r) = \varepsilon_0 \mathbf{E}^{\mathbf{Ext}}(r) = -\varepsilon_0 \varepsilon_r \nabla \psi_i(r) \tag{8.16}$$

where $\varepsilon_r\psi_i(r)$ is the Coulombic potential of the test charge in vacuum. For a charge density with an electric field permeating the solution, the following definition applies:[67]

$$\mathbf{D}(r) = \varepsilon_0\mathbf{E}(r) + \mathbf{P}(r) \tag{8.17}$$

being $\mathbf{P}(r)$ is the polarization vector of the electrolyte and $\mathbf{E}(r) = \nabla\psi_i^{av}(r)$. Thus, as ions are being introduced into an electrolyte, a polarization response of the electrolyte is to be expected.

It then follows that:

$$\mathbf{P}(r) = \varepsilon_0\left(\nabla\psi_i^{av}(r) - \varepsilon_r\nabla\psi_i(r)\right) \tag{8.18}$$

For a macroscopic dielectric from equation (2.101), the function $(\varepsilon_r - 1)$ is called the relative dielectric susceptibility.[67] In direct analogy, the function $\left(\nabla\psi_i^{av}(r) - \varepsilon_r\nabla\psi_i(r)\right)$ relates to the dielectric susceptibility of the electrolyte.[42]

Furthermore, the potential $\nabla\psi_i^{av}(r)$ is a function of the charge density and the charge density restructures itself by a polarization response upon addition of more ions into the electrolyte. Thus, an infinitesimal increment of charge in a point $r$ of the electrolyte results in a total potential at $r$ that is equal to the potential of the external charge being introduced and a $\rho_P(r')$ polarization density response of the electrolyte:[96]

$$\psi_i^{av}(r) = \psi_i + \int \phi(|r - r'|)\rho_P(r')dr' \tag{8.19}$$

The polarization response of the charge density of the electrolyte, i.e. equation (8.14), is then given by:[96]

$$\rho_P(r) = -\int \alpha(|r - r'|)\psi_i^{av}(r')dr' \tag{8.20}$$

In Fourier space, equation (8.19) is expressed as follows:[96]

$$\begin{aligned} \hat{\psi}_i^{av}(\mathrm{k}) &= \hat{\psi}_i(\mathrm{k}) + \hat{\psi}_i^{av}(\mathrm{k})\hat{\alpha}(k)\hat{\phi}(k) \\ \frac{\hat{\psi}_i(\mathrm{k})}{\hat{\psi}_i^{av}(\mathrm{k})} &= 1 - \hat{\alpha}(k)\hat{\phi}(k) = \hat{\varepsilon}_r(k) \end{aligned} \tag{8.21}$$

where $1 - \hat{\alpha}(k)\hat{\phi}(k) = \hat{\varepsilon}_r(k)$ is termed the dielectric function, related to the dielectric susceptibility of the electrolyte, which gives origin[48,96] to the necessity of the dielectric

factor $E$ in the unit Coulomb potential. Consequently, the dielectric factor is introduced in equation (2.64) of the main text. $\hat{\varepsilon}_r(k)$ is divided into a singular and non-singular components in Fourier space.[96] These correspond to $\mathcal{E}'$ and $\mathcal{E}''$ in real space and take part in the Coulomb potential.

*Supplement to Multiple Decay Extension of the Debye-Hückel Theory (MDE-DH)*

In the main text, equation (2.79) is introduced as the result from the electroneutrality condition. This result is easily visualized by applying equation (2.65) in equation (2.78) as follows:

$$q_i = 4\pi\varepsilon_0\varepsilon_r \int_a^\infty \left( \frac{(\kappa')^2 q_i^{*'} \exp(-\kappa' r)}{4\pi\varepsilon_0\varepsilon_r \mathcal{E}' r} + \frac{(\kappa'')^2 q_i^{*''} \exp(-\kappa'' r)}{4\pi\varepsilon_0\varepsilon_r \mathcal{E}'' r} \right) r\mathrm{d}r$$

$$= \int_a^\infty \left( \frac{(\kappa')^2 q_i \left( \frac{\exp(\kappa' a)}{(1+\kappa' a)} \right) \exp(-\kappa' r)}{\mathcal{E}' r} + \frac{(\kappa'')^2 q_i \left( \frac{\exp(\kappa'' a)}{(1+\kappa'' a)} \right) \exp(-\kappa'' r)}{\mathcal{E}'' r} \right) r\mathrm{d}r$$

$$= \frac{q_i \left( \frac{\exp(\kappa' a)}{(1+\kappa' a)} \right) \frac{(1+\kappa' a)}{\exp(\kappa' a)}}{\mathcal{E}'} + \frac{q_i \left( \frac{\exp(\kappa'' a)}{(1+\kappa'' a)} \right) \frac{(1+\kappa'' a)}{\exp(\kappa'' a)}}{\mathcal{E}''} = \frac{q_i}{\mathcal{E}'} + \frac{q_i}{\mathcal{E}''}$$

Above the Kirkwood crossover the Euler formula is applied with the definitions in the main text to obtain the electroneutrality condition as:

$$\frac{1}{|\mathcal{E}|} \cdot \left( \cos\vartheta + \mathrm{i} \cdot \sin\vartheta + \frac{\cos\vartheta - \mathrm{i} \cdot \sin\vartheta}{\cos^2\vartheta + \sin^2\vartheta} \right) = 1$$

The calculation of the mean ionic activity coefficient above the Kirkwood crossover is:

$$\ln\left(\gamma_i^{el}\right) = -\frac{\beta q_i^2}{8\pi\varepsilon\varepsilon_r} \left[ \frac{\kappa_\Re + \mathrm{i}\kappa_\Im}{\mathcal{E}'((1+\kappa_\Re a) + \mathrm{i}\kappa_\Im a)} + \frac{\kappa_\Re - \mathrm{i}\kappa_\Im}{\mathcal{E}''((1+\kappa_\Re a) - \mathrm{i}\kappa_\Im a)} \right]$$

$$= -\frac{\beta q_i^2}{8\pi\varepsilon\varepsilon_r} \left\{ \frac{\cos\vartheta \cdot \left[ e^{\mathrm{i}\vartheta} \left( \kappa_\Re + \kappa_\Re^2 a + \mathrm{i}\kappa_\Im - \mathrm{i}^2 a\kappa_\Im^2 \right) + e^{-\mathrm{i}\vartheta} \left( \kappa_\Re + \kappa_\Re^2 a - \mathrm{i}\kappa_\Im - \mathrm{i}^2 a\kappa_\Im^2 \right) \right]}{2\cos^2\vartheta \cdot \left( (1+\kappa_\Re a)^2 + a\kappa_\Im^2 \right)} \right\}$$

$$= -\frac{\beta q_i^2}{8\pi\varepsilon\varepsilon_r} \left\{ \frac{\left[ 2\cos\vartheta \left( \kappa_\Re + \kappa_\Re^2 a + a\kappa_\Im^2 \right) + \mathrm{i}^2 2\kappa_\Im \sin\vartheta \right]}{2\cos\vartheta \cdot \left( (1+\kappa_\Re a)^2 + a\kappa_\Im^2 \right)} \right\}$$

$$= -\frac{\beta q_i^2}{8\pi\varepsilon\varepsilon_r} \left\{ \frac{\kappa_\Re + \kappa_\Re^2 a + a\kappa_\Im^2 - \kappa_\Im \tan\vartheta}{(1+\kappa_\Re a)^2 + a\kappa_\Im^2} \right\}$$

which the result from equation (2.86), where the Euler formula was once again applied to reduce the terms into a simpler form.

Finally, the phase shift is given by:

$$\tan\vartheta = \left\{ e^{a\kappa_{\Re}} - \left[1 + a\kappa_{\Re} + \frac{(a\kappa_{\Re})^2}{2} + \frac{(a\kappa_{\Re})^3}{6} - \frac{(a\kappa_{\Im})^2}{2}(1 + a\kappa_{\Re})\right]\cos a\kappa_{\Im} - a\kappa_{\Im}\left[1 + a\kappa_{\Re} + \frac{(a\kappa_{\Re})^2}{2} - \frac{(a\kappa_{\Im})^2}{6}\right]\sin a\kappa_{\Im}\right\} / \left\{\left[1 + a\kappa_{\Re} + \frac{(a\kappa_{\Re})^2}{2} + \frac{(a\kappa_{\Re})^3}{6} - \frac{(a\kappa_{\Im})^2}{2}(1 + a\kappa_{\Re})\right]\sin a\kappa_{\Im} - a\kappa_{\Im}\left[1 + a\kappa_{\Re} + \frac{(a\kappa_{\Re})^2}{2} - \frac{(a\kappa_{\Im})^2}{6}\right]\cos a\kappa_{\Im}\right\}$$

## 8.2 Supplement to the Modified and Modified Extended Pitzer-Debye-Hückel Terms

*Supplement to the modified parameter of closest approach*

The scaling of the parameter of closest approach is based on approximating equation (6.7) repeated here:

$$\frac{\kappa}{\kappa_D} = \sqrt{1 - \alpha_1\Lambda^2}$$

using equation (6.9) at infinite dilution, repeated here:

$$\frac{\kappa^{\infty}}{\kappa_D^{\infty}} = \frac{1}{\sqrt{1 + \alpha_1(\Lambda^{\infty})^2}}$$

Firstly, the limiting law derived from the DIT cannot be applied at large concentrations. The same applies to equation (6.7), which becomes complex valued when $\alpha_1\Lambda^2 > 1$. Equations (6.7) and (6.9) are evidently not equal at higher concentrations, but closely approximate each other at infinite dilution. It can be shown that:

$$\lim_{\kappa_D \to 0} \sqrt{1 - \alpha_1(\Lambda^{\infty})^2} = \lim_{\kappa_D \to 0} \frac{1}{\sqrt{1 + \alpha_1(\Lambda^{\infty})^2}}$$

This is can be visualized at infinite dilution in Figure 19, where equations (6.7) and (6.9) become equal and agree with Bjerrum's theory. Thus, equation (6.9) is a simple expression that can be used to scale the parameter of closest approach in Pitzer's equations and reproduce literature values.

The modified parameter of closest approach is a semi-empirical correlation obtained by the introduction of the scaling factor from equation (6.10) into the physical parameter of closest approach to yield equation (6.13) of the main text repeated here:

$$b_{mod}^{(m)} = \frac{1}{\sqrt{I^{(m)}}} \cdot \kappa_D a \cdot f_{sc(2)} = b^{(m)} + \left( \sqrt{\frac{1}{I^{(m)}} + \frac{\alpha_1 \Lambda^2}{I^{(m)}}} - \frac{1}{\sqrt{I^{(m)}}} \right)$$

Gibbs-Duhem consistency requires $b_{mod}^{(m)}$ to be a constant. For strong ion-ion coupling in low permittivity values the term $\frac{\alpha_1 \Lambda^2}{I^{(m)}}$ is dominant and for high permittivity values the correction term itself becomes negligible. Furthermore, at the ionic liquid limit, the terms $\frac{1}{I^{(m)}}$ and $\frac{1}{\sqrt{I^{(m)}}}$ vanish. Thus, given the fully empirical nature of the correction, these were neglected for simplicity.

Introducing the association constant from Ebeling ($K_{assoc}$ is applied in m$^3$/mol and the result has consistent units kg/mol), the second term of the square root is given by:

$$\frac{\alpha_1 \Lambda^2}{I^{(m)}} = \frac{K_{assoc}}{8\pi N_A \lambda_B^3} \frac{\kappa_D^2 \lambda_B^2}{I^{(m)}} = \frac{K_{assoc}}{8\pi N_A} \left( \frac{2 N_A d_s e^2}{\varepsilon_0 \varepsilon_r k_B T} \right) \left( \frac{e^2}{4\pi \varepsilon_0 \varepsilon_r k_B T} \right)^{-1}$$

$$= \frac{K_{assoc}}{8\pi N_A} \left( \frac{N_A d_s e^2}{\varepsilon_0 \varepsilon_r k_B T} \right) \left( \frac{8\pi \varepsilon_0 \varepsilon_r k_B T}{e^2} \right) = d_s \cdot K_{assoc}$$

$$= 8\pi d_s N_A (\alpha_{sc} a)^3 \sum_{n=1}^{\infty} \frac{(\lambda_B / (\alpha_{sc} a))^{2n+2}}{(2n+2)! \cdot (2n-1)}$$

The resulting expression in the molality scale corresponds to equation (6.15) of the main text which results in equation (6.17) in the mole fraction scale.

Taking into consideration that the first term of the summation is fully dominant when $\alpha_{sc}$ takes large enough values, it then follows that equation (6.17) can be simplified as follows:

$$b_{mod}^{(x)} \equiv \frac{3}{2}b^{(x)} + \sqrt{\frac{d_s}{M_s}\cdot 8\pi N_A(\alpha_{sc}a)^3\sum_{n=1}^{\infty}\frac{(\lambda_B/(\alpha_{sc}a))^{2n+2}}{(2n+2)!\cdot(2n-1)}}$$

$$= \frac{3}{2}b^{(x)} + \sqrt{\frac{d_s}{M_s}\cdot 8\pi N_A(\alpha_{sc}a)^3\frac{(\lambda_B/(\alpha_{sc}a))^4}{4!}}$$

$$= \frac{3}{2}b^{(x)} + \sqrt{\frac{d_s}{M_s}\cdot 8\pi N_A\lambda_B a^2\left(\frac{\lambda_B}{a}\right)^3\left(\frac{\alpha_{sc}^2}{4!\,\alpha_{sc}^3}\right)}$$

$$= \frac{3}{2}b^{(x)} + a\sqrt{\frac{d_s}{M_s}\cdot 8\pi N_A\lambda_B}\sqrt{\left(\frac{\lambda_B}{a}\right)^3\left(\frac{\alpha_{sc}^2}{4!\,\alpha_{sc}^3}\right)} = \frac{3}{2}b^{(x)} + b^{(x)}\sqrt{\left(\frac{\lambda_B}{a}\right)^3\left(\frac{1}{4!\,\alpha_{sc}}\right)}$$

$$\equiv \frac{3}{2}b^{(x)} + b^{(x)}\sqrt{\left(\frac{\lambda_B}{a\cdot(4!\,\alpha_{sc})^{1/3}}\right)^3} = b^{(x)}\left[\omega_{(0)} + \left(\omega_{(1)}\frac{\lambda_B}{a}\right)^{3/2}\right]$$

where $\omega_{(0)} = \frac{3}{2}$ and, if $\alpha_{sc} \approx 30$ to reproduce literature values, then $\omega_{(1)} \approx \frac{1}{9}$ and this equation corresponds to equations (6.18) and (6.28) of the main text.

*Supplement to the E-PDH term*

The full derivative of equation (2.49) is expressed as follows:

$$\ln(\gamma_i^{E-PDH}) = -A_\phi^{(x)}\left\{\overbrace{\frac{2z_i^2}{b^{(x)}}\ln\left(1+b^{(x)}I_x^{1/2}\right)}^{term\ 1} + \overbrace{\frac{z_i^2 I_x^{1/2} - 2I_x^{3/2}}{1+b^{(x)}I_x^{1/2}}}^{term\ 2} - \overbrace{\frac{4n_T I_x}{b^{(x)^2}}\ln\left(1+b^{(x)}I_x^{1/2}\right)\cdot\frac{\partial b^{(x)}}{\partial n_i}}^{term\ 3}\right.$$
$$\left. + \overbrace{\frac{4I_x^{3/2}n_T}{b^{(x)}\left(1+b^{(x)}I_x^{1/2}\right)}\cdot\frac{\partial b^{(x)}}{\partial n_i}}^{term\ 4}\right\} - \overbrace{\frac{4n_T I_x}{b^{(x)}}\ln\left(1+b^{(x)}I_x^{1/2}\right)\cdot\frac{\partial A_\phi}{\partial n_i}}^{term\ 5}$$

One may observe that terms 1 and 2 correspond to the conventional derivation from Pitzer,[40] for which all concentration dependencies of $A_\phi^{(x)}$ and $b^{(x)}$ are absent and therefore $\frac{\partial b^{(x)}}{\partial n_i} = \frac{\partial A_\phi^{(x)}}{\partial n_i} = 0$. If these concentration dependencies are accounted for through a concentration dependent permittivity, density and molar mass, as shown in section 6.2.1, then the following definitions ensue:

$$\left(\frac{\partial A_\phi}{\partial n_i}\right)_{\varepsilon_m, d_m} = -\frac{A_\phi}{2M_m}\cdot\frac{\partial M_m}{\partial n_i}$$

$$\left(\frac{\partial A_\phi}{\partial n_i}\right)_{\varepsilon_m, M_m} = \frac{A_\phi}{2d_m} \cdot \frac{\partial d_m}{\partial n_i}$$

$$\left(\frac{\partial A_\phi}{\partial n_i}\right)_{d_m, M_m} = -\frac{3A_\phi}{2\varepsilon_m} \cdot \frac{\partial \varepsilon_m}{\partial n_i}$$

for the Debye-Hückel slope. Likewise for the parameter of closest approach:

$$\left(\frac{\partial b^{(x)}}{\partial n_i}\right)_{\varepsilon_m, d_m} = -\frac{b^{(x)}}{2M_m} \cdot \frac{\partial M_m}{\partial n_i}$$

$$\left(\frac{\partial b^{(x)}}{\partial n_i}\right)_{\varepsilon_m, M_m} = \frac{b^{(x)}}{2d_m} \cdot \frac{\partial d_m}{\partial n_i}$$

$$\left(\frac{\partial b^{(x)}}{\partial n_i}\right)_{d_m, M_m} = -\frac{b^{(x)}}{2\varepsilon_m} \cdot \frac{\partial \varepsilon_m}{\partial n_i}$$

Use of the aforementioned equations leads to the E-PDH term from equation (6.21).

*Supplement to the ME-PDH term*

The same procedure from the E-PDH term is followed for the ME-PDH term but with application of the modified $b_{mod}^{(x)}$. The modified parameter of closest approach has the following definitions and corresponding derivatives:

$$b_{mod}^{(x)} = b_{(0)}^{(x)} + b_{(1)}^{(x)}$$

$$b_{(0)}^{(x)} = \omega_{(0)} b^{(x)}$$

$$b_{(1)}^{(x)} = \left(\omega_{(1)} \frac{\lambda_B}{a}\right)^{3/2} b^{(x)}$$

$$\left(\frac{\partial b_{mod}^{(x)}}{\partial n_i}\right)_{\varepsilon_m, d_m} = -\frac{b_{mod}^{(x)}}{2M_m} \cdot \frac{\partial M_m}{\partial n_i}$$

$$\left(\frac{\partial b_{mod}^{(x)}}{\partial n_i}\right)_{\varepsilon_m, M_m} = \frac{b_{mod}^{(x)}}{2d_m} \cdot \frac{\partial d_m}{\partial n_i}$$

$$\left(\frac{\partial b_{mod}^{(x)}}{\partial n_i}\right)_{d_m, M_m} = -\frac{b_{mod}^{(x)} + 3b_{(1)}^{(x)}}{2\varepsilon_m} \cdot \frac{\partial \varepsilon_m}{\partial n_i}$$

Application of these definitions in the full derivative of equation (2.49) leads to the ME-PDH term shown in equation (6.29).

*Supplement to volume fraction based mixing rules for extended LR electrostatics*

As briefly shown in Table 2, Giese et al.[82] proposed an empirical model for the concentration dependent relative permittivity of aqueous electrolytes. The model consists of considering a volume fraction determined by unbound water molecules that do not participate in the solvation shell of an ion and a volume fraction that consists of solvated ions. The volume fraction of the free water molecules is applied with the salt-free permittivity and the solvated ion volume fraction is applied with a hypothetical value $\varepsilon_e = 2$. The molar volume of the solvated ions was kept constant.

Based on these ideas and the discussion on mixing rules provided by Kaatze et al.[79], one may propose a concentration dependency for the volume fraction that corresponds to the bound solvent molecules that participate in the solvation shell. This dependency must respect the logical requirements that the moles of molecular and ionic species remain constant and that the total volume is preserved when neglecting entropic disorder and electrostriction effects $\Delta \mathrm{v}^d = \Delta \mathrm{v}^{el} = 0$. These conditions are expressed as:

$$x_{\mathcal{U}} + x_{\mathcal{B}} + \sum_j x_j = x_s + \sum_j x_j = 1$$
$$\mathrm{v}_T = x_{\mathcal{U}}(\mathrm{v}_s + \Delta \mathrm{v}^d) + x_{\mathcal{B}}(\mathrm{v}_s + \Delta \mathrm{v}^{el}) + \sum_j x_j \mathrm{v}_j = x_s \mathrm{v}_s + \sum_j x_j \mathrm{v}_j \quad \text{if} \quad \Delta \mathrm{v}^{el} = \Delta \mathrm{v}^d = 0 \tag{8.22}$$

where the subscript $\mathcal{U}$ stands for unbound (free) solvent fraction, $\mathcal{B}$ stands for bound solvent fraction and $\mathrm{v}_T$ stands for the total molar volume of the mixture. The subscripts $i$, $j$, $s$ are used here for all species, ionic species and solvent species, respectively. The unbound solvent mole fraction is defined by $x_{\mathcal{U}} = x_s - x_{\mathcal{B}}$. A conceptually similar (concentration dependent solvation shells), Debye-Hückel-theory-based approach was published by Mollerup and Breil.[360]

Following these assumptions, a mixing rule for a property $\mathcal{P}_m$ of an electrolyte mixture (single solvent) is reformulated as follows:

$$\mathcal{P}_m = \frac{x_{\mathcal{B}}\mathrm{v}_s}{\mathrm{v}_T}(\mathcal{P}_{\mathcal{B}} - \mathcal{P}_s) + \sum_i \phi_i \mathcal{P}_i = \phi_{\mathcal{B}}(\mathcal{P}_{\mathcal{B}} - \mathcal{P}_s) + \sum_i \phi_i \mathcal{P}_i \tag{8.23}$$

which constitutes a bound fraction model: a volume fraction mixing rule that attempts to account for some additional phenomenology by introducing a concentration dependent fraction of the dielectric volume that takes part in the ionic solvation shell. If $x_B \to 0 \therefore \phi_{\mathcal{B}} \to 0$, then the expression reduces to conventional volume fraction. The term $\phi_{\mathcal{B}}(\mathcal{P}_{\mathcal{B}} - \mathcal{P}_s)$ represents a rough phenomenological correction, assumes that the molar volume of the bound solvent has not changed and does not account for structural effects (i.e. neglected $\Delta\mathrm{v}^{el} = \Delta\mathrm{v}^{d}$). Most systematic modelling approaches of the density and relative permittivity with broad electrolyte databases remain empirical and oversimplified.[91,125,184,262,321] The case is not different for a blunt mixing rule, yet one may introduce some complementary phenomenology.

The corresponding partial derivatives of the terms on the right-hand side of equation (8.23) are given by:

$$\begin{gathered}\frac{\partial}{\partial n_i}\left(\sum_i \phi_i \mathcal{P}_i\right) = \frac{\mathrm{v}_i}{n_T \mathrm{v}_T}\left(\mathcal{P}_i - \sum_i \phi_i \mathcal{P}_i\right) \\ \frac{\partial}{\partial n_i}[\phi_{\mathcal{B}}(\mathcal{P}_{\mathcal{B}} - \mathcal{P}_s)] = \mathrm{v}_s(\mathcal{P}_{\mathcal{B}} - \mathcal{P}_s)\left\{\frac{1}{\mathrm{v}_T}\frac{\partial}{\partial n_i}(x_{\mathcal{B}}) - \frac{x_{\mathcal{B}}\left(\delta_{is}\mathrm{v}_s + \delta_{ij}\mathrm{v}_j - \mathrm{v}_T\right)}{n_T \mathrm{v}_T^2}\right\}\end{gathered} \tag{8.24}$$

where $\delta_{ik}$ is a Kronecker delta: $\delta_{ik} = 1 \;\forall\; i = k$ and $\delta_{ik} = 0 \;\forall\; i \neq k$ and the subscript convention $s$ and $j$ is being used for solvents and ions, respectively, and $i, k$ for any arbitrary species.

If $\mathcal{P}_m$ is the relative permittivity of the mixture then, in line with the work from Giese et al.,[82] and the work of Mollerup and Breil,[360] the local relative permittivity of the bound solvent can be assumed to be in the vicinity of $1 \leq \varepsilon_{\mathcal{B}} \leq 2$. If equation (8.23) were to be used with $\varepsilon_{IL} = \varepsilon_{\mathcal{B}}$ and a $x_{\mathcal{B}} = \mathcal{S}x_j$ ratio ($\mathcal{S}$ is some system specific constant) where the molar volume of the solvated ion is $x_j(\mathcal{S}\mathrm{v}_s + \mathrm{v}_j)$, then the model conceptually corresponds to that of Giese et al.,[82] reformulated as a mixing rule.

A concentration dependent definition of the bound fraction $x_{\mathcal{B}}$ can be proposed as a function of ion concentration, molar volumes, salt-free permittivity, dipole moments, among other criteria, developing into a complex theoretical undertaking. For bound water

alone, Kaatze et al.[79] discuss the effects on relaxation times observed in aqueous mixtures which can be strongly dependent on the nature and concentration of other species due to the coupling between hydrodynamics and dielectrics, structural effects (e.g. the enhancement of the mobility of water) and coulombic charge, among others. In view of these hurdles a pragmatic possibility could be to suggest treating the solvation shell with simplified reaction-like kinetics:

$$\sum_j x_j + x_{\mathcal{U}} \overset{K_{\mathcal{B}}}{\rightarrow} x_{\mathcal{B}}$$

$$x_{\mathcal{B}} = \frac{K_{\mathcal{B}} x_s \sum_j x_j}{1 + K_{\mathcal{B}} \sum_j x_j} \tag{8.25}$$

where a bound fraction constant $K_{\mathcal{B}} \geq 0$ applies. The previous equation fulfills the logical requirement $x_{\mathcal{B}} = 0$ for the salt-free and solvent-free states, and provides a straightforward expression for the missing compositional derivative in equation set (8.24):

$$\frac{\partial}{\partial n_i}(x_{\mathcal{B}}) = \left(\frac{K_{\mathcal{B}}}{n_T}\right) \frac{x_s\left(\delta_{ij} - \sum_j x_j\right) + \sum_j x_j\,(\delta_{is} - x_s)}{1 + K_{\mathcal{B}} \sum_j x_j} - \left(\frac{K_{\mathcal{B}} \sqrt{x_s \sum_j x_j}}{1 + K_{\mathcal{B}} \sum_j x_j}\right)^2 \left(\frac{\delta_{ij} - \sum_j x_j}{n_T}\right) \tag{8.26}$$

The problem reduces to defining the hypothetical limiting value $\varepsilon_{IL}$ for the molten (hypothetical metastable subcooled, given the case) ionic state and a bound fraction constant $K_{\mathcal{B}}$. This approach could be more universally applicable compared to fitting a series of specific parameters for quadratic or cubic volume fraction mixing rules. It may also provide some rough pragmatic improvements while excluding the need for rigorous modelling of a highly complex and poorly understood phenomenon in such a vast database. Due to time limitations, this blunt idea was not properly explored, is left here for documentation purposes and has been partially programmed in the "equilibrium properties" code of the model. It must be clearly pointed out that the missing effects in all COSMO-RS-ES and COSMO-RS-ES+ models that result in an overestimation of $\gamma_{\pm}$ in neat organic solvents are neither purely attributed to the dielectric decrement nor purely attributed to ion-pairing, but a delicate combination of both. Furthermore, the latter is subdivided into coulombic (Poisson-Boltzmann related) and non-coulombic (solvation related) ion pairing.

## 8.3 Supplement to COSMO-RS based calculations

The logarithmic mean ionic activity coefficients (MIACs) of the charged species and activity coefficients of the solvents are calculated based on two contributions as follows:

$$\ln(\gamma_{\pm}) = \ln\left(\gamma_{\pm}^{SR}\right) + \ln\left(\gamma_{\pm}^{LR}\right)$$
$$\ln(\gamma_s) = \ln(\gamma_s^{SR}) + \ln(\gamma_s^{LR}) \tag{8.27}$$

where the subscript $s$ stands for solvents. In the COSMO-RS-ES mode the short-range (SR) contribution is always COSMO-RS based and the long-range (LR) contribution (also equivalent to superscript *el* for electrostatic) is always Pitzer-Debye-Hückel-term-based unless explicitly stated otherwise.

LLE calculations follow the condition given by equation (2.15) as criterion for all compounds and the salt-free state of one of the two liquid phases is taken as reference state to calculate the activity coefficients of the other, thereby calculating free energies of transfer from one phase to the other, as shown further ahead in equation (5.3).

Solubility calculations can be divided into two interpretations: solid salt solubility (SLE for solid-liquid equilibrium in a single or mixed solvent) and IL solubility, which stands for the LLE of a binary, ionic-liquid-containing system (e.g. solubility of an IL in water).

Salt solubility calculations are estimated based on the known solubility in water i.e. water is the reference solvent to estimate the solubility constant $K_{sp}$. If the solubility of a salt in water is known, then the logarithmic solubility constant corresponds to:

$$\ln\left(K_{sp}\right) = v \cdot \ln\left(x_{\pm}\gamma_{\pm}\right) \text{ at } x_{\pm} \equiv exp.solubility \tag{8.28}$$

where the reference state is infinite dilution. The $K_{sp}$ value in turn is applied for the calculation of the solubility of the salt in solvents other than water. It then follows that with a reference solvent, the solubility is calculated in any other solvent via transfer energetics:

$$\ln\left(\gamma_{t,x\to s}\right) = \ln\left(\frac{\gamma_{\pm,ref}}{\gamma_{\pm,s}}\right) = \ln\left(\frac{x_{\pm,s}}{x_{\pm,ref}}\right) \tag{8.29}$$

The method has the advantage of keeping the asymmetric convention for salts in order to avoid depending on experimentally measured thermodynamic properties of the molten state. The disadvantages are that the solubility of the salt in water needs to be known and that the precision of the solubility calculations are dependent on the precision of the calculated/predicted $\gamma_{\pm}$ values in water.

Gibbs-free energies of transfer of ions from water to organic solvents and mixed solvents are included in the database. The calculation of Gibbs-free energies of transfer takes place at infinite dilution with reference state infinite dilution for single ions. Very roughly stated: these data describe the free energy required to strip a single ion from its solvation state in water, introduce it into another solvent and allow it to reach a new solvation state. Ion-ion electrostatic contributions are absent and single-ion transfer energetics at infinite dilution are entirely given by the short-range contribution.

Infinite dilution activity coefficients (IDACs) of neutral molecules in pure ILs are included in the dataset. The reference state for IDAC calculations is always symmetric for the neutral molecule (regardless of the reference state of the salt/IL) and has both a short- and LR contributions except for openCOSMO-RS related validations.

### *Correlation for the temperature dependent properties of water*

The following correlations were applied to estimate the temperature dependent density and relative permittivity of water involved in the long-range term calculations to estimate the MIAC of salts in water at various temperatures (Figure 38 – Right).

For the density, the correlation provided by Maribo-Mogensen et al.[164] was applied:

$$d_w(T) = d_0 + \omega_1(T\backslash K - T_0) + \omega_2(T\backslash K - T_0)^{\omega_3} \tag{8.30}$$

with the parameters $d_0 = 0.99984\ g/cm^3$, $T_0 = 298.15\ K$, $\omega_1 = 1.51782 \cdot 10^{-4}\ g/cm^3/K$, $\omega_2 = -4.50573 \cdot 10^{-5}\ g/cm^3/K^{\omega_3}$ and $\omega_3 = 1.55$.

For the relative permittivity, Pátek et al.[348] provided the following correlation:

$$\varepsilon_w(T) = \sum_{i=1}^{4} e_i \left(\frac{T\backslash K}{300}\right)^{f_i} \tag{8.31}$$

**Appendix Table 1. Parameters for equation (8.31) obtained with the experimental data from Uematsu and Franck.[361]**

| $i$ | $e_i$ | $f_i$ |
|---|---|---|
| 1 | -0.4737 | 3.817 |
| 2 | 194.137 | -2.3674 |
| 3 | -281.1995 | -2.8235 |
| 4 | 165.4053 | -2.6576 |

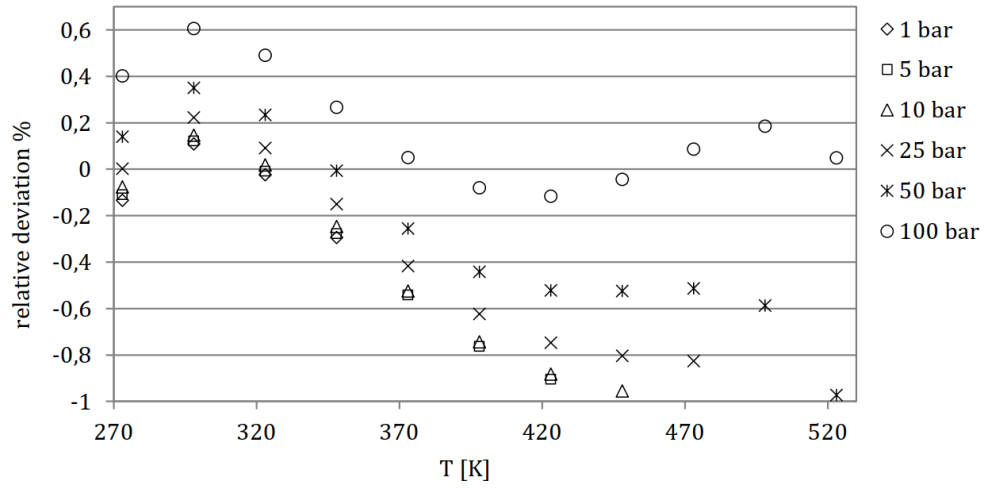


**Appendix Figure 2. Relative error of the temperature dependent relative permittivity of water as calculated with equation (8.31) using the parameters provided by Pátek et al.[352] with an ARD of 0.0035.**

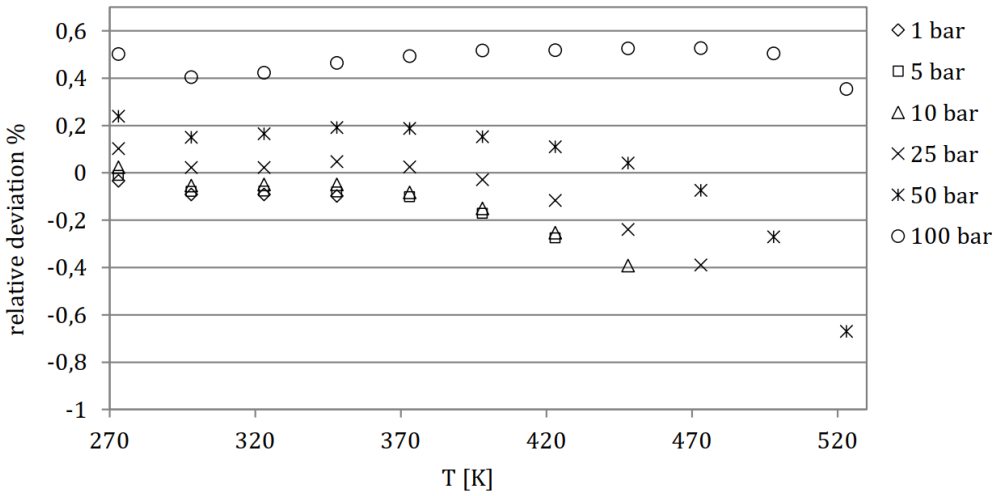


**Appendix Figure 3. Relative error of the temperature dependent relative permittivity of water as calculated with equation (8.31) using the parameters provided in Appendix Table 1 with an ARD of 0.0021.**

## *Parameters for IL-dedicated openCOSMO-RS parameterizations*

In section 6.3.2 openCOSMO-RS was parameterized with the IDAC and IL-LLE datasets in order to improve its performance in the description of ionic liquid systems. The

corresponding COSMO-RS equations that were applied are described for all pertaining interactions in Table 13 of the main text. The optimized interactions involve the first equation in equation set (6.52), repeated here:

$$A_{IJ} = F_{IJ}^{mf} \cdot E_{IJ}^{mf} + F_{IJ}^{hb} \cdot G_{IJ}^{hb} \tag{8.32}$$

where the misfit interaction energy applies the conventional misfit term without orthogonalization. Though not detailed in the main text, the reason for this is that ion interactions seem to provide better minima when the orthogonalization of the misfit term is not used. As briefly discussed by Klamt,[107] the formulation of the misfit term should theoretically involve additional considerations for ions. So far, and to the best of the writing author's knowledge, this has not been explored in the literature.

The parameters for the IL-dedicated parameterizations that correspond to the results presented in Table 14 are shown in the following tables:

**Appendix Table 2. Parameters for ionic liquid-dedicated parameterizations with openCOSMO-RS.**

<u>openCOSMO-RS</u>

Misfit scaling factors $F_{IJ}^{mf}$

| | PC | PA | MA | $H_2O$ | Org. |
|---|---|---|---|---|---|
| PC | | 4.202 | 4.285 | 2.353 | 2.895 |
| PA | | | | 3.193 | 3.207 |
| MA | | | | 1.000 | 2.233 |
| H2O | | | | | |
| Org. | | | | | |

Hydrogen-Bonding scaling factors $F_{IJ}^{hb}$

| | PC | PA | MA | $H_2O$ | Org. |
|---|---|---|---|---|---|
| PC | | 3.117 | 7.365 | 3.498 | 2.055 |
| PA | | | | 2.741 | 2.892 |
| MA | | | | 2.513 | 2.386 |
| H2O | | | | | |
| Org. | | | | | |

<u>openCOSMO-RS + ME-PDH</u>

Misfit scaling factors $F_{IJ}^{mf}$

| | PC | PA | MA | $H_2O$ | Org. |
|---|---|---|---|---|---|
| PC | | 2.989 | 2.562 | 1.880 | 2.606 |
| PA | | | | 1.122 | 2.804 |
| MA | | | | 28.228 | 2.290 |
| H2O | | | | | |
| Org. | | | | | |

Hydrogen-Bonding scaling factors $F_{IJ}^{hb}$

| | PC | PA | MA | $H_2O$ | Org. |
|---|---|---|---|---|---|
| PC | | 1.236 | 1.610 | 2.632 | 1.695 |
| PA | | | | 1.282 | 1.654 |
| MA | | | | 3.308 | 1.787 |
| H2O | | | | | |
| Org. | | | | | |

Normal COSMO-RS*
Normal COSMO-RS**

PC: polyatomic cation
PA: polyatomic anion
MA: monoatomic anion
Org.: organic solvent

ME-PDH parameters:

$\varepsilon_A = 3.1414$
$\varepsilon_B = 1.8907$
$F_a = 0.6472$

## *Extension to the Training Set*

The training sets from Gerlach et al.[14] and Müller et al.[15] were extended with the new datasets from this work. The latter are further detailed in the following figures and tables:

**Appendix Figure 4. Selected 21634 IDAC datapoints extracted from IL-Thermo[296,297] and broken down by solvent and temperature range.**

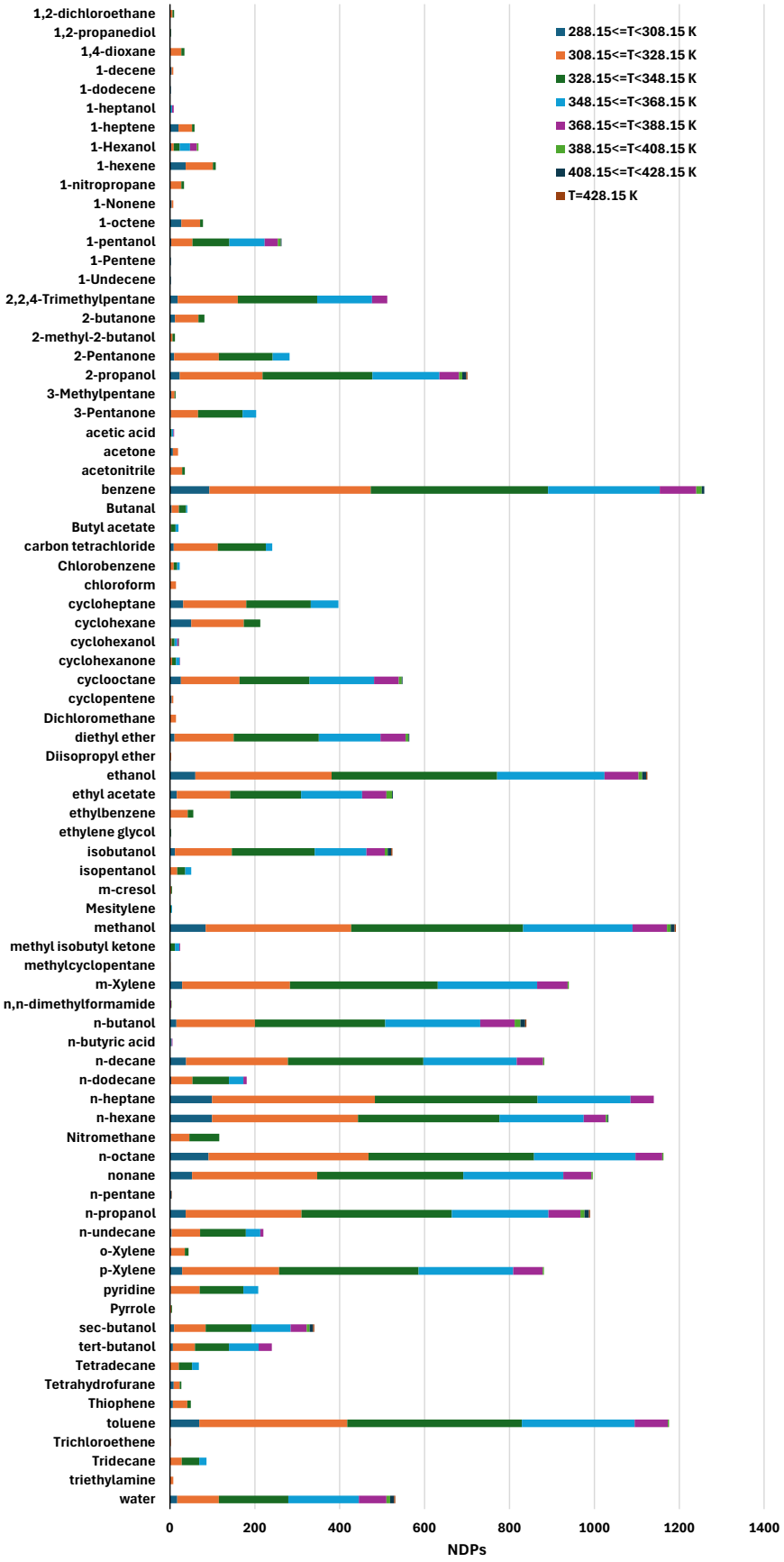

**Appendix Table 3. Ternary LLE systems with an ionic liquid compound applied for evaluation and parameterization in the present work. The "source" code corresponds to the sources and data provided in the supporting information from Paduszynski.**[115]

| Solvent 1 | Solvent 2 | IL-cation | IL-anion | T [°C] | DP | Source |
|---|---|---|---|---|---|---|
| 2-phenylethanol | water | diethyl(methyl)sulfanium | bis(trifluoromethylsulfonyl)azanide | 35 | 5 | S053 |
| 2-propanol | butanone | 1,3-dimethyl-1H-imidazol-3-ium | methyl sulfate | 25 | 7 | S169 |
| 2-propanol | butanone | 1-butyl-3-methyl-1H-imidazol-3-ium | hexafluorophosphate | 25 | 10 | S169 |
| 2-propanol | di-iso-propyl ether | 4-(2-methoxyethyl)-4-methylmorpholin-4-ium | bis(trifluoromethylsulfonyl)azanide | 25 | 16 | S056 |
| 2-propanol | di-iso-propyl ether | 1-(2-methoxyethyl)-1-methylpiperidin-1-ium | bis(trifluoromethylsulfonyl)azanide | 25 | 12 | S056 |
| 2-propanol | di-iso-propyl ether | 1-(2-methoxyethyl)-1-methylpyrrolidin-1-ium | bis(trifluoromethylsulfonyl)azanide | 25 | 11 | S056 |
| 2-propanol | ethyl acetate | 1,3-dimethyl-1H-imidazol-3-ium | methyl sulfate | 25 | 7 | S171 |
| 2-propanol | ethyl acetate | 1-butyl-3-methyl-1H-imidazol-3-ium | hexafluorophosphate | 25 | 12 | S171 |
| 2-propanol | ethyl acetate | 3-hexyl-1-methyl-1H-imidazol-3-ium | hexafluorophosphate | 25 | 11 | S171 |
| 2-propanol | n-heptane | 3-hexyl-1-methyl-1H-imidazol-3-ium | tetrafluoroborate | 25 | 2 | S025 |
| 2-propanol | n-heptane | 3-hexyl-1-methyl-1H-imidazol-3-ium | bis(trifluoromethylsulfonyl)azanide | 25 | 2 | S025 |
| 2-propanol | n-heptane | 3-hexyl-1-methyl-1H-imidazol-3-ium | trifluoromethanesulfonate | 25 | 3 | S132 |
| 2-propanol | water | 1-butyl-3-methyl-1H-imidazol-3-ium | bis(trifluoromethylsulfonyl)azanide | 10 | 7 | S022 |
| 2-propanol | water | 1-butyl-3-methyl-1H-imidazol-3-ium | bis(trifluoromethylsulfonyl)azanide | 30 | 5 | S022 |
| 2-propanol | water | 1-butyl-3-methyl-1H-imidazol-3-ium | bis(trifluoromethylsulfonyl)azanide | 50 | 4 | S022 |
| 2-propanol | water | 3-hexyl-1-methyl-1H-imidazol-3-ium | bis(trifluoromethylsulfonyl)azanide | 25 | 6 | S026 |
| 2-propanol | water | 3-methyl-1-octyl-1H-imidazol-3-ium | bis(trifluoromethylsulfonyl)azanide | 25 | 5 | S026 |
| 2-propanol | water | 1-decyl-3-methyl-1H-imidazol-3-ium | bis(trifluoromethylsulfonyl)azanide | 5 | 2 | S044 |
| 2-propanol | water | 1-decyl-3-methyl-1H-imidazol-3-ium | bis(trifluoromethylsulfonyl)azanide | 15 | 4 | S044 |
| 2-propanol | water | 1-decyl-3-methyl-1H-imidazol-3-ium | bis(trifluoromethylsulfonyl)azanide | 25 | 4 | S026 |
| 2-propanol | water | 1-butyl-1-methylpyrrolidin-1-ium | bis(trifluoromethylsulfonyl)azanide | 10 | 6 | S022 |
| 2-propanol | water | 1-butyl-1-methylpyrrolidin-1-ium | bis(trifluoromethylsulfonyl)azanide | 30 | 6 | S022 |
| 2-propanol | water | 1-butyl-1-methylpyrrolidin-1-ium | bis(trifluoromethylsulfonyl)azanide | 50 | 5 | S022 |
| 3-methylpyridine | n-heptane | 2-octylisoquinolin-2-ium | thiocyanate | 25 | 6 | S061 |
| acetic acid | water | 1-ethyl-3-methyl-1H-imidazol-3-ium | bis(trifluoromethylsulfonyl)azanide | 20 | 9 | S014 |
| acetic acid | water | 1-butyl-3-methyl-1H-imidazol-3-ium | bis(trifluoromethylsulfonyl)azanide | 20 | 12 | S014 |
| acetic acid | water | 1-butyl-2,3-dimethyl-1H-imidazol-3-ium | bis(trifluoromethylsulfonyl)azanide | 20 | 9 | S014 |
| acetic acid | water | 3-hexyl-1-methyl-1H-imidazol-3-ium | bis(trifluoromethylsulfonyl)azanide | 20 | 15 | S014 |
| acetic acid | water | 3-methyl-1-octyl-1H-imidazol-3-ium | bis(trifluoromethylsulfonyl)azanide | 20 | 9 | S014 |
| acetic acid | water | 1-decyl-3-methyl-1H-imidazol-3-ium | bis(trifluoromethylsulfonyl)azanide | 20 | 8 | S014 |
| acetic acid | water | trihexyl(tetradecyl)phosphanium | chloride | 20 | 2 | S014 |
| acetic acid | water | 1-butyl-1-methylpyrrolidin-1-ium | bis(trifluoromethylsulfonyl)azanide | 20 | 5 | S014 |
| acetone | water | 3-hexyl-1-methyl-1H-imidazol-3-ium | hexafluorophosphate | 20 | 8 | S174 |
| acetone | water | 3-hexyl-1-methyl-1H-imidazol-3-ium | hexafluorophosphate | 25 | 8 | S174 |
| acetone | water | 3-hexyl-1-methyl-1H-imidazol-3-ium | hexafluorophosphate | 30 | 7 | S174 |
| benzene | cyclohexane | 1-methyl-imidazolium | dibutyl phosphate | 25 | 9 | S228 |
| benzene | cyclohexane | 1,3-dimethyl-1H-imidazol-3-ium | dimethyl phosphate | 40 | 3 | S222 |
| benzene | cyclohexane | 1-ethyl-3-methyl-1H-imidazol-3-ium | diethyl phosphate | 25 | 2 | S222 |
| benzene | cyclohexane | 1-ethyl-3-methyl-1H-imidazol-3-ium | diethyl phosphate | 40 | 3 | S222 |
| benzene | cyclohexane | 1-butyl-4-methylpyridin-1-ium | tetrafluoroborate | 30 | 11 | S093 |
| benzene | n-dodecane | 3-hexyl-1-methyl-1H-imidazol-3-ium | tetrafluoroborate | 25 | 7 | S084 |
| benzene | n-dodecane | 3-hexyl-1-methyl-1H-imidazol-3-ium | hexafluorophosphate | 25 | 7 | S084 |
| benzene | n-dodecane | 3-methyl-1-octyl-1H-imidazol-3-ium | chloride | 25 | 4 | S152 |

| | | | | | | |
|---|---|---|---|---|---|---|
| benzene | n-heptane | 1-ethyl-3-methyl-1H-imidazol-3-ium | 2-(2-methoxyethoxy)ethyl sulfate | 25 | 2 | S229 |
| benzene | n-heptane | 1-ethyl-3-methyl-1H-imidazol-3-ium | octyl sulfate | 25 | 4 | S229 |
| benzene | n-heptane | 3-hexyl-1-methyl-1H-imidazol-3-ium | tetrafluoroborate | 25 | 12 | S084 |
| benzene | n-heptane | 3-hexyl-1-methyl-1H-imidazol-3-ium | hexafluorophosphate | 25 | 12 | S084 |
| benzene | n-heptane | 3-methyl-1-octyl-1H-imidazol-3-ium | chloride | 25 | 3 | S152 |
| benzene | n-hexadecane | 1-ethyl-3-methyl-1H-imidazol-3-ium | 2-(2-methoxyethoxy)ethyl sulfate | 25 | 4 | S229 |
| benzene | n-hexadecane | 1-ethyl-3-methyl-1H-imidazol-3-ium | octyl sulfate | 25 | 5 | S229 |
| benzene | n-hexadecane | 3-hexyl-1-methyl-1H-imidazol-3-ium | tetrafluoroborate | 25 | 8 | S084 |
| benzene | n-hexadecane | 3-hexyl-1-methyl-1H-imidazol-3-ium | hexafluorophosphate | 25 | 4 | S084 |
| benzene | n-hexane | 3-methyl-1-octyl-1H-imidazol-3-ium | bis(trifluoromethylsulfonyl)azanide | 25 | 1 | S015 |
| benzene | n-hexane | 1-decyl-3-methyl-1H-imidazol-3-ium | bis(trifluoromethylsulfonyl)azanide | 25 | 2 | S015 |
| benzene | n-hexane | 1-dodecyl-3-methyl-1H-imidazol-3-ium | bis(trifluoromethylsulfonyl)azanide | 25 | 2 | S015 |
| benzene | n-hexane | (2-hydroxyethyl)trimethylazanium | bis(trifluoromethylsulfonyl)azanide | 40 | 1 | S059 |
| benzene | n-hexane | 1-butyl-3-methylpyridin-1-ium | tricyanomethide | 30 | 8 | S142 |
| benzene | n-hexane | 1-butyl-3-methylpyridin-1-ium | tricyanomethide | 55 | 8 | S142 |
| benzene | n-hexane | 1-butyl-3-methylpyridin-1-ium | dicyanoazanide | 30 | 7 | S108 |
| benzene | n-hexane | 1-butyl-3-methylpyridin-1-ium | dicyanoazanide | 55 | 5 | S108 |
| benzene | n-hexane | 1-butyl-3-methylpyridin-1-ium | tetracyanoboranuide | 30 | 13 | S137 |
| benzene | n-hexane | 1-butyl-3-methylpyridin-1-ium | tetracyanoboranuide | 55 | 13 | S137 |
| benzene | n-hexane | 1-butyl-4-methylpyridin-1-ium | tetrafluoroborate | 40 | 6 | S092 |
| benzene | n-hexane | 1-butyl-4-methylpyridin-1-ium | tetrafluoroborate | 75 | 6 | S092 |
| benzene | n-nonane | 1-butyl-3-methyl-1H-imidazol-3-ium | hexafluorophosphate | 25 | 5 | S164 |
| benzene | n-nonane | 3-methyl-1-octyl-1H-imidazol-3-ium | hexafluorophosphate | 25 | 4 | S177 |
| benzene | n-undecane | 1-butyl-3-methyl-1H-imidazol-3-ium | hexafluorophosphate | 25 | 5 | S164 |
| benzene | n-undecane | 3-methyl-1-octyl-1H-imidazol-3-ium | hexafluorophosphate | 25 | 4 | S177 |
| benzene | water | tetrabutylazanium | bromide | 45 | 7 | S231 |
| benzene | water | tetrabutylazanium | bromide | 55 | 7 | S231 |
| benzene | water | tetrabutylazanium | bromide | 65 | 8 | S231 |
| butanone | cyclohexane | 3-hexyl-1-methyl-1H-imidazol-3-ium | hexafluorophosphate | 25 | 6 | S175 |
| butanone | cyclohexane | 3-methyl-1-octyl-1H-imidazol-3-ium | hexafluorophosphate | 25 | 3 | S175 |
| butyric acid | n-hexane | 3-hexyl-1-methyl-1H-imidazol-3-ium | bis(trifluoromethylsulfonyl)azanide | 30 | 4 | S012 |
| cumene | n-nonane | 1-butyl-3-methylpyridin-1-ium | dicyanoazanide | 30 | 9 | S108 |
| cumene | n-nonane | 1-butyl-3-methylpyridin-1-ium | dicyanoazanide | 55 | 9 | S108 |
| di-iso-propyl ether | water | 1-ethyl-3-methyl-1H-imidazol-3-ium | ethyl sulfate | 30 | 9 | S083 |
| di-iso-propyl ether | water | 1-ethyl-3-methyl-1H-imidazol-3-ium | ethyl sulfate | 40 | 8 | S083 |
| di-iso-propyl ether | water | 1-butyl-3-methyl-1H-imidazol-3-ium | tetrafluoroborate | 30 | 9 | S083 |
| di-iso-propyl ether | water | 1-butyl-3-methyl-1H-imidazol-3-ium | tetrafluoroborate | 40 | 7 | S083 |
| ethanol | 1-heptene | 3-hexyl-1-methyl-1H-imidazol-3-ium | tetrafluoroborate | 25 | 8 | S085 |
| ethanol | 1-heptene | 3-hexyl-1-methyl-1H-imidazol-3-ium | hexafluorophosphate | 25 | 13 | S085 |
| ethanol | 1-hexene | 3-hexyl-1-methyl-1H-imidazol-3-ium | tetrafluoroborate | 25 | 12 | S085 |
| ethanol | 1-hexene | 3-hexyl-1-methyl-1H-imidazol-3-ium | hexafluorophosphate | 25 | 13 | S085 |
| ethanol | butanone | 1,3-dimethyl-1H-imidazol-3-ium | methyl sulfate | 25 | 7 | S187 |
| ethanol | butanone | 1-butyl-3-methyl-1H-imidazol-3-ium | hexafluorophosphate | 25 | 6 | S169 |
| ethanol | ethyl acetate | 1-ethyl-3-methyl-1H-imidazol-3-ium | acetate | 15 | 7 | S148 |
| ethanol | ethyl acetate | 1-ethyl-3-methyl-1H-imidazol-3-ium | acetate | 26 | 7 | S148 |
| ethanol | ethyl acetate | 1-ethyl-3-methyl-1H-imidazol-3-ium | acetate | 35 | 7 | S148 |
| ethanol | ethyl acetate | 1-ethyl-3-methyl-1H-imidazol-3-ium | tetrafluoroborate | 25 | 9 | S076 |

| | | | | | | |
|---|---|---|---|---|---|---|
| ethanol | ethyl acetate | 1-ethyl-2,3-methyl-imidazolium | tetrafluoroborate | 25 | 8 | S076 |
| ethanol | ethyl acetate | 1-(2-hydroxyethyl)-3-methyl-1H-imidazol-3-ium | tetrafluoroborate | 25 | 8 | S076 |
| ethanol | ethyl acetate | 1-(2-hydroxyethyl)-2,3-dimethyl-imidazolium | tetrafluoroborate | 25 | 8 | S076 |
| ethanol | n-dodecane | 1,3-dimethyl-1H-imidazol-3-ium | methyl sulfate | 25 | 4 | S182 |
| ethanol | n-dodecane | 1-ethyl-3-methyl-1H-imidazol-3-ium | methyl sulfate | 25 | 4 | S182 |
| ethanol | n-dodecane | 1-butyl-3-methyl-1H-imidazol-3-ium | methyl sulfate | 25 | 4 | S182 |
| ethanol | n-dodecane | 3-methyl-1-octyl-1H-imidazol-3-ium | chloride | 25 | 4 | S153 |
| ethanol | n-heptane | 1-ethyl-3-methyl-1H-imidazol-3-ium | thiocyanate | 25 | 7 | S116 |
| ethanol | n-heptane | 1-ethyl-3-methyl-1H-imidazol-3-ium | ethyl sulfate | 25 | 2 | S205 |
| ethanol | n-heptane | 3-hexyl-1-methyl-1H-imidazol-3-ium | tetrafluoroborate | 25 | 4 | S025 |
| ethanol | n-heptane | 3-hexyl-1-methyl-1H-imidazol-3-ium | trifluoromethanesulfonate | 25 | 3 | S132 |
| ethanol | n-heptane | 3-methyl-1-octyl-1H-imidazol-3-ium | chloride | 25 | 3 | S153 |
| ethanol | n-heptane | 3-methyl-1-octyl-1H-imidazol-3-ium | hexafluorophosphate | 25 | 11 | S172 |
| ethanol | n-heptane | 1-ethyl-3-methylpyridin-1-ium | bis(trifluoromethylsulfonyl)azanide | 25 | 3 | S040 |
| ethanol | n-heptane | 3-methyl-1-propylpyridin-1-ium | bis(trifluoromethylsulfonyl)azanide | 25 | 3 | S040 |
| ethanol | n-hexadecane | 3-methyl-1-octyl-1H-imidazol-3-ium | chloride | 25 | 2 | S153 |
| ethanol | n-hexane | 1-ethyl-3-methyl-1H-imidazol-3-ium | bis(trifluoromethylsulfonyl)azanide | 25 | 3 | S009 |
| ethanol | n-hexane | 1-ethyl-3-methyl-1H-imidazol-3-ium | ethyl sulfate | 25 | 3 | S205 |
| ethanol | n-hexane | 1-butyl-3-methyl-1H-imidazol-3-ium | bis(trifluoromethylsulfonyl)azanide | 25 | 3 | S009 |
| ethanol | n-hexane | 3-hexyl-1-methyl-1H-imidazol-3-ium | hexafluorophosphate | 25 | 8 | S172 |
| ethanol | n-hexane | 3-methyl-1-octyl-1H-imidazol-3-ium | hexafluorophosphate | 25 | 11 | S172 |
| ethanol | n-hexane | hexyl(2-hydroxyethyl)dimethylazanium | tetrafluoroborate | 25 | 3 | S100 |
| ethanol | n-hexane | 1-ethyl-3-methylpyridin-1-ium | bis(trifluoromethylsulfonyl)azanide | 25 | 3 | S040 |
| ethanol | n-hexane | 3-methyl-1-propylpyridin-1-ium | bis(trifluoromethylsulfonyl)azanide | 25 | 4 | S040 |
| ethanol | n-hexane | 1-butyl-3-methylpyridin-1-ium | bis(trifluoromethylsulfonyl)azanide | 25 | 5 | S009 |
| ethanol | tert-butylethyl ether | 1-ethyl-3-methyl-1H-imidazol-3-ium | trifluoromethanesulfonate | 25 | 3 | S129 |
| ethanol | tert-butylethyl ether | 1-ethyl-3-methyl-1H-imidazol-3-ium | methanesulfonate | 25 | 4 | S129 |
| ethanol | tert-butylethyl ether | 1-ethyl-3-methyl-1H-imidazol-3-ium | ethyl sulfate | 25 | 4 | S206 |
| ethanol | trichloromethane | 1-ethyl-3-methyl-1H-imidazol-3-ium | trifluoromethanesulfonate | 20 | 9 | S130 |
| ethanol | trichloromethane | 1-ethyl-3-methyl-1H-imidazol-3-ium | trifluoromethanesulfonate | 50 | 12 | S130 |
| ethanol | water | 1-butyl-3-methyl-1H-imidazol-3-ium | bis(trifluoromethylsulfonyl)azanide | 10 | 10 | S021 |
| ethanol | water | 1-butyl-3-methyl-1H-imidazol-3-ium | bis(trifluoromethylsulfonyl)azanide | 30 | 8 | S021 |
| ethanol | water | 1-butyl-3-methyl-1H-imidazol-3-ium | bis(trifluoromethylsulfonyl)azanide | 50 | 6 | S021 |
| ethanol | water | 1-butyl-3-methyl-1H-imidazol-3-ium | hexafluorophosphate | 10 | 24 | S170 |
| ethanol | water | 1-butyl-3-methyl-1H-imidazol-3-ium | hexafluorophosphate | 30 | 12 | S170 |
| ethanol | water | 1-butyl-3-methyl-1H-imidazol-3-ium | hexafluorophosphate | 50 | 6 | S170 |
| ethanol | water | 1-decyl-3-methyl-1H-imidazol-3-ium | bis(trifluoromethylsulfonyl)azanide | 25 | 3 | S043 |
| ethanol | water | 1-butyl-1-methylpyrrolidin-1-ium | bis(trifluoromethylsulfonyl)azanide | 10 | 7 | S038 |
| ethanol | water | 1-butyl-1-methylpyrrolidin-1-ium | bis(trifluoromethylsulfonyl)azanide | 30 | 6 | S038 |
| ethanol | water | 1-butyl-1-methylpyrrolidin-1-ium | bis(trifluoromethylsulfonyl)azanide | 50 | 4 | S038 |
| ethanol | water | 1-butyl-1-methylpyrrolidin-1-ium | bis(trifluoromethylsulfonyl)azanide | 60 | 6 | S038 |
| ethyl acetate | n-hexane | 3-hexyl-1-methyl-1H-imidazol-3-ium | tetrafluoroborate | 25 | 4 | S086 |
| ethyl acetate | n-hexane | 3-hexyl-1-methyl-1H-imidazol-3-ium | trifluoromethanesulfonate | 25 | 2 | S086 |
| ethyl acetate | n-hexane | 3-hexyl-1-methyl-1H-imidazol-3-ium | hexafluorophosphate | 25 | 8 | S176 |
| ethyl acetate | n-hexane | 3-methyl-1-octyl-1H-imidazol-3-ium | tetrafluoroborate | 25 | 2 | S086 |
| ethyl acetate | n-hexane | 3-methyl-1-octyl-1H-imidazol-3-ium | trifluoromethanesulfonate | 25 | 4 | S086 |
| ethyl acetate | n-hexane | 3-methyl-1-octyl-1H-imidazol-3-ium | hexafluorophosphate | 25 | 7 | S176 |

| | | | | | | |
|---|---|---|---|---|---|---|
| ethylbenzene | cyclohexane | 1-butyl-4-methylpyridin-1-ium | tetrafluoroborate | 30 | 12 | S093 |
| ethylbenzene | n-octane | 1-ethyl-3-methyl-1H-imidazol-3-ium | trifluorotris(pentafluoroethyl)-$\lambda^5$-phosphanuide | 20 | 1 | S121 |
| ethylbenzene | n-octane | 1-ethyl-3-methyl-1H-imidazol-3-ium | bis(trifluoromethylsulfonyl)azanide | 25 | 2 | S004 |
| ethylbenzene | n-octane | 1-butyl-4-methylpyridin-1-ium | tetrafluoroborate | 40 | 6 | S092 |
| ethylbenzene | styrene | 1-butyl-3-methyl-1H-imidazol-3-ium | dicyanoazanide | 25 | 3 | S104 |
| ethylbenzene | styrene | 3-methyl-1-(prop-2-en-1-yl)-1H-imidazol-3-ium | dicyanoazanide | 25 | 3 | S104 |
| methanol | dimethyl carbonate | 1,3-dimethyl-1H-imidazol-3-ium | dimethyl phosphate | 25 | 8 | S225 |
| methanol | dimethyl carbonate | 1-ethyl-3-methyl-1H-imidazol-3-ium | diethyl phosphate | 25 | 8 | S225 |
| methanol | methyl acetate | 1,3-dimethyl-1H-imidazol-3-ium | dimethyl phosphate | 25 | 11 | S235 |
| methanol | methyl acetate | 1,3-dimethyl-1H-imidazol-3-ium | dimethyl phosphate | 40 | 11 | S235 |
| methanol | n-heptane | 3-methyl-1-octyl-1H-imidazol-3-ium | chloride | 25 | 1 | S153 |
| methanol | n-hexadecane | 3-methyl-1-octyl-1H-imidazol-3-ium | chloride | 25 | 5 | S153 |
| methanol | trichloromethane | 1-ethyl-3-methyl-1H-imidazol-3-ium | trifluoromethanesulfonate | 20 | 14 | S128 |
| methanol | trichloromethane | 1-ethyl-3-methyl-1H-imidazol-3-ium | trifluoromethanesulfonate | 40 | 14 | S128 |
| m-xylene | n-nonane | 1-butyl-3-methyl-1H-imidazol-3-ium | hexafluorophosphate | 25 | 5 | S164 |
| m-xylene | n-nonane | 3-methyl-1-octyl-1H-imidazol-3-ium | hexafluorophosphate | 25 | 4 | S177 |
| m-xylene | n-octane | 1-butyl-4-methylpyridin-1-ium | tetrafluoroborate | 40 | 9 | S092 |
| m-xylene | n-octane | 1-butyl-4-methylpyridin-1-ium | tetrafluoroborate | 75 | 9 | S092 |
| m-xylene | n-undecane | 1-butyl-3-methyl-1H-imidazol-3-ium | hexafluorophosphate | 25 | 4 | S164 |
| m-xylene | n-undecane | 3-methyl-1-octyl-1H-imidazol-3-ium | hexafluorophosphate | 25 | 5 | S177 |
| n-dodecane | water | trihexyl(tetradecyl)phosphanium | bis(trifluoromethylsulfonyl)azanide | 75 | 1 | S032 |
| n-dodecane | water | trihexyl(tetradecyl)phosphanium | bis(2,4,4-trimethylpentyl)phosphinate | 25 | 1 | S233 |
| o-xylene | cyclohexane | 1-butyl-4-methylpyridin-1-ium | tetrafluoroborate | 30 | 12 | S093 |
| o-xylene | n-hexane | 1-ethyl-3-methylpyridin-1-ium | ethyl sulfate | 25 | 1 | S217 |
| o-xylene | n-octane | 1-ethyl-3-methyl-1H-imidazol-3-ium | trifluorotris(pentafluoroethyl)-$\lambda^5$-phosphanuide | 20 | 9 | S121 |
| propionic acid | n-hexane | 1-butyl-3-methyl-1H-imidazol-3-ium | tetrafluoroborate | 25 | 5 | S081 |
| propionic acid | n-hexane | 1-butyl-3-methyl-1H-imidazol-3-ium | hexafluorophosphate | 25 | 2 | S081 |
| p-xylene | n-hexane | 1-butyl-3-methylpyridin-1-ium | dicyanoazanide | 30 | 9 | S108 |
| p-xylene | n-octane | 4-butyl-4-methylmorpholin-4-ium | tricyanomethide | 25 | 3 | S140 |
| p-xylene | n-octane | 1-butyl-3-methylpyridin-1-ium | tricyanomethide | 30 | 3 | S142 |
| p-xylene | n-octane | 1-butyl-3-methylpyridin-1-ium | tetracyanoboranuide | 30 | 13 | S137 |
| p-xylene | n-octane | 1-butyl-3-methylpyridin-1-ium | tetracyanoboranuide | 55 | 13 | S137 |
| pyridine | n-heptane | 1-ethyl-3-methyl-1H-imidazol-3-ium | thiocyanate | 25 | 2 | S115 |
| pyridine | n-heptane | 1-butyl-3-methyl-1H-imidazol-3-ium | tricyanomethide | 25 | 1 | S141 |
| pyridine | n-heptane | 4-butyl-4-methylmorpholin-4-ium | tricyanomethide | 25 | 4 | S141 |
| pyridine | n-heptane | 1-butyl-4-methylpyridin-1-ium | tricyanomethide | 25 | 4 | S141 |
| pyridine | n-heptane | 2-hexylisoquinolin-2-ium | thiocyanate | 25 | 1 | S061 |
| pyridine | n-heptane | 2-octylisoquinolin-2-ium | thiocyanate | 25 | 11 | S061 |
| pyridine | n-hexane | 1-ethyl-3-methyl-1H-imidazol-3-ium | bis(trifluoromethylsulfonyl)azanide | 25 | 4 | S007 |
| pyridine | n-hexane | 1-ethyl-3-methyl-1H-imidazol-3-ium | diethyl phosphate | 25 | 1 | S144 |
| pyridine | n-hexane | 1-ethyl-3-methyl-1H-imidazol-3-ium | ethyl sulfate | 25 | 1 | S030 |
| pyridine | n-hexane | 3-methyl-1-octyl-1H-imidazol-3-ium | tetrafluoroborate | 25 | 4 | S030 |
| pyridine | n-hexane | 3-methyl-1-octyl-1H-imidazol-3-ium | bis(trifluoromethylsulfonyl)azanide | 25 | 7 | S030 |
| pyridine | n-hexane | 1-hexyl-3,5-dimethylpyridin-1-ium | bis(trifluoromethylsulfonyl)azanide | 25 | 8 | S074 |
| pyridine | n-hexane | 1-hexyl-3,5-dimethylpyridin-1-ium | bis(trifluoromethylsulfonyl)azanide | 25 | 2 | S075 |
| pyridine | toluene | 1-butyl-3-methyl-1H-imidazol-3-ium | perchlorate | 25 | 6 | S189 |
| pyridine | toluene | 1-butyl-3-methyl-1H-imidazol-3-ium | dihydrogen phosphate | 25 | 4 | S189 |

| | | | | | | |
|---|---|---|---|---|---|---|
| pyridine | toluene | 1-butyl-3-methyl-1H-imidazol-3-ium | hydrogen sulfate | 25 | 5 | S189 |
| tert-butylethyl ether | water | 1-ethyl-3-methyl-1H-imidazol-3-ium | ethyl sulfate | 25 | 9 | S082 |
| tert-butylethyl ether | water | 1-butyl-3-methyl-1H-imidazol-3-ium | tetrafluoroborate | 25 | 8 | S082 |
| thiophene | 2,2,4-trimethylpentane | 3-methyl-1-octyl-1H-imidazol-3-ium | bis(trifluoromethylsulfonyl)azanide | 25 | 5 | S028 |
| thiophene | cyclohexane | 3-methyl-1-octyl-1H-imidazol-3-ium | tetrafluoroborate | 25 | 9 | S087 |
| thiophene | cyclohexane | 3-methyl-1-octyl-1H-imidazol-3-ium | bis(trifluoromethylsulfonyl)azanide | 25 | 8 | S029 |
| thiophene | methylcyclohexane | 3-methyl-1-octyl-1H-imidazol-3-ium | tetrafluoroborate | 25 | 3 | S088 |
| thiophene | n-dodecane | 3-methyl-1-octyl-1H-imidazol-3-ium | bis(trifluoromethylsulfonyl)azanide | 25 | 10 | S029 |
| thiophene | n-dodecane | 1-hexyl-3,5-dimethylpyridin-1-ium | bis(trifluoromethylsulfonyl)azanide | 25 | 4 | S075 |
| thiophene | n-heptane | 1,3-dimethyl-1H-imidazol-3-ium | hydrogen methylphosphonate | 30 | 1 | S115 |
| thiophene | n-heptane | 1-ethyl-3-methyl-1H-imidazol-3-ium | acetate | 25 | 3 | S145 |
| thiophene | n-heptane | 1-ethyl-3-methyl-1H-imidazol-3-ium | thiocyanate | 30 | 2 | S115 |
| thiophene | n-heptane | 1-ethyl-3-methyl-1H-imidazol-3-ium | ethyl sulfate | 25 | 2 | S200 |
| thiophene | n-heptane | 1-butyl-3-methyl-1H-imidazol-3-ium | acetate | 25 | 1 | S145 |
| thiophene | n-heptane | 1-butyl-3-methyl-1H-imidazol-3-ium | trifluoromethanesulfonate | 25 | 2 | S131 |
| thiophene | n-heptane | 3-hexyl-1-methyl-1H-imidazol-3-ium | acetate | 25 | 7 | S145 |
| thiophene | n-heptane | 3-methyl-1-octyl-1H-imidazol-3-ium | acetate | 25 | 7 | S145 |
| thiophene | n-heptane | 3-methyl-1-octyl-1H-imidazol-3-ium | bis(trifluoromethylsulfonyl)azanide | 25 | 2 | S027 |
| thiophene | n-heptane | tris(2-hydroxyethyl)(methyl)azanium | methyl sulfate | 30 | 2 | S115 |
| thiophene | n-heptane | tributyl(ethyl)phosphonium | diethyl phosphate | 35 | 9 | S070 |
| thiophene | n-hexadecane | 3-methyl-1-octyl-1H-imidazol-3-ium | bis(trifluoromethylsulfonyl)azanide | 25 | 7 | S027 |
| thiophene | n-hexadecane | 1-hexyl-3,5-dimethylpyridin-1-ium | bis(trifluoromethylsulfonyl)azanide | 25 | 1 | S075 |
| thiophene | n-hexane | 1-ethyl-3-methyl-1H-imidazol-3-ium | ethyl sulfate | 25 | 5 | S200 |
| thiophene | n-hexane | 3-methyl-1-octyl-1H-imidazol-3-ium | bis(trifluoromethylsulfonyl)azanide | 25 | 1 | S027 |
| thiophene | toluene | 3-methyl-1-octyl-1H-imidazol-3-ium | bis(trifluoromethylsulfonyl)azanide | 25 | 5 | S028 |
| toluene | cyclohexane | 1-butyl-4-methylpyridin-1-ium | tetrafluoroborate | 30 | 11 | S093 |
| toluene | methylcyclohexane | 1-butyl-3-methyl-1H-imidazol-3-ium | tetracyanoboranuide | 20 | 2 | S134 |
| toluene | methylcyclohexane | 3-hexyl-1-methyl-1H-imidazol-3-ium | tetracyanoboranuide | 20 | 2 | S134 |
| toluene | n-heptane | 1,3-dimethyl-1H-imidazol-3-ium | methyl sulfate | 75 | 14 | S094 |
| toluene | n-heptane | 1-ethyl-3-methyl-1H-imidazol-3-ium | ethyl sulfate | 75 | 19 | S094 |
| toluene | n-heptane | 1-butyl-3-methyl-1H-imidazol-3-ium | dicyanoazanide | 30 | 5 | S105 |
| toluene | n-heptane | 1-butyl-3-methyl-1H-imidazol-3-ium | dicyanoazanide | 55 | 5 | S105 |
| toluene | n-heptane | 1-butyl-3-methyl-1H-imidazol-3-ium | thiocyanate | 30 | 5 | S105 |
| toluene | n-heptane | 1-butyl-3-methyl-1H-imidazol-3-ium | thiocyanate | 55 | 5 | S105 |
| toluene | n-heptane | 1-butyl-3-methyl-1H-imidazol-3-ium | methyl sulfate | 40 | 6 | S094 |
| toluene | n-heptane | 1-butyl-3-methyl-1H-imidazol-3-ium | methyl sulfate | 75 | 5 | S094 |
| toluene | n-heptane | 3-hexyl-1-methyl-1H-imidazol-3-ium | hydrogen sulfate | 30 | 1 | S188 |
| toluene | n-heptane | 1-butyl-3-methylpyridin-1-ium | tricyanomethide | 30 | 9 | S142 |
| toluene | n-heptane | 1-butyl-3-methylpyridin-1-ium | tricyanomethide | 55 | 9 | S142 |
| toluene | n-heptane | 1-butyl-3-methylpyridin-1-ium | dicyanoazanide | 30 | 5 | S105 |
| toluene | n-heptane | 1-butyl-3-methylpyridin-1-ium | dicyanoazanide | 55 | 5 | S105 |
| toluene | n-heptane | 1-butyl-3-methylpyridin-1-ium | tetracyanoboranuide | 30 | 13 | S137 |
| toluene | n-heptane | 1-butyl-3-methylpyridin-1-ium | tetracyanoboranuide | 55 | 12 | S137 |
| toluene | n-heptane | 1-butyl-4-methylpyridin-1-ium | tetrafluoroborate | 75 | 5 | S094 |
| toluene | n-nonane | 1-butyl-3-methyl-1H-imidazol-3-ium | hexafluorophosphate | 25 | 3 | S164 |
| toluene | n-nonane | 3-methyl-1-octyl-1H-imidazol-3-ium | hexafluorophosphate | 25 | 4 | S177 |
| toluene | n-undecane | 1-butyl-3-methyl-1H-imidazol-3-ium | hexafluorophosphate | 25 | 4 | S164 |

| | | | | | | |
|---|---|---|---|---|---|---|
| toluene | n-undecane | 3-methyl-1-octyl-1H-imidazol-3-ium | hexafluorophosphate | 25 | 5 | S177 |
| 1-butanol | butyl acetate | 3-hexyl-1-methyl-1H-imidazol-3-ium | chloride | 90 | 17 | S151 |
| 1-butanol | butyl acetate | 3-methyl-1-octyl-1H-imidazol-3-ium | hexafluorophosphate | 15 | 11 | S178 |
| 1-butanol | water | 1-(2-hydroxyethyl)-3-methyl-1H-imidazol-3-ium | tetrafluoroborate | 20 | 10 | S090 |
| 1-butanol | water | 1-(2-hydroxyethyl)-2,3-dimethyl-imidazolium | tetrafluoroborate | 20 | 9 | S090 |
| 1-butanol | water | 3-hexyl-1-methyl-1H-imidazol-3-ium | tetracyanoboranuide | 35 | 14 | S135 |
| 1-butanol | water | 1-(2-methoxyethyl)-1-methylpiperidin-1-ium | bis(trifluoromethylsulfonyl)azanide | 25 | 23 | S058 |
| 1-butanol | water | 1-butyl-1-methylpiperidin-1-ium | bis(trifluoromethylsulfonyl)azanide | 25 | 13 | S058 |
| 1-butanol | water | 1-(2-methoxyethyl)-1-methylpyrrolidin-1-ium | bis(trifluoromethylsulfonyl)azanide | 25 | 24 | S058 |
| 1-phenylethanol | n-hexane | 1-ethyl-3-methyl-1H-imidazol-3-ium | 4-methylbenzene-1-sulfonate | 25 | 3 | S081 |
| 1-phenylethanol | n-hexane | 1-butyl-3-methyl-1H-imidazol-3-ium | hexafluorophosphate | 25 | 3 | S081 |
| 1-propanol | n-heptane | 3-hexyl-1-methyl-1H-imidazol-3-ium | tetrafluoroborate | 25 | 4 | S025 |
| 1-propanol | n-heptane | 3-hexyl-1-methyl-1H-imidazol-3-ium | trifluoromethanesulfonate | 25 | 5 | S132 |
| 1-propanol | water | 1-ethyl-3-methyl-1H-imidazol-3-ium | bis(trifluoromethylsulfonyl)azanide | 10 | 7 | S011 |
| 1-propanol | water | 1-ethyl-3-methyl-1H-imidazol-3-ium | bis(trifluoromethylsulfonyl)azanide | 30 | 6 | S011 |
| 1-propanol | water | 1-ethyl-3-methyl-1H-imidazol-3-ium | bis(trifluoromethylsulfonyl)azanide | 50 | 5 | S011 |
| 1-propanol | water | 3-hexyl-1-methyl-1H-imidazol-3-ium | bis(trifluoromethylsulfonyl)azanide | 10 | 5 | S011 |
| 1-propanol | water | 3-hexyl-1-methyl-1H-imidazol-3-ium | bis(trifluoromethylsulfonyl)azanide | 30 | 6 | S011 |
| 1-propanol | water | 3-hexyl-1-methyl-1H-imidazol-3-ium | bis(trifluoromethylsulfonyl)azanide | 50 | 7 | S011 |
| 1-propanol | water | 1-decyl-3-methyl-1H-imidazol-3-ium | bis(trifluoromethylsulfonyl)azanide | 25 | 3 | S043 |
| 2-pentanol | n-hexane | 3-hexyl-1-methyl-1H-imidazol-3-ium | bis(trifluoromethylsulfonyl)azanide | 30 | 6 | S012 |
| benzene | cyclohexane | 1,3-dimethyl-1H-imidazol-3-ium | dimethyl phosphate | 25 | 5 | S222 |
| toluene | n-heptane | 1,3-dimethyl-1H-imidazol-3-ium | methyl sulfate | 40 | 7 | S094 |
| toluene | n-heptane | 1-ethyl-3-methyl-1H-imidazol-3-ium | ethyl sulfate | 40 | 17 | S094 |
| toluene | n-heptane | 1-butyl-4-methylpyridin-1-ium | tetrafluoroborate | 40 | 2 | S094 |

# 9 Bibliography


(1) Vaque Aura, S.; Roa Pinto, J.-S.; Ferrando, N.; de Hemptinne, J.-C.; ten Kate, A.; Kuitunen, S.; Diamantonis, N.; Gerlach, T.; Heilig, M.; Becker, G.; Brehelin, M. Data Analysis for Electrolyte Systems: A Method Illustrated on Alkali Halides in Water. *J. Chem. Eng. Data* **2021**, *66* (8), 2976–2990. https://doi.org/10.1021/acs.jced.1c00105.

(2) Kontogeorgis, G. M.; Dohrn, R.; Economou, I. G.; de Hemptinne, J.-C.; ten Kate, A.; Kuitunen, S.; Mooijer, M.; Žilnik, L. F.; Vesovic, V. Industrial Requirements for Thermodynamic and Transport Properties: 2020. *Ind. Eng. Chem. Res.* **2021**, *60* (13), 4987–5013. https://doi.org/10.1021/acs.iecr.0c05356.

(3) Kontogeorgis, G. M.; Maribo-Mogensen, B.; Thomsen, K. The Debye-Hückel Theory and Its Importance in Modeling Electrolyte Solutions. *Fluid Phase Equilib.* **2018**. https://doi.org/10.1016/j.fluid.2018.01.004.

(4) Prausnitz, J. M. *Molecular Thermodynamics of Fluid-Phase Equilibria*, 3rd ed.; Prentice-Hall international series in the physical and chemical engineering sciences; Prentice Hall PTR: Upper Saddle River, N.J, 1999.

(5) Held, C. Thermodynamic $g^{E}$ Models and Equations of State for Electrolytes in a Water-Poor Medium: A Review. *J. Chem. Eng. Data* **2020**, acs.jced.0c00812. https://doi.org/10.1021/acs.jced.0c00812.

(6) Kontogeorgis, G. M.; Schlaikjer, A.; Olsen, M. D.; Maribo-Mogensen, B.; Thomsen, K.; von Solms, N.; Liang, X. A Review of Electrolyte Equations of State with Emphasis on Those Based on Cubic and Cubic-Plus-Association (CPA) Models. *Int J Thermophys* **2022**, *43* (4), 54. https://doi.org/10.1007/s10765-022-02976-4.

(7) Klamt, A.; Jonas, V.; Bürger, T.; Lohrenz, J. C. Refinement and Parametrization of COSMO-RS. *J. Phys. Chem. A* **1998**, *102* (26), 5074–5085.

(8) Klamt, A. Conductor-like Screening Model for Real Solvents: A New Approach to the Quantitative Calculation of Solvation Phenomena. *J. Phys. Chem.* **1995**, *99* (7), 2224–2235.

(9) Ingram, T.; Gerlach, T.; Mehling, T.; Smirnova, I. Extension of COSMO-RS for Monoatomic Electrolytes: Modeling of Liquid–Liquid Equilibria in Presence of Salts. *Fluid Phase Equilibria* **2011**, *314*, 29–37. https://doi.org/10.1016/j.fluid.2011.09.021.

(10) Hsieh, M.-T.; Lin, S.-T. A Predictive Model for the Excess Gibbs Free Energy of Fully Dissociated Electrolyte Solutions. *AIChE Journal* **2011**, *57* (4), 1061–1074. https://doi.org/10.1002/aic.12325.

(11) Toure, O.; Audonnet, F.; Lebert, A.; Dussap, C.-G. COSMO-RS-PDHS: A New Predictive Model for Aqueous Electrolytes Solutions. *Chemical Engineering Research and Design* **2014**, *92* (12), 2873–2883. https://doi.org/10.1016/j.cherd.2014.06.020.

(12) Toure, O.; Lebert, A.; Dussap, C.-G. Extension of the COSMO-RS-PDHS Model to the Prediction of Activity Coefficients in Concentrated {water-Electrolyte} and {water-

Polyol} Solutions. *Fluid Phase Equilibria* **2016**, *424*, 90–104. https://doi.org/10.1016/j.fluid.2015.11.005.

(13) Wang, S.; Song, Y.; Chen, C.-C. Extension of COSMO-SAC Solvation Model for Electrolytes. *Industrial & Engineering Chemistry Research* **2011**, *50* (1), 176–187. https://doi.org/10.1021/ie100689g.

(14) Gerlach, T.; Müller, S.; Smirnova, I. Development of a COSMO-RS Based Model for the Calculation of Phase Equilibria in Electrolyte Systems. *AIChE J.* **2018**, *64* (1), 272–285. https://doi.org/10.1002/aic.15875.

(15) Müller, S.; González de Castilla, A.; Taeschler, C.; Klein, A.; Smirnova, I. Evaluation and Refinement of the Novel Predictive Electrolyte Model COSMO-RS-ES Based on Solid-Liquid Equilibria of Salts and Gibbs Free Energies of Transfer of Ions. *Fluid Phase Equilib.* **2018**. https://doi.org/10.1016/j.fluid.2018.10.023.

(16) Müller, S.; González de Castilla, A.; Taeschler, C.; Klein, A.; Smirnova, I. Calculation of Thermodynamic Equilibria with the Predictive Electrolyte Model COSMO-RS-ES: Improvements for Low Permittivity Systems. *Fluid Phase Equilibria* **2020**, *506*, 112368. https://doi.org/10.1016/j.fluid.2019.112368.

(17) González de Castilla, A.; Müller, S.; Smirnova, I. On the Analogy between the Restricted Primitive Model and Capacitor Circuits: Semi-Empirical Alternatives for over- and Underscreening in the Calculation of Mean Ionic Activity Coefficients. *Journal of Molecular Liquids* **2021**, *326*, 115204. https://doi.org/10.1016/j.molliq.2020.115204.

(18) González de Castilla, A.; Müller, S.; Smirnova, I. On the Analogy between the Restricted Primitive Model and Capacitor Circuits. Part II: A Generalized Gibbs-Duhem Consistent Extension of the Pitzer-Debye-Hückel Term with Corrections for Low and Variable Relative Permittivity. *Journal of Molecular Liquids* **2022**, *360*, 119398. https://doi.org/10.1016/j.molliq.2022.119398.

(19) Marques, H.; González de Castilla, A.; Müller, S.; Smirnova, I. Impact of Extended Long-Range Electrostatics on the Correlation of Liquid-Liquid Equilibria in Aqueous Ionic Liquid Systems. *Fluid Phase Equilibria* **2023**, *569*, 113765. https://doi.org/10.1016/j.fluid.2023.113765.

(20) Arrad, M.; Thomsen, K.; Müller, S.; Smirnova, I. Thermodynamic Modeling Using Extended UNIQUAC and COSMO-RS-ES Models: Case Study of the Cesium Nitrate - Water System over a Large Range of Temperatures. *Fluid Phase Equilibria* **2024**, 114037. https://doi.org/10.1016/j.fluid.2024.114037.

(21) Smith, J. M.; Ness, H. C. V.; Abbott, M. *Introduction to Chemical Engineering Thermodynamics*; McGraw-Hill Education, 2005.

(22) Kjellander, R. *Statistical Mechanics of Liquids and Solutions. Intermolecular Forces, Structure and Surface Interactions.*, 1st ed.; CRC Press, 2020; Vol. 1.

(23) McQuarrie, D. A.; A, M. D. *Statistical Mechanics*; Harper & Row, 1975.

(24) Atkins, P. W.; De Paula, J. *Elements of Physical Chemistry*, 5th ed.; Oxford University Press: Oxford ; New York, 2009.

(25) Barthel, J.; Krienke, H.; Kunz, W. *Physical Chemistry of Electrolyte Solutions: Modern Aspects*; Topics in physical chemistry; Steinkopf ; Springer: Darmstadt : [New York], 1998.

(26) Brown, W. F.; Franz, W.; Forsbergh, P. W. *Dielectrics / Dielektrika*; Elektrisches und magnetisches Verhalten der Materie / Electric and Magnetic Behavior of Matter; Springer-Verlag: Berlin Heidelberg, 1956. https://doi.org/10.1007/978-3-642-45841-5.

(27) Pitzer, K. S. Electrolyte Theory-Improvements since Debye and Hückel. *Accounts of Chemical Research* **1977**, *10* (10), 371–377.

(28) Born, M. Volumen Und Hydratationswärme Der Ionen. *Zeitschrift für Physik A Hadrons and Nuclei* **1920**, *1* (1), 45–48.

(29) Bondi, A. Van Der Waals Volumes and Radii. *J. Phys. Chem.* **1964**, *68* (3), 441–451. https://doi.org/10.1021/j100785a001.

(30) Marcus, Y. Ionic Radii in Aqueous Solutions. *Chem. Rev.* **1988**, *88* (8), 1475–1498. https://doi.org/10.1021/cr00090a003.

(31) Debye, P.; Hückel, E. Zur Theorie Der Elektrolyte 1: Gefrierpunktserniedrigung Und Verwandte Erscheinungen. *Phys. Z* **1923**, *24* (9), 185–207.

(32) Kjellander, R. Modified Debye-Hueckel Approximation with Effective Charges: An Application of Dressed Ion Theory for Electrolyte Solutions. *J. Phys. Chem.* **1995**, *99* (25), 10392–10407. https://doi.org/10.1021/j100025a048.

(33) Glueckauf, E. Effect of the Dielectric Constant on the Activity Coefficients of Electrolytes in Aqueous Solutions. *Transactions of the Faraday Society* **1964**, *60*, 776. https://doi.org/10.1039/tf9646000776.

(34) McMillan, W. G., Jr.; Mayer, J. E. The Statistical Thermodynamics of Multicomponent Systems. *The Journal of Chemical Physics* **1945**, *13* (7), 276–305. https://doi.org/10.1063/1.1724036.

(35) Lee, L. L. Thermodynamic Consistency and Reference Scale Conversion in Multisolvent Electrolyte Solutions. *Journal of Molecular Liquids* **2000**, *87* (2), 129–147. https://doi.org/10.1016/S0167-7322(00)00117-3.

(36) Pitzer, K. S. Thermodynamics of Electrolytes. I. Theoretical Basis and General Equations. *J. Phys. Chem. A* **1973**, *77* (2), 268–277.

(37) Rasaiah, J. C.; Friedman, H. L. Integral Equation Methods in the Computation of Equilibrium Properties of Ionic Solutions. *The Journal of Chemical Physics* **1968**, *48* (6), 2742–2752. https://doi.org/10.1063/1.1669510.

(38) Pitzer, K. S.; Mayorga, G. Thermodynamics of Electrolytes. II. Activity and Osmotic Coefficients for Strong Electrolytes with One or Both Ions Univalent. *J. Phys. Chem. A* **1973**, *77* (19), 2300–2308.

(39) Attard, P. *Thermodynamics and Statistical Mechanics: Equilibrium by Entropy Maximisation*; Academic Press, 2002.

(40) Pitzer, K. S. Electrolytes. From Dilute Solutions to Fused Salts. *Journal of the American Chemical Society* **1980**, *102* (9), 2902–2906.

(41) Kjellander, R.; Mitchell, D. J. An Exact but Linear and Poisson—Boltzmann-like Theory for Electrolytes and Colloid Dispersions in the Primitive Model. *Chemical Physics Letters* **1992**, *200* (1), 76–82. https://doi.org/10.1016/0009-2614(92)87048-T.

(42) Kjellander, R.; Mitchell, D. J. Dressed-ion Theory for Electrolyte Solutions: A Debye–Hückel-like Reformulation of the Exact Theory for the Primitive Model. *J. Chem. Phys.* **1994**, *101* (1), 603–626. https://doi.org/10.1063/1.468116.

(43) Kjellander, R. Ion-Ion Correlations and Effective Charges in Electrolyte and Macroion Systems. *Berichte der Bunsengesellschaft für physikalische Chemie* **1996**, *100* (6), 894–904. https://doi.org/10.1002/bbpc.19961000635.

(44) Ulander, J.; Kjellander, R. The Decay of Pair Correlation Functions in Ionic Fluids: A Dressed Ion Theory Analysis of Monte Carlo Simulations. *J. Chem. Phys.* **2001**, *114* (11), 4893–4904. https://doi.org/10.1063/1.1350449.

(45) Ulander, J.; Kjellander, R. Screening and Asymptotic Decay of Pair Distributions in Asymmetric Electrolytes. *J. Chem. Phys.* **1998**, *109* (21), 9508–9522. https://doi.org/10.1063/1.477613.

(46) Ulander, J.; Greberg, H.; Kjellander, R. Primary and Secondary Effective Charges for Electrical Double Layer Systems with Asymmetric Electrolytes. *J. Chem. Phys.* **2001**, *115* (15), 7144–7160. https://doi.org/10.1063/1.1398587.

(47) Forsberg, B.; Ulander, J.; Kjellander, R. Dressed Ion Theory of Size-Asymmetric Electrolytes: Effective Ionic Charges and the Decay Length of Screened Coulomb Potential and Pair Correlations. *The Journal of Chemical Physics* **2005**, *122* (6), 064502. https://doi.org/10.1063/1.1843811.

(48) Kjellander, R. The Intimate Relationship between the Dielectric Response and the Decay of Intermolecular Correlations and Surface Forces in Electrolytes. *Soft Matter* **2019**, 10.1039.C9SM00712A. https://doi.org/10.1039/C9SM00712A.

(49) Kjellander, R. A Multiple Decay-Length Extension of the Debye-Hückel Theory: To Achieve High Accuracy Also for Concentrated Solutions and Explain under-Screening in Dilute Symmetric Electrolytes. *Phys. Chem. Chem. Phys.* **2020**, *22*, 23952–23985. https://doi.org/10.1039/D0CP02742A.

(50) Kirkwood, J. G. On the Theory of Strong Electrolyte Solutions. *The Journal of Chemical Physics* **1934**, *2* (11), 767–781. https://doi.org/10.1063/1.1749393.

(51) Stillinger, F. H.; Lovett, R. Ion-Pair Theory of Concentrated Electrolytes. I. Basic Concepts. *The Journal of Chemical Physics* **1968**, *48* (9), 3858–3868. https://doi.org/10.1063/1.1669709.

(52) Lovett, R.; Stillinger, F. H. Ion-Pair Theory of Concentrated Electrolytes. II. Approximate Dielectric Response Calculation. *The Journal of Chemical Physics* **1968**, *48* (9), 3869–3884. https://doi.org/10.1063/1.1669710.

(53) Blum, L. Primitive Electrolytes in the Mean Spherical Approximation. In *Theoretical Chemistry*; Eyring, H., Henderson, D., Eds.; Academic Press, 1980; pp 1–66. https://doi.org/10.1016/B978-0-12-681905-2.50007-4.

(54) Percus, J. K.; Yevick, G. J. Analysis of Classical Statistical Mechanics by Means of Collective Coordinates. *Phys. Rev.* **1958**, *110* (1), 1–13. https://doi.org/10.1103/PhysRev.110.1.

(55) Blum, L. Mean Spherical Model for a Mixture of Charged Spheres and Hard Dipoles. *Chemical Physics Letters* **1974**, *26* (2), 200–202. https://doi.org/10.1016/0009-2614(74)85396-0.

(56) Blum, L. Mean Spherical Model for Asymmetric Electrolytes. *Molecular Physics* **1975**, *30* (5), 1529–1535. https://doi.org/10.1080/00268977500103051.

(57) Blum, L.; Bernard, O. The General Solution of the Binding Mean Spherical Approximation for Pairing Ions. *J Stat Phys* **1995**, *79* (3), 569–583. https://doi.org/10.1007/BF02184871.

(58) Bernard, O.; Kunz, W.; Turq, P.; Blum, L. Conductance in Electrolyte Solutions Using the Mean Spherical Approximation. *J. Phys. Chem.* **1992**, *96* (9), 3833–3840. https://doi.org/10.1021/j100188a049.

(59) Simonin, J.-P.; Blum, L.; Turq, P. Real Ionic Solutions in the Mean Spherical Approximation. 1. Simple Salts in the Primitive Model. *J. Phys. Chem.* **1996**, *100* (18), 7704–7709. https://doi.org/10.1021/jp953567o.

(60) Hamer, W. J.; Wu, Y.-C. Osmotic Coefficients and Mean Activity Coefficients of Uni-Univalent Electrolytes in Water at 25°C. *Journal of Physical and Chemical Reference Data* **1972**, *1* (4), 1047. https://doi.org/10.1063/1.3253108.

(61) Marcus, Y. *Ions in Solution and Their Solvation: Marcus/Ions in Solution and Their Solvation*; John Wiley & Sons, Inc: Hoboken, NJ, 2015.

(62) Collins, K. D. Charge Density-Dependent Strength of Hydration and Biological Structure. *Biophysical Journal* **1997**, *72* (1), 65–76. https://doi.org/10.1016/S0006-3495(97)78647-8.

(63) Collins, K. D. The Behavior of Ions in Water Is Controlled by Their Water Affinity. *Quarterly Reviews of Biophysics* **2019**, *52*, e11. https://doi.org/10.1017/S0033583519000106.

(64) Hasted, J. B.; Sabeh, S. H. M. E. The Dielectric Properties of Water in Solutions. *Trans. Faraday Soc.* **1953**, *49* (0), 1003–1011. https://doi.org/10.1039/TF9534901003.

(65) Hasted, J. B.; Ritson, D. M.; Collie, C. H. Dielectric Properties of Aqueous Ionic Solutions. Parts I and II. *The Journal of Chemical Physics* **1948**, *16* (1), 1–21. https://doi.org/10.1063/1.1746645.

(66) Mazzini, V.; Liu, G.; Craig, V. S. J. Probing the Hofmeister Series beyond Water: Specific-Ion Effects in Non-Aqueous Solvents. *The Journal of Chemical Physics* **2018**, *148* (22), 222805. https://doi.org/10/gdq2bj.

(67) Scaife, B. K. P. *Principles of Dielectrics*; Monographs on the physics and chemistry of materials; Clarendon Press, 1989.

(68) Kontogeorgis, G. M.; Coutsikos, P. Thirty Years with EoS/GE Models—What Have We Learned? *Ind. Eng. Chem. Res.* **2012**, *51* (11), 4119–4142. https://doi.org/10/gdncf6.

(69) Onsager, L. Electric Moments of Molecules in Liquids. *J. Am. Chem. Soc.* **1936**, *58* (8), 1486–1493. https://doi.org/10.1021/ja01299a050.

(70) Rysselberghe, P. V. Remarks Concerning the Clausius-Mossotti Law. *The Journal of Physical Chemistry* **1932**, *36* (4), 1152–1155.

(71) Kirkwood, J. G. On the Theory of Dielectric Polarization. *J. Chem. Phys.* **1936**, *4* (9), 592–601. https://doi.org/10.1063/1.1749911.

(72) Kohns, M.; Marx, J.; Langenbach, K. Relative Permittivity of Stockmayer-Type Model Fluids from MD Simulations and COFFEE. *J. Chem. Eng. Data* **2020**, *65* (12), 5891–5896. https://doi.org/10.1021/acs.jced.0c00769.

(73) Langenbach, K.; Kohns, M. Relative Permittivity of Dipolar Model Fluids from Molecular Simulation and from the Co-Oriented Fluid Functional Equation for Electrostatic Interactions. *J. Chem. Eng. Data* **2020**, *65* (3), 980–986. https://doi.org/10.1021/acs.jced.9b00296.

(74) Gaudin, T.; Ma, H. A Molecular Contact Theory for Simulating Polarization: Application to Dielectric Constant Prediction. *Phys. Chem. Chem. Phys.* **2019**, *21* (27), 14846–14857. https://doi.org/10.1039/C9CP02358E.

(75) Kirkwood, J. G. The Dielectric Polarization of Polar Liquids. *J. Chem. Phys.* **1939**, *7* (10), 911–919. https://doi.org/10.1063/1.1750343.

(76) Hasted, J. B. Dielectric Properties. In *Water in Crystalline Hydrates Aqueous Solutions of Simple Nonelectrolytes*; Franks, F., Ed.; Water; Springer US: Boston, MA, 1973; pp 405–458. https://doi.org/10.1007/978-1-4757-6958-6_7.

(77) Hubbard, J.; Onsager, L. Dielectric Dispersion and Dielectric Friction in Electrolyte Solutions. I. *J. Chem. Phys.* **1977**, *67* (11), 4850–4857. https://doi.org/10.1063/1.434664.

(78) Hubbard, J. B.; Onsager, L.; Beek, W. M. van; Mandel, M. Kinetic Polarization Deficiency in Electrolyte Solutions. *PNAS* **1977**, *74* (2), 401–404. https://doi.org/10.1073/pnas.74.2.401.

(79) Kaatze, U. Bound Water: Evidence from and Implications for the Dielectric Properties of Aqueous Solutions. *Journal of Molecular Liquids* **2011**, *162* (3), 105–112. https://doi.org/10/dkfcd3.

(80) Hückel, E. Zur Theorie Konzentrierter Wässriger Lösungen Starker Elektrolyte. *Phys. Z* **1925**, *26*, 93–147.

(81) Tikanen, A. C.; Fawcett, W. R. Application of the Mean Spherical Approximation and Ion Association to Describe the Activity Coefficients of Aqueous 1:1 electrolytes1Dedicated to Professor K.B. Oldham on the Occasion of His Retirement from Trent University.1. *Journal of Electroanalytical Chemistry* **1997**, *439* (1), 107–113. https://doi.org/10.1016/S0022-0728(97)00376-8.

(82) Giese, K.; Kaatze, U.; Pottel, R. Permittivity and Dielectric and Proton Magnetic Relaxation of Aqueous Solutions of the Alkali Halides. *J. Phys. Chem.* **1970**, *74* (21), 3718–3725. https://doi.org/10/fb6df2.

(83) Simonin, J.-P.; Bernard, O.; Blum, L. Ionic Solutions in the Binding Mean Spherical Approximation: Thermodynamic Properties of Mixtures of Associating Electrolytes. *J. Phys. Chem. B* **1999**, *103* (4), 699–704. https://doi.org/10/cxjd55.

(84) Wang, P.; Anderko, A. Computation of Dielectric Constants of Solvent Mixtures and Electrolyte Solutions. *Fluid Phase Equilibria* **2001**, *186* (1–2), 103–122. https://doi.org/10.1016/S0378-3812(01)00507-6.

(85) Koeberg, M.; Wu, C.-C.; Kim, D.; Bonn, M. THz Dielectric Relaxation of Ionic Liquid:Water Mixtures. *Chemical Physics Letters* **2007**, *439* (1–3), 60–64. https://doi.org/10/fwb8v7.

(86) Bennett, E. L.; Song, C.; Huang, Y.; Xiao, J. Measured Relative Complex Permittivities for Multiple Series of Ionic Liquids. *Journal of Molecular Liquids* **2019**, *294*, 111571. https://doi.org/10.1016/j.molliq.2019.111571.

(87) Marcus, Y. *Ionic Liquid Properties*; Springer International Publishing: Cham, 2016. https://doi.org/10.1007/978-3-319-30313-0.

(88) Jin, H.; Baker, G. A.; Arzhantsev, S.; Dong, J.; Maroncelli, M. Solvation and Rotational Dynamics of Coumarin 153 in Ionic Liquids: Comparisons to Conventional Solvents. *J. Phys. Chem. B* **2007**, *111* (25), 7291–7302. https://doi.org/10.1021/jp070923h.

(89) Marcus, Y. On the Molar Volumes and Viscosities of Electrolytes. *J Solution Chem* **2006**, *35* (9), 1271–1286. https://doi.org/10.1007/s10953-006-9058-5.

(90) Millero, F. J. Molal Volumes of Electrolytes. *Chem. Rev.* **1971**, *71* (2), 147–176. https://doi.org/10.1021/cr60270a001.

(91) Nguyen, N. H.; Hussain, F.; Chen, C.-C. Correlations for Densities of Aqueous Electrolyte Solutions. *J. Chem. Eng. Data* **2016**, *61* (2), 740–747. https://doi.org/10.1021/acs.jced.5b00491.

(92) Liu, W.; Zhao, T.; Zhang, Y.; Wang, H.; Yu, M. The Physical Properties of Aqueous Solutions of the Ionic Liquid [BMIM][BF4]. *J Solution Chem* **2006**, *35* (10), 1337–1346. https://doi.org/10.1007/s10953-006-9064-7.

(93) Yu, Y.; Chen, Y. Density Prediction of Ionic Liquids at Different Temperatures Using the Average Free Volume Model. *ACS Omega* **2021**, *6* (23), 14869–14874. https://doi.org/10.1021/acsomega.1c00547.

(94) Marcus, Y.; Hefter, G. Ion Pairing. *Chemical Reviews* **2006**, *106* (11), 4585–4621. https://doi.org/10.1021/cr040087x.

(95) Bjerrum, N. Untersuchungen über Ionenassoziation. I. Der Einfluss der Ionenassoziation auf die Aktivität der Ionen bei Mittleren Assoziationsgraden. *Kgl. Danske Vidensk. Selskab.* **1926**, *7* (9).

(96) Kjellander, R. Nonlocal Electrostatics in Ionic Liquids: The Key to an Understanding of the Screening Decay Length and Screened Interactions. *J. Chem. Phys.* **2016**, *145* (12), 124503. https://doi.org/10.1063/1.4962756.

(97) Onsager, Lars. A Correction to the Poisson-Boltzmann Equation for Unsymmetrical Electrolytes. *J. Am. Chem. Soc.* **1964**, *86* (17), 3421–3423. https://doi.org/10.1021/ja01071a004.

(98) LaMer, V. K.; Mason, C. F. ACTIVITY COEFFICIENTS OF ELECTROLYTES. II. THE UNSYMMETRIC VALENCE-TYPE EFFECT IN HIGHLY DILUTE SOLUTIONS1. *J. Am. Chem. Soc.* **1927**, *49* (2), 410–426. https://doi.org/10.1021/ja01401a012.

(99) Onsager, L. Theories of Concentrated Electrolytes. *Chemical Reviews* **1933**, *13* (1), 73–89.

(100) Barthel, J. *Ionen in Nichtwässrigen Lösungen*; Jost, W., Series Ed.; Fortschritte der Physikalischen Chemie; Steinkopff: Heidelberg, 1976; Vol. 10. https://doi.org/10.1007/978-3-642-72321-6.

(101) Fuoss, R. M. Ionic Association. III. The Equilibrium between Ion Pairs and Free Ions. *Journal of the American Chemical Society* **1958**, *80* (19), 5059–5061. https://doi.org/10.1021/ja01552a016.

(102) Fuoss, R. M.; Kraus, C. A. Properties of Electrolytic Solutions. III. The Dissociation Constant. *Journal of the American Chemical Society* **1933**, *55* (3), 1019–1028. https://doi.org/10.1021/ja01330a023.

(103) Lindenbaum, S.; Boyd, G. E. Osmotic and Activity Coefficients for the Symmetrical Tetraalkyl Ammonium Halides in Aqueous Solution at 25° [1]. *The Journal of Physical Chemistry* **1964**, *68* (4), 911–917. https://doi.org/10.1021/j100786a038.

(104) Lindenbaum, S.; Leifer, L.; Boyd, G. E.; Chase, J. W. Variation of Osmotic Coefficients of Aqueous Solutions of Tetraalkylammonium Halides with Temperature. Thermal and Solute Effects on Solvent Hydrogen Bonding. *J. Phys. Chem.* **1970**, *74* (4), 761–764. https://doi.org/10.1021/j100699a014.

(105) Naseri Boroujeni, S.; Maribo-Mogensen, B.; Liang, X.; Kontogeorgis, G. M. Binding Debye–Hückel Theory for Associative Electrolyte Solutions. *The Journal of Chemical Physics* **2023**, *159* (15), 154503. https://doi.org/10.1063/5.0170146.

(106) Klamt, A.; Schüürmann, G. COSMO: A New Approach to Dielectric Screening in Solvents with Explicit Expressions for the Screening Energy and Its Gradient. *J. Chem. Soc., Perkin Trans. 2* **1993**, No. 5, 799–805.

(107) Klamt, A. *COSMO-RS: From Quantum Chemistry to Fluid PhaseThermodynamics and Drug Design*; Elsevier, 2005.

(108) Springborg, M.; Zhou, M. Quantum Chemistry: An Introduction. In *Quantum Chemistry*; De Gruyter, 2021. https://doi.org/10.1515/9783110742206.

(109) Tomasi, J.; Mennucci, B.; Cammi, R. Quantum Mechanical Continuum Solvation Models. *Chem. Rev.* **2005**, *105* (8), 2999–3094. https://doi.org/10.1021/cr9904009.

(110) TURBOMOLE V7.3.

(111) Klamt, A.; Eckert, F. COSMO-RS: A Novel and Efficient Method for the a Priori Prediction of Thermophysical Data of Liquids. *Fluid Phase Equilib.* **2000**, *172* (1), 43–72. https://doi.org/10.1016/S0378-3812(00)00357-5.

(112) Klamt, A. The COSMO and COSMO-RS Solvation Models. *Wiley Interdiscip. Rev.: Comput. Mol. Sci.* **2018**, *8* (1), e1338. https://doi.org/10.1002/wcms.1338.

(113) Klamt, A.; Krooshof, G. J.; Taylor, R. COSMOSPACE: Alternative to Conventional Activity-Coefficient Models. *AIChE journal* **2002**, *48* (10), 2332–2349.

(114) Gerlach, T.; Müller, S.; de Castilla, A. G.; Smirnova, I. An Open Source COSMO-RS Implementation and Parameterization Supporting the Efficient Implementation of Multiple Segment Descriptors. *Fluid Phase Equilibria* **2022**, *560*, 113472. https://doi.org/10.1016/j.fluid.2022.113472.

(115) Paduszyński, K. Extensive Evaluation of the Conductor-like Screening Model for Real Solvents Method in Predicting Liquid–Liquid Equilibria in Ternary Systems of Ionic Liquids with Molecular Compounds. *J. Phys. Chem. B* **2018**, *122* (14), 4016–4028. https://doi.org/10/gddtxs.

(116) Paduszyński, K. An Overview of the Performance of the COSMO-RS Approach in Predicting the Activity Coefficients of Molecular Solutes in Ionic Liquids and Derived Properties at Infinite Dilution. *Phys. Chem. Chem. Phys.* **2017**, *19* (19), 11835–11850. https://doi.org/10.1039/C7CP00226B.

(117) Alhadid, A.; Jandl, C.; Mokrushina, L.; Minceva, M. Experimental Investigation and Modeling of Cocrystal Formation in L-Menthol/Thymol Eutectic System. *Crystal Growth & Design* **2021**, *21* (11), 6083–6091. https://doi.org/10.1021/acs.cgd.1c00306.

(118) Lin, S.-T.; Sandler, S. I. A Priori Phase Equilibrium Prediction from a Segment Contribution Solvation Model. *Industrial & Engineering Chemistry Research* **2002**, *41* (5), 899–913. https://doi.org/10.1021/ie001047w.

(119) Bell, I. H.; Mickoleit, E.; Hsieh, C.-M.; Lin, S.-T.; Vrabec, J.; Breitkopf, C.; Jäger, A. A Benchmark Open-Source Implementation of COSMO-SAC. *J. Chem. Theory Comput.* **2020**, *16* (4), 2635–2646. https://doi.org/10.1021/acs.jctc.9b01016.

(120) BIOVIA COSMOtherm. Dassault Systèmes, Http://Www.3ds.Com.

(121) Kalidas, C.; Hefter, G.; Marcus, Y. Gibbs Energies of Transfer of Cations from Water to Mixed Aqueous Organic Solvents. *Chem. Rev.* **2000**, *100* (3), 819–852. https://doi.org/10.1021/cr980144k.

(122) Osakai, T.; Naito, Y.; Eda, K.; Yamamoto, M. Prediction of the Standard Gibbs Energy of Transfer of Organic Ions Across the Interface between Two Immiscible Liquids. *The Journal of Physical Chemistry B* **2015**, *119* (41), 13167–13176. https://doi.org/10.1021/acs.jpcb.5b06544.

(123) Marcus, Y. Gibbs Energies of Transfer of Anions from Water to Mixed Aqueous Organic Solvents. *Chemical Reviews* **2007**, *107* (9), 3880–3897. https://doi.org/10.1021/cr068045r.

(124) Hendriks, E.; Kontogeorgis, G. M.; Dohrn, R.; de Hemptinne, J.-C.; Economou, I. G.; Žilnik, L. F.; Vesovic, V. Industrial Requirements for Thermodynamics and Transport Properties. *Ind. Eng. Chem. Res.* **2010**, *49* (22), 11131–11141. https://doi.org/10.1021/ie101231b.

(125) Novak, N.; Kontogeorgis, G. M.; Castier, M.; Economou, I. G. Extension of the eSAFT-VR Mie Equation of State from Aqueous to Non-Aqueous Electrolyte Solutions. *Fluid Phase Equilibria* **2023**, *565*, 113618. https://doi.org/10.1016/j.fluid.2022.113618.

(126) Płotka-Wasylka, J.; de la Guardia, M.; Andruch, V.; Vilková, M. Deep Eutectic Solvents vs Ionic Liquids: Similarities and Differences. *Microchemical Journal* **2020**, *159*, 105539. https://doi.org/10.1016/j.microc.2020.105539.

(127) Singh, S. K.; Savoy, A. W. Ionic Liquids Synthesis and Applications: An Overview. *Journal of Molecular Liquids* **2020**, *297*, 112038. https://doi.org/10.1016/j.molliq.2019.112038.

(128) González de Castilla, A.; Bittner, J. P.; Müller, S.; Jakobtorweihen, S.; Smirnova, I. Thermodynamic and Transport Properties Modeling of Deep Eutectic Solvents: A Review on gE-Models, Equations of State, and Molecular Dynamics. *J. Chem. Eng. Data* **2019**. https://doi.org/10.1021/acs.jced.9b00548.

(129) Simonin, J.-P. On the Solution of the Mean-Spherical Approximation (MSA) for Ions in a Dipolar Solvent in the General Case. *AIP Advances* **2020**, *10* (9), 095213. https://doi.org/10.1063/5.0022864.

(130) Martínez-Borquez, A.; Gil-Villegas, A.; Lira-Galeana, C. Asphaltene Precipitation Described with a Yukawa SAFT-VR/MSA Equation of State. *Fluid Phase Equilibria* **2023**, *572*, 113827. https://doi.org/10.1016/j.fluid.2023.113827.

(131) Theiss, M.; Gross, J. Nonprimitive Model Electrolyte Solutions: Comprehensive Data from Monte Carlo Simulations. *J. Chem. Eng. Data* **2020**, acs.jced.9b00855. https://doi.org/10.1021/acs.jced.9b00855.

(132) Fürst, W.; Renon, H. Representation of excess properties of electrolyte solutions using a new equation of state. *AIChE Journal* **1993**, *39* (2), 335–343. https://doi.org/10.1002/aic.690390213.

(133) Simon, H.-G.; Kistenmacher, H.; Prausnitz, J. M.; Vortmeyer, D. An Equation of State for Systems Containing Electrolytes and Nonelectrolytes. *Chemical Engineering and Processing: Process Intensification* **1991**, *29* (3), 139–146. https://doi.org/10.1016/0255-2701(91)85013-E.

(134) Zuo, Y.-X.; Fürst, W. Use of an Electrolyte Equation of State for the Calculation of Vapor–Liquid Equilibria and Mean Activity Coefficients in Mixed Solvent Electrolyte Systems. *Fluid Phase Equilibria* **1998**, *150–151* (Supplement C), 267–275. https://doi.org/10.1016/S0378-3812(98)00326-4.

(135) Zuo, J. Y.; Zhang, D.; Fürst, W. Predicting LLE in Mixed-Solvent Electrolyte Systems by an Electrolyte EOS. *AIChE J.* **2000**, *46* (11), 2318–2329. https://doi.org/10.1002/aic.690461122.

(136) Kosinski, J. J.; Anderko, A. Equation of State for High-Temperature Aqueous Electrolyte and Nonelectrolyte Systems. *Fluid Phase Equilibria* **2001**, *183–184*, 75–86. https://doi.org/10/dn2xcv.

(137) Myers, J. A.; Sandler, S. I.; Wood, R. H. An Equation of State for Electrolyte Solutions Covering Wide Ranges of Temperature, Pressure, and Composition. *Ind. Eng. Chem. Res.* **2002**, *41* (13), 3282–3297. https://doi.org/10.1021/ie011016g.

(138) Chapman, W. G.; Gubbins, K. E.; Jackson, G.; Radosz, M. New Reference Equation of State for Associating Liquids. *Ind. Eng. Chem. Res.* **1990**, *29* (8), 1709–1721.

(139) Wu, J.; Prausnitz, J. M. Phase Equilibria for Systems Containing Hydrocarbons, Water, and Salt: An Extended Peng–Robinson Equation of State. *Ind. Eng. Chem. Res.* **1998**, *37* (5), 1634–1643. https://doi.org/10.1021/ie9706370.

(140) Inchekel, R.; de Hemptinne, J.-C.; Fürst, W. The Simultaneous Representation of Dielectric Constant, Volume and Activity Coefficients Using an Electrolyte Equation of State. *Fluid Phase Equilibria* **2008**, *271* (1), 19–27. https://doi.org/10.1016/j.fluid.2008.06.013.

(141) Maribo-Mogensen, B.; Kontogeorgis, G. M.; Thomsen, K. Modeling of Dielectric Properties of Aqueous Salt Solutions with an Equation of State. *J. Phys. Chem. B* **2013**, *117* (36), 10523–10533. https://doi.org/10.1021/jp403375t.

(142) Maribo-Mogensen, B.; Thomsen, K.; Kontogeorgis, G. M. An Electrolyte CPA Equation of State for Mixed Solvent Electrolytes. *AIChE Journal* **2015**, *61* (9), 2933–2950. https://doi.org/10.1002/aic.14829.

(143) Schlaikjer, A.; Thomsen, K.; Kontogeorgis, G. M. eCPA: An Ion-Specific Approach to Parametrization. *Fluid Phase Equilibria* **2017**. https://doi.org/10/gc4jh2.

(144) Schlaikjer, A.; Thomsen, K.; Kontogeorgis, G. M. Simultaneous Description of Activity Coefficients and Solubility with eCPA. *Industrial & Engineering Chemistry Research* **2017**, *56* (4), 1074–1089. https://doi.org/10.1021/acs.iecr.6b03333.

(145) Olsen, M. D.; Kontogeorgis, G. M.; Liang, X.; von Solms, N. Investigation of the Performance of E-CPA for a Wide Range of Properties for Aqueous NaCl Solutions. *Fluid Phase Equilibria* **2021**, *548*, 113167. https://doi.org/10.1016/j.fluid.2021.113167.

(146) Roosta, A.; Rezaei, N. Modification of E-CPA for Estimating Phase Equilibria and Development of Predictive Models for Electrical Conductivity in Aqueous Electrolyte Solutions. *Chemical Engineering Science* **2024**, *284*, 119481. https://doi.org/10.1016/j.ces.2023.119481.

(147) Shaahmadi, F.; Smith, S. A.; Schwarz, C. E.; Burger, A. J.; Cripwell, J. T. Group-Contribution SAFT Equations of State: A Review. *Fluid Phase Equilibria* **2023**, *565*, 113674. https://doi.org/10.1016/j.fluid.2022.113674.

(148) Ji, X.; Adidharma, H. Ion-Based Statistical Associating Fluid Theory (SAFT2) to Represent Aqueous Single-Salt Solutions at Temperatures and Pressures up to 473.15 K and 1000 Bar. *Ind. Eng. Chem. Res.* **2007**, *46* (13), 4667–4677. https://doi.org/10/bhr8h5.

(149) Gil-Villegas, A.; Galindo, A.; Whitehead, P. J.; Mills, S. J.; Jackson, G.; Burgess, A. N. Statistical Associating Fluid Theory for Chain Molecules with Attractive Potentials of Variable Range. *The Journal of Chemical Physics* **1997**, *106* (10), 4168–4186. https://doi.org/10.1063/1.473101.

(150) Galindo, A.; Gil-Villegas, A.; Jackson, G.; Burgess, A. N. SAFT-VRE: Phase Behavior of Electrolyte Solutions with the Statistical Associating Fluid Theory for Potentials of Variable Range. *J. Phys. Chem. B* **1999**, *103* (46), 10272–10281. https://doi.org/10.1021/jp991959f.

(151) GIL-VILLEGAS, A.; GALINDO, A.; JACKSON, G. A Statistical Associating Fluid Theory for Electrolyte Solutions (SAFT-VRE). *Molecular Physics* **2001**, *99* (6), 531–546. https://doi.org/10.1080/00268970010018666.

(152) Patel, B. H.; Paricaud, P.; Galindo, A.; Maitland, G. C. Prediction of the Salting-Out Effect of Strong Electrolytes on Water + Alkane Solutions. *Ind. Eng. Chem. Res.* **2003**, *42* (16), 3809–3823. https://doi.org/10.1021/ie020918u.

(153) Schreckenberg, J. M. A.; Dufal, S.; Haslam, A. J.; Adjiman, C. S.; Jackson, G.; Galindo, A. Modelling of the Thermodynamic and Solvation Properties of Electrolyte Solutions with the Statistical Associating Fluid Theory for Potentials of Variable Range. *Molecular Physics* **2014**, *112* (17), 2339–2364. https://doi.org/10.1080/00268976.2014.910316.

(154) Lafitte, T.; Apostolakou, A.; Avendaño, C.; Galindo, A.; Adjiman, C. S.; Müller, E. A.; Jackson, G. Accurate Statistical Associating Fluid Theory for Chain Molecules Formed from Mie Segments. *J Chem Phys* **2013**, *139* (15), 154504. https://doi.org/10.1063/1.4819786.

(155) Dufal, S.; Lafitte, T.; Haslam, A. J.; Galindo, A.; Clark, G. N. I.; Vega, C.; Jackson, G. The A in SAFT: Developing the Contribution of Association to the Helmholtz Free Energy within a Wertheim TPT1 Treatment of Generic Mie Fluids. *Molecular Physics* **2015**, *113* (9–10), 948–984. https://doi.org/10.1080/00268976.2015.1029027.

(156) Dufal, S.; Lafitte, T.; Galindo, A.; Jackson, G.; Haslam, A. J. Developing Intermolecular-Potential Models for Use with the SAFT-VR Mie Equation of State. *AIChE Journal* **2015**, *61* (9), 2891–2912. https://doi.org/10.1002/aic.14808.

(157) Eriksen, D. K.; Lazarou, G.; Galindo, A.; Jackson, G.; Adjiman, C. S.; Haslam, A. J. Development of Intermolecular Potential Models for Electrolyte Solutions Using an Electrolyte SAFT-VR Mie Equation of State. *Molecular Physics* **2016**, *114* (18), 2724–2749. https://doi.org/10.1080/00268976.2016.1236221.

(158) Lecce, S. D.; Lazarou, G.; Khalit, S. H.; Adjiman, C. S.; Jackson, G.; Galindo, A.; McQueen, L. Modelling and Prediction of the Thermophysical Properties of Aqueous Mixtures of Choline Geranate and Geranic Acid (CAGE) Using SAFT-γ Mie. *RSC Adv.* **2019**, *9* (65), 38017–38031. https://doi.org/10.1039/C9RA07057E.

(159) Selam, M. A.; Economou, I. G.; Castier, M. A Thermodynamic Model for Strong Aqueous Electrolytes Based on the eSAFT-VR Mie Equation of State. *Fluid Phase Equilibria* **2018**, *464*, 47–63. https://doi.org/10/gc4mz7.

(160) Novak, N.; Kontogeorgis, G. M.; Castier, M.; Economou, I. G. Modeling of Gas Solubility in Aqueous Electrolyte Solutions with the eSAFT-VR Mie Equation of State. *Ind. Eng. Chem. Res.* **2021**, *60* (42), 15327–15342. https://doi.org/10.1021/acs.iecr.1c02923.

(161) Nikolaidis, I. K.; Novak, N.; Kontogeorgis, G. M.; Economou, I. G. Rigorous Phase Equilibrium Calculation Methods for Strong Electrolyte Solutions: The Isothermal Flash. *Fluid Phase Equilibria* **2022**, *558*, 113441. https://doi.org/10.1016/j.fluid.2022.113441.

(162) Walker, P. J.; Liang, X.; Kontogeorgis, G. M. Importance of the Relative Static Permittivity in Electrolyte SAFT-VR Mie Equations of State. *Fluid Phase Equilibria* **2022**, *551*, 113256. https://doi.org/10.1016/j.fluid.2021.113256.

(163) Valiskó, M.; Boda, D. The Effect of Concentration- and Temperature-Dependent Dielectric Constant on the Activity Coefficient of NaCl Electrolyte Solutions. *The Journal of Chemical Physics* **2014**, *140* (23), 234508. https://doi.org/10.1063/1.4883742.

(164) Maribo-Mogensen, B.; Kontogeorgis, G. M.; Thomsen, K. Comparison of the Debye–Hückel and the Mean Spherical Approximation Theories for Electrolyte Solutions. *Industrial & Engineering Chemistry Research* **2012**, *51* (14), 5353–5363. https://doi.org/10.1021/ie2029943.

(165) Silva, G. M.; Liang, X.; Kontogeorgis, G. M. How to Account for the Concentration Dependency of Relative Permittivity in the Debye–Hückel and Born Equations. *Fluid Phase Equilibria* **2023**, *566*, 113671. https://doi.org/10.1016/j.fluid.2022.113671.

(166) Silva, G. M.; Liang, X.; Kontogeorgis, G. M. On the Derivations of the Debye–Hückel Equations. *Molecular Physics* **2022**, *120* (10), e2064353. https://doi.org/10.1080/00268976.2022.2064353.

(167) Novak, N.; Kontogeorgis, G. M.; Castier, M.; Economou, I. G. Theoretical Considerations on Single and Mixed Solvent Electrolyte Solutions. *Fluid Phase Equilibria* **2023**, 113924. https://doi.org/10.1016/j.fluid.2023.113924.

(168) Novak, N.; Kontogeorgis, G. M.; Castier, M.; Economou, I. G. Mixed Solvent Electrolyte Solutions: A Review and Calculations with the eSAFT-VR Mie Equation of State. *Ind. Eng. Chem. Res.* **2023**. https://doi.org/10.1021/acs.iecr.3c00717.

(169) Gross, J.; Sadowski, G. Application of the Perturbed-Chain SAFT Equation of State to Associating Systems. *Ind. Eng. Chem. Res.* **2002**, *41* (22), 5510–5515. https://doi.org/10/dmfwjm.

(170) Gross, J.; Sadowski, G. Perturbed-Chain SAFT: An Equation of State Based on a Perturbation Theory for Chain Molecules. *Ind. Eng. Chem. Res.* **2001**, *40* (4), 1244–1260. https://doi.org/10/dt7kgb.

(171) Cameretti, L. F.; Sadowski, G.; Mollerup, J. M. Modeling of Aqueous Electrolyte Solutions with Perturbed-Chain Statistical Associated Fluid Theory. *Industrial & Engineering Chemistry Research* **2005**, *44* (9), 3355–3362. https://doi.org/10.1021/ie0488142.

(172) Lee, B.-S.; Kim, K.-C. Modeling of Aqueous Electrolyte Solutions Based on Perturbed-Chain Statistical Associating Fluid Theory Incorporated with Primitive Mean Spherical Approximation. *Korean J. Chem. Eng.* **2009**, *26* (6), 1733–1747. https://doi.org/10.1007/s11814-009-0286-4.

(173) Held, C.; Cameretti, L. F.; Sadowski, G. Modeling Aqueous Electrolyte Solutions. *Fluid Phase Equilibria* **2008**, *270* (1–2), 87–96. https://doi.org/10.1016/j.fluid.2008.06.010.

(174) Held, C.; Sadowski, G. Modeling Aqueous Electrolyte Solutions. Part 2. Weak Electrolytes. *Fluid Phase Equilibria* **2009**, *279* (2), 141–148. https://doi.org/10.1016/j.fluid.2009.02.015.

(175) Reschke, T.; Naeem, S.; Sadowski, G. Osmotic Coefficients of Aqueous Weak Electrolyte Solutions: Influence of Dissociation on Data Reduction and Modeling. *J. Phys. Chem. B* **2012**, *116* (25), 7479–7491. https://doi.org/10.1021/jp3005629.

(176) Held, C.; Prinz, A.; Wallmeyer, V.; Sadowski, G. Measuring and Modeling Alcohol/Salt Systems. *Chemical Engineering Science* **2011**, *68* (1), 328–339. https://doi.org/10.1016/j.ces.2011.09.040.

(177) Held, C.; Cameretti, L. F.; Sadowski, G. Measuring and Modeling Activity Coefficients in Aqueous Amino-Acid Solutions. *Industrial & Engineering Chemistry Research* **2011**, *50* (1), 131–141. https://doi.org/10.1021/ie100088c.

(178) Reschke, T.; Brandenbusch, C.; Sadowski, G. Modeling Aqueous Two-Phase Systems: I. Polyethylene Glycol and Inorganic Salts as ATPS Former. *Fluid Phase Equilibria* **2014**, *368*, 91–103. https://doi.org/10.1016/j.fluid.2014.02.016.

(179) Reschke, T.; Brandenbusch, C.; Sadowski, G. Modeling Aqueous Two-Phase Systems: III. Polymers and Organic Salts as ATPS Former. *Fluid Phase Equilibria* **2015**, *387*, 178–189. https://doi.org/10.1016/j.fluid.2014.12.011.

(180) Mohammad, S.; Held, C.; Altuntepe, E.; Köse, T.; Gerlach, T.; Smirnova, I.; Sadowski, G. Salt Influence on MIBK/Water Liquid–Liquid Equilibrium: Measuring and Modeling with ePC-SAFT and COSMO-RS. *Fluid Phase Equilibria* **2016**, *416*, 83–93. https://doi.org/10.1016/j.fluid.2015.11.018.

(181) Held, C.; Reschke, T.; Mohammad, S.; Luza, A.; Sadowski, G. ePC-SAFT Revised. *Chemical Engineering Research and Design* **2014**, *92* (12), 2884–2897. https://doi.org/10.1016/j.cherd.2014.05.017.

(182) Bülow, M.; Ji, X.; Held, C. Incorporating a Concentration-Dependent Dielectric Constant into ePC-SAFT. An Application to Binary Mixtures Containing Ionic Liquids. *Fluid Phase Equilibria* **2019**, *492*, 26–33. https://doi.org/10.1016/j.fluid.2019.03.010.

(183) Bülow, M.; Ascani, M.; Held, C. ePC-SAFT Advanced - Part I: Physical Meaning of Including a Concentration-Dependent Dielectric Constant in the Born Term and in the Debye-Hückel Theory. *Fluid Phase Equilibria* **2021**, *535*, 112967. https://doi.org/10.1016/j.fluid.2021.112967.

(184) Ascani, M.; Held, C. Prediction of Salting-out in Liquid-liquid Two-phase Systems with ePC-SAFT: Effect of the Born Term and of a Concentration-dependent Dielectric Constant. *Z. anorg. allg. Chem.* **2021**, zaac.202100032. https://doi.org/10.1002/zaac.202100032.

(185) Ascani, M.; Sadowski, G.; Held, C. Calculation of Multiphase Equilibria Containing Mixed Solvents and Mixed Electrolytes: General Formulation and Case Studies. *J. Chem. Eng. Data* **2022**, *67* (8), 1972–1984. https://doi.org/10.1021/acs.jced.1c00866.

(186) Schick, D.; Arrad, M.; Figiel, P.; Sadowski, G.; Held, C. Modeling the Temperature-Dependent Solubility of Salts in Organic Solvents. *Fluid Phase Equilibria* **2023**, *572*, 113828. https://doi.org/10.1016/j.fluid.2023.113828.

(187) Yu, G.; Zhang, X.; Hubach, T.; Chen, B.; Held, C. Highly Efficient Lithium Extraction from Magnesium-Rich Brines with Ionic Liquid-Based Collaborative Extractants: Thermodynamics and Molecular Insights. *Chemical Engineering Science* **2023**, 119682. https://doi.org/10.1016/j.ces.2023.119682.

(188) Schick, D.; Bierhaus, L.; Strangmann, A.; Figiel, P.; Sadowski, G.; Held, C. Predicting CO2 Solubility in Aqueous and Organic Electrolyte Solutions with ePC-SAFT Advanced. *Fluid Phase Equilibria* **2023**, *567*, 113714. https://doi.org/10.1016/j.fluid.2022.113714.

(189) Ascani, M.; Pabsch, D.; Klinksiek, M.; Gajardo-Parra, N.; Sadowski, G.; Held, C. Prediction of pH in Multiphase Multicomponent Systems with ePC-SAFT Advanced. *Chem. Commun.* **2022**, *58* (60), 8436–8439. https://doi.org/10.1039/D2CC02943J.

(190) Rozmus, J.; de Hemptinne, J.-C.; Galindo, A.; Dufal, S.; Mougin, P. Modeling of Strong Electrolytes with ePPC-SAFT up to High Temperatures. *Industrial & Engineering Chemistry Research* **2013**, *52* (29), 9979–9994. https://doi.org/10.1021/ie303527j.

(191) Yang, F.; Kontogeorgis, G. M.; de Hemptinne, J.-C. Systematic Evaluation of Parameterization Approaches for the ePPC-SAFT Model for Aqueous Alkali Halide Solutions. II. Alkali Bromides, Iodides, Fluorides, and Lithium Halides. *Fluid Phase Equilibria* **2023**, *573*, 113853. https://doi.org/10.1016/j.fluid.2023.113853.

(192) Ahmed, S.; Ferrando, N.; Hemptinne, J.-C. de; Simonin, J.-P.; Bernard, O.; Baudouin, O. Modeling of Mixed-Solvent Electrolyte Systems. *Fluid Phase Equilibria* **2018**, *459*, 138–157. https://doi.org/10.1016/j.fluid.2017.12.002.

(193) Olsen, M. D.; Kontogeorgis, G. M.; de Hemptinne, J.-C.; Liang, X.; von Solms, N. Comparisons of Equation of State Models for Electrolytes: E-CPA and e-PPC-SAFT. *Fluid Phase Equilibria* **2023**, *571*, 113804. https://doi.org/10.1016/j.fluid.2023.113804.

(194) Renon, H.; Prausnitz, J. M. Local Compositions in Thermodynamic Excess Functions for Liquid Mixtures. *AIChE J.* **1968**, *14* (1), 135–144. https://doi.org/10.1002/aic.690140124.

(195) Chen, C.-C.; Evans, L. B. A Local Composition Model for the Excess Gibbs Energy of Aqueous Electrolyte Systems. *AIChE J.* **1986**, *32* (3), 444–454.

(196) Chen, C.-C.; Britt, H. I.; Boston, J. F.; Evans, L. B. Local Composition Model for Excess Gibbs Energy of Electrolyte Systems. Part I: Single Solvent, Single Completely Dissociated Electrolyte Systems. *AIChE J.* **1982**, *28* (4), 588–596.

(197) Liu, Y.; Harvey, A. H.; Prausnitz, J. M. THERMODYNAMICS OF CONCENTRATED ELECTROLYTE SOLUTIONS. *Chemical Engineering Communications* **1989**, *77* (1), 43–66. https://doi.org/10.1080/00986448908940172.

(198) Chen, C.-C.; Song, Y. Generalized Electrolyte-NRTL Model for Mixed-Solvent Electrolyte Systems. *AIChE J.* **2004**, *50* (8), 1928–1941. https://doi.org/10.1002/aic.10151.

(199) Song, Y.; Chen, C.-C. Symmetric Electrolyte Nonrandom Two-Liquid Activity Coefficient Model. *Ind. Eng. Chem. Res.* **2009**, *48* (16), 7788–7797. https://doi.org/10.1021/ie9004578.

(200) Chen, C.-C.; Song, Y. Solubility Modeling with a Nonrandom Two-Liquid Segment Activity Coefficient Model. *Ind. Eng. Chem. Res.* **2004**, *43* (26), 8354–8362. https://doi.org/10.1021/ie049463u.

(201) Chen, C.-C.; Song, Y. Extension of Nonrandom Two-Liquid Segment Activity Coefficient Model for Electrolytes. *Industrial & Engineering Chemistry Research* **2005**, *44* (23), 8909–8921. https://doi.org/10.1021/ie0503592.

(202) Song, Y.; Chen, C.-C. Symmetric Nonrandom Two-Liquid Segment Activity Coefficient Model for Electrolytes. *Ind. Eng. Chem. Res.* **2009**, *48* (11), 5522–5529. https://doi.org/10.1021/ie900006g.

(203) Olaya, M. M.; Marcilla, A.; Serrano, M. D.; Botella, A.; Reyes-Labarta, J. A. Simultaneous Correlation of Liquid−Liquid, Liquid−Solid, and Liquid−Liquid−Solid Equilibrium Data for Water + Organic Solvent + Salt Ternary Systems. Anhydrous Solid Phase. *Industrial & Engineering Chemistry Research* **2007**, *46* (21), 7030–7037. https://doi.org/10.1021/ie0705610.

(204) Christensen, C.; Sander, B.; Fredenslund, Aa.; Rasmussen, P. Towards the Extensionof UNIFAC to Mixtures with Electrolytes. *Fluid Phase Equilibria* **1983**, *13*, 297–309. https://doi.org/10.1016/0378-3812(83)80101-0.

(205) Sander, B.; Fredenslund, A.; Rasmussen, P. Calculation of Vapour-Liquid Equilibria in Mixed Solvent/Salt Systems Using an Extended UNIQUAC Equation. *Chemical Engineering Science* **1986**, *41* (5), 1171–1183. https://doi.org/10.1016/0009-2509(86)87090-7.

(206) Sander, B.; Rasmussen, P.; Fredenslund, A. Calculation of Solid-Liquid Equilibria in Aqueous Solutions of Nitrate Salts Using an Extended UNIQUAC Equation. *Chemical*

*Engineering Science* **1986**, *41* (5), 1197–1202. https://doi.org/10.1016/0009-2509(86)87092-0.

(207) Iliuta, M. C.; Thomsen, K.; Rasmussen, P. Extended UNIQUAC Model for Correlation and Prediction of Vapour–Liquid–Solid Equilibria in Aqueous Salt Systems Containing Non-Electrolytes. Part A. Methanol–Water–Salt Systems. *Chemical Engineering Science* **2000**, *55* (14), 2673–2686.

(208) Iliuta, M. C.; Thomsen, K.; Rasmussen, P. Modeling of Heavy Metal Salt Solubility Using the Extended UNIQUAC Model. *AIChE J.* **2002**, *48* (11), 2664–2689. https://doi.org/10.1002/aic.690481125.

(209) Thomsen, K.; C. Iliuta, M.; Rasmussen, P. Extended UNIQUAC Model for Correlation and Prediction of Vapor–Liquid–Liquid–Solid Equilibria in Aqueous Salt Systems Containing Non-Electrolytes. Part B. Alcohol (Ethanol, Propanols, Butanols)–Water–Salt Systems. *Chemical Engineering Science* **2004**, *59* (17), 3631–3647. https://doi.org/10.1016/j.ces.2004.05.024.

(210) Li, J.; Polka, H.-M.; Gmehling, J. A gE Model for Single and Mixed Solvent Electrolyte Systems: 1. Model and Results for Strong Electrolytes. *Fluid Phase Equilibria* **1994**, *94*, 89–114.

(211) Polka, H.-M.; Li, J.; Gmehling, J. A g E Model for Single and Mixed Solvent Electrolyte Systems: 2. Results and Comparison with Other Models. *Fluid phase equilibria* **1994**, *94*, 115–127.

(212) Li, M.-Y.; Wang, L.-S.; Jiang, B.; Gmehling, J. Generalized LIQUAC Model for the Single- and Mixed-Solvent Strong Electrolyte Systems. *AIChE Journal* **2011**, *57* (9), 2535–2546. https://doi.org/10.1002/aic.12445.

(213) Li, M.-Y.; Wang, L.-S.; Gmehling, J. Thermodynamics of Phase Equilibria in Aqueous Strong Electrolyte Systems. *Ind. Eng. Chem. Res.* **2011**, *50* (6), 3621–3631. https://doi.org/10.1021/ie101428j.

(214) Li, M.-Y.; Wang, L.-S.; Wang, K.-P.; Jiang, B.; Gmehling, J. Experimental Measurement and Modeling of Solubility of LiBr and LiNO3 in Methanol, Ethanol, 1-Propanol, 2-Propanol and 1-Butanol. *Fluid Phase Equilibria* **2011**, *307* (1), 104–109. https://doi.org/10.1016/j.fluid.2011.03.017.

(215) Li, M.; Constantinescu, D.; Wang, L.; Mohs, A.; Gmehling, J. Solubilities of NaCl, KCl, LiCl, and LiBr in Methanol, Ethanol, Acetone, and Mixed Solvents and Correlation Using the LIQUAC Model. *Industrial & Engineering Chemistry Research* **2010**, *49* (10), 4981–4988. https://doi.org/10.1021/ie100027c.

(216) Mohs, A.; Gmehling, J. A Revised LIQUAC and LIFAC Model (LIQUAC*/LIFAC*) for the Prediction of Properties of Electrolyte Containing Solutions. *Fluid Phase Equilibria* **2013**, *337*, 311–322. https://doi.org/10.1016/j.fluid.2012.09.023.

(217) Anderko, A.; Wang, P.; Rafal, M. Electrolyte Solutions: From Thermodynamic and Transport Property Models to the Simulation of Industrial Processes. *Fluid Phase Equilibria* **2002**, *194*, 123–142.

(218) Wang, P.; Springer, R. D.; Anderko, A.; Young, R. D. Modeling Phase Equilibria and Speciation in Mixed-Solvent Electrolyte Systems. *Fluid Phase Equilibria* **2004**, *222–223*, 11–17. https://doi.org/10.1016/j.fluid.2004.06.008.

(219) Wang, P.; Anderko, A.; Young, R. D. A Speciation-Based Model for Mixed-Solvent Electrolyte Systems. *Fluid Phase Equilibria* **2002**, *203* (1), 141–176.

(220) Kolář, P.; Nakata, H.; Tsuboi, A.; Wang, P.; Anderko, A. Measurement and Modeling of Vapor–Liquid Equilibria at High Salt Concentrations. *Fluid Phase Equilibria* **2005**, *228–229*, 493–497. https://doi.org/10/cxdccq.

(221) Yan, W.; Topphoff, M.; Rose, C.; Gmehling, J. Prediction of Vapor–Liquid Equilibria in Mixed-Solvent Electrolyte Systems Using the Group Contribution Concept. *Fluid Phase Equilibria* **1999**, *162* (1–2), 97–113. https://doi.org/10.1016/S0378-3812(99)00201-0.

(222) Zuend, A.; Marcolli, C.; Luo, B. P.; Peter, T. A Thermodynamic Model of Mixed Organic-Inorganic Aerosols to Predict Activity Coefficients. *Atmospheric Chemistry and Physics* **2008**, *8* (16), 4559–4593.

(223) Kiepe, J.; Noll, O.; Gmehling, J. Modified LIQUAC and Modified LIFAC A Further Development of Electrolyte Models for the Reliable Prediction of Phase Equilibria with Strong Electrolytes. *Industrial & Engineering Chemistry Research* **2006**, *45* (7), 2361–2373. https://doi.org/10.1021/ie0510122.

(224) Zuend, A.; Marcolli, C.; Booth, A. M.; Lienhard, D. M.; Soonsin, V.; Krieger, U. K.; Topping, D. O.; McFiggans, G.; Peter, T.; Seinfeld, J. H. New and Extended Parameterization of the Thermodynamic Model AIOMFAC: Calculation of Activity Coefficients for Organic-Inorganic Mixtures Containing Carboxyl, Hydroxyl, Carbonyl, Ether, Ester, Alkenyl, Alkyl, and Aromatic Functional Groups. *Atmospheric Chemistry and Physics* **2011**, *11* (17), 9155–9206. https://doi.org/10.5194/acp-11-9155-2011.

(225) Ganbavale, G.; Zuend, A.; Marcolli, C.; Peter, T. Improved AIOMFAC Model Parameterisation of the Temperature Dependence of Activity Coefficients for Aqueous Organic Mixtures. *Atmospheric Chemistry and Physics* **2015**, *15* (1), 447–493. https://doi.org/10.5194/acp-15-447-2015.

(226) Wang, S.; Sandler, S. I.; Chen, C.-C. Refinement of COSMO–SAC and the Applications. *Ind. Eng. Chem. Res.* **2007**, *46* (22), 7275–7288. https://doi.org/10.1021/ie070465z.

(227) Gerlach, T.; Ingram, T.; Sieder, G.; Smirnova, I. Modeling the Solubility of CO2 in Aqueous Methyl Diethanolamine Solutions with an Electrolyte Model Based on COSMO-RS. *Fluid Phase Equilibria* **2018**, *461*, 39–50. https://doi.org/10/gcz7k5.

(228) Toure, O.; Audonnet, F.; Lebert, A.; Dussap, C.-G. Development of a Thermodynamic Model of Aqueous Solution Suited for Foods and Biological Media. Part A: Prediction of Activity Coefficients in Aqueous Mixtures Containing Electrolytes. *The Canadian Journal of Chemical Engineering* **2015**, *93* (2), 443–450. https://doi.org/10.1002/cjce.22075.

(229) Lustig, S. R. Speciation in Electrolytes Using the COSMO-RS Solution Model. *Fluid Phase Equilibria* **2020**, *521*, 112717. https://doi.org/10.1016/j.fluid.2020.112717.

(230) Silva, L. P.; Fernandez, L.; Conceição, J. H. F.; Martins, M. A. R.; Sosa, A.; Ortega, J.; Pinho, S. P.; Coutinho, J. A. P. Design and Characterization of Sugar-Based Deep Eutectic Solvents Using Conductor-like Screening Model for Real Solvents. *ACS*

*Sustainable Chemistry & Engineering* **2018**, *6* (8), 10724–10734. https://doi.org/10.1021/acssuschemeng.8b02042.

(231) Dai, C.; Yu, G.; Lei, Z. Chapter 7 - Predictive Molecular Thermodynamic Models for Ionic Liquids. In *Theoretical and Computational Approaches to Predicting Ionic Liquid Properties*; Joseph, A., Mathew, S., Eds.; Elsevier, 2021; pp 209–241. https://doi.org/10.1016/B978-0-12-820280-7.00004-8.

(232) Lazzús, J. A. A GROUP CONTRIBUTION METHOD TO PREDICT ρ-T-P OF IONIC LIQUIDS. *Chemical Engineering Communications* **2010**, *197* (7), 974–1015. https://doi.org/10/c2fr8r.

(233) Albert, J.; Müller, K. A Group Contribution Method for the Thermal Properties of Ionic Liquids. *Ind. Eng. Chem. Res.* **2014**, *53* (44), 17522–17526. https://doi.org/10/f6pt6d.

(234) Nebig, S.; Gmehling, J. Prediction of Phase Equilibria and Excess Properties for Systems with Ionic Liquids Using Modified UNIFAC: Typical Results and Present Status of the Modified UNIFAC Matrix for Ionic Liquids. *Fluid Phase Equilibria* **2011**, *302* (1), 220–225. https://doi.org/10/cnq2bq.

(235) Lubben, M. J.; Canales, R. I.; Lyu, Y.; Held, C.; Gonzalez-Miquel, M.; Stadtherr, M. A.; Brennecke, J. F. A Promising Thiolanium Ionic Liquid for Extraction of Aromatics from Aliphatics: Experiments and Modeling. *Ind. Eng. Chem. Res.* **2020**. https://doi.org/10.1021/acs.iecr.0c02292.

(236) Thangarajoo, N.; Matheswaran, P.; Johari, K.; Kurnia, K. A. Overview of Activity Coefficient of Methanol at Infinite Dilution in Ionic Liquids and Their Modeling Using Group Contribution Model. *J. Chem. Eng. Data* **2019**, *64* (4), 1760–1769. https://doi.org/10.1021/acs.jced.8b01246.

(237) Thangarajoo, N.; Taqvi, S. A. A.; Matheswaran, P.; Johari, K.; Noh, M. H. Prediction of Infinite Dilution Activity Coefficient of Alcohol in Ionic Liquids Using Group Contribution Method. *Journal of Molecular Liquids* **2021**, *324*, 114723. https://doi.org/10.1016/j.molliq.2020.114723.

(238) Lee, S.; Kim, C.; Do, T. N.; Kim, J. Machine-Learning Based Prediction of Infinite-Dilution Activity Coefficients of Ionic Liquids Using Physicochemical Properties. In *Computer Aided Chemical Engineering*; Montastruc, L., Negny, S., Eds.; 32 European Symposium on Computer Aided Process Engineering; Elsevier, 2022; Vol. 51, pp 1453–1458. https://doi.org/10.1016/B978-0-323-95879-0.50243-5.

(239) Li, J.; Anderson, J. L.; Smith, E. A. Determination of Infinite Dilution Activity Coefficients of Molecular Solutes in Ionic Liquids and Deep Eutectic Solvents by Factorization-Machine-Based Neural Networks. *ACS Sustainable Chem. Eng.* **2022**, *10* (42), 13927–13935. https://doi.org/10.1021/acssuschemeng.2c02600.

(240) Benimam, H.; Moussa, C. S.; Hentabli, M.; Hanini, S.; Laidi, M. Dragonfly-Support Vector Machine for Regression Modeling of the Activity Coefficient at Infinite Dilution of Solutes in Imidazolium Ionic Liquids Using σ-Profile Descriptors. *J. Chem. Eng. Data* **2020**, *65* (6), 3161–3172. https://doi.org/10.1021/acs.jced.0c00168.

(241) Dong, Y.; Huang, S.; Guo, Y.; Lei, Z. COSMO-UNIFAC Model for Ionic Liquids. *AIChE Journal* **2020**, *66* (1), e16787. https://doi.org/10.1002/aic.16787.

(242) Diedenhofen, M.; Eckert, F.; Klamt, A. Prediction of Infinite Dilution Activity Coefficients of Organic Compounds in Ionic Liquids Using COSMO-RS. *J. Chem. Eng. Data* **2003**, *48* (3), 475–479. https://doi.org/10.1021/je025626e.

(243) Anantharaj, R.; Banerjee, T. COSMO-RS-Based Screening of Ionic Liquids as Green Solvents in Denitrification Studies. *Industrial & Engineering Chemistry Research* **2010**, *49* (18), 8705–8725. https://doi.org/10.1021/ie901341k.

(244) Freire, M. G.; Ventura, S. P. M.; Santos, L. M. N. B. F.; Marrucho, I. M.; Coutinho, J. A. P. Evaluation of COSMO-RS for the Prediction of LLE and VLE of Water and Ionic Liquids Binary Systems. *Fluid Phase Equilibria* **2008**, *268* (1–2), 74–84. https://doi.org/10.1016/j.fluid.2008.04.009.

(245) Youqi, Z.; Qinqin, Z.; Hua, X.; Meiheng, L.; Zhigang, Z. COSMO-RS Prediction, Liquid-Liquid Equilibrium Experiment and Quantum Chemistry Calculation for the Separation of n-Butanol and n-Heptane System Using Ionic Liquids. *The Journal of Chemical Thermodynamics* **2022**, *167*, 106719. https://doi.org/10.1016/j.jct.2021.106719.

(246) Qin, H.; Wang, Z.; Zhou, T.; Song, Z. Comprehensive Evaluation of COSMO-RS for Predicting Ternary and Binary Ionic Liquid-Containing Vapor–Liquid Equilibria. *Ind. Eng. Chem. Res.* **2021**, *60* (48), 17761–17777. https://doi.org/10.1021/acs.iecr.1c03940.

(247) Lyu, Y.; Brennecke, J. F.; Stadtherr, M. A. Review of Recent Aromatic–Aliphatic–Ionic Liquid Ternary Liquid–Liquid Equilibria and Their Modeling by COSMO-RS. *Ind. Eng. Chem. Res.* **2020**, *59* (19), 8871–8893. https://doi.org/10.1021/acs.iecr.0c00581.

(248) Ferreira, A. R.; Freire, M. G.; Ribeiro, J. C.; Lopes, F. M.; Crespo, J. G.; Coutinho, J. A. P. Overview of the Liquid–Liquid Equilibria of Ternary Systems Composed of Ionic Liquid and Aromatic and Aliphatic Hydrocarbons, and Their Modeling by COSMO-RS. *Ind. Eng. Chem. Res.* **2012**, *51* (8), 3483–3507. https://doi.org/10.1021/ie2025322.

(249) Tsai, C.-C.; McNeeley, A.; Lin, S.-T.; Liu, Y. A. Evaluation of Thermophysical Data, COSMO-SAC Predictions, and Feed Simplifications for Aromatic Extraction Process Simulation Using Ionic Liquid [EMIM][NTf2]. *AIChE Journal* **2023**, *69* (2), e17916. https://doi.org/10.1002/aic.17916.

(250) Yang, J.; Hou, Z.; Wen, G.; Cui, P.; Wang, Y.; Gao, J. A Brief Review of the Prediction of Liquid–Liquid Equilibrium of Ternary Systems Containing Ionic Liquids by the COSMO-SAC Model. *J Solution Chem* **2019**, *48* (11), 1547–1563. https://doi.org/10.1007/s10953-019-00934-7.

(251) Królikowska, M.; Skonieczny, M.; Paduszyński, K.; Zawadzki, M. Vapor Pressure and Physicochemical Properties of {LiBr + IL-Based Additive + Water} Mixtures: Experimental Data and COSMO-RS Predictions. *J Solution Chem* **2021**, *50* (4), 473–502. https://doi.org/10.1007/s10953-021-01071-w.

(252) Diedenhofen, M.; Klamt, A. COSMO-RS as a Tool for Property Prediction of IL Mixtures—A Review. *Fluid Phase Equilib.* **2010**, *294* (1–2), 31–38. https://doi.org/10.1016/j.fluid.2010.02.002.

(253) Paduszyński, K.; Królikowska, M. Extensive Evaluation of Performance of the COSMO-RS Approach in Capturing Liquid–Liquid Equilibria of Binary Mixtures of Ionic Liquids with Molecular Compounds. *Ind. Eng. Chem. Res.* **2020**, *59* (25), 11851–11863. https://doi.org/10.1021/acs.iecr.0c00449.

(254) Ferreira, A. R.; Freire, M. G.; Ribeiro, J. C.; Lopes, F. M.; Crespo, J. G.; Coutinho, J. A. P. An Overview of the Liquid–Liquid Equilibria of (Ionic Liquid + Hydrocarbon) Binary Systems and Their Modeling by the Conductor-like Screening Model for Real Solvents. *Industrial & Engineering Chemistry Research* **2011**, *50* (9), 5279–5294. https://doi.org/10.1021/ie102471b.

(255) Fernandez, L.; Silva, L. P.; Martins, M. A. R.; Ferreira, O.; Ortega, J.; Pinho, S. P.; Coutinho, J. A. P. Indirect Assessment of the Fusion Properties of Choline Chloride from Solid-Liquid Equilibria Data. *Fluid Phase Equilibria* **2017**, *448*, 9–14. https://doi.org/10.1016/j.fluid.2017.03.015.

(256) Han, J.; Dai, C.; Yu, G.; Lei, Z. Parameterization of COSMO-RS Model for Ionic Liquids. *Green Energy & Environment* **2018**. https://doi.org/10/gdnd4w.

(257) Schneider, R.; Gerber, R. P.; Soares, R. de P. Extension of the F-SAC Model to Ionic Liquids. *Fluid Phase Equilibria* **2018**, *477*, 87–97. https://doi.org/10/gfc3zd.

(258) Lee, B.-S.; Lin, S.-T. Prediction of Phase Behaviors of Ionic Liquids over a Wide Range of Conditions. *Fluid Phase Equilibria* **2013**, *356*, 309–320. https://doi.org/10.1016/j.fluid.2013.07.046.

(259) Lee, B.-S.; Lin, S.-T. A Priori Prediction of Dissociation Phenomena and Phase Behaviors of Ionic Liquids. *Ind. Eng. Chem. Res.* **2015**, *54* (36), 9005–9012. https://doi.org/10.1021/acs.iecr.5b01762.

(260) Lee, B.-S.; Lin, S.-T. The Origin of Ion-Pairing and Redissociation of Ionic Liquid. *J. Phys. Chem. B* **2017**, *121* (23), 5818–5823. https://doi.org/10/gbg5ng.

(261) Lee, B.-S.; Lin, S.-T. Prediction and Screening of Solubility of Pharmaceuticals in Single- and Mixed-Ionic Liquids Using COSMO-SAC Model. *AIChE J.* **2017**, *63* (7), 3096–3104. https://doi.org/10/gbjrvm.

(262) Chang, C.-K.; Lin, S.-T. Extended Pitzer–Debye–Hückel Model for Long-Range Interactions in Ionic Liquids. *J. Chem. Eng. Data* **2019**, acs.jced.9b00368. https://doi.org/10.1021/acs.jced.9b00368.

(263) Chang, C.-K.; Lin, S.-T. Improved Prediction of Phase Behaviors of Ionic Liquid Solutions with the Consideration of Directional Hydrogen Bonding Interactions. *Ind. Eng. Chem. Res.* **2020**, *59* (8), 3550–3559. https://doi.org/10.1021/acs.iecr.9b03741.

(264) Chang, C.-K.; Chen, W.-L.; Wu, D. T.; Lin, S.-T. Improved Directional Hydrogen Bonding Interactions for the Prediction of Activity Coefficients with COSMO-SAC. *Ind. Eng. Chem. Res.* **2018**, *57* (32), 11229–11238. https://doi.org/10/gdwrq5.

(265) Gebbie, M. A.; Smith, A. M.; Dobbs, H. A.; Lee, A. A.; Warr, G. G.; Banquy, X.; Valtiner, M.; Rutland, M. W.; Israelachvili, J. N.; Perkin, S.; Atkin, R. Long Range Electrostatic Forces in Ionic Liquids. *Chem. Commun.* **2017**, *53* (7), 1214–1224. https://doi.org/10.1039/C6CC08820A.

(266) Gebbie, M. A.; Valtiner, M.; Banquy, X.; Fox, E. T.; Henderson, W. A.; Israelachvili, J. N. Ionic Liquids Behave as Dilute Electrolyte Solutions. *PNAS* **2013**, *110* (24), 9674–9679. https://doi.org/10.1073/pnas.1307871110.

(267) Maia, F. M.; Tsivintzelis, I.; Rodriguez, O.; Macedo, E. A.; Kontogeorgis, G. M. Equation of State Modelling of Systems with Ionic Liquids: Literature Review and Application with the Cubic Plus Association (CPA) Model. *Fluid Phase Equilibria* **2012**, *332*, 128–143. https://doi.org/10.1016/j.fluid.2012.06.026.

(268) Ji, X.; Adidharma, H. Thermodynamic Modeling of Ionic Liquid Density with Heterosegmented Statistical Associating Fluid Theory. *Chemical Engineering Science* **2009**, *64* (9), 1985–1992. https://doi.org/10.1016/j.ces.2009.01.018.

(269) Paduszyński, K.; Domańska, U. Thermodynamic Modeling of Ionic Liquid Systems: Development and Detailed Overview of Novel Methodology Based on the PC-SAFT. *The Journal of Physical Chemistry B* **2012**, *116* (16), 5002–5018. https://doi.org/10.1021/jp3009207.

(270) Gharehzadeh Shirazi, S.; Shahabadi, S.; Shekaari, H.; Golmohammadi, B. Thermodynamic Properties of Binary Mixtures Containing Ionic Liquid 1-Butyl-3-Methylimidazolium Thiocyanate and Ethanolamines at Different Temperatures: Measurement and PC-SAFT Modeling. *J. Chem. Eng. Data* **2023**, *68* (12), 3126–3134. https://doi.org/10.1021/acs.jced.3c00374.

(271) Andreu, J. S.; Vega, L. F. Capturing the Solubility Behavior of CO2 in Ionic Liquids by a Simple Model. *J. Phys. Chem. C* **2007**, *111* (43), 16028–16034. https://doi.org/10.1021/jp074353x.

(272) Crespo, E. A.; Silva, L. P.; Correia, C. I. P.; Martins, M. A. R.; Gardas, R. L.; Vega, L. F.; Carvalho, P. J.; Coutinho, J. A. P. Development of a Robust Soft-SAFT Model for Protic Ionic Liquids Using New High-Pressure Density Data. *Fluid Phase Equilibria* **2021**, *539*, 113036. https://doi.org/10.1016/j.fluid.2021.113036.

(273) Guzmán, O.; Ramos Lara, J. E.; del Río, F. Liquid–Vapor Equilibria of Ionic Liquids from a SAFT Equation of State with Explicit Electrostatic Free Energy Contributions. *J. Phys. Chem. B* **2015**, *119* (18), 5864–5872. https://doi.org/10.1021/jp511571h.

(274) Ji, X.; Held, C.; Sadowski, G. Modeling Imidazolium-Based Ionic Liquids with ePC-SAFT. *Fluid Phase Equilibria* **2012**, *335*, 64–73. https://doi.org/10.1016/j.fluid.2012.05.029.

(275) Ji, X.; Held, C.; Sadowski, G. Modeling Imidazolium-Based Ionic Liquids with ePC-SAFT. Part II. Application to H2S and Synthesis-Gas Components. *Fluid Phase Equilibria* **2014**, *363*, 59–65. https://doi.org/10.1016/j.fluid.2013.11.019.

(276) Ji, X.; Held, C. Modeling the Density of Ionic Liquids with ePC-SAFT. *Fluid Phase Equilibria* **2016**, *410*, 9–22. https://doi.org/10.1016/j.fluid.2015.11.014.

(277) Shen, G.; Held, C.; Lu, X.; Ji, X. Modeling Thermodynamic Derivative Properties of Ionic Liquids with ePC-SAFT. *Fluid Phase Equilibria* **2015**, *405*, 73–82. https://doi.org/10.1016/j.fluid.2015.07.018.

(278) Shen, G.; Laaksonen, A.; Lu, X.; Ji, X. Developing Electrolyte Perturbed-Chain Statistical Associating Fluid Theory Density Functional Theory for CO2 Separation by Confined Ionic Liquids. *J. Phys. Chem. C* **2018**, *122* (27), 15464–15473. https://doi.org/10/gdzwcj.

(279) Sun, Y.; Zuo, Z.; Laaksonen, A.; Lu, X.; Ji, X. How to Detect Possible Pitfalls in ePC-SAFT Modelling: Extension to Ionic Liquids. *Fluid Phase Equilibria* **2020**, *519*, 112641. https://doi.org/10.1016/j.fluid.2020.112641.

(280) Dai, Z.; Chen, Y.; Sun, Y.; Zuo, Z.; Lu, X.; Ji, X. Screening Ionic Liquids for Developing Advanced Immobilization Technology for CO2 Separation. *Frontiers in Chemistry* **2022**, *10*.

(281) Jiřiště, L.; Klajmon, M. Predicting the Thermodynamics of Ionic Liquids: What to Expect from PC-SAFT and COSMO-RS? *J. Phys. Chem. B* **2022**, *126* (20), 3717–3736. https://doi.org/10.1021/acs.jpcb.2c00685.

(282) Marques, H.; Velho, P.; Gómez, E.; Macedo, E. A. Determining the Dissociation Extent of Ionic Liquids in Water Using the PDH + UNIQUAC Model. *Journal of Molecular Liquids* **2022**, *348*, 118403. https://doi.org/10.1016/j.molliq.2021.118403.

(283) Wang, P.; Anderko, A. Modeling Chemical Equilibria, Phase Behavior, and Transport Properties in Ionic Liquid Systems. *Fluid Phase Equilibria* **2011**, *302* (1–2), 74–82. https://doi.org/10.1016/j.fluid.2010.08.011.

(284) Shariatmadar Tehrani, M. A.; Haghtalab, A. Correlation of Ternary Aqueous Two-Phase Systems Containing Ionic Liquids and Salts Using Symmetric Electrolyte Local Composition Models: NRTL-NRF, UNIQUAC-NRF, and UNIQUAC. *J. Chem. Eng. Data* **2019**. https://doi.org/10.1021/acs.jced.9b00612.

(285) Ganguly, A.; Bairagya, P.; Banerjee, T.; Kundu, D. Application of Nature-Inspired Algorithms with Generalized Pitzer-Debye-Hückel (PDH) Refinement for Liquid Liquid Equilibria (LLE) Correlation in Cyclic Di-Ether Systems. *AIChE Journal* **2022**, *68* (2), e17434. https://doi.org/10.1002/aic.17434.

(286) Lin, Y.-J.; Hossain, N.; Chen, C.-C. Modeling Dissociation of Ionic Liquids with Electrolyte NRTL Model. *Journal of Molecular Liquids* **2021**, *329*, 115524. https://doi.org/10.1016/j.molliq.2021.115524.

(287) May, P. M.; Murray, K. JESS, A Joint Expert Speciation System—I. Raison d'être. *Talanta* **1991**, *38* (12), 1409–1417. https://doi.org/10/bp8x55.

(288) May, P. M.; Muray, K. Jess, a Joint Expert Speciation System—II. The Thermodynamic Database. *Talanta* **1991**, *38* (12), 1419–1426. https://doi.org/10/bmkfz5.

(289) May, P. M.; Murray, K. JESS, a Joint Expert Speciation System—III. Surrogate Functions. *Talanta* **1993**, *40* (6), 819–825. https://doi.org/10/fdh599.

(290) Rowland, D.; May, P. M. JESS, a Joint Expert Speciation System—V: Approaching Thermodynamic Property Prediction for Multicomponent Concentrated Aqueous Electrolyte Solutions. *Talanta* **2010**, *81* (1), 149–155. https://doi.org/10/bfghsf.

(291) May, P. M.; Rowland, D. JESS, a Joint Expert Speciation System – VI: Thermodynamically-Consistent Standard Gibbs Energies of Reaction for Aqueous Solutions. *New J. Chem.* **2018**, *42* (10), 7617–7629. https://doi.org/10/gd8fc8.

(292) Gulaboski, R.; Mirčeski, V.; Scholz, F. An Electrochemical Method for Determination of the Standard Gibbs Energy of Anion Transfer between Water and N-Octanol. *Electrochemistry Communications* **2002**, *4* (4), 277–283. https://doi.org/10.1016/S1388-2481(02)00264-3.

(293) Olaya, A. J.; Méndez, M. A.; Cortes-Salazar, F.; Girault, H. H. Voltammetric Determination of Extreme Standard Gibbs Ion Transfer Energy. *Journal of Electroanalytical Chemistry* **2010**, *644* (1), 60–66. https://doi.org/10.1016/j.jelechem.2010.03.030.

(294) Marcus, Y. Thermodynamic Functions of Transfer of Single Ions from Water to Nonaqueous and Mixed Solvents: Part I - Gibbs Free Energies of Transfer to Nonaqueous Solvents. *pac* **1983**, *55* (6), 977–1021. https://doi.org/10.1351/pac198355060977.

(295) Kihara, S.; Suzuki, M.; Sugiyama, M.; Matsui, M. The Transfer of Carboxylate and Sulphonate Anions at the Aqueous/Organic Solution Interface Studied by Polarography with the Electrolyte Solution Dropping Electrode. *Journal of Electroanalytical Chemistry and Interfacial Electrochemistry* **1988**, *249* (1), 109–122. https://doi.org/10.1016/0022-0728(88)80352-8.

(296) Kazakov, A. F.; Magee, J. W.; Chirico, R. D.; Diky, V.; Kroenlein, K. G.; Muzny, C. D.; Frenkel, M. D. Ionic Liquids Database - ILThermo (v2.0). *NIST* **2013**.

(297) Dong, Q.; Muzny, C. D.; Kazakov, A. F.; Diky, V.; Magee, J. W.; Widegren, J. A.; Chirico, R. D.; Marsh, K. N.; Frenkel, M. D. ILThermo: A Free-Access Web Database for Thermodynamic Properties of Ionic Liquids. *NIST* **2007**, *52*, 1151–1159.

(298) COSMOconf 3.

(299) Marcus, Y. Thermodynamic Functions of Transfer of Single Ions from Water to Nonaqueous and Mixed Solvents: Part 4-The Selection of Extra Thermodynamic Assumptions. *Pure and Applied Chemistry* **1986**, *58* (12), 1721–1736.

(300) Lee, A. A.; Perez-Martinez, C. S.; Smith, A. M.; Perkin, S. Underscreening in Concentrated Electrolytes. *Faraday Discuss.* **2017**, *199* (0), 239–259. https://doi.org/10.1039/C6FD00250A.

(301) Smith, A. M.; Lee, A. A.; Perkin, S. The Electrostatic Screening Length in Concentrated Electrolytes Increases with Concentration. *The Journal of Physical Chemistry Letters* **2016**, *7* (12), 2157–2163. https://doi.org/10.1021/acs.jpclett.6b00867.

(302) Smith, A. M.; Maroni, P.; Trefalt, G.; Borkovec, M. Unexpectedly Large Decay Lengths of Double Layer Forces in Solutions of Symmetric, Multivalent Electrolytes. *J. Phys. Chem. B* **2019**. https://doi.org/10.1021/acs.jpcb.8b12246.

(303) Stojimirović, B.; Galli, M.; Trefalt, G. Forces between Silica Particles in Isopropanol Solutions of 1:1 Electrolytes. *Phys. Rev. Res.* **2020**, *2* (2), 023315. https://doi.org/10.1103/PhysRevResearch.2.023315.

(304) Barthel, J.; Neueder, R.; Poepke, H.; Wittmann, H. Osmotic Coefficients and Activity Coefficients of Nonaqueous Electrolyte Solutions. Part 2. Lithium Perchlorate in the Aprotic Solvents Acetone, Acetonitrile, Dimethoxyethane, and Dimethylcarbonate. *Journal of solution chemistry* **1999**, *28* (5), 489–503.

(305) Nordness, O.; Brennecke, J. F. Ion Dissociation in Ionic Liquids and Ionic Liquid Solutions. *Chemical Reviews* **2020**. https://doi.org/10.1021/acs.chemrev.0c00373.

(306) Outhwaite, C. W. A Modified Poisson-Boltzmann Equation in the Double Layer. *Chemical Physics Letters* **1970**, *7* (6), 636–638. https://doi.org/10.1016/0009-2614(70)87027-0.

(307) Outhwaite, C. W. Numerical Solution of a Poisson–Boltzmann Theory for a Primitive Model Electrolyte with Size and Charge Asymmetric Ions. *J. Chem. Soc., Faraday Trans. 2* **1987**, *83* (6), 949–959. https://doi.org/10.1039/F29878300949.

(308) Outhwaite. A Modified Poisson-Boltzmann Approach to Homogeneous Ionic Solutions. *Condensed Matter Physics* **2004**, *7* (4), 719. https://doi.org/10/gftg6w.

(309) Abbas, Z.; Gunnarsson, M.; Ahlberg, E.; Nordholm, S. Corrected Debye–Hückel Theory of Salt Solutions: Size Asymmetry and Effective Diameters. *J. Phys. Chem. B* **2002**, *106* (6), 1403–1420. https://doi.org/10/bqrk6x.

(310) Fraenkel, D. Correction to Negative Deviations from the Debye–Hückel Limiting Law for High-Charge Polyvalent Electrolytes: Are They Real? *J. Chem. Theory Comput.* **2018**, *14* (12), 6741–6741. https://doi.org/10/gfrbqv.

(311) Lei, Q.; Peng, B.; Sun, L.; Luo, J.; Chen, Y.; Kontogeorgis, G. M.; Liang, X. Predicting Activity Coefficients with the Debye–Hückel Theory Using Concentration Dependent Static Permittivity. *AIChE Journal* **2020**, *66* (11), e16651. https://doi.org/10.1002/aic.16651.

(312) Ebeling, W. Zur Theorie Der Bjerrumschen Ionenassoziation in Elektrolyten. *Zeitschrift für Physikalische Chemie* **1968**, *238O* (1), 400–402. https://doi.org/10.1515/zpch-1968-23847.

(313) Yokoyama, H.; Yamatera, H. A Theory of Ion Association as a Complement of the Debye-Hückel Theory. *Bulletin of the Chemical Society of Japan* **1975**, *48* (6), 1770–1776. https://doi.org/10.1246/bcsj.48.1770.

(314) Robinson, R. A.; Stokes, R. H. *Electrolyte Solutions*, 2nd rev. ed.; Dover Publications: Mineola, NY, 2002.

(315) Haghtalab, A.; Peyvandi, K. Electrolyte-UNIQUAC-NRF Model for the Correlation of the Mean Activity Coefficient of Electrolyte Solutions. *Fluid Phase Equilibria* **2009**, *281* (2), 163–171. https://doi.org/10.1016/j.fluid.2009.04.013.

(316) Pinho, S. P.; Macedo, E. A. Experimental Measurement and Modelling of KBr Solubility in Water, Methanol, Ethanol, and Its Binary Mixed Solvents at Different Temperatures. *The Journal of Chemical Thermodynamics* **2002**, *34* (3), 337–360. https://doi.org/10.1006/jcht.2001.0856.

(317) González de Castilla, A.; Müller, S.; Smirnova, I. Corrigendum to 'On the Analogy between the Restricted Primitive Model and Capacitor Circuits: Semi-Empirical Alternatives for over- and Underscreening in the Calculation of Mean Ionic Activity Coefficients.' *Journal of Molecular Liquids* **2021**, *331*, 115640. https://doi.org/10.1016/j.molliq.2021.115640.

(318) Wolery, T. J. On the Thermodynamic Framework of Solutions (with Special Reference to Aqueous Electrolyte Solutions). *American Journal of Science* **1990**, *290* (3), 296–320. https://doi.org/10.2475/ajs.290.3.296.

(319) Pitzer, K. S. A Consideration of Pitzer's Equations for Activity and Osmotic Coefficients in Mixed Electrolytes. *J. Chem. Soc., Faraday Trans. 1* **1984**, *80* (12), 3451–3454. https://doi.org/10.1039/F19848003451.

(320) van Bochove, G. H.; Krooshof, G. J.; de Loos, T. W. Modelling of Liquid–Liquid Equilibria of Mixed Solvent Electrolyte Systems Using the Extended Electrolyte NRTL. *Fluid Phase Equilib.* **2000**, *171* (1), 45–58.

(321) Chang, C.-K.; Lin, S.-T. Improved Prediction of Phase Behaviors of Ionic Liquid Solutions with Consideration of Directional Hydrogen Bonding Interactions. *Ind. Eng. Chem. Res.* **2020**. https://doi.org/10.1021/acs.iecr.9b03741.

(322) Bülow, M.; Ji, X.; Held, C. Incorporating a Concentration-Dependent Dielectric Constant into ePC-SAFT. An Application to Binary Mixtures Containing Ionic Liquids. *Fluid Phase Equilibria* **2019**, *492*, 26–33. https://doi.org/10.1016/j.fluid.2019.03.010.

(323) Huang, M.-M.; Jiang, Y.; Sasisanker, P.; Driver, G. W.; Weingärtner, H. Static Relative Dielectric Permittivities of Ionic Liquids at 25 °C. *J. Chem. Eng. Data* **2011**, *56* (4), 1494–1499. https://doi.org/10.1021/je101184s.

(324) Wakai, C.; Oleinikova, A.; Ott, M.; Weingärtner, H. How Polar Are Ionic Liquids? Determination of the Static Dielectric Constant of an Imidazolium-Based Ionic Liquid by Microwave Dielectric Spectroscopy. *J. Phys. Chem. B* **2005**, *109* (36), 17028–17030. https://doi.org/10.1021/jp053946+.

(325) De M. Cardoso, M. J. E.; O'Connell, J. P. Activity Coefficients in Mixed Solvent Electrolyte Solutions. *Fluid Phase Equilibria* **1987**, *33* (3), 315–326. https://doi.org/10.1016/0378-3812(87)85043-4.

(326) Breil, M. P.; Mollerup, J. M. The McMillan–Mayer Framework and the Theory of Electrolyte Solutions. *Fluid Phase Equilibria* **2006**, *242* (2), 129–135. https://doi.org/10.1016/j.fluid.2006.01.018.

(327) Michelsen, M. L.; Mollerup, J. M. *Thermodynamic Models: Fundamentals & Computational Aspects*, 2. ed.; Tie-Line Publications: Holte, 2007.

(328) Friedman, H. L. Lewis-Randall to McMillan-Mayer Conversion for the Thermodynamic Excess Functions of Solutions. Part I. Partial Free Energy Coefficients. *J Solution Chem* **1972**, *1* (5), 387–412. https://doi.org/10.1007/BF00645603.

(329) Friedman, H. L. Lewis-Randall to McMillan-Mayer Conversion for the Thermodynamic Excess Functions of Solutions. Part II. Excess Energy and Volume. *J Solution Chem* **1972**, *1* (5), 413–417. https://doi.org/10.1007/BF00645604.

(330) Friedman, H. L. Lewis-Randall to McMillan-Mayer Conversion for the Thermodynamic Excess Functions of Solutions. Part III. Common-Ion Mixtures of Two Electrolytes. *J Solution Chem* **1972**, *1* (5), 419–431. https://doi.org/10.1007/BF00645605.

(331) Bernard, O. Theory of Charge Asymmetric Electrolytes. Onsager's Approach Revisited. *Journal of Molecular Liquids* **2022**, 120163. https://doi.org/10.1016/j.molliq.2022.120163.

(332) Simonin, J.-P.; Bernard, O. Insight into the Ionic Atmosphere Effect: Comparison of Theories for Electrolytes at the Primitive Level. *Fluid Phase Equilibria* **2023**, *571*, 113805. https://doi.org/10.1016/j.fluid.2023.113805.

(333) Skrzecz, A.; Lisov, N. I.; Sazonov, N. V. IUPAC-NIST Solubility Data Series. 83. Acetonitrile: Ternary and Quaternary Systems. *Journal of Physical and Chemical Reference Data* **2007**, *36* (3), 733. https://doi.org/10.1063/1.2539811.

(334) Pinho, S. P.; Macedo, E. A. Solubility of NaCl, NaBr, and KCl in Water, Methanol, Ethanol, and Their Mixed Solvents. *J. Chem. Eng. Data* **2005**, *50* (1), 29–32. https://doi.org/10.1021/je049922y.

(335) Hernández-Luis, F.; Rodríguez-Raposo, R.; Galleguillos, H. R.; Morales, J. W. Solubility of Sodium Halides in Aqueous Mixtures with ε-Increasing Cosolvents: Formamide, *N* -Methylformamide, and *N* -Methylacetamide at 298.15 K. *Industrial & Engineering Chemistry Research* **2016**, *55* (3), 812–819. https://doi.org/10.1021/acs.iecr.5b04614.

(336) Seidell, A. *Solubilities of Inorganic and Organic Compounds; a Compilation of Quantitative Solubility Data from the Periodical Literature*, 2nd ed.; New York, Van Nostrand, 1919.

(337) Barthel, J.; Krüger, J.; Schollmeyer, E. Untersuchungen Zur Dispersion Der Komplexen Dielektrizitätskonstante Wäßriger Und Nichtwäßriger Elektrolytlösungen. *Zeitschrift für Physikalische Chemie* **1977**, *104* (1–3), 59–72. https://doi.org/10.1524/zpch.1977.104.1-3.059.

(338) Wu, X.; Gong, Y.; Xu, S.; Yan, Z.; Zhang, X.; Yang, S. Electrical Conductivity of Lithium Chloride, Lithium Bromide, and Lithium Iodide Electrolytes in Methanol, Water, and Their Binary Mixtures. *J. Chem. Eng. Data* **2019**, *64* (10), 4319–4329. https://doi.org/10.1021/acs.jced.9b00405.

(339) Banerjee, T.; Verma, K. K.; Khanna, A. Liquid-Liquid Equilibrium for Ionic Liquid Systems Using COSMO-RS: Effect of Cation and Anion Dissociation. *AIChE Journal* **2008**, *54* (7), 1874–1885. https://doi.org/10.1002/aic.11495.

(340) Coutinho, J. A. P.; Carvalho, P. J.; Oliveira, N. M. C. Predictive Methods for the Estimation of Thermophysical Properties of Ionic Liquids. *RSC Advances* **2012**, *2* (19), 7322. https://doi.org/10.1039/c2ra20141k.

(341) Wang, K.; Peng, D.; Alhadid, A.; Minceva, M. Assessment of COSMO-RS for Predicting Liquid–Liquid Equilibrium in Systems Containing Deep Eutectic Solvents. *Ind. Eng. Chem. Res.* **2024**, *63* (25), 11110–11120. https://doi.org/10.1021/acs.iecr.4c00796.

(342) Landrum, G.; Tosco, P.; Kelley, B.; sriniker; gedeck; NadineSchneider; Vianello, R.; Ric; Dalke, A.; Cole, B.; AlexanderSavelyev; Swain, M.; Turk, S.; N, D.; Vaucher, A.; Kawashima, E.; Wójcikowski, M.; Probst, D.; godin, guillaume; Cosgrove, D.; Pahl, A.; JP; Berenger, F.; strets123; JLVarjo; O'Boyle, N.; Fuller, P.; Jensen, J. H.; Sforna, G.; DoliathGavid. Rdkit/Rdkit: 2020_03_1 (Q1 2020) Release, 2020. https://doi.org/10.5281/zenodo.3732262.

(343) Slattery, J. M.; Daguenet, C.; Dyson, P. J.; Schubert, T. J. S.; Krossing, I. How to Predict the Physical Properties of Ionic Liquids: A Volume-Based Approach. *Angewandte Chemie International Edition* **2007**, *46* (28), 5384–5388. https://doi.org/10.1002/anie.200700941.

(344) Preiss, U. P. R. M.; Slattery, J. M.; Krossing, I. In Silico Prediction of Molecular Volumes, Heat Capacities, and Temperature-Dependent Densities of Ionic Liquids. *Ind. Eng. Chem. Res.* **2009**, *48* (4), 2290–2296. https://doi.org/10.1021/ie801268a.

(345) Grzetic, D. J.; Delaney, K. T.; Fredrickson, G. H. Contrasting Dielectric Properties of Electrolyte Solutions with Polar and Polarizable Solvents. *Phys. Rev. Lett.* **2019**, *122* (12), 128007. https://doi.org/10.1103/PhysRevLett.122.128007.

(346) Weingärtner, H. The Static Dielectric Constant of Ionic Liquids. *Zeitschrift für Physikalische Chemie* **2006**, *220* (10), 1395–1405. https://doi.org/10.1524/zpch.2006.220.10.1395.

(347) Kaatze, U.; Schumacher, A.; Pottel, R. The Dielectric Properties of Tert.-Butanol/Water Mixtures as a Function of Composition. *Berichte der Bunsengesellschaft für physikalische Chemie* **1991**, *95* (5), 585–592. https://doi.org/10.1002/bbpc.19910950508.

(348) Kannan Kottummal, T.; Pilathottathil, S.; Thayyil, M. S.; Mahadevan Perumal, P.; Nagarajan Sreekala, K. K.; Guruswamy, G.; Vellikkandi Chaluvalappil, S.; Manal Poovingal, N. N. Dielectric Relaxation and Electrochemical Studies on Trihexyl Tetradecyl Phosphonium Chloride [P14,6,6,6][Cl] Ionic Liquid. *Journal of Molecular Liquids* **2018**, *252*, 488–494. https://doi.org/10.1016/j.molliq.2017.12.146.

(349) Rowley, R. L.; Wilding, W. V.; Oscarson, J. L.; Yang, Y.; Zundel, N. A.; Daubert, T. E.; Danner, R. P. *DIPPR Data Compilation of Pure Compound Properties*; Design Institute for Physical Properties, 2003.

(350) Every, A. G.; McCardy, A. K. *Numerical Data and Fundamental Relationships in Science and Technology (New Series, Group III of Landolt-Bernstein Vol 29a) Ed DF Nelson*; Berlin: Springer, 1992.

(351) *CRC Handbook of Chemistry and Physics: A Ready-Reference Book of Chemical and Physical Data*, 86. ed.; Chemical Rubber Company, Lide, D. R., Eds.; CRC Press: Boca Raton, 2005.

(352) Pátek, J.; Hrubý, J.; Klomfar, J.; Součková, M.; Harvey, A. H. Reference Correlations for Thermophysical Properties of Liquid Water at 0.1 MPa. *Journal of Physical and Chemical Reference Data* **2009**, *38* (1), 21. https://doi.org/10.1063/1.3043575.

(353) Miller, C. G.; Maass, O. DETERMINATION OF DIELECTRIC CONSTANT IN BINARY ORGANIC SYSTEMS. *Can. J. Chem.* **1960**, *38* (9), 1606–1616. https://doi.org/10.1139/v60-221.

(354) Pramanik, S.; Das, B. Thermodynamic Properties of Aqueous Sodium Nitrate Solutions Under Superambient Conditions. *J Solution Chem* **2019**, *48* (2), 167–179. https://doi.org/10.1007/s10953-019-00852-8.

(355) Freire, M. G.; Neves, C. M. S. S.; Carvalho, P. J.; Gardas, R. L.; Fernandes, A. M.; Marrucho, I. M.; Santos, L. M. N. B. F.; Coutinho, J. A. P. Mutual Solubilities of Water and Hydrophobic Ionic Liquids. *The Journal of Physical Chemistry B* **2007**, *111* (45), 13082–13089. https://doi.org/10.1021/jp076271e.

(356) Pereiro, A. B.; Rodríguez, A. Experimental Liquid–Liquid Equilibria of 1-Alkyl-3-Methylimidazolium Hexafluorophosphate with 1-Alcohols. *J. Chem. Eng. Data* **2007**, *52* (4), 1408–1412. https://doi.org/10.1021/je700099w.

(357) Pereiro, A. B.; Rodríguez, A. Study on the Phase Behaviour and Thermodynamic Properties of Ionic Liquids Containing Imidazolium Cation with Ethanol at Several Temperatures. *The Journal of Chemical Thermodynamics* **2007**, *39* (6), 978–989. https://doi.org/10.1016/j.jct.2006.10.017.

(358) Nordness, O.; Simoni, L. D.; Stadtherr, M. A.; Brennecke, J. F. Characterization of Aqueous 1-Ethyl-3-Methylimidazolium Ionic Liquids for Calculation of Ion

Dissociation. *J. Phys. Chem. B* **2019**, *123* (6), 1348–1358. https://doi.org/10.1021/acs.jpcb.8b11892.

(359) Bülow, M.; Ascani, M.; Held, C. ePC-SAFT Advanced – Part II: Application to Salt Solubility in Ionic and Organic Solvents and the Impact of Ion Pairing. *Fluid Phase Equilibria* **2021**, *537*, 112989. https://doi.org/10.1016/j.fluid.2021.112989.

(360) Mollerup, J. M.; Breil, M. P. Modeling the Permittivity of Electrolyte Solutions. *AIChE Journal* **2015**, *61* (9), 2854–2860. https://doi.org/10.1002/aic.14799.

(361) Uematsu, M.; Franck, E. U. Static Dielectric Constant of Water and Steam. *Journal of Physical and Chemical Reference Data* **1980**, *9* (4), 1291–1306. https://doi.org/10.1063/1.555632.

# 10 Student Theses

The following theses were supervised during my stay as a research assistant at Hamburg University of Technology. These have contributed to some sections of the present manuscript:

- Daniel Wenser. "*Extension of the COSMO-RS-ES model for temperature dependency in aqueous electrolytes based on data from the Joint Expert Speciation System*". Bachelor Thesis. 2021.
- Julian Schilling. "*Development of a temperature dependent non-aqueous electrolyte systems database by means of experimental data and the Pitzer equations".* Bachelor Thesis. 2022. Shared supervision with Dr.-Ing. Simon Müller.
- Bálint Szikszai. "*Evaluation of long-range electrostatics on the modelling of ionic liquids with COSMO-RS based methods*". Project Thesis. 2023

In addition, the students Lukas Maksimowski, Tim-Julian Brandt, Inma Mundokkil Nisht Kumar and Hassan Raza also contributed to the results of the present work.

The following theses were supervised during my stay as research assistant at Hamburg University of Technology. These theses focused on topics that are not included in this manuscript:

- Sadi Tomtulu. "*Modelling the solubility curves of choline chloride based deep eutectic solvents with NRTL and extended long-range electrostatics*". Project Thesis. 2023.
- Tien Ching Ma. "*Development of novel porous materials by a combination of cryoextraction and supercritical drying technologies*". Master Thesis. 2019. Shared supervision with Jun. Prof. Pavel Gurikov and Dr.-Ing. Sheila Ruiz Barbero.
- Kevin Joel de la Asunción López. "*Development of a model for the relative permittivity in organic liquids: A COSMO based approach".* Master Thesis. 2022. Shared supervision with Dr.-Ing. Simon Müller.